The geology and geochemistry of the ultrabasic rocks ad associated chromite deposits of the andizlik-zimparalik area, fethiye, southwest Turkey

T. Engin

THE GEOLOGY AND GEOCHEMISTRY OF THE ULTRABASIC ROCKS AND ASSOCIATED CHROMITE DEPOSITS OF THE ANDIZLIK-ZIMPARALIK AREA, FETHIYE, SOUTHWEST TURKEY

T. ENGIN, Dip. Geol/Geophys. Istanbul, 1962

Thesis submitted for the degree of
Doctor of Philosophy in the
University of Durham

VOLUME 1

Graduate Society

February 1969

ABSTRACT

The serpentinised ultramafics and associated chromites selected for study are derived from the Andizlik-Zimparalik peridotite body situated near Fethiye, Southwest Turkey, towards the eastern end of the northern peridotite body.

The peridotite is bounded by large, inward dipping faults. The country rocks are unmetamorphosed and mainly comprise Paleozoic and Mesozoic limestones and Miocene flysch.

Structural features including faults, joints, and internal contacts conform to two dominant planes trending either northeast-southwest, dipping northwest or northwest-southeast, dipping northeast. These planes make acute angles in the east-west direction suggesting that the final tectonic emplacement to the present level, took place under the influence of maximum principal pressures from the east-west direction.

The peridotites are mainly harzburgite with subordinate dunites. Pyroxenite veins and basic dykes are late stage features.

The ultramafics show wide variation in degree of serpentinisation which is invariably intense near the margins of the body, along fault zones and along internal tectonic contacts.

Chemical analyses of the ultramafics reveal little variation throughout the peridotite body. When the harzburgite

analyses are recalculated on a water free basis the chemistry remains constant except for loses in respect of some minor constituents, notably Al_2O_3 and CaO, in fully serpentinised rocks. An equation representing isochemical (except for hydration) serpentinisation of harzburgite implies expansion of approximately 39 percent of the original volume during the process, higher than values derived from density calculations.

The area is a source of chrome ore. The chemistry of the chromites has been examined in relation to type of ore, situation and structural disposition. Cr_2O_3 content increases from stratiform through disseminated and massive to nodular types, while the eastern chromites have relatively low Cr/Fe, Cr/Al and Mg/Fe ratios. Chemical analyses of the chromites have been correlated with measurements of unit cell size and reflectivity.

The peridotite is believed to have been generated near the crust-mantle boundary where the bulk of the chromite and associated peridotite crystallized. Tectonic uplift, associated with the Alpine orogeny, raised the body to a mid-crustal position producing the podiform disposition, of chrome ore bodies by differential movement in crystal mush. In the mid-crust final ultramafic crystallization resulted in the formation of limited stratiform chromite. This was followed by autointrusion of residual gabbroic magma along

pre-determined structural directions, high temperature hydrothermal formation of pyroxenite, and serpentinisation. Expansion resulting from serpentinisation probably provided the impetus for continued uplift to the present level in the crust, this probably took place during the Laramide phase of Alpine orogeny.

ACKNOWLEDGEMENTS

The author wishes to acknowledge a research studentship provided by the Mineral Research and Exploration Institute, Ankara, Turkey (M.T.A.) who also financed the field work in Turkey. Thanks are due to the Etibank, Uckopru, chrome-ore mining company for providing facilities in the field and access to underground chrome-ore workings, Messrs. Y. Ertem, S. Aydas, G.Berk and F.Yilmaz of this Company were particularly helpful. Professor, Dr. Van der Kaaden introduced the author to this chrome-ore field in 1965.

The author wishes to thank Professor Dr. K.C. Dunham and his successor, Professor Dr. G.M. Brown for providing research facilities in the Department of Geology, University of Durham. Professor Dunham's supervision during the first year of research is gratefully acknowledged. The author is indebted to Dr. D.M. Hirst for his supervision of this research during the remaining period of time, for his advice, direction, encouragement and assistance in transcribing the English from the continental to the insular. He wishes to record his thanks to Mr. R. Phillips for his advice on economic geology and particularly for the assistance with ore microscopy, and to Professor Dr. M.H.P. Bott for his suggestions relating to the structural geology. Dr. J.G. Holland has given freely of advice and assistance with X-ray fluorescence

analysis and computing for which the author is most grateful. Dr. P. de Graciansky of Ecole Nationale Superieure des Mines de Paris is gratefully acknowledged for his suggestions and access to his field maps. Dr. J.W. Aucott has given assistance with the electron microprobe analyses and computing and Mr. M.C. George has provided a computer programme for cell size calculations of cubic minerals. M.T.A. of Turkey and Albright and Wilson Ltd. have kindly provided the analysed chrome ore samples which were used as standards for the X-ray fluorescence analysis. Finally the author wishes to record his thanks to Mr. G. Wilson and the technical personnel of the Department of Geology.

LIST OF FIGURES

LIST OF PLATES

LIST OF TABLES

CONTENTS

CHAPTER 1

INTRODUCTION

General Setting

The area under consideration is situated in southwest Turkey, 40 km north of Fethiye, it lies at the eastern end of a large peridotite body extending from the Datça peninsula in the west, fig.1. It is bounded in the south by the Çal dere and Gürleyik köy, in the north by Damdir, in the east by Kizlan mahallesi and in the northwest by the Dalaman Çay, (river) fig.2, fig.4.

The terrain is mountainous, the highest peak in the immediate vicinity being Çal dag 2185 m. In the actual field the lowest point is on the Dalaman Çay at 250 m and the highest point is Madenoyugu tepe at 1622 m. The area is covered in places by pine trees, a reflection of the elevation; vegetation did not impede the field work.

The climate is Mediterranean, dry with temperatures reaching 35°C - 40°C during the summer, while in winter temperatures are moderate with thundery rain; snow is not common and only covers the high peaks.

The population is concentrated in the towns of Mugla, Köycegiz and Fethiye. The field under consideration is sparsley populated. The three main chrome ore mine groups, Uçköprü in the south, Andizlik and Zimparalik in the centre and Damdir in the north, together with some other small mining hamlets are the only populated places. Mining and forestery are the two main occupations.

BASIC AND ULTRABASIC ROCKS IN TURKEY

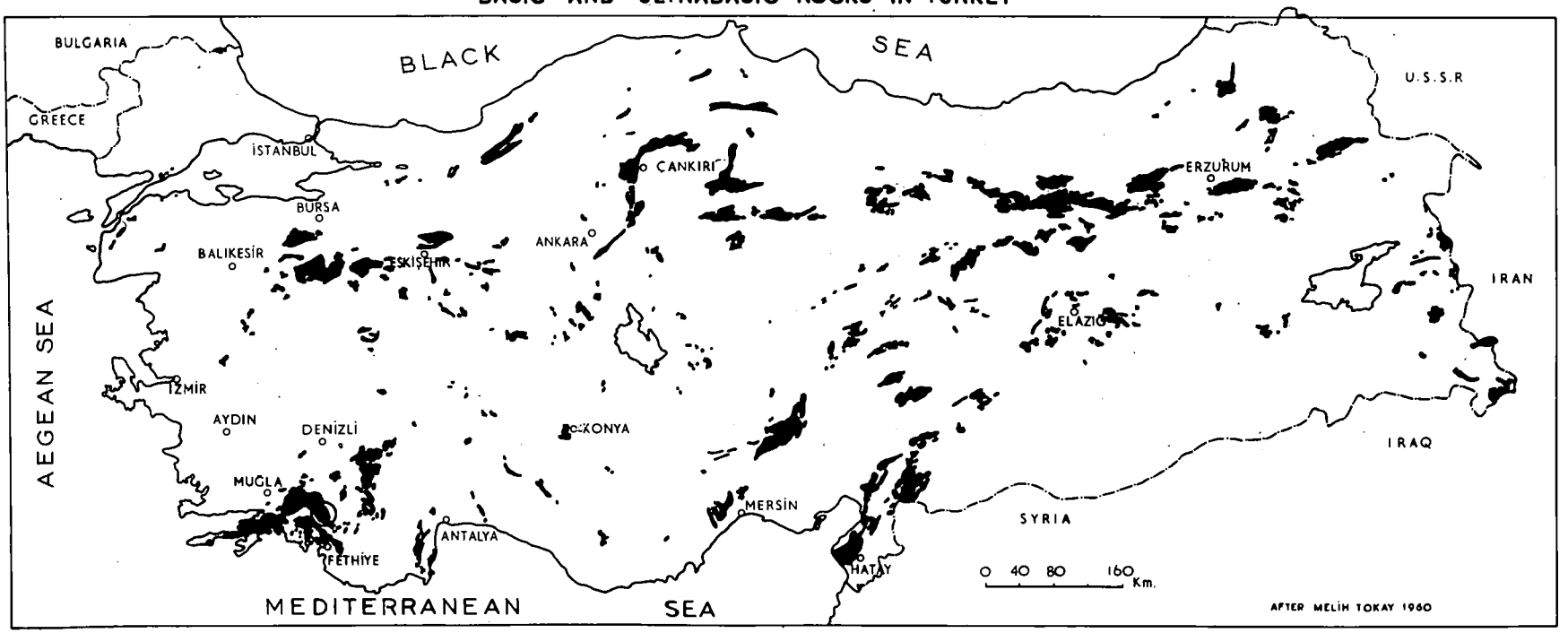

○ Andızlık–Zımparalık area

FIG. 1

Because of the mountainous character, the accessability of the district as a whole is poor, and comprised only of unsurfaced highways, the nearest railway line passes about 150 km to the north; it is connected to Aydin. The road conditions have improved in recent years due to the increased production of chrome ore and to an increase in tourist activity. The chrome ores are transported by road to the coastal village of Göcek and stored or shipped from there. The distance between the mines and the storage station is about 40-60 km but the loaded transport takes at least 4-5 hours for the journey.

The history of chrome ore discovery and mining in Turkey, goes back to 1848, the first discoveries being in the Bursa-Harmancik area south of the Marmara sea. In the Fethiye district chrome ore mining started in 1887, with exploitation by private companies, while from 1916 until 1945 the chrome ore mining rights of the area were State controlled. In 1945 M.T.A. (Mineral research and exploration institute) of Turkey undertook chrome ore prospecting in the area and in 1957 the mining rights were given to the self supporting State mining company "Etibank". Since then, despite poor world chrome ore markets, Etibank has made remarkable progress in the district. At present they are producing 200 tons of metallurgical grade ore daily from the Andizlik and Zimparalik mines, the other relatively small mines contributing an additional 40-50 tons.

GENERAL GEOLOGY OF SW TURKEY

FIG.2

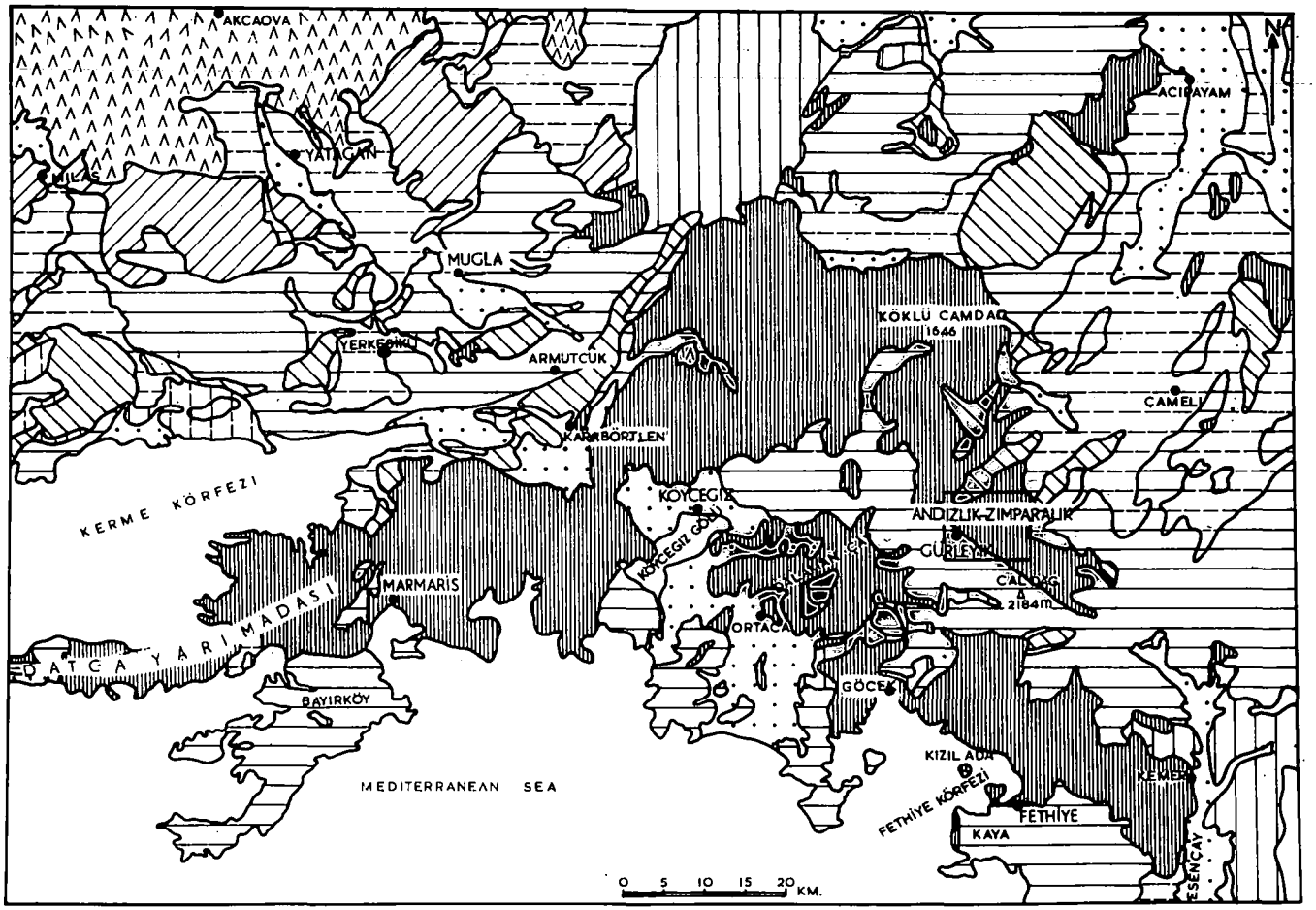

AFTER H.N.PAMİR 1964

- QUATERNARY
- PLIOCENE
- EOCENE-OLIGOCENE
- MESOZOIC–TERTIARY
- TRIASSIC
- PERMIAN–MESOZOIC
- PALEOZOIC
- GNEISS MICASCHIST AMPHIBOLITE
- PERIDOTITE

Geological Setting

The Andizlik-Zimparalik peridotite lies at the eastern end of a large peridotite mass extending from the Datça peninsula on the Mediterranean coast. The peridotite has been divided into two units, north and south, fig.2. The northern unit starts from the Datça Peninsula and covers over 2100 km^2 running in a southwest-northeast direction for 125 km from the coast and then taking a southeast direction. The southern unit, situated to the north of Fethiye and southeast of Köycegiz, is about 70 km long and 15 km wide with a northwest-southeast trend. The two groups of peridotites have been interpreted as the continuation of the peridotites of the Balkans, Greece, Crete and Cyprus. Wijkerslooth (1942) placed all the peridotites in the south of Turkey into the same group which he termed "the Southern Peridotite Belt", fig.3. This belt is about 1500 km long, 250 km wide and extends into Iran in the east. The peridotite is uniform in appearance throughout this southern peridotite belt but the ages ascribed to various localities range from early Palaeozoic to Eocene. Such variation suggests that it would probably be wiser to alter the original term into "the Southern Peridotite Belts". Hiessleitner (1954) places the peridotites of the Balkans and Greece in the early Palaeozoic and relates them to the peridotites of southern Turkey in general. Borchert (1958) however, suggests that they are Mesozoic, mainly Upper Jurassic, and correlates them with the southern peridotite unit. Borchert (1958) further correlates the Upper Cretaceous-Eocene peridotites of southwest Greece, Crete and Cyprus with those of Mersin-Iskenderun and the eastern Anatolian chromite

province. These two groups of peridotites are separated by Mesozoic rocks in the east, but the two units get closer to each other in the west, south of Köycegiz they are separated only by a zone of disturbance on which Köycegiz lake is situated.

The peridotites are mainly harzburgites. Serpentinisation is particularly common along the disturbance zones. Dunite and lherzolite are the less common rock types, while pyroxenite veins and basic dykes are of subsidiary importance. Van der Kaaden (1960) says "Pyroxenite veins, basic dykes and lherzolites are more common in the northern unit, the southern unit being richer in chromite deposits". He also suggests that the two peridotite units were emplaced during the early Palaeozoic, their present disposition and tectonic setting being due to alpine movements.

The Southern Peridotite Unit

This unit is elongated in a northwest-southeast direction and is approximately 70 km long and 15 km wide. To the northwest this peridotite is separated from the northern unit by a zone of disturbance. To the southeast the peridotite can be followed to the Esen Çay valley where it is cut off by a north-south fault trending along the valley, (Colin, 1962). The peridotites are mainly slightly serpentinised harzburgite, pyroxenites and dunites are less common rock types. Later basic dykes are common, they are mainly norite, olivine gabbro, diorite and quartz diorite. In some localities p 46-47 Colin (1962) has reported that peridotites grade into gabbroic rocks as the result

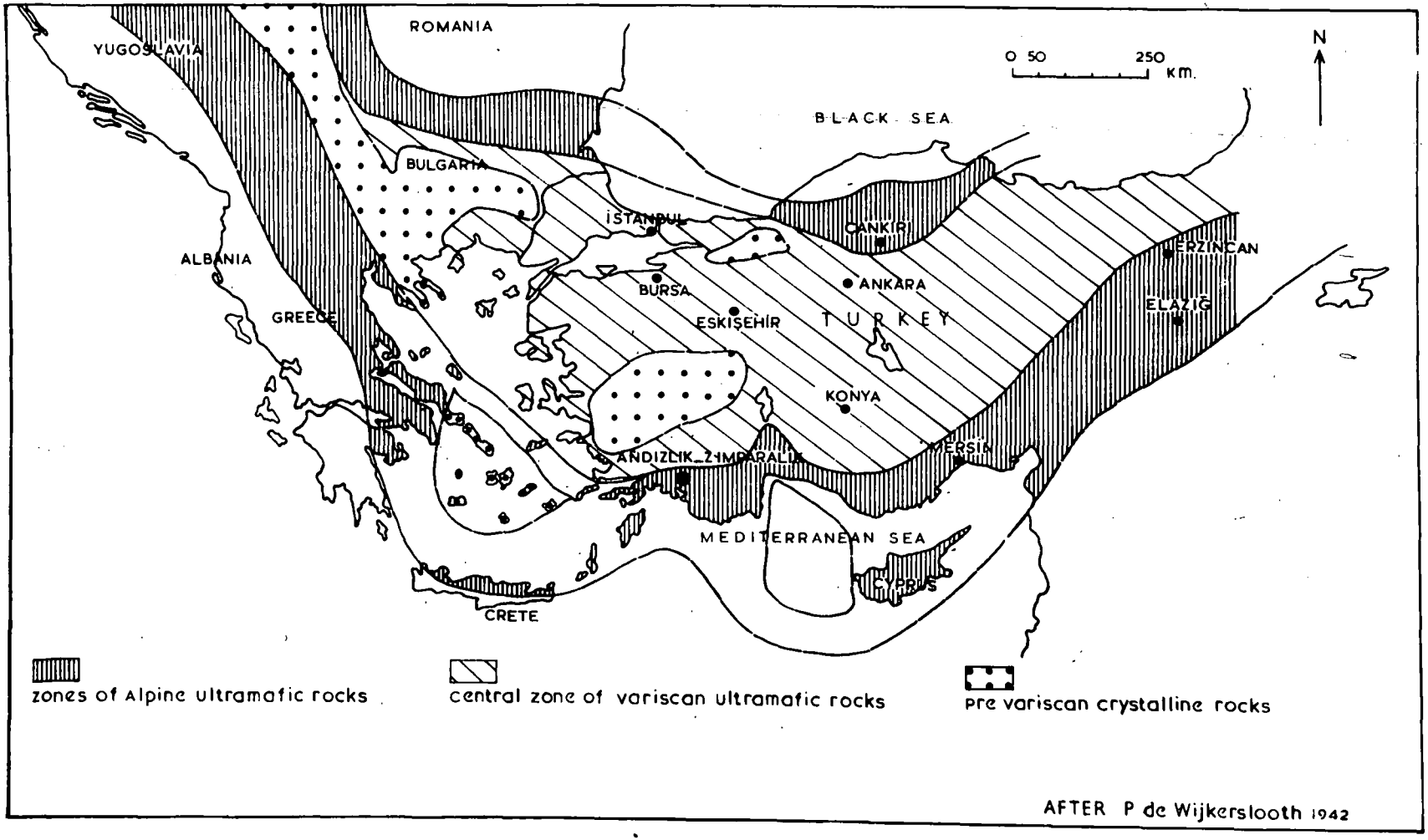

CORRELATION OF THE ULTRAMAFIC ROCKS OF THE BALKANS AND TURKEY

FIG.3

of normal differentiation processes. Both northern and southern contacts of the peridotite are tectonic, the peridotite being faulted against the surrounding sedimentary rocks.

Palaeozoic rocks are not common in the immediate vicinity of the peridotite. To the north of the peridotite Palaeozoic reddish grey, fossiliferous limestones are interbedded with quartzites, the fauna indicates a Carboniferous to Permian age. These Palaeozoic rocks lie beneath a succession which comprises spilitic tuffs on which rest red-green cherts followed by dark grey sandy limestones which are lithologically similar to those further north, though unfossiliferous to date. At other localities the spilites are interbedded with Cretaceous limestones. Occasionally the peridotites are in fault contact with basic effusives of Cretaceous age. At the southern end of the peridotite, Upper Jurassic to Lower Cretaceous limestones have been located in a very restricted area with indications that they underlie the peridotite. In Kizil ada (red island) lithologically similar limestones clearly do underlie the peridotite, (Colin 1962).

Eocene formations are widespread to the east and southeast of the peridotite but do not occur in the immediate vicinity. They are represented by conglomeratic limestones, partly silicified grey limestones, and also by flysch facies. The limestones are Upper Eocene and the flysch is younger than the Lutetian. In the Kaya Peninsula conglomerates and partly silicified grey limestones lie discomformably on the Senomanian limestones. The Eocene flysch formations are light brown, sandy, thin bedded, narrowly folded limestones

and marls. They include fragments of peridotite, (Van der Kaaden, 1959). Oligocene and Miocene rocks are represented by dark limey sandstones, marls, limestones and limestone conglomerates, they rest on the peridotite and other older formations.

Pliocene deposits are represented by basic rock and peridotite pebble conglomerates and pinkish white marls which include some lignite. They cover very large areas to the north and east but are also seen to the south of the peridotite along the Esen Çay valley.

In the east around Elmali are marine marls and bituminous shales of suspected Neogene age, they overlie Upper Cretaceous formations.

Chromite Deposits

According to Van der Kaaden (1960) the southern peridotite is richer in chromite deposits than the northern unit; this area was the most productive in Turkey prior to the development of the eastern Anatolian (Guleman-Elazig) province. The ore is, in general, massive or nodular with chromite pods mainly aligned north-south or northeast - southwest. Most of the ores are of metallurgical grade with Cr/Fe ratios between 3.52 and 3.54. Some of the deposits have been followed to depths of 130 m for example at Cenger and Sandalbaşi. In places the chromite pods have been cut by dolerite dykes, cracks in the chromite being filled with kammererite and smaragdite veins. Chrome hornblende, with serpentine, is quite common in association with nodular chromite.

The Northern Peridotite Unit

In the west this unit is elongated in a southwest-northeast direction then trends northwest-southeast; it covers more than 2100 km^2. The main rock type is again harzburgite with subsidiary dunite and lherzolite. Basic dykes and pyroxenite veins are very common. Serpentinisation is well advanced particularly along tectonically disturbed zones. The southern contact of this peridotite is marked by a thrust on which peridotite overides the Palaeozoic and Mesozoic formations. These formations include the continuation of the Cretaceous limestones seen to the north of the southern unit. Along the southern contact, near Gürleyik köy, Eocene limestones and Miocene flysch formations are known. They envelope tectonically emplaced mountains of Palaeozoic and Mesozoic limestone. Along this zone of disturbance, as in the north, amphibolite and quartzite lenses are common, particularly in the southwest. They are believed to have been introduced with the peridotite during tectonic emplacement.

In the north, peridotite is again separated from the surrounding units by a zone of disturbance characterized by dislodged material including radiolarian cherts, crystalline schists, amphibolites, breccias, Mesozoic and Eocene limestones and peridotite blocks. A phyllitic schist zone of Devonian age occurs along the northern contact, it consists of quartzites and muscovite and chloritoid schists.

Ula and Mugla marbles, including emery deposits, cover a large area to the north of the peridotite. They are sub-horizontal

and in some localities are interbedded with "Karabörtlen schists". Overlying the marbles are well stratified, unmetamorphosed, fossiliferous, Upper Cretaceous limestones. Further north are crystalline rocks which are mainly amphibolites, amphibole schists, quartzites and gneisses. The main constituents of these rocks are green amphibole, albite, oligoclase, quartzite, clinoziosite, epidote, chlorite and muscovite. These crystalline rocks are isolated from the main Menderes crystalline schist massif, but are very similar. They occasionally form a foot-wall to the peridotite when a tremolite schist zone is often developed, with a regular transition from the peridotite to the tremolite. Van der Kaaden (1960) suggests that this tremolite schist zone may be the result of Mg metasomatism by the peridotite intrusion.

In some localities the crystalline schists underlie the peridotite, also in parts the peridotites are seen beneath the Middle Cretaceous, with a normal contact, Van der Kaaden (1960). In the southwest the Mesozoic to Tertiary rocks range from Triassic to Eocene. They comprise both massive and thin bedded limestones with intercalations of radiolarian cherts; reef formations are known in the Trias and Upper Cretaceous. Reef, nummulitic and flysch facies also occur in the Eocene. Spilitic rocks again occur with the middle Cretaceous limestones, but they are not as common here as was apparent in association with the southern peridotite unit.

Alpine orogenesis resulted in the development of overthrusts

and thrust faults in the region. In the southwest nappes are indicated by Eocene underlying older Mesozoic rocks to the northeast of Köycegiz. To the southwest of Marmaris, in Bayirköy, Eocene and Cretaceous flysch is suspected underlying Triassic limestones.

Chromite Deposits

Van der Kaaden (1960) reports that the northern unit is not so rich in chromite deposits as the southern unit, chromite deposits do however occur throughout. The general directions of the chromites are north-south and east-west, dipping to the north and east. Disseminated, massive and nodular ores are common, the grade ranging from refractory to metallurgical. Because of the complex tectonic history of the region many of the chromites have lost their genetic ties. It is quite common to find different types, or different grades, of ore at the same locality.

Occasionally the chromites have normal magmatic contacts with the surrounding peridotites, but commonly the contacts between the chromites and the peridotites are very sharp and faulted.

Hiessleitner (1951-1952) and Van der Kaaden and Metz (1954) have attempted a stratigraphic correlation of the chromites within the peridotite by considering their Al_2O_3/MgO and FeO/MgO ratios, on this basis they have subdivided the body into several units. Despite the complicated tectonic history of the region a broad measure of success was achieved by this subdivision.

Previous work in southwest Turkey.

The first geological reconnaissance of southwest Turkey was made by Tchihatcheff (1886), while from 1910 to 1915 Philipson made several visits to the area (Philipson, 1910-1915), Van der Kaaden (1953) has mapped the Andizlik-Zimparalik area on the scale of 1:25000 and attempted to establish a genetic and tectonic control of the chromite ore bodies; this work led to the development of chrome ore mining in the area. Van der Kaaden and Muller (1953) studied the chemical variations of the chromite from different parts of the northern and southern peridotite units and correlated the chromites with those of the Balkans. Van der Kaaden and Metz (1954), mapping on a regional scale, have examined the regional setting of the district, covering the area from the Datça peninsula in the west to east of the Dalaman Çay. Hiessleitner (1954) has published a brief account of the Andizlik-Zimparalik area, while Altinli (1955) has described the area extending from south of Denizli to north of Gurleyik koy. Van der Kaaden (1959) has described field and chemical investigations of the chromites in the northern and southern units, drawing attention to chromite compositional changes in various parts of the peridotites. Again Van der Kaaden (1960) published an account describing the geological-tectonic setting of the northern and southern peridotite units. Borchert (1961) visited the chromite occurrences and attempted to establish the structural control of the chromites through a record of very minor structural details in and around

the ore bodies. Colin (1962) has described the Fethiye-Antalya, Kas Kinike region of southwest Turkey, with particular emphasis on the sedimentary environment of the peridotites. P. de Graciansky has mapped the sedimentary units surrounding the peridotites and published an account describing some of the major tectonic features, (P. de Graciansky, 1967).

Objects of research

The Andizlik-Zimparalik peridotite is an economic source of chrome ore, it is situated at the eastern end of an extensive alpine peridotite body. The main subject of this study was thus an evaluation of the geology and geochemistry of the host rock peridotite and associated chrome ores.

Field relations of the different units, and their structural control, were an obvious prerequisite to the chemical and petrological work, they were achieved by constructing a 1:25000 scale geological map covering about 50 km^2, 1:1000 scale maps of the Andizlik-Zimparalik mine areas, each covering 1 km^2 and 1:500 scale subsurface geological maps of these mines.

Petrological and mineralogical studies were conducted to evaluate the rock types and their mineralogical composition. Mineralogical compositional variation was studied by electron microprobe and X-ray diffraction analyses of olivines and X-ray diffraction analyses of pyroxenes and serpentine minerals.

Attempts have been made to evaluate compositional changes within the peridotite and to investigate whether such changes

conform to a recognisable pattern. The degree of serpentinisation and the process of serpentinisation have also been investigated.

The chemical composition of intrusive basic dykes and numerous pyroxenite veins in the peridotite have been examined in an attempt to assess their relationship to the main ultramafic mass.

The chrome ores have been analysed to investigate any chemical changes dependent on their location within the peridotite or significant differences between the physically recognisable types of ore.

The common occurrence of tremolite veins in the chrome ore bodies, has been investigated and their composition viewed with respect to the possible effects of hydrothermal solutions on the chrome ore bodies. Variation in composition within single chromite grains have been studied in this context.

Finally attempts have been made to evaluate the genetic history of the peridotite and associated chrome ore bodies in the light of the field and experimental studies, the area has been compared with others of similar nature and similar probable mode of origin.

CHAPTER 2

FIELD RELATIONS AND STRUCTURE

The Andizlik-Zimparalik area is shown in fig.2., it lies at the southeastern end of the northern peridotite unit which extends from the Datca peninsula in the west, and is joined to this northern unit at the Dalaman Cay.

Marginal thrust zones

The peridotite is bounded by thrusts both to the south and the north. The southern thrust zone is very sharp, Plates 1,2,3, and in places follows the northern bank of the Cal dere (stream) with a northwest-southeast trend. This thrust zone can be followed towards the southeast for 30 km to the Esen Cay valley where it is terminated by a north-south trending fault along the valley, (Colin 1962). To the northwest the southern thrust zone extends round Dikmen tepe and passes to the southern bank of the Dalaman Cay where the contact makes a west facing "V"; the zone leaves the Dalaman Cay with a northwest trend. This thrust zone is very sharp and always dips towards the peridotite with an angle varying from 27° to 53°. Hanging wall breccias in the peridotite occur all along the contact. Slickensides on the limestones at the contact have measurements which indicate movement in the northwest-southeast direction (056/29; 17° right, 016/53; 10° right). No metamorphic effects are visible at this southern contact.

The northern contact is irregular in trend, and often ill-defined. The peridotite, with a smooth topography, contrasts markedly with

Plate 1 Southern thrust zone to the south of Incebel tepe (looking north).

Plate 2 Eastern continuation of the southern thrust zone. The localities of the Andizlik and Zimparalik mines are marked in the background. The locality marked in the thrust zone is shown in plate 5 (looking north-east).

the surrounding limestones characterized by scarp topography and a development of canyons. The northern contact partly follows the southern bank of the Dalaman Cay from where it extends to the north of Ulas dere for about 2 km with a north-south trend. The contact then runs east-west for 3 km flanking Buyuk and Kucuk Hisar tepes (hills). From this point the contact again takes the north-south direction to Gozyeri tepe, west of Damdir koy. The contact again turns east-west and leaves the area to the north of Madenoyugu tepe with a northeast trend. The contact dips towards the peridotite with an angle varying from 28° to 44°; breccias are again prominent along the contact.

A tongue of small peridotite extends beyond the general southern thrust zone at Kizlansenir sirti fig.4 (see volume 2). The relations with the main peridotite are not clear, Cal dere (stream) occupying ground between the two units. The contacts of this small unit are marked with breccias, they are sharp along the eastern and western sides of the tongue but are obscured by debris to the north and south. It seems reasonable to interpret these two peridotite units as part of the same body with the same tectonic history.

Plate 4 shows the Uckopru mine in the foreground and the peridotite tongue, extending towards the south in the background.

Sedimentary rocks

The oldest known units in the surrounding sediments are fossiliferous Permo-Carboniferous shales, quartzites, sandstones

Plate 3 Southern thrust zone (looking west).

Plate 4 Uckopru mine. A peridotite tongue extending southwards beyond the southern thrust zone can be seen in the background.

and limestones. These rocks are mainly in fault contact with other sediments and have no direct contact with the peridotite. They occur at three isolated localities, to the west of Kalabak tepe, and to the east and southeast of Kizlansenir sirti, fig.4 (see volume 2). Permian limestones are widespread, though invariably highly fractured. They are in contact with the peridotite in the northwest. Despite their disturbed nature the Permian limestones dip towards the peridotite along the contact.

The Upper Permian is represented by arkoses; their upper surface is taken as the boundary to the overlying Trias.

Triassic rocks are mainly dolomitic limestones and quartzites and are of limited extent in the vicinity of the peridotite.

Brecciated Upper Jurassic and Lower Cretaceous silicified limestones are common along the contact with the peridotite. Bedding is evident at some localities, dipping towards the peridotite. In places these limestones rest unconformably on Permian limestones but they have normal contact relations with the Triassic dolomitic limestones.

Upper Cretaceous limestones are very restricted, outcropping mainly in the southeastern part of the area; they include silicified limestone bands. Eocene, in this part, is represented by the Nummulitic limestones. Miocene is represented by limestones and flysch formations; together they form the largest sedimentary

unit. They are composed of arenaceous and argillaceous limestones and include peridotite fragments and blocks of Carboniferous and Cretaceous limestone. They are thinly bedded, very narrowly folded, and have fault contacts with the surrounding rocks.

Sedimentary rocks to the north of the peridotite have not been mapped in detail. The peridotite has faulted contact with Palaeozoic and Mesozoic limestones. Flysch formations similar to those occurring south of the peridotite surround these limestones. Apparently unfossiliferous sedimentary rocks, lithologically similar to many of the above units, are enclosed within the peridotite near both northern and southern contacts. Identification of some of these included blocks as Upper Jurassic to Lower Cretaceous limestones, (P. de Graciansky, personal communication) suggests that the peridotite was emplaced subsequently, during the Laramian phase of the alpine orogenic movements (Ketin, 1966). Upper Pliocene and Quarternary conglomerates and marls overlie the peridotite in the east and northeast, Plate 5. They extend away from the area to the north, and may be followed to Denizli. In the west near Kertebel tepe, isolated conglomerates also rest on the peridotite. These deposits have a northwest-southeast strike and dip at 10° to 20° towards the northeast. The conglomerates are dark red in colour and include pebbles of peridotite, dolerite and gabbro. The size of the pebbles varies from a few mm up to a several centimetres. Overlying the conglomerates are white or pinkish-white marls. The boundary between the conglomerates and

the marls is gradational and marls are also sometimes interbedded with the conglomerates. In places the marls contain small lignite deposits.

Ultramafic and Basic rocks

Away from the contact zone the main rock type is harzburgite, composed of forsteritic olivine, orthopyroxene, serpentine minerals and accessory clinopyroxene, chromite, magnetite and pyrite. Other varieties such as dunite and lherzolite, are not easily distinguished in the field.

The peridotites are serpentinised and are also weathered to a reddish appearance. Serpentinisation and brecciation are particularly noticeable along fault zones and at the contacts. The breccias are formed of angular fragments which include basic rocks, peridotite and sometimes chromite. The grain size of the fragments varies from about 0.5 cm up to 20 cm in diameter. The cementing material is serpentinised peridotite. Magnesite also occurs in the eastern part of the area particularly around the Upper Pliocene to Quaternary conglomerates.

Pyroxenites occur as veins cutting the peridotite, they have a thickness which varies from a few cm up to 30 to 40 cm and can seldom be followed for more than 1-3 metres on the surface. The veins are resistant to weathering and ~~are~~ stand out in outcrop, Plate 6. The constituent minerals are mainly the orthopyroxene, enstatite with accessory clinopyroxene, amphibole and chromite.

According to Bowen and Tuttle (1949) water vapour, saturated

Plate 5 Pliocene-Quaternary conglomerates and marls resting on the peridotite, situated in the northeast of the area.

Plate 6 An orthopyroxenite vein cutting across harzburgite.

with SiO_2, streaming through cracks in the peridotite at temperatures above 650°C could convert the wallrock to pyroxenite. The pyroxenite veins are too small to be included on the 1:25000 scale map, fig.4 (see volume 2), but are plotted in detail on the 1:1000 scale geological map of the Andizlik and Zimparalik mines, figs. 5A, 6A (see volume 2). The general strike and dip direction of the veins is parallel to other structural features such as faults and joints. They occur throughout the area, but are particularly common around Andizlik and Zimparalik, as described below.

Basic dykes are common forming about 9 percent of the peridotite area, characterised by a rugged appearance, they stand out from the more easily weathered peridotite. Contacts to peridotite are usually sharp and marked by cooked, serpentinised, brecciated or sheared peridotite, Plate 7. The dykes vary from 50 cm to 250 m in thickness and they can be followed for distances of up to 2 km in the strike direction. The main constituents are clinopyroxene, plagioclase feldspar and skeletal ilmenite. Their texture and plagioclase composition indicates that many are diorites; dolerite dykes also occur. The dykes exhibit no compositional layering.

The dykes are limited to the peridotite body, only in one locality (Van der Kaaden, 1959) does a basic dyke transgress to the surrounding sediments, this is on the western continuation of the peridotite, near Datça.

The dykes are heavily concentrated in the south and north of

Plate 7 A contact between a basic dyke and peridotite which is brecciated and serpentinised.

Plate 8 A zeolite vein cutting a basic dyke.

the field, and in many localities they follow the contact of the peridotite with the surrounding rocks. Around Üçköprü, in the south, and Damdir, in the north, small dykes are numerous and of complicated pattern; they cause difficulty with underground mining, particularly at Damdir. The general strike direction of the dykes, despite small variations, is parallel to the southern and northern thrust zones with northwest-southeast orientation dominant. Towards the west, near Kertebel tepe the strike direction turns to north northwest parallel to the contact in this area, fig.4 (see volume 2). The dykes dip to the southwest or to the northeast, to the northeast the dip is about 38° but this direction changes to the southwest south of Kilcan dere, fig.7. The southwesterly dip of the dykes is maintained up to the southern thrust zone where the dip direction again changes to the northeast. The data from the southern contact area is not as conclusive as that from the north.

Measurements on the dykes have been plotted on an equal area stereogram (Schmidt net) as poles normal to the plane of orientation, produced into the lower hemisphere, fig.8B shows that 14 and 10 percent centers represent the dykes oriented in the northwest-southeast direction, dipping southwest. A 4 percent concentration represents the dykes to the north of Kilcan dere, oriented to the northwest-southeast, but dipping northeast, and a 2 percent concentration relates to dykes along the southern contact again oriented to the northwest-southeast and dipping northeast.

Near the southern contact, in particular, the basic dykes

ORIENTATION OF BASIC DYKES IN THE ANDIZLIK_ZIMPARALIK AREA FIG.7

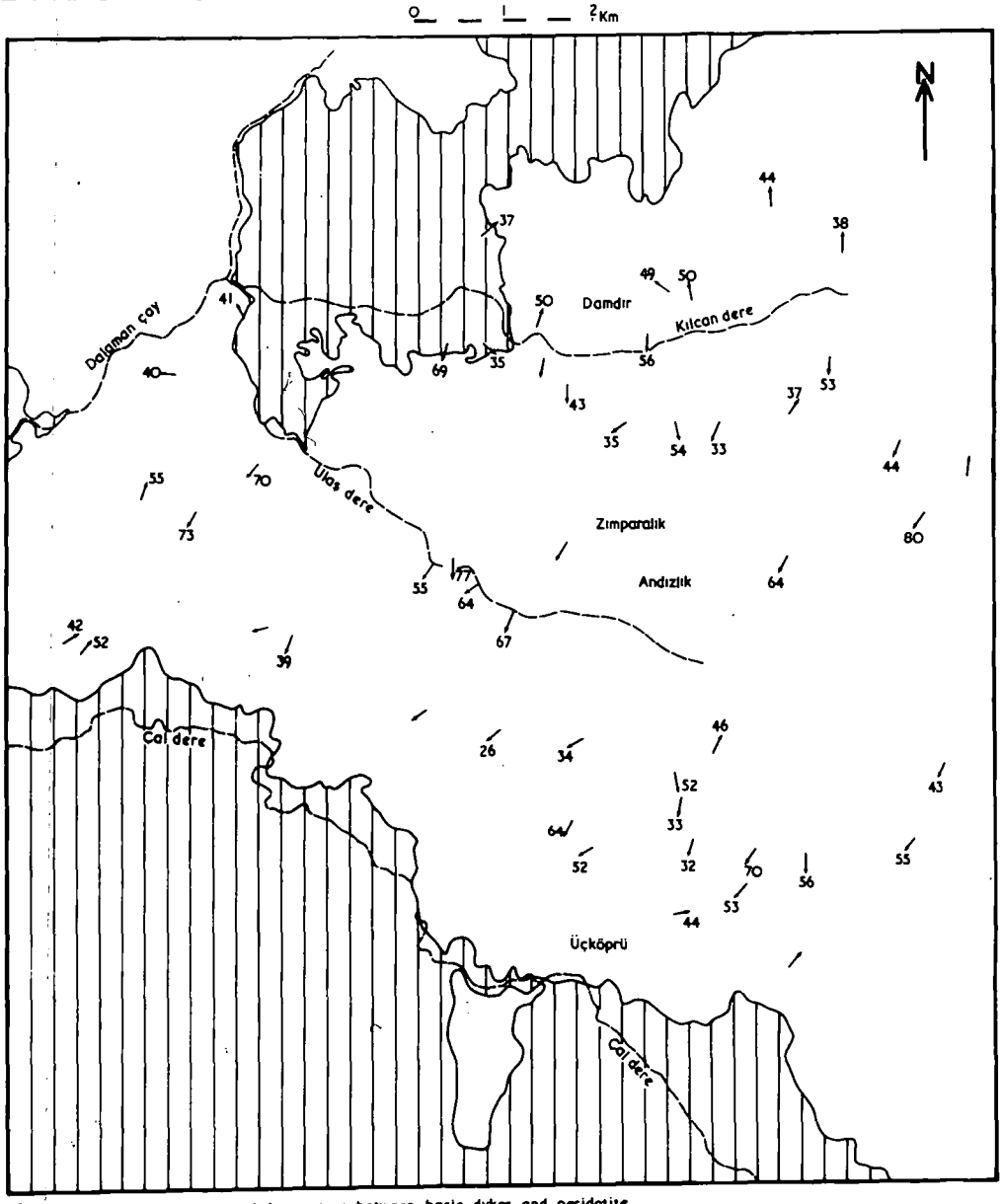

32 Dip direction and angle of the contact between basic dykes and peridotite

are cut by veins 4 to 5 cm thick, carrying a fibrous zeolite, Plate 8. Basic dykes cut chromite pods at Damdir, Karakaya and Dagdibi tepe they have a thin chilled margins against the chromite, Plate 9; the texture is porphyritic. The association of basic dykes with peridotite is common in many alpine complexes; the dykes are almost invariably limited to the mafic plutons. Their origin may be ascribed to movement of interstitial residual magma into fractures (low pressure areas) after consolidation of the peridotite.

Chromite deposits

Chromite, ubiquitous as an accessory mineral in the peridotite, is also concentrated into economically viable deposits at a number of localities. At present only three mine groups are operating, Uckopru mine in the south, Damdir mine in the north and the Andizlik and Zimparalik mines in the central part of the area. Other occurrences of economic importance include the Kuru dere - Karakaya, Sarikaya, Bagdibi, Harmancik, Dikmen, Kesmelik, Yassitepe, Tavuktarlasi and Madenoyugu occurrences. Individual chrome ore occurrences, together with the active mine groups have been plotted on fig.4 (see volume 2).

The chromite deposits are of podiform type, the ore grading from disseminated through nodular to massive varieties. The matrix of the chromite is serpentine, serpentinised harzburgite-dunite or, in some cases, tremolite and chlorite. The chromite

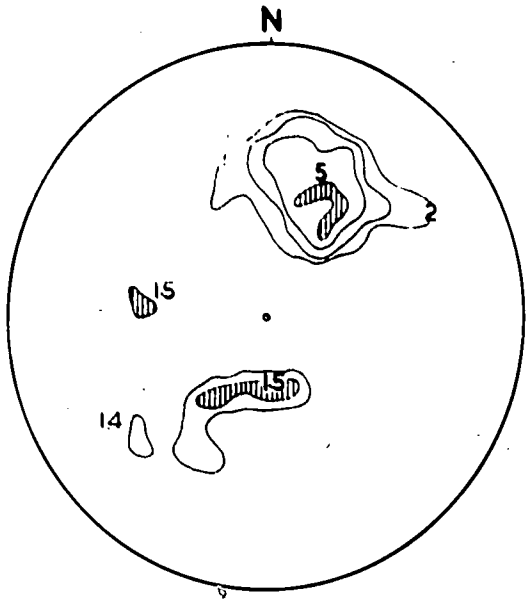

A

656 Joint planes

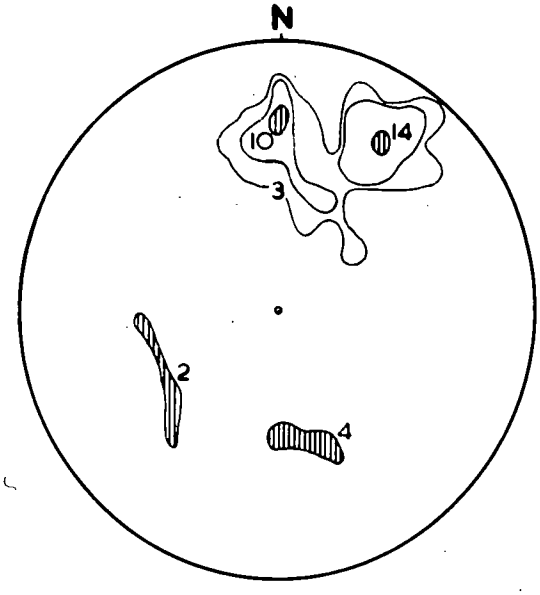

B

51 Basic dyke boundary planes

Fig 8

bodies, though in places shapeless, are, in general, in the form of elongated, lenticular pods. The size of the individual pods varies from 1 to 2 m up to 50 m in length and the thickest part from 0.50 m to 7 - 8 m. The lenticular form of the bodies is not well represented in the outcrops although a fine example is seen in the Tavuk tarlâsi outcrop. The shape of some of the chromite bodies as seen in the gallery walls are shown in fig.9.

Boundaries between chromite and the surrounding rocks are mostly very sharp, Plate 10, and comprise a 10 to 20 cm thick serpentine zone with slickensides indicating differential movement. In the Üçköprü and Sarikaya areas the contact between the chromite and the enclosing dunite or harzburgite is sharp and primary in some cases, and in others gradational. Primary magmatic contact relations are, however, of very restricted occurrence. Both massive and disseminated chrome ore are often seen together but separated where the boundary is clear by a zone of mechanical disruption.

Stratiform or banded chromites occur in very limited amount. They form 3 to 4 mm thick bands of anhedral to euhedral chromite grains, Plate 14. They cannot be followed for more than about 50 cm in the strike direction. Localities F19 and F68, fig.10, are of stratiform type.

Nodular chromite in a serpentine matrix, is widespread. The nodules vary in size from a few mm to 2-3 cm in length and

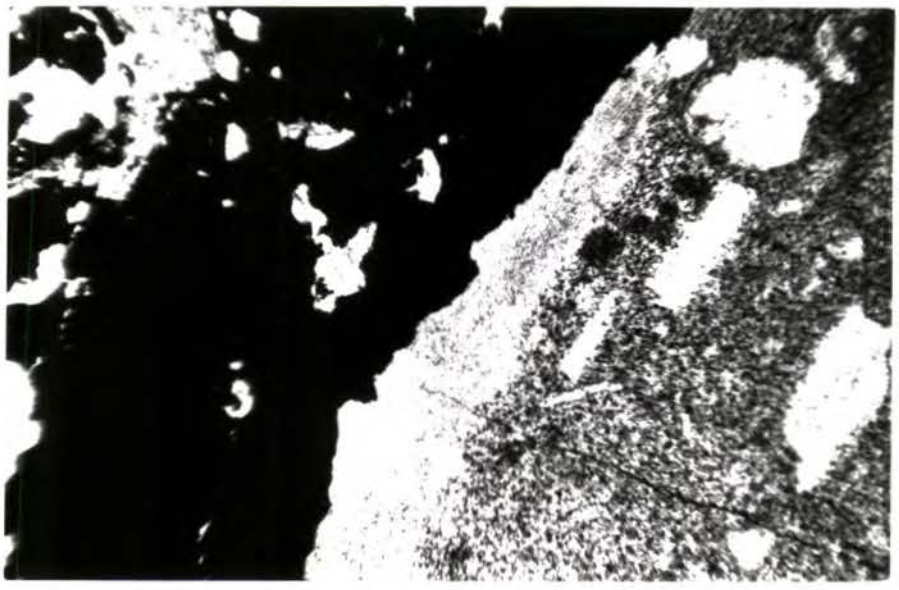

Plate 9 The chilled margin of a porphyritic basic dyke in contact with chromite (crossed polars, X20).

Plate 10 Chromite-peridotite contact.

up to 1 cm in diameter at the thickest part, Plate 11. The nodules are a miniture counterpart of the chromite pods and are elongated in some circumstances in a regular manner. This elongation of the nodules (lineation) resembles the lineation apparent in many metamorphic rocks and is believed to have formed during their emplacement with the host peridotite.

The origin of nodular chromite is controversial. A widely held theory suggests that early chromite crystallizing in the upper parts of a magma chamber sinks and rolls down banks of silicate, increasing heat during the descent causing corrosion and resulting in formation of nodular chromite. This theory does not explain why nodular chromite is only related to alpine peridotites. Clearly the tectonic history must have a role in the formation of nodular chromite and should account for their similarity to metamorphic textures. The nodules are generally composed of imperfectly formed crystals, or of crystals that have suffered resorption. Thayer (1943) suggests that the minor features of nodular chromite indicate that abrøasion is not responsible for their form. Chromite may have separated from the peridotite magma as globules which settled on the floor of the magma chamber. Coalescence and flattening of the nodules suggest plastic deformation at an early stage in their history. Remnants of nodules are known in disseminated ore some of which may have been formed by disintegration of nodules and mixing with

The position of some of the chromite bodies as they are seen on the gallery walls

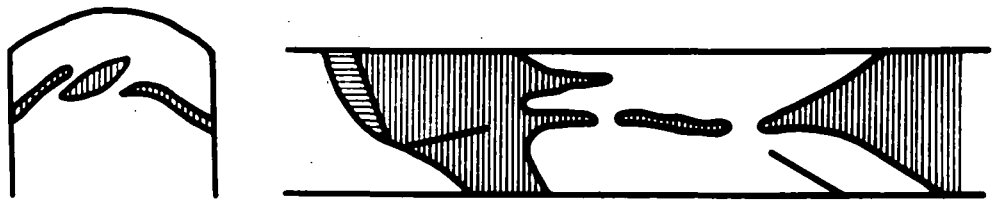

ZIMPARALIK 1205m LEVEL AT ZU40

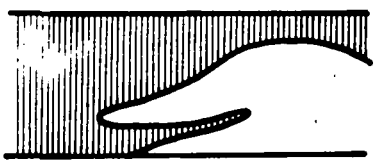

ZIMPARALIK 121537m LEVEL AT ZU46

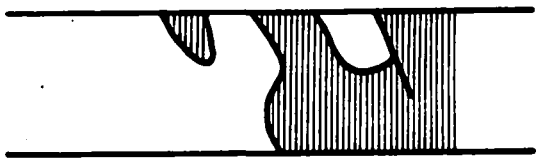

ZIMPARALIK 1240m LEVEL AT ZU6

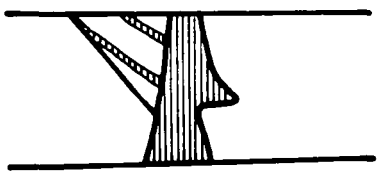

ANDIZLIK, 147554m LEVEL AT AU21

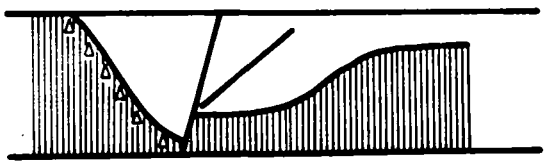

ANDIZLIK 147438m LEVEL AT AU13

PERIDOTITE

MASSIVE CHROMITE

DISSEMINATED CHROMITE

FAULTS

BRECCIAS

STRATIFOM CHROMITES

0 1 2 m

FIG.9

peridotite by differential flow. Bowen (1928) has pointed out that the unmixing of liquids takes place by the formation of globules. In discussing the possible mechanism for the formation of nodular chromites Bilgrami (1964) says that the possibility of liquid immiscibility in chromite rich melts should be considered. Bearing Bowen's findings in mind Bilgrami says if these globules were generated from the unmixing of the liquids which existed in the natural magmas and were preserved, they may explain the formation of nodular chromites.

Tremolite veins, mainly visible underground, cut the chromite pods. These veins are light to dark green in colour, of irregular pattern, filling fractures from a few mm to 20 cm in thickness. The tremolite veins cannot usually be followed for more than 50 cm before they branch in an irregular manner. Occasionally veins of 5 to 10 cm thickness can be traced for 2-3 m, A17, fig.5A (see Volume 2).

The orientation of the chromite pods is regular, mainly either northwest-southeast or northeast-southwest. This is clearly demonstrated in the Zimparalik mine area, fig.6A.(see Volume 2). Numerous chromite deposits occur along the southern contact from Dikmen in the west to Karakaya in the east.

The chromite deposits around Dikmen are mainly massive though nodular varieties are also present. Late tremolite veins are common. South of Incebel tepe, chromite occurs in weathered peridotite, it is mainly of nodular type. At Dagdibi tepe the chromite is cut by basic dykes, though of massive type, the

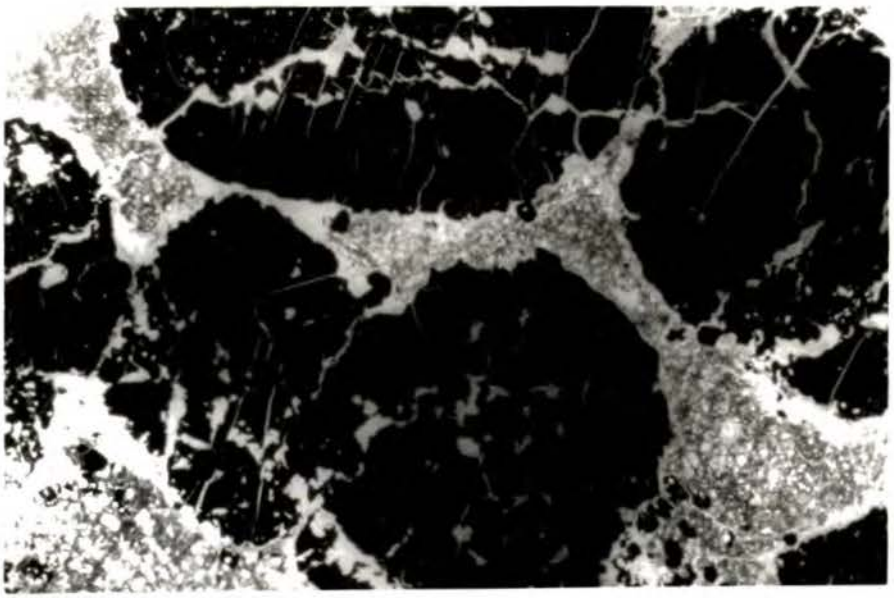

Plate 11 Nodular chromite (X6).

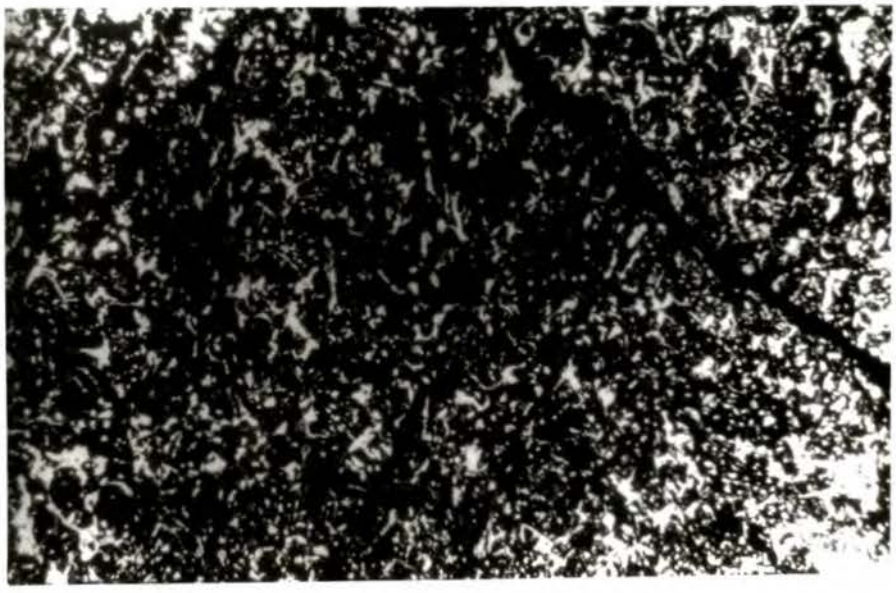

Plate 12 Massive chromite (X6).

deposit is very limited in extent. Nodular chromite occurs at Bagdibi, the cementing material is weathered, serpentinised harzburgite. Massive, though brecciated, chromite also occurs. At Kumocak the ore is sand like in appearance.

Üçköprü is the oldest known working chromite deposit in the area, with outcrops covering a large area. The ore is mainly massive but other types are also known, contact relations with the host peridotite are sharp and mechanical, though occasionally relics of primary magmatic contacts are seen. Chromite pods are oriented north 10° to 20° east and dip westwards at about 60°. Tremolite, filling fractures in the chromite, is common. Several chromite outcrops also occur at Karadünek, some are cut by basic dykes. The Sarikaya deposits in the southeast are of disseminated type, cemented by serpentinised harzburgite, the ore is of refractory grade. Massive disseminated and nodular types of chromite occur at Karakaya and Kurudere, north of Sarikaya tepe. The ore is cut by basic dykes and irregular, 3-4 cm thick, serpentine bands in the ore are abundant. Disseminated chromite outcrops occur at Kizlan mahallesi (fig.4. (F218), in highly weathered peridotite; the ore is cemented by serpentinised harzburgite.

The Yassitepe deposits are mainly nodular but grade into both massive and disseminated types. Outcrops covering a large area comprise the Kesmelik deposits north of Incebel tepe. The ore is mainly of disseminated type although other types are known

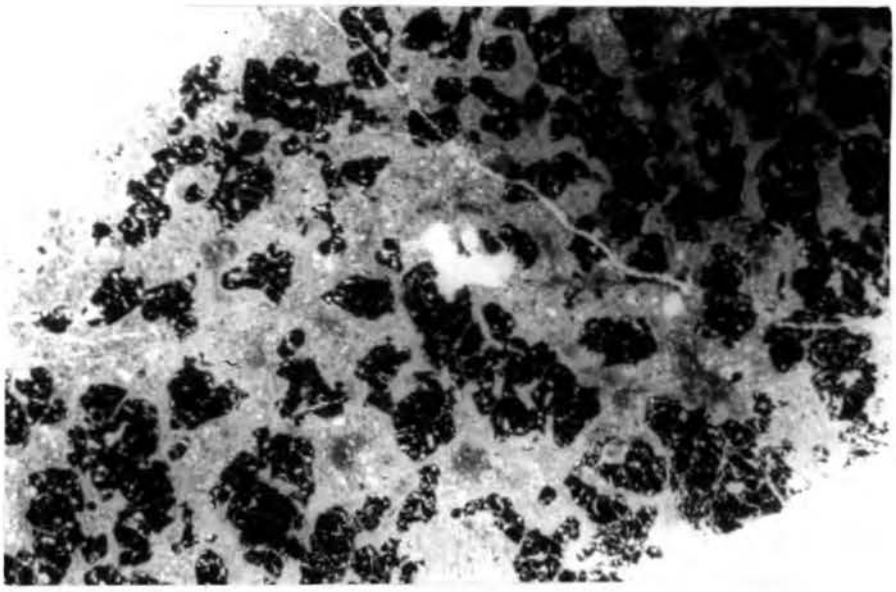

Plate 13 Disseminated chromite (X6).

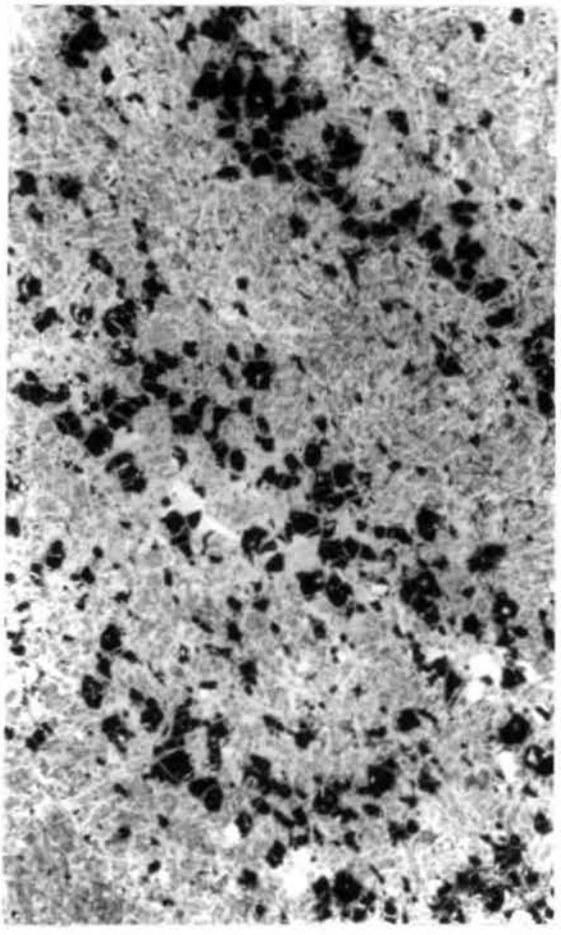

Plate 14 Stratiform chromite (X6).

tremolite veins, cutting the chromite, are common. Primary magmatic contacts between chromite and the surrounding peridotite are better displayed than elsewhere in the field. The contact dips northwest at 71°. A lens shaped pod, about 2 m thick and 15 m wide, is clearly seen in outcrop at Tavuk tarlasi. The ore is massive but brecciated. Disseminated chromite deposits are also known in this area. The deposits at Damdir, in the north cover a large area. They are mainly of massive chromite but nodular and disseminated types are also common. The deposits are cut by numerous basic dykes which cause considerable difficulty in underground mining. The pods have an east-west strike and dip northwards. Tremolite veins are rare.

Borchert (1961) claims that magmatic layering is present in the Andızlik-Zimparalik area with a northeast-southwest strike and dipping to the northwest; he does not describe the layering. Layering believed to have been caused by magmatic flowage during the emplacement of the peridotite is obscure and joints can easily be mistaken for layering. At one locality only, to the south of Madenoyugu tepe, 4-5 cm thick pyroxene rich bands, Plate 15, occur in the harzburgite, they cannot however be followed for more than 1 to 2 m along the strike direction.

Joints are common in the peridotite and in the basic dykes, and they present a complicated pattern in the field. 656 joint planes in the peridotite have been measured, and measurements plotted on an equal area stereogram, fig.8A. The poles of the

joint planes are relatively concentrated in four sectors. The greatest concentration lies in the northeast sector comprising 5 percent of the poles with a 211/42 dip direction and angle (211 is the dip direction and 42 is the dip angle). 1.5 percent of the poles are concentrated at 093/41, and at 016/21 while 1.4 percent indicate 047/57 as the dominant direction. The remaining poles are scattered with concentrations less than 1 percent.

Detailed geology and structure of the area around the Andizlik- and Zimparalik mines.

The Andizlik and Zimparalik mines are situated in the central part of the field. The Zimparalik sub-area, mapped on a scale of 1:1000, fig. 6A, (see volume 2), covers the top half of a large hill, the lowest point is at 1160 m and the highest at 1270 m. The summit is relatively flat and covered by heavy bush with a considerable thickness of soil. At Andizlik the ground gains height towards the southeast. The lowest elevation in the mapped area is 1220 m and the highest 1502 m, fig. 5A (see volume 2). The area was staked with surveying posts to increase the accuracy of the geological mapping. These posts were provided by the mining company "Etibank", and located by theodolite. The area is unaffected by the strong brecciation associated with either the northern or southern thrust zones. The geology is shown in figs. 5A and 6A (see volume 2).

The dominant rock type is serpentinised harzburgite which is highly brecciated along fault zones. Weathering is extensive, particularly in the Zimparalik sub-area. The most intensely weathered part

SPECIMEN LOCALITY MAP

FIG.10

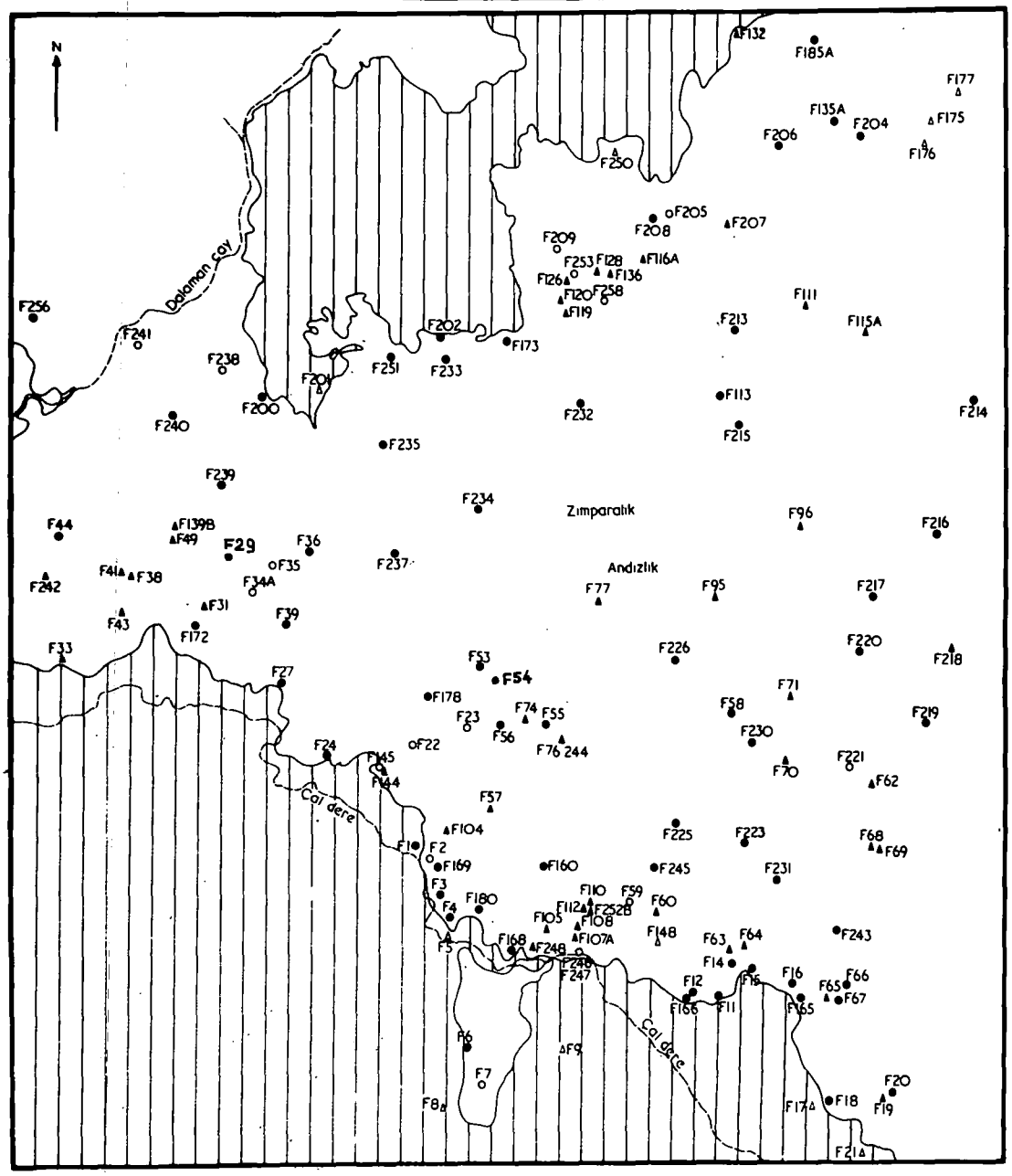

●Ultramafic rocks ○Basic rocks ▲Chromites △Sedimentary rocks

Excluding specimens from the Andizlik and Zimparalik mine areas

covers the higher ground at Zimparalik, the boundary with fresher harzburgite has been mapped and is shown on fig.6A (see Volume 2). Jointing and faulting are strongly developed in the area but magmatic layering has not been identified.

Pyroxenite veins occur throughout the area with thicknesses varying from 1 cm to 30-40 cm. They cannot generally be followed more than 1-2 m on the surface though occasionally they can be followed for 50-60 m, Z14 and A54. The pyroxenite veins are shown in figs. 5A and 6A (see Volume 2). They are composed of the orthopyroxene, enstatite with minor clinopyroxene, olivine and chromite, and maintain constant composition throughout the area. Their boundaries are sharp and marked by a narrow zone of serpentinisation in the peridotite.

The dispositions of 114 pyroxenite veins from Andizlik and 34 from Zimparalik were measured and plotted on equal area stereograms, figs. 11A and 11B. For the Andizlik sub-area, the stereogram has 10.5 and 7 percent concentrations of the poles in the southwest and southeast parts of the diagram respectively. The former indicates a 308/54 dip direction and the latter a 027/57 dip direction. The remaining poles are scattered in the northeast and southwest quadrants of the stereogram. The Zimparalik diagram shows three heavy concentrations of poles in the southwest and southeast quadrants. The most powerful, with a 13 percent concentration, lies in the southeast and indicates a 305/60 dip

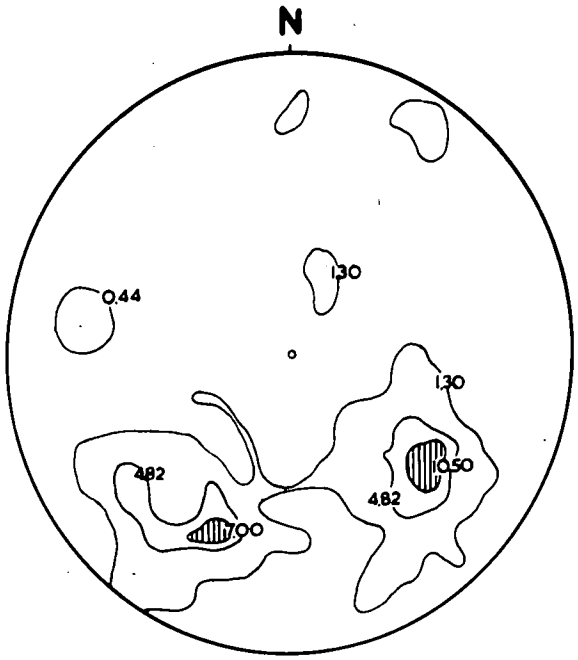

A

114 Pyroxenite veins from the Andızlık mine area

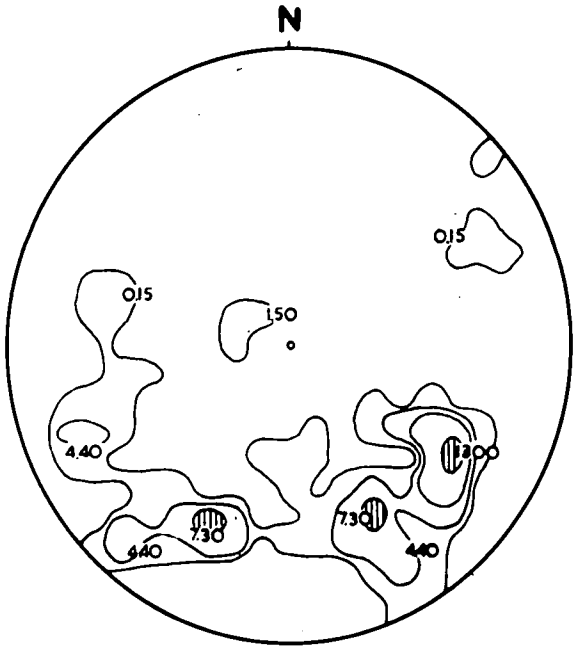

B

34 Pyroxenite veins from the Zımparalık mine area

Fig 11

direction, the other two have 7.3 percent concentrations of poles and indicate 332/56 and 026/57 dip directions. The two stereograms demonstrate the consistant character of the pyroxenite veins with clear orientations at about 308/54 and 027/57. Pyroxenite veins from other parts of the field have orientations which coincide with one or other of these two dominant directions.

Dioritic or doleritic dykes are infrequent in the Andizlik sub-area and generally small, from 1-5 m long and up to 1 m thick; three such dykes are seen in the eastern part. In the Zimparalik sub-area dykes occur in the southwest and east but with nothing like the frequency found at Damdir or Uckopru. The boundaries with the peridotite sometimes show slight chilling and have mostly ~~cooked~~ baked, serpentinised and brecciated the peridotite. These dykes are in the group which is oriented to the northwest-southeast dipping southwest, shown in fig.8B. Chromite occurs as an accessory mineral in the harzburgite and pyroxenite but is not present in the basic dykes.

In the Andizlik sub-area the chrome ore is mainly massive though nodular and disseminated types are known. Underground chromite bodies have been projected on to the surface map fig.5A (see volume 2), to assist in correlation. A line of outcrops can be followed from A1 in the west for about 330 m, towards the southeast, to A17, where a northwest-southeast trending fault is inferred causing a northwest lateral shift of about 150m. The outcrops can then be followed in a north-northeasterly direction for about 300 m. At A1 the chromite is massive with an east-west elongation and is

enveloped by serpentine and weathered peridotite. A7 comprises a small disseminated chromite outcrop in the highly weathered peridotite. A6, A10 and A17 were being worked as an open cut, and included several small peridotite lenses. The ore itself is mainly massive, though brecciated and cut by irregular green-whitish green tremolite veins up to 15 cm thick. A small fault with northwest-southeast trend cuts the exposure with a displacement of about 10 m in the northwest direction. The large fault east of A17 cannot be observed on the surface because of a cover of loose blocks. The orientation of the chromite pods and of other small parallel faults is strongly in favour of the existance of this fault. All the outcrops have been mined at some time and underground workings have been extensively developed to the east of the inferred fault. The chromite pods have sharp faulted contacts with the peridotite and are bounded by a 15-20 cm thick brecciated, serpentinised zone.

Measurements from 80 chromite boundary planes from the Andizlik mine area are plotted on fig.12A. There are three 5.60 percent and one 4.37 percent concentrations of poles situated in the southwest and southeast segments of the diagram. They indicate 044/73, 023/54, 318/47 and 284/36 dip directions respectively. The northwest part of the Andizlik sub-area is cut by a nobtheast-southwest trending fault running along the Ulaş dere and dipping 42° to 78° to the southeast. The northeast part of this large

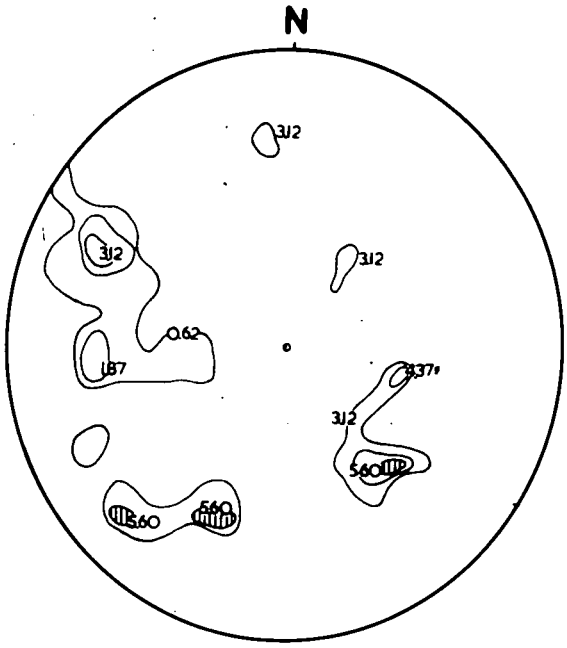

A

80 Chromite boundary faults in the Andızlık mine

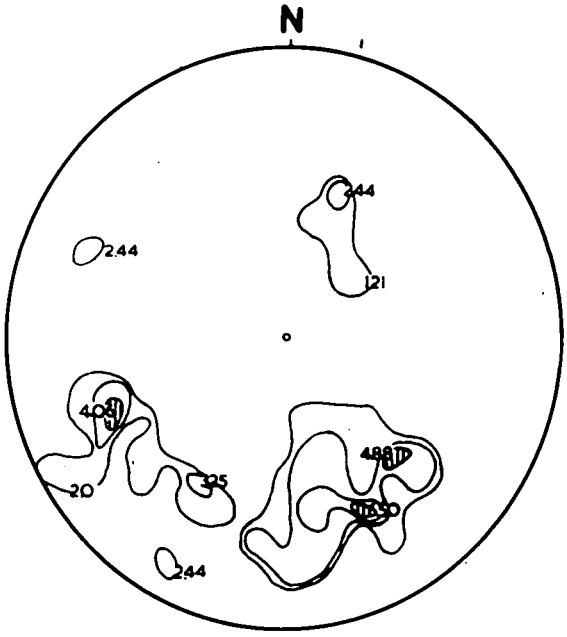

B

123 Chromite boundary faults in the Zimparalık mine

Fig 12

fault is characterized by a thick brecciated zone and several smaller parallel faults. Minor faults are plotted on both the 1:1000 scale surface map fig.5A (see Volume 2), and the 1:500 scale subsurface plan fig.5B, 5C (see Volume 2). Four sets of faults can be discerned. Two groups run in the northeast-southwest direction and dip northwest or southeast, a third one runs north-south and dips to the west while the fourth group has a northwest-southeast direction and dips northeast.

Measurements were made on 97 fault planes at the surface and 200 underground, they are plotted in figs. 13A and 13B. The surface diagram has four 4.5 percent concentrations of poles which have 162/74, 132/47, 030/59 and 271/52 dip directions. The diagram for underground fault planes has 4.75 percent pole concentrations with 034/62 and 329/48 dip and a 2.75 percent concentration indicating a 280/42 dip direction. Taken together 034/62 and 030/59 planes and 271/52 and 280/42 planes are common to surface and underground faults. The remainder have similar strike but dip in the opposite directions. A less strong concentration in the northwest sector indicates a northeast-southwest strike and southeast dip.

In the Zimparalik sub-area the chromite outcrops are grouped in the southeast. They cannot be followed far on the surface in the strike direction because of the topography. The ore is massive, but nodular and disseminated types are associated in places. Outcrops at Z56, Z58, Z59 and Z68 fig.6A, are oriented in a

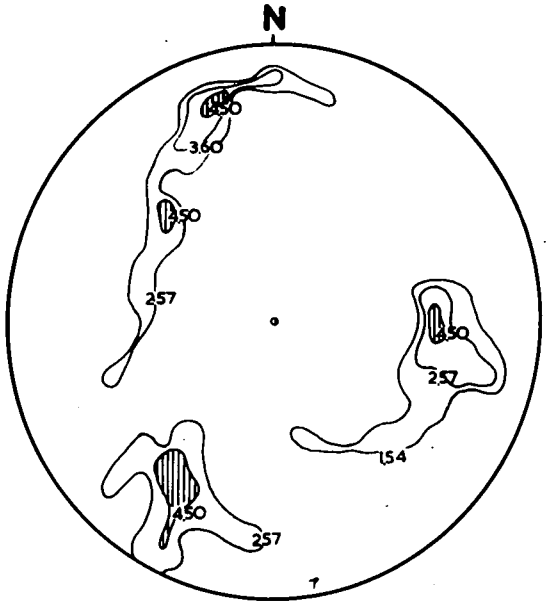

A

97 Surface faults from the Andizlik mine area

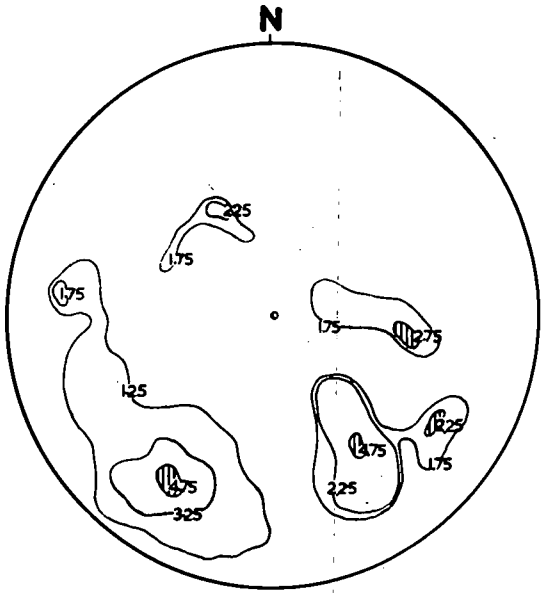

B

200 Underground faults from the Andizlik mine

Fig 13

northwest-southeast direction and dip to the northeast while those at Z1, Z55, Z67, Z65, Z70 are oriented in a north-northeast-south southwest direction and dip northwest. The outcrop at Z1 can be followed for about 30 m when it tails off. The ore is of disseminated and nodular type, and the nodules show a good lineation. Measured on the 174/77 plane the lineation is 051 (Pitch) left. The chromite at Z57, Z58 and Z59 is massive while Z54, Z56 and Z70 are of disseminated type; Z68 is a nodular chromite, while Z65 is a nodular, stratiform variety with bands 1-2 cm thick striking northeast-southwest and dipping to the northwest at 45°. The nodules are elongated but the elongation bears no relation to the banding. The outcrop can be followed for about 2 m along the strike direction. All of these outcrops occur in a heavily weathered harzburgite. The boundaries of the chromite pods are sharp and, in most localities, are marked by a 10-15 cm thick, brecciated serpentine zone, as at Andizlik. Measurements of 123 boundary planes from surface and underground are plotted in fig.12B, the poles are mainly concentrated in the southeast and southwest sectors of the diagram. There are concentrations of 6.50, 4.88, 4.06, 325 percent and three of 2.44 percent, they have orientations of 335/56, 315/48, 067/58, 031/50, 029/78, 113/68 and 199/44 respectively. When examined in conjunction with the field map the 335/56, 315/48, 031/50 and 029/78 planes indicate a folding of the pods on a 341° axis plunging at 51°. The 067/58 plane represents the northwest-southeast oriented

chromite pods. The surface fault pattern at Zimparalik is simpler than at Andizlik. A northwest-southeast trending fault cuts through the southwest of the sub-area and other small faults have the same trend. 41 surface, and 367 underground, fault plane measurements are plotted in fig. 14A and 14B. The surface data has a 9.75 percent and two 6.10 percent concentrations of poles at 067/77, 046/72 and 252/84 respectively. The underground pattern is more complicated with poles relatively concentrated at 9 centres. The strongest are two 3.27 percent concentrations oriented at 352/59 and 163/36. A 3.0 percent concentration occurs at 036/68, a 2.72 percent pole at 289/27, three 2.18 percent concentrations at 284/70, 334/77 and 215/59 respectively, and two 1.63 percent concentrations have 097/71 and 197/55 disposition. The planes 067/77 and 046/72 are probably common with the 036/68, ~~031/50~~ and ~~029/78~~ planes of the underground diagram. The powerful 252/84 plane of the surface diagram appears to be only weakly developed underground. The absence of the other poles from the underground pattern on the surface diagram can be explained by the weathered nature of the surface peridotites and the complicating factors of topography.

Development of chrome ore mining and detailed plans of the underground workings.

Surface outcrops were initially worked in open pits, e.g. the group in the Zimparalik mine area Z54, Z56, Z57, Z58, Z59, and in the

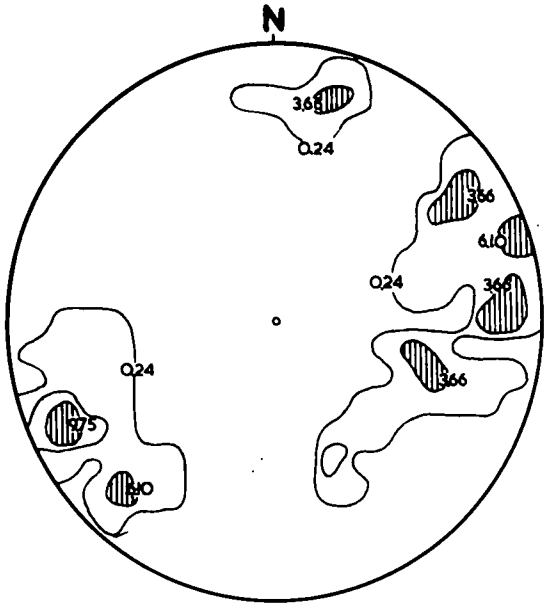

A

41 Surface faults from the Zimparalik mine area

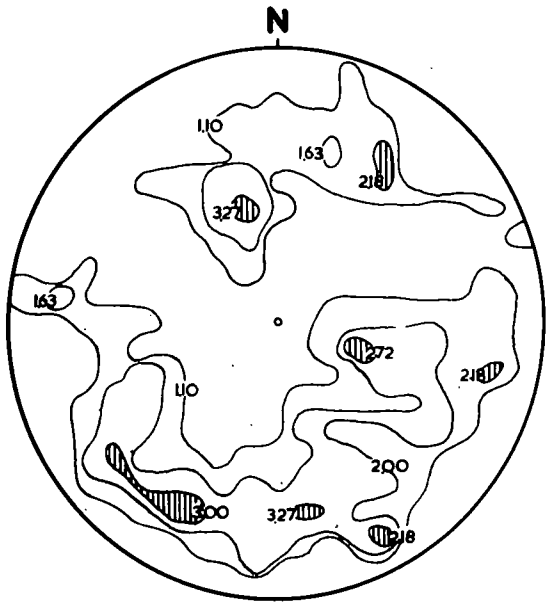

B

367 Underground faults from the Zimparalik mine

Fig 14

Andizlik mine area A17, A78, A81 etc., fig. 5A and 6A (see volume 2).

Underground mining commenced in 1951 with an exploration drive at the 1271 m level in Zimparalik. Since the mining follows the pods as closely as possible the shape of the production galleries changes from day to day.

A total of 1114 m of underground galleries at Andizlik and 1115 m at Zimparalik have been mapped on a scale of 1:500. Base plans, where available, were provided by the mining company, otherwise plans were prepared by Brunton compass and tape surveying during the geological mapping. The plans record features on a plane at a height of 90 cm above the ground (belt level). The mine plans presented here, figs. 5B, 5C, 6B, 6C and 6D (see volume 2), represent the situation between 1st August 1966 and 29th September 1966.

At Andizlik there are galleries at nine levels, figs 5B and 5C (see volume 2); 1275 m, 1305 m, 1326 m, 1340 m, 1421 m, 1458 m, 1475 m and 1501 m; the levels are not connected. Among these, the levels at 1340, 1421 and 1458 m are of major importance.

The 1275 m level is situated below outcrop A1 extends in a northeast-southwest direction. No chromite was found in the gallery.

The 1305 m level runs 20 m east-west, turns northwest-southeast for 5 m and finally trends northeast-southwest. Disseminated chromite occurs at the entrance to the gallery

and extends for about 20 m until it is stopped by a northwest-southeast fault dipping to the northeast. The chromite itself is also affected by a fault of similar trend and dip. Slicken sides measured on the terminal fault plane are oriented 029/67; 30 right. The northeast-southwest extension of the gallery is parallel to a prominent fault dipping at 37°-40° to the northwest. Slickenside measurements are oriented 352/39; 45 right and 327/40; 48 right. The 1326 m level extends for about 20 m first in a northeast-southwest direction then with a northwest-southeast trend. Chromite pods, dipping 49° northeast, are known from the latter region of the gallery.

The 1340 m level is one of the most productive galleries in the Andizlik mine. The main level is 100 m long extending east-west. Chromite pods occur throughout the length dipping 32° to 63° northwards. The pods have been followed up dip, through a series of galleries, to an elevation of 1358 m at the surface. Their downward continuation has been established to 1308 m by drilling from the 1340 m level.

The chromite is mainly massive and in places brecciated though nodular and disseminated types are common. The nodules show consistent elongation; 219/71; 50 left (AU22), 185/83; 53 left (AU24), 149/85; 38 left (AU23), 301/48; 66 right and 039/74; 35 right. Northwest-southeast trending faults dipping to the northeast offset the chromite pods.

The 1421 m level is situated to the northeast of the inferred

major fault described above. The gallery extends for 110 m in a northwest-southeast direction, in relatively fresh harzburgite, then branches to the northeast-southwest where several chromite pods are encountered dipping northwest at 14° - 42°. This pattern is complicated at the northeast end of the gallery where the dip direction changes to south. The ore is massive, in places strongly brecciated, and includes peridotite lenses. The pods can be followed up to present production levels. Tremolite veins are noticeable.

The 1458 m level, at one time connected to the 1421 m level, extends in a north-south direction then forks east-west. The continuation of the north-south gallery has been filled and the walls are heavily timbered. A large, massive chromite pod occurs in the east-west gallery, dipping northwest at 46°. Small harzburgite inclusions occur in the chromite. Small dislocations along northwest faults are present.

The 1470 m level extends in a northeast-southwest direction and exhibits two disseminated chromite pods dipping at 68° northwest.

The 1475 m level runs for 15 m in the northwest-southeast direction, it contains a 35 cm thick, fault bounded, northeast-southwest oriented, disseminated chromite pod, dipping northwest at 71°.

The 1501 m level is 20 m long in the northwest-southeast direction. No chromite is present in the gallery.

The Zimparalik mine has three main underground galleries at the 1205 m, 1240 m and 1271 m levels; all levels are interconnected, figs. 6B, 6C and 6D (see volume 2)

Plate 15 Pyroxene-rich layers in peridotite.

Plate 16 Olivine with serpentinised rims (X20).

The 1205 m level is oriented mainly northeast-southwest in serpentinised harzburgite. Chromite, at ZU30, is very brecciated and follows a shear zone, while the chromite at ZU34 is massive with a northeast-southwest strike and dips northwest at 44° to 74°. ZU36 is from a 70 m long, north northeast-south southwest trending chromite pod. Though somewhat irregular in shape, the pod has an east-west strike and dips north to northwest at 38° to 64°. Chromites from the western part of the gallery have dips in the opposite sense to the general pattern. The chromite is mainly massive, though in places it is very brecciated. Disseminated chromite is enclosed within the same structural frame in the east-west pod but is separated from the massive chromite by a sharp fault plane. The boundaries of the chromite pods are very distinctly marked in the peridotite on the gallery walls but the shape of the pods are very irregular, fig.9. These pods can be followed upwards to the present production levels where tremolite veins are abundant, e.g. ZU45. Continuation down dip has been proved by drilling and a gallery on the 1146 m level was under construction to reach these ores.

The 1240 m level runs northeast-southwest for about 150 m, in serpentinised peridotite, then forks into a northwest-southeast direction. Two chromite pods 25 m long (ZU6) and 20 m long (ZU5) are encountered, comprised of massive, but heavily brecciated ore dipping northeast at 45° to 84°. These pods wedge out down dip and are not known in the 1205 m

level. These two pods (ZU5 and ZU6) are the clear representation of the northwest-southeast trending bodies in the underground workings. Along an east-west gallery, part of the northwest-southeast drive, there are a number of chromite pods dipping northwards. This line of pods is the continuation of chromites seen at the 1205 m level.

The 1271 m level is mainly oriented in the northwest-southeast direction though towards the northwest, it makes several forks and has several stopes 2-3 m above and below the main gallery. This gallery is close to the surface and most of the features have lost their original disposition. Chromites dipping northwards at 36°-64° are the continuation of those seen at lower levels. The chromites at ZU16 and ZU17 are of stratifrom type with bands dipping northwards at 68°. The gallery walls are heavily timbered and the westward continuation of these bands cannot be followed.

Conclusions

During the fieldwork a total of 1763 pyroxenite veins, basic dykes, fault planes, joint planes and chromite boundary planes have been measured. Individually prepared stereographic diagrams suggest that basic dykes follow the dominant joint direction which is northwest-southeast, dipping southwest. The remaining features, pyroxenite veins, faults and chromite boundary planes

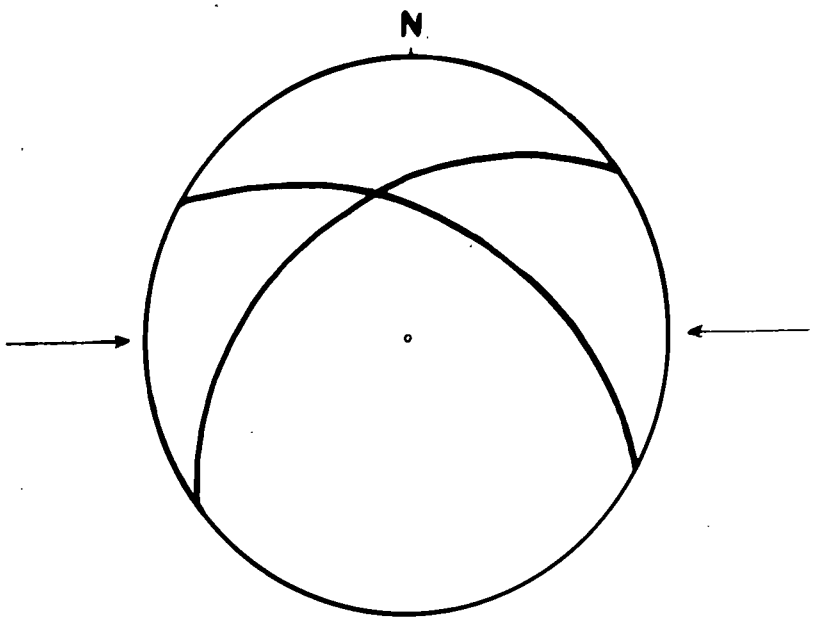

A

Pressure direction causing the dominant structural features

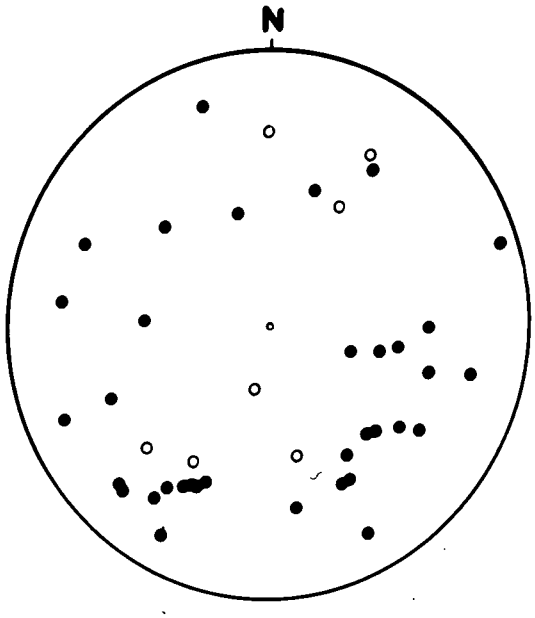

B

Generalised pattern of the powerfull poles

o JOINTS AND BASIC DYKES

● FAULTS, PYROXENITE VEINS, CHROME ORE BOUNDARY PLANES

Fig 15

are oriented in two dominant directions, northeast-southwest dipping northwest and northwest-southeast dipping northeast. The maximum concentrations of poles for each of these features have been plotted together on a stereogram, fig.15B. Although the poles present a scattered pattern, the heaviest concentrations are in the southeast and southwest sections of the diagram, indicating that the most dominant structural planes are running northwest-southeast dipping northeast and northeast-southwest dipping northwest, fig.15A. After rotating these two planes to the vertical position, they make an acute angle in the east-west direction. This suggests that the maximum pressure causing this pattern may have come in the east-west direction Phillips (1963), Badgley (1959).

Peridotite may have originally been uplifted by forces acting parallel to the north-south direction (normal to the alpine trend). From the stereographic data there is a suggestion that the peridotite may have been thrust to its present position by the forces acting in an east-west direction. Slickensides measured on the southern thrust zone indicate movement in the northwest-southeast direction which corresponds with one set of the dominant structural planes. Lineation measured on the elongated chromite nodules shows a southwest trend plunging at 45°, fig.16. This direction conforms with that of the northeast-southwest chromite pods. Field evidence suggests that the faults trending northwest-southeast were still operative at a later stage then the northeast-

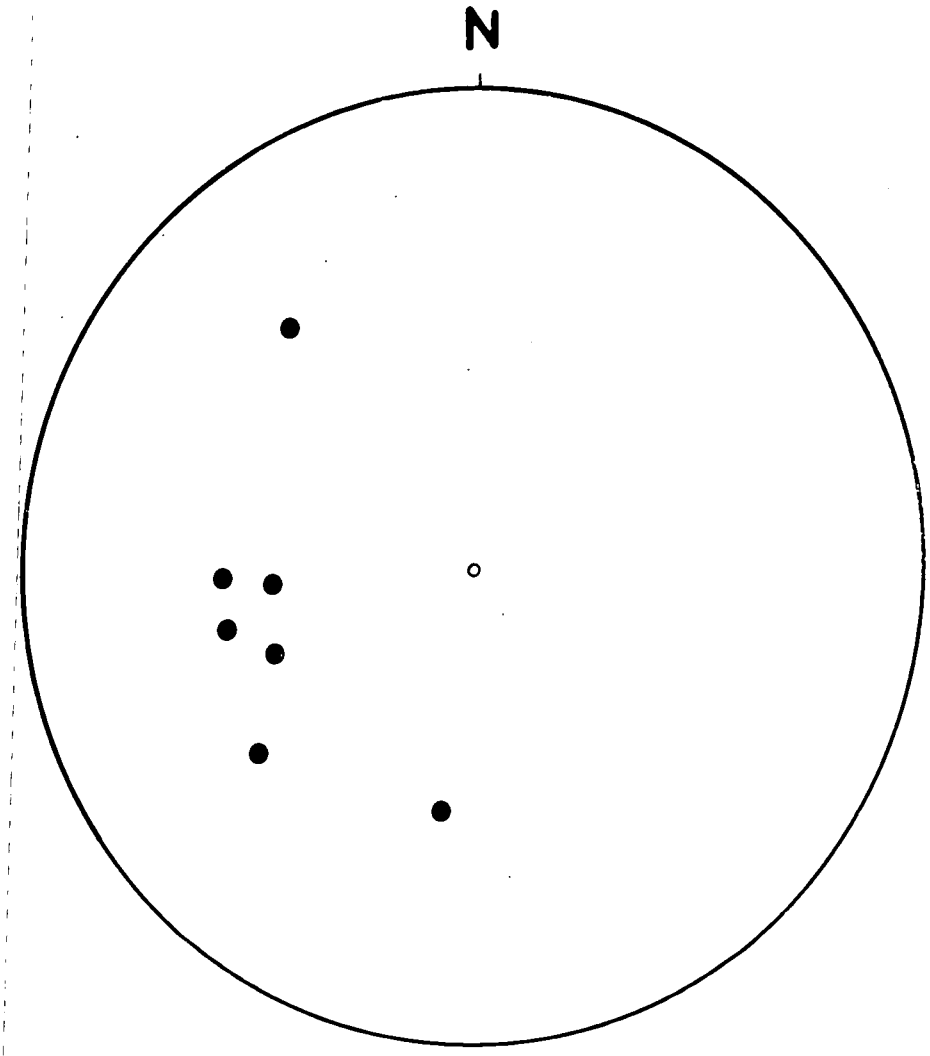

Lineation from the chromite nodules

Fig16

southwest faults, causing displacement of chromite pods. This pattern is difficult to reconcile with the regional alpine trend.

CHAPTER 3

PETROLOGY OF THE ULTRAMAFIC AND BASIC ROCKS

The ultramafic rocks are mainly serpentinised harzburgites, harzburgites and serpentinite with limited dunite, pyroxenite, tremolite and amphibolite. The basic rocks are those of the dioritic and doleritic dykes.

Sampling

Sampling was designed to cover all the representative rock types and to allow study of the chemical changes within the peridotite body. Special attention was paid to the Andizlik and Zimparalik mine areas. Specimens collected during the regional mapping have been marked with F (e.g. F1 - F259). Specimens from the Andizlik mine area are marked with A (e.g. A1 - A91) and underground specimens with AU (e.g. AU1 - AU34). In the same way specimens from the Zimparalik mine area are marked with Z (e.g. Z1 - Z107) and underground specimens with ZU (e.g. ZU1 - ZU48). Sample localities in the Andizlik and Zimparalik mine areas are shown on the surface and underground geological maps figs. 5A, 5B, 5C, 6A, 6B, 6C, 6D (see volume 2). Sample localities in the regional scale are shown on fig.10.

Harzburgite

The harzburgite is mainly composed of olivine and orthopyroxene together with minor amounts of clinopyroxene and chromite. The representative fresh hand specimen is black to dark olivė green in colour; individual crystals are not easily seen with the naked eye. In reddish-brown weathered specimens olive green, rounded

olivine, lathlike pyroxene and pin-head chromite crystals can be distinguished. In many places the harzburgite is highly serpentinised, the degree of serpentinisation varying from zero to fully serpentinised. In general the peridotite is over 50 percent serpentinised.

The dominant mineral in the harzburgite is olivine comprising up to 82 percent of unserpentinised specimens. Locality F251, fig.10, is least altered, the rock is light olive green in colour and has a glassy appearance; pyroxene and chromite crystals can be detected.

Modal analysis by integrating point counter gives olivine 82 percent, orthopyroxene 18 percent, and chromite 0.4 percent. There is no evidence of serpentinisation.

Olivine

Olivine is anhedral, of fine to medium grain size, up to 2 mm in length and has second order birefringence. The optic axial angles are equal to or greater than 87°. In most specimens it is partially altered to serpentine, individual grains being surrounded by a serpentine rim and veined by serpentine, Plate 16. In the less serpentinised harzburgites lamellae are common, Plate 17, accompanied by undulose extinction. Undulose extinction may still occur in olivines which are free from the lamellar structure. The occurence of such lamellae in olivine is explained by Turner

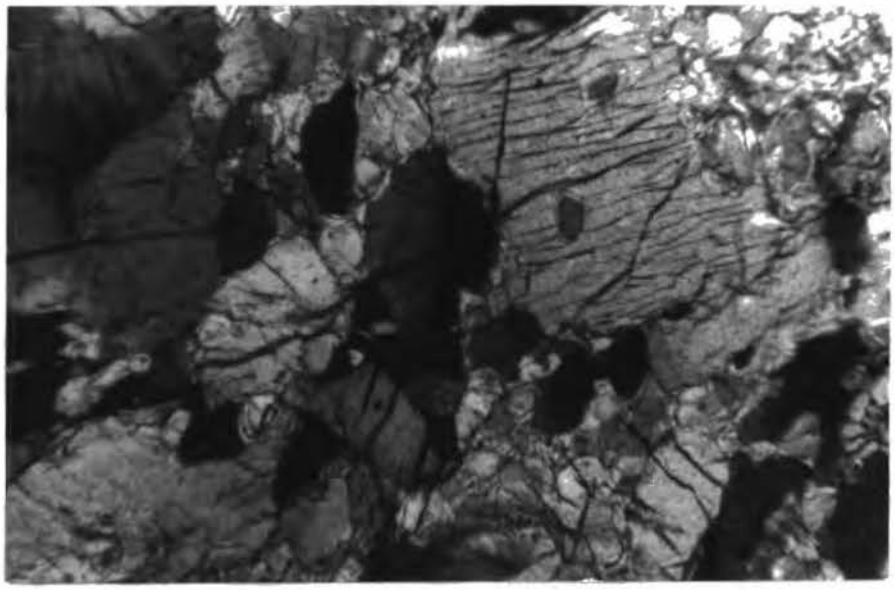

Plate 17 Lamellar structure in olivine (crossed polars, X20).

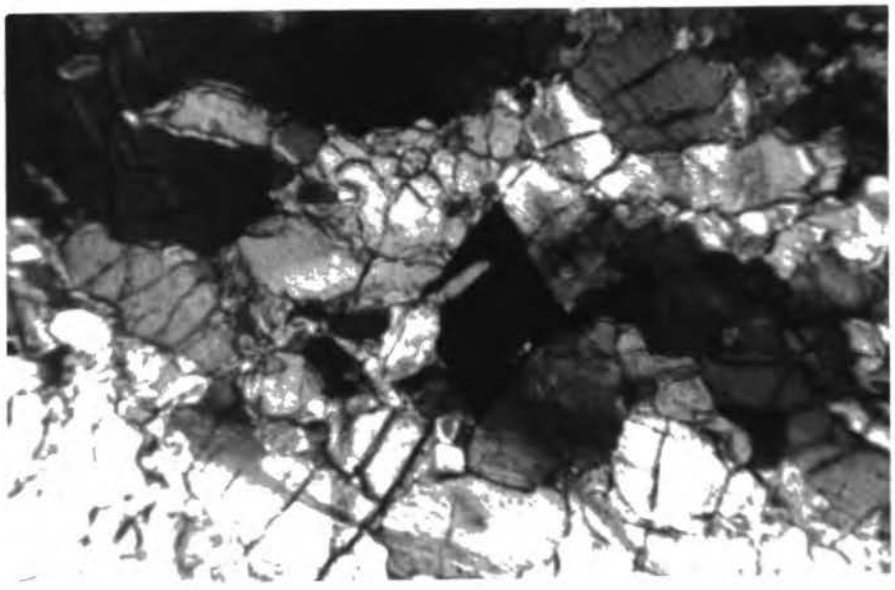

Plate 18 A chromite crystal enclosed by fresh olivine (X20).

(1942) as the result of translation gliding. Brothers (1960) has suggested that these features might be the result of gravity deformation by a load of overlying crystallites in a magma chamber. Lamellar structure in the olivine is more common near the fault contacts with the surrounding sedimentary rocks, than in the central part of the peridotite. The lamellar structure may thus have been formed during the tectonic emplacement of the peridotite, or as a result of the internal pressures set up during serpentinisation. The olivines include chromite crystals and are themselves included within chromite and pyroxene, Plates 18 and 19.

Olivine compositions have been determined by the X-ray diffraction method of Yoder and Sahama (1957), fig 17, and by electron probe analysis. The specimens analysed by X-ray diffractometer were examined as smear mounts using the Philips high-angle diffractometer. Scans were made over the range 28° to 33° 2Θ using CuKα radiation. Pulse height discrimination was used to increase peak to background ratios. The observed 2Θ position of the (130) reflection, fig.18, was corrected by means of the silicon (111) reflection at 28.4662 ; silicon was added as an internal standard. The results, table 1, show that the olivine composition varies from about Fo 80 to Fo 95. Duplicated runs show some variation, up to $\pm$ 10 percent.

The olivines in 10 peridotite specimens from different parts

FIG.17

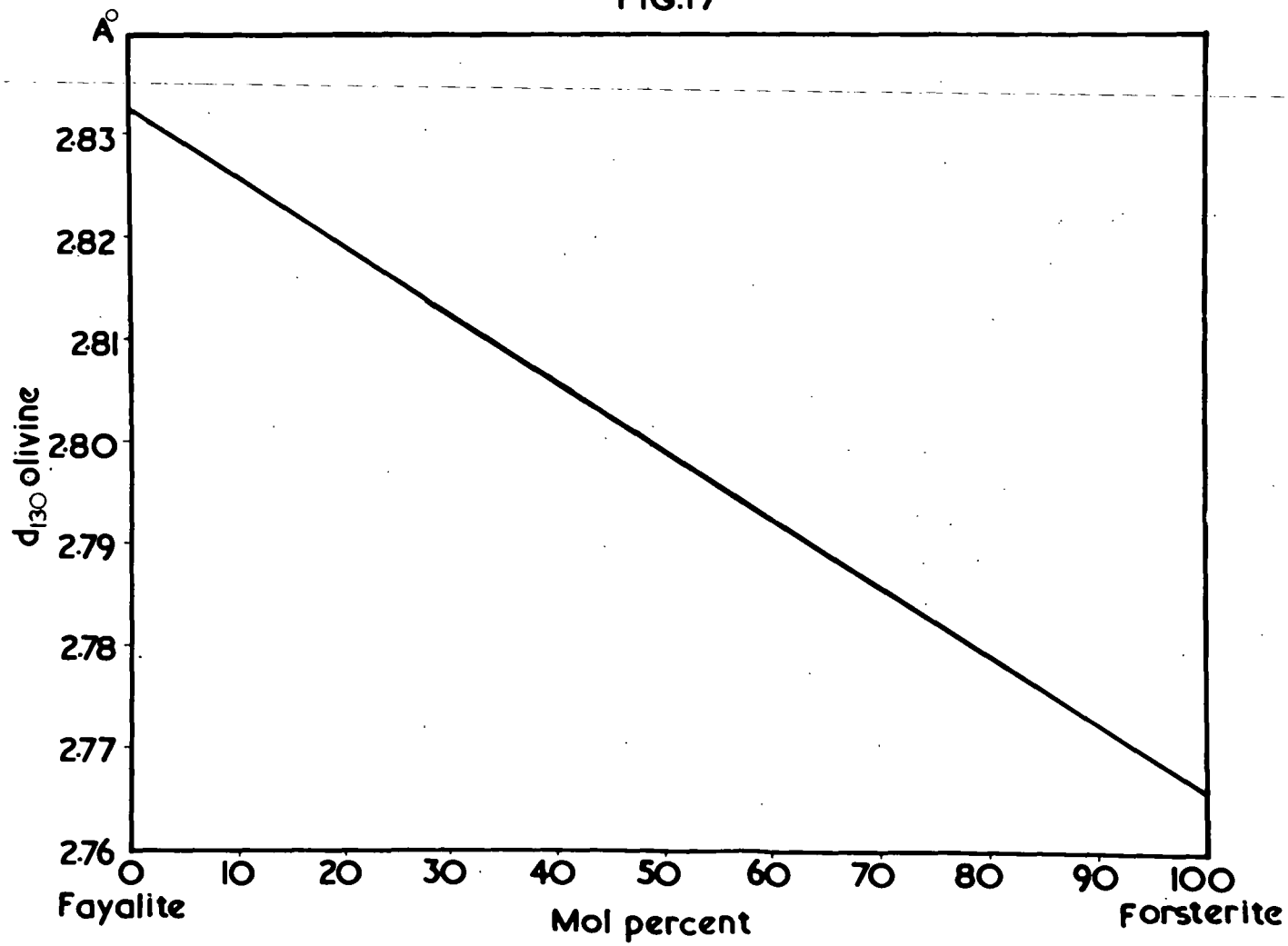

Olivine determinative curve (Yoder and Sahama 1957)

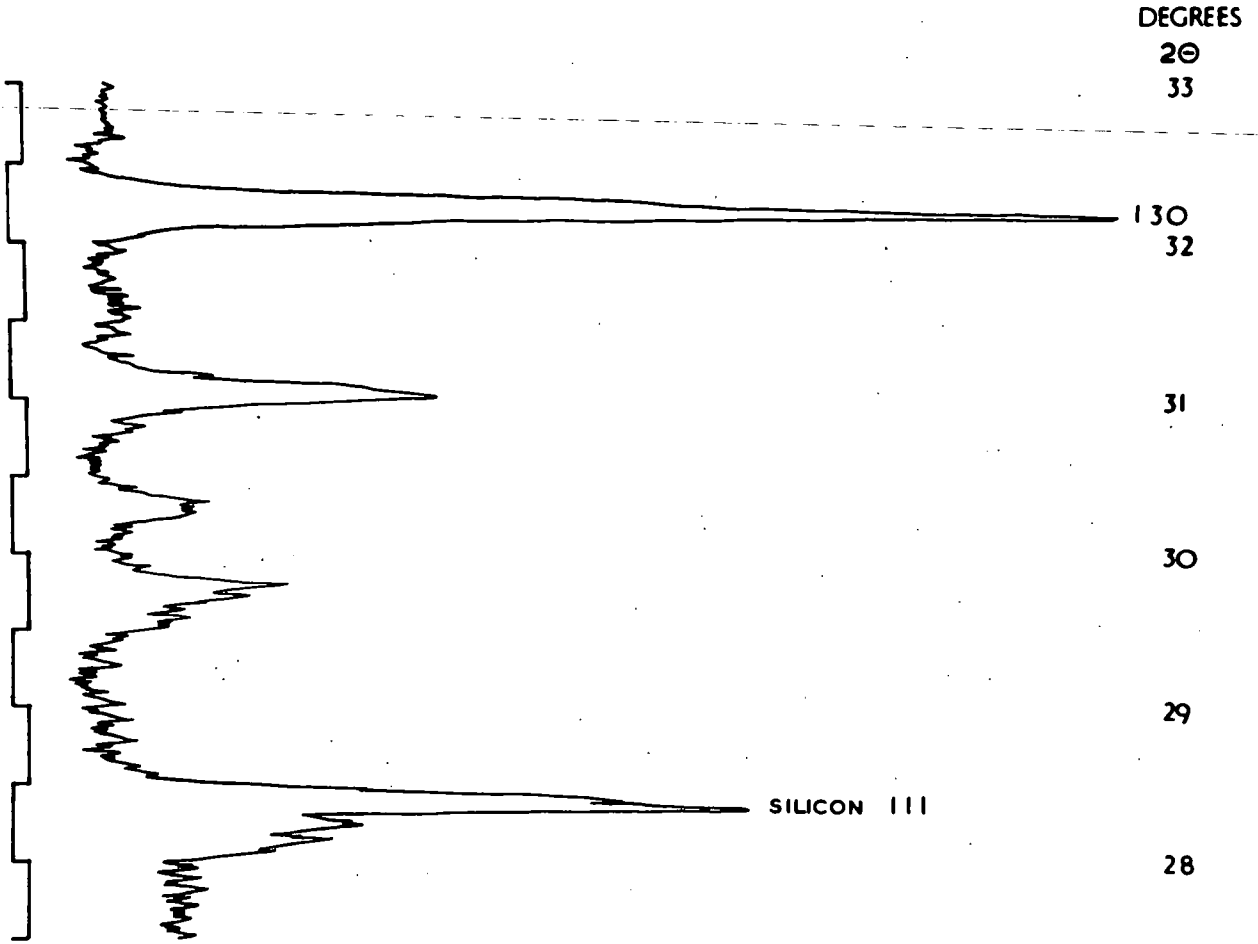

DIFFRACTOMETER RECORD OF OLIVINE NO F256 CuKα RADIATION

FIG.18

of the peridotite have been analysed by electron probe using chemically analysed $Fo_{81.20}$, $Fa_{19.17}$ olivine as the standard. Mass absorbtion and dead time corrections were made by means of a computer program (J.W. Aucott, personal communication). Results reveal the constancy of olivine composition throughout different parts of the intrusion with values occupying the range Fo_{88} - Fo_{91}, table 1. Traverses made in the same olivine grain reveal no obvious zoning.

Orthopyroxene

Orthopyroxene is the second most abundant mineral in the harzburgite, the content ranging from 8 to 25 percent by volume but mostly around 14 percent. The orthopyroxene occurs as lath like, subhedral to euhedral crystals with a grain size reaching 5 to 6 mm in length. They have low first and second order birefringence and the optic angle gives values from 77° to 80°. On the basis of optical identification the orthopyroxenes are either enstatite or bronzite though both may occur in the same rock. Bronzites show very faint, lightbrown pleochroism and are optically negative, while the enstatite is non-pleochroic and optically positive.

In many sections the cleavage traces of the orthopyroxenes suggest that crystals are bent or broken. Many orthopyroxene laths are divided into sharply defined sections of different optical orientation, with boundaries known as kink bands, Plate 20.

Table 1 Forsterite content (Mol Percent) of olivines from harzburgites determined by electron microprobe and X-ray diffractometer.

	Electron Probe analyses						Average of E.Probe analyses	X-ray diffractometer
No	Fo	Fo	Fo	Fo	Fo	Fo	Fo	Fo
F6								90
F11								94
F14								92
F19	88	88	88	88			88	
F29	87	87	88	88	87		87	80
F39								93
F44	88	88	89				88	86
F45								82
F53								90
F54	91	91	91	91	91	91	91	
F56								95
F59								93
F67								93
F68	89	89	90	90	88		89	
F169	88	88	88	87	87		88	
F173								91
F200								94
F204								89
F206	87	87	87	87	87		87	
F208								85
F214	88	88	88				88	91
F215	88	87	88	88	88		88	95
F217								91
F220								94
F223								90
F225								95
F231								94
F233								91
F234								94
F237								90
F239								89
F240								91
F243								91
F245								95
F251	88	89	89	89			89	94
F256								94
A13								95
Z82								94
Z103								94

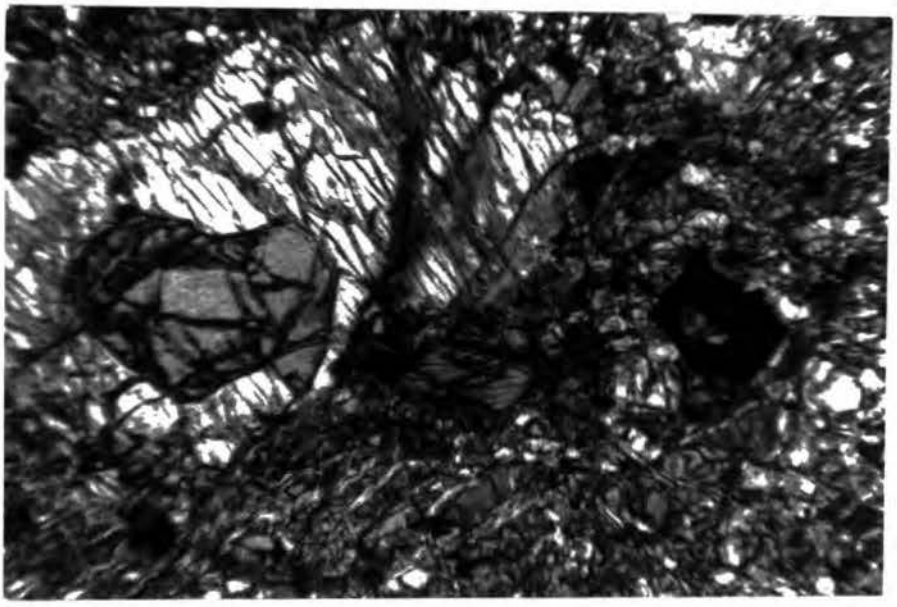

Plate 19 Olivine inclusions in orthopyroxene and chromites (crossed polars, X20).

Plate 20 Kink bands in orthopyroxene (crossed polars, X80).

These bands become more irregular with increasing deformation until the crystals actually rupture and are torn apart along the sector boundaries. This structure has been produced artificially by deformation of pyroxenite at pressures of 5000 bars/cm^2 and temperatures of 500°C and 800°C. The kink bands are attributed to translation gliding during rotation about the (010) axis (Turner, Heard and Griggs, 1960). This may be a result of internal pressures imposed during the expansion resulting from serpentinisation, as discussed below.

The orthopyroxenes include thin clinopyroxene exsolution lamellae which are mainly parallel to the 110 cleavage trace, Plate 21. The lamellae show high birefringence and have oblique extinction. In some sections they are not strictly parallel to the cleavage trace. The exsolution takes place such that the lamellae and host have common b and c axis and (100) plane. This is the only plane on which the clinopyroxene and orthopyroxene have similar structure and might thus be expected to give the lowest energy interface between the two structures. Hess (1960) considers that the exsolution plane may also be related to the ease of migrations of ions in the structure, rather than to differences between the two structures. This may explain those exsolution lamellae which are not parallel to the (100) plane.

The harzburgites generally show a poikilitic texture, orthopyroxenes enclosing rounded olivine, chrome spinel and rare

Plate 21 Clinopyroxene exsolution lamellae and a chromite inclusion in orthopyroxene (crossed polars, X32).

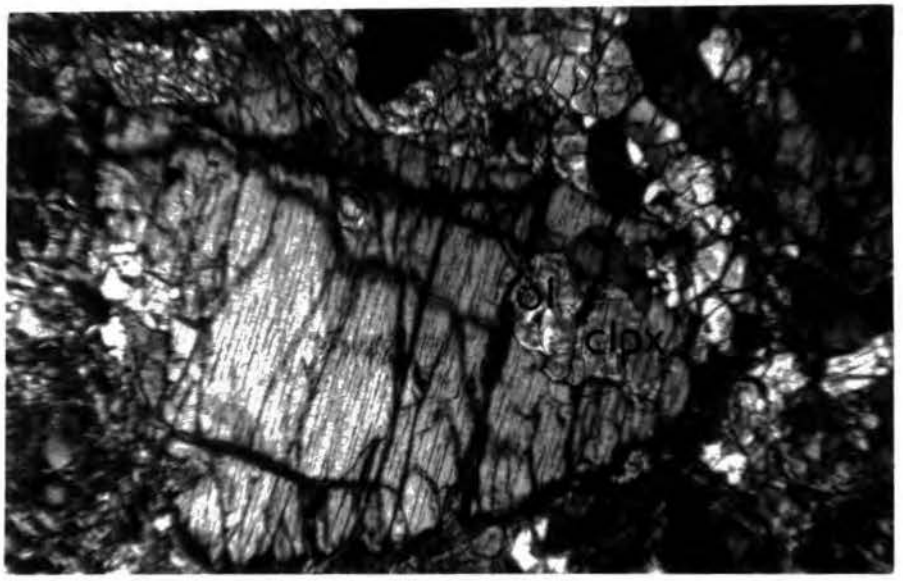

Plate 22 Olivine and clinopyroxene inclusions in orthopyroxene (crossed polars, X20).

clinopyroxenes, Plate 21 and 22. The orthopyroxene crystals are in random orientation, occasionally they embay olivine but no reaction rim is produced at the junction. Serpentinisation of the orthopyroxene may be seen in many sections, particularly near the northern and southern thrust zones where orthopyroxenes may be partly or completely altered to bastite, Plate 23.

Hess (1952) and Kuno (1954) have shown that orthopyroxenes exhibit ideal solid solution, the unit cell parameter varying regularly with Mg content. Zwan (1954) showed that the d spacings (10 3 1) and (0 60) fig.19, change systematically with variation in En for a series of low alumina orthopyroxenes.

Hancock (1964) plotted the spacing (060) against the spacing (10 3 1) for a series of low alumina orthopyroxenes from Hess (1952). He established a straight line relationship from which the molecular percent En could be estimated in the range En_{40} to En_{100}. fig.20. Separated orthopyroxenes from 10 harzburgite specimens have been examined by X-ray diffraction over the angular range 55° to 64°2Θ, using CuKα radiation, and added silicon as internal standard. Duplicate scans were made for each specimen and the average spacings (10 3 1) and (060) used to determine composition from the curve produced by Hancock (1964). With the exception of the F18 the specimens plot very close to the curve and give values ranging from En_{89} to En_{99}, table 2, in agreement with their optical identification as enstatite and bronzite.

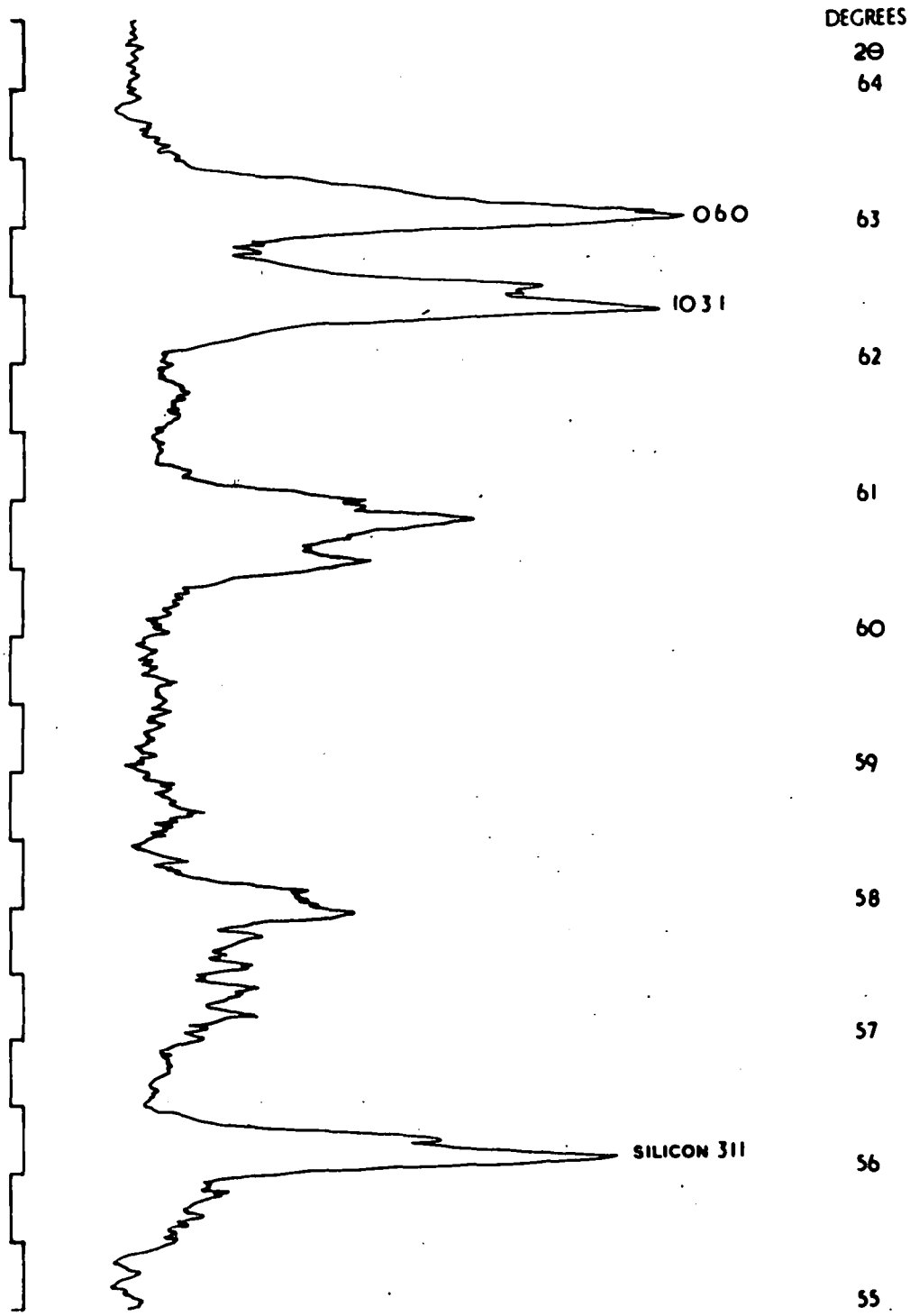

DIFFRACTOMETER RECORD OF ORTHOPYROXENE NO A18 CuKα RADIATION

FIG.19

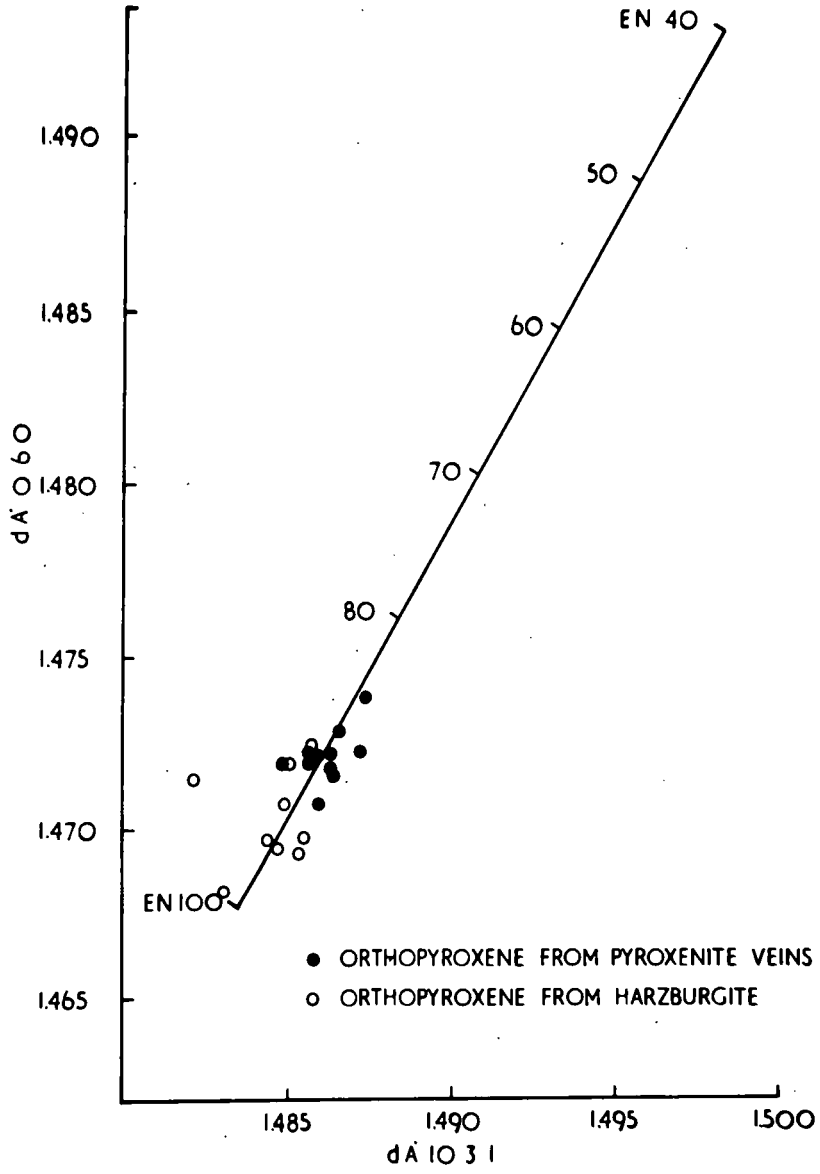

Orthopyroxene x-ray determinative curve (after Hancock 1964)

FIG.20

Table 2 En content of Orthopyroxenes (mol percent) from harzburgites and pyroxenites determined by X-ray diffractometer.

(a) Orthopyroxenes from harzburgites

No	d 1031	d 060	En
A22	1.4851	1.4718	91
F4	1.4844	1.4694	95.5
F18	1.4821	1.4713	94?
F200	1.4855	1.4697	94
F214	1.4848	1.4706	93
F216	1.4857	1.4723	89
F223	1.4847	1.4693	95.5
F245	1.4831	1.4681	99.5
F249	1.4853	1.4692	95

(b) Orthopyroxenes from pyroxenites

A18	1.4859	1.4721	89.5
A34	1.4865	1.4728	87.5
A54	1.4874	1.4738	85
A55	1.4856	1.4722	89.5
A76	1.4857	1.4719	90
Z3	1.4863	1.4722	89
Z14	1.4872	1.4723	88
Z25	1.4863	1.4717	89.5
F15	1.4849	1.4719	91
F20A	1.4859	1.4707	92
F36	1.4864	1.4715	90.5

Clinopyroxene

Clinopyroxenes are very minor in amount; in some specimens they are completely absent while in others 1 or 2 grains can be identified. In the western part of the field, around Incebel tepe, there is a slight increase in the amount of clinopyroxene to 3 to 4 percent, but insufficient to term the rock lherzolite. They occur as subhedral to euhedral crystals with well developed cleavage and oblique extinction. Orthopyroxene exsolution lamellae are occasionally present. Clinopyroxenes are identified as diopsidic augite. The clinopyroxenes are the least altered silicate mineral in the harzburgite although they do show slight signs of alteration to a light green chlorite, and tremolite.

Chromite

Accessory chromite, about 1 percent, is generally found in the harzburgite. In the weathered specimens pin-head chromite crystals are easily seen, the grain size reaches 1 mm. In thin sections they ~~form~~ are reddish brown to reddish darkbrown, although they are mostly anhedral corroded crystals in some cases euhedral forms have been preserved, Plate 24. The chromite crystals are mostly corroded and they often have silicate inclusions. The chromites are usually enclosed in olivine or orthopyroxene, Plate 18 and 21, and are rarely interstitial to these minerals. The chromite shows no orientation.

Episcopic study reveals no evidence of compositional zoning

Plate 23 Bastitised orthopyroxene (X32).

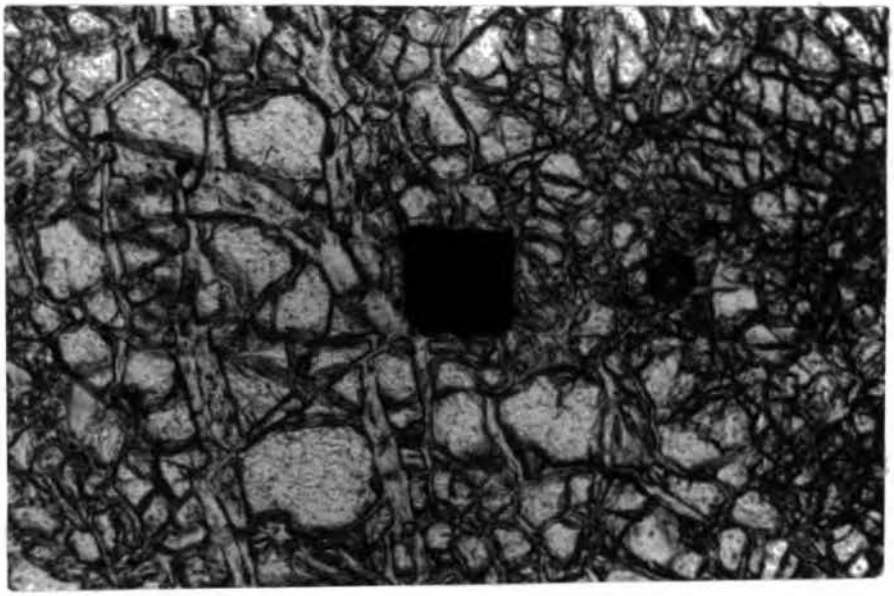

Plate 24 A euhedral chromite crystal in harzburgite (X32).

in the chromite. Very fine grained magnetite, and occasional pyrite and chalcopyrite are found in the serpentinised part of the peridotites.

Dunite

Dunites are of very limited extent and their distinction from harzburgite is difficult in hand specimen. The amount of chromite discernable in hand specimen is a rough guide in distinguishing one from the other, the dunite carrying more chromite. Dunites are restricted to the immediate vicinity of the chromite occurrences, but adjacent to the podiform chromites, the peridotite is often a sheared serpentinite of heavily serpentinised harzburgite-dunite. Normal contacts between chromite and the enclosing rock do however involve dunite which is usually heavily serpentinised; relict olivines can be seen in thin section. Representative dunite occurs at F19, F68, F54 and F208, fig.10.

The dunite is composed of olivine and minor chromite and is usually heavily serpentinised, more so than the harzburgites. The chromites are mostly euhedral to subhedral and are interstitial to the olivine. The chromite content is around 2 percent while pyroxene may reach 0.3 volume percent.

Lineation is not noticeable except that the chromite may show a banding, visible, for example, in specimens F19 and F68, Plate 14. The chromite is dark-brown in thin section.

Serpentinites

The peridotite is in general serpentinised to over 50 percent. Around the chromite bodies, adjacent to basic dykes and along the tectonic zones the peridotites are generally fully serpentinised. The serpentine texture is controlled by the original rock type and the degree of post serpentinisation shearing. The sheared serpentinites are composed of a mass of small serpentine flakes showing undulose extinction, and traversed by numerous thin serpentine veins. In the peridotites olivine, pyroxene and chromite are usually surrounded by a thin serpentine zone, Plate 16. Serpentinisation starts from the margin and advances towards the centre where relict olivine may still be seen. Serpentinised olivine forms brownish green mesh textured serpentine with small euhedral magnetite crystals or magnetite dust occurring along cracks and representing iron liberated during the serpentinisation process. The rims of this mesh textured material are composed of fibrous serpentine which is length fast and termed α serpentine by Tertsch (1922).

The "hour-glass" structure is quite common, Plate 25. In this structure the collar and the core are both composed of α serpentine. Late stage chrysotile veins fill cracks resulting from shearing, and cut across the previously formed serpentine. These veins are composed of length fast α serpentine fibres.

Orthopyroxene is altered to bastite during serpentinisation,

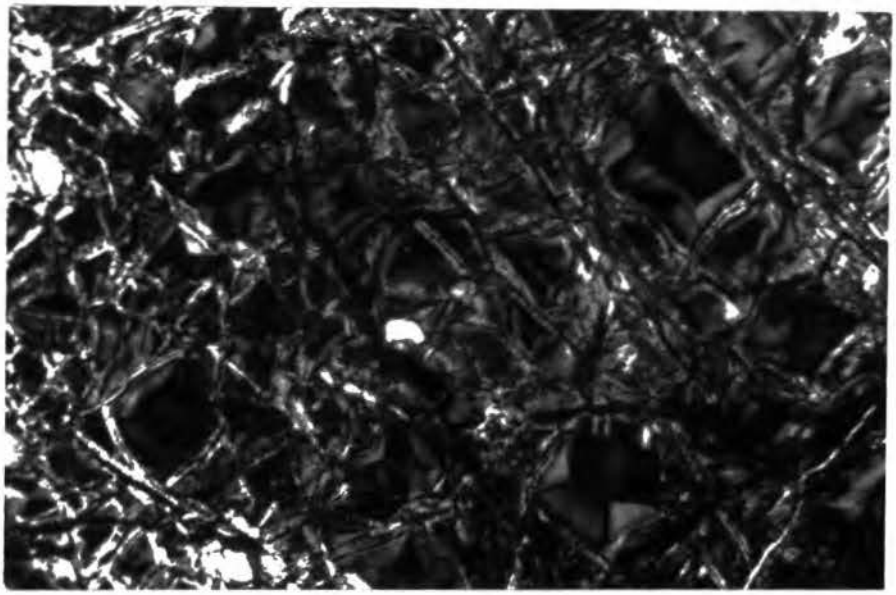

Plate 25 Serpentine psuedomorphs after olivine, showing hourglass structure (crossed polars, X20).

Plate 26 Granulation in harzburgite (crossed polars, X20).

but original crystal outlines are often preserved. This feature has been used to argue against volume increase during serpentinisation. In many of these relict orthopyroxenes and clinopyroxene exsolution lamellae can still be seen. The bastite is length slow α serpentine. According to Whittaker (1953) serpentine has a layered structure consisting of a pseudo-hexagonal network of SiO_4 tetrahedra. The main polymorphs of serpentine are chrysotile, antigorite and lizardite.

Chrysotile consists of fibres of the order of 200 A° in diameter, packed in trigonal array along their length (Page, 1968). Electron microscope studies reveal that chrysotile has a morphology similar to that of a hollow tube. Whittaker (1953) has recognised three varieties of chrysotile from single fibre studies; clinochrysotile, orthochrysotile and parachrysotile. Ortho and parachrysotile are orthorhombic while clinochrysotile is monoclinic. In clino and orthochrysotile the fibres are curved about the a axis while parachrysotile has curvature about the b axis.

Lizardite has a platey morphology and is disordered in three ways:

a) The crystals are macroscopically bent about more than one crystallographic axis.

b) Some layers are rotated relative to the others by 180°.

c) Some layers are displaced.

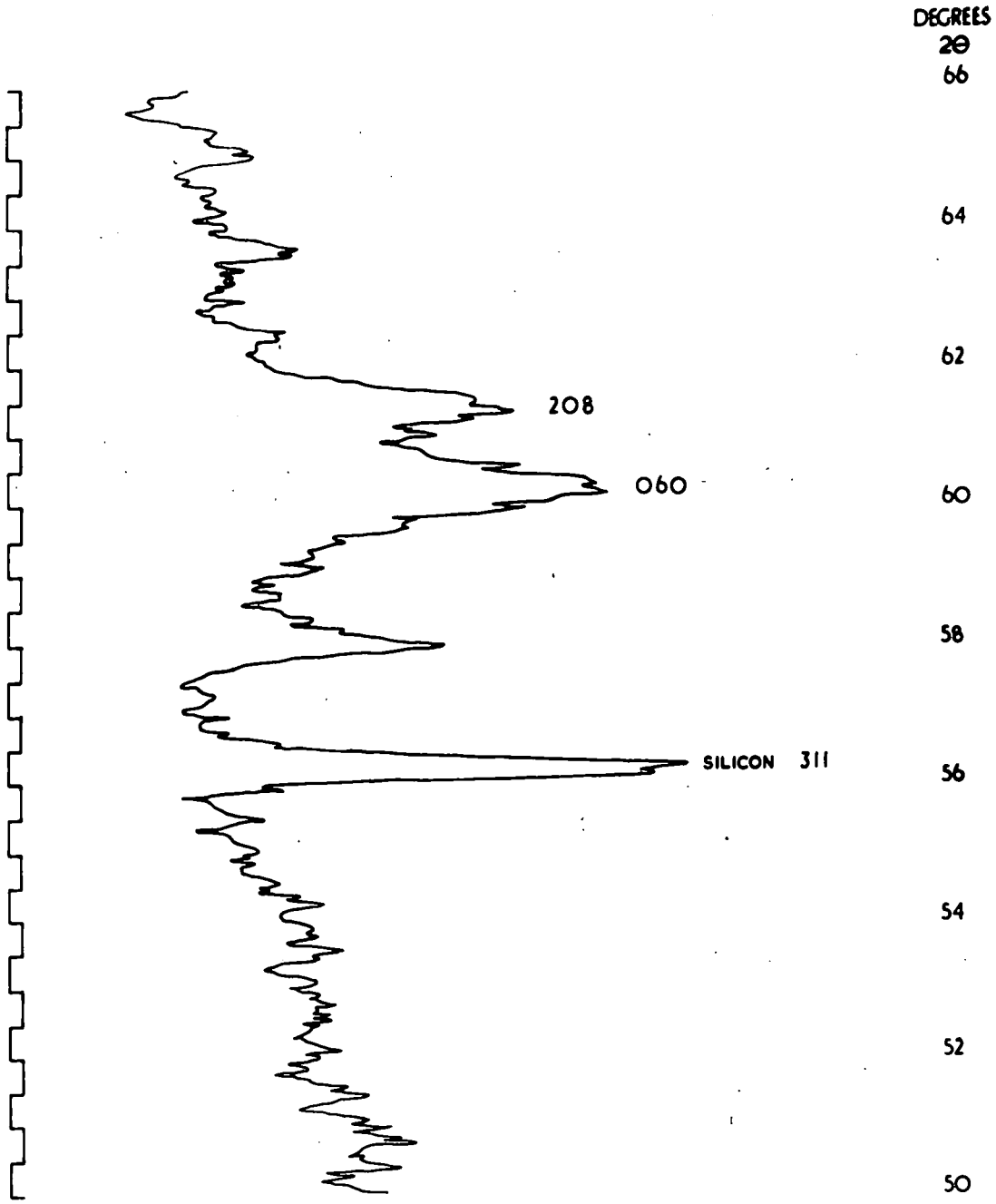

DIFFRACTOMETER RECORD OF LIZARDITE NO F75 CuKα RADIATION

FIG.21

Table 3 d spacings of serpentines

WZ*		A2		F58		Z72		F75		F101		F142		
dA°	Intensity	dA°	Intensity	dA°	Intensity	dA°	Intensity	dA°	Intensity	dA°	Intensity	dA°	Intensity	hkl
7.360	vs	7.300	100	7.312	100	7.335	80	7.360	100	7.355	100	7.317	100	002
4.580	m	4.564	20	4.550	25	4.541	18	4.580	11	4.585	16	4.576	14	020
3.660	vs	3.652	90	3.653	90	3.659	100	3.658	39	3.664	90	3.659	98	004
-				2.827	6									
2.617	w					2.620	17							201
2.498	s	2.495	31	2.498	24	2.499	51	2.495	90	2.502	58	2.505	28	202
-				2.455	16			2.457	6	2.461	5			202
2.340	mw													203
2.150	mw	2.147	9			2.150	16	2.148	11	2.149	9	2.149	8	204
-		2.093	9											204
1.968	w													205
1.830	w													008
1.797	w					1.794	7	1.796	8			1.799	6	206
-		1.749	19									1.749	6	106
1.739	mw													110
1.640	w													207
1.534	s	1.537	16	1.532	24	1.532	25	1.535	18	1.536	16	1.539	24	060
1.504	m	1.502	7	1.503	6	1.507	7	1.507	5	1.503	7	1.506	6	208
1.464	w													

WZ* d spacings of serpentine from Whittaker and Zussman (1956) p.117, column 22.

Antigorite exhibits both platey and fibrous morphology. It is a single layered serpentine with c and b dimensions similar to those of lizardite but with a larger a parameter in many cases approximating 40A°.

Serpentine forming the matrix to chromite ore, specimens Z72A, F75, F101, the serpentine in normal magmatic contact with chromite, specimen F142, serpentine in fault contact with chromite, specimen A2, and serpentine specimen F58 from a basic dyke-peridotite contact have been investigated using a Philips high angle diffractometer. Scans were made over the angular range 6° to 65° 2Θ using CuKα radiation and peak positions corrected by means of known peaks from silicon which was added as an internal standard. The d spacings have been correlated with values derived by Whittaker and Zussman (1956); they are shown in table 3. The existance of the (060) reflection at 1.547-1.532A° and of the (208) reflection at 1.502-1.507A° table 3, fig.21, suggests that the serpentine is mainly lizardite. The presence of the (204) spacing at 2.09A° the (206) spacing at 1.749A° and the (202) spacing at 2.45A° suggest that chrysotile is also present.

No peaks specifically attributable to antigorite could be identified in the diffraction patterns, fig.22. The absence of antigorite was checked by comparison with diffraction patterns of a fibrous antigorite (picrolite) from the Durham University

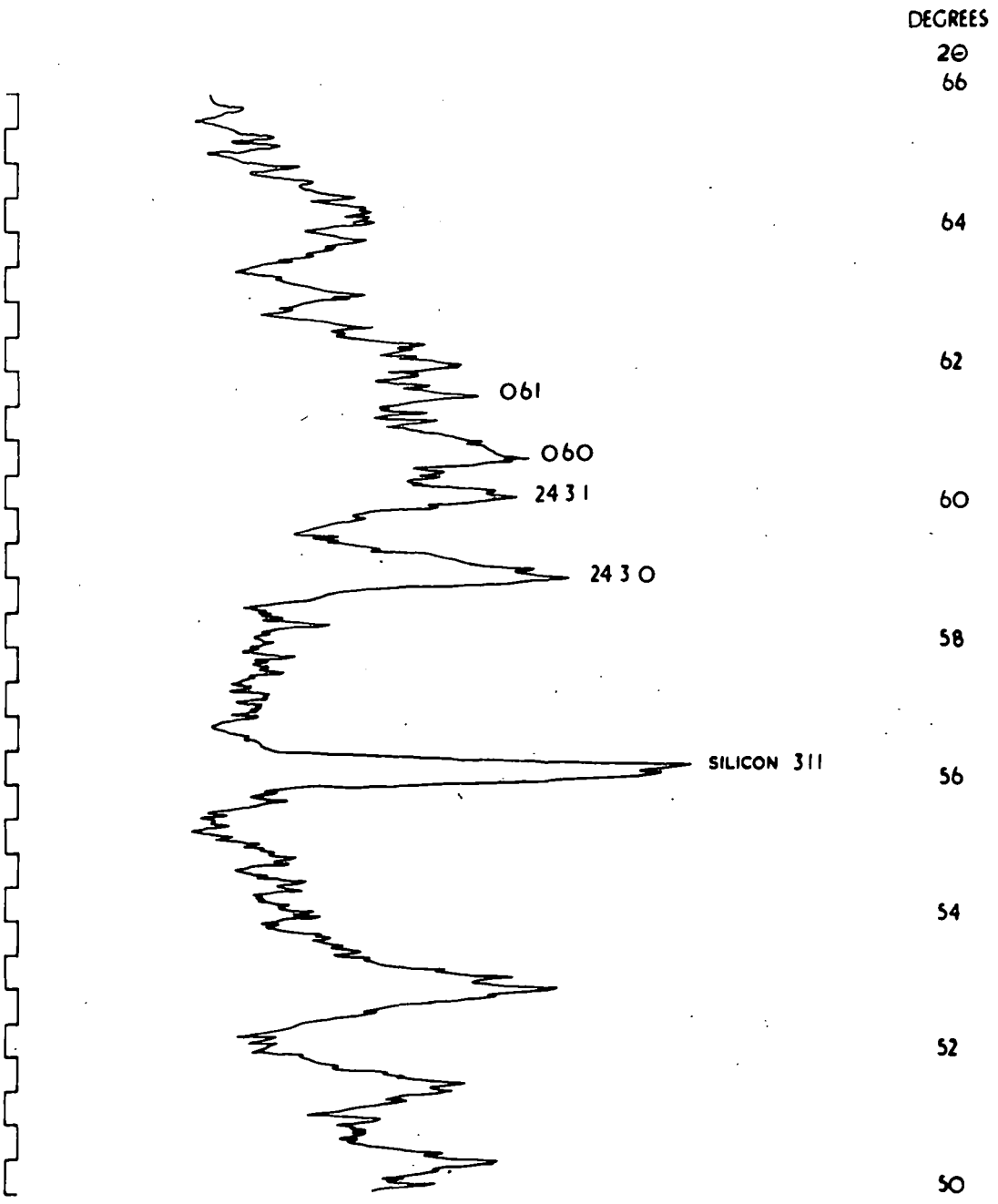

DIFFRACTOMETER RECORD OF ANTIGORITE NO 8243 CuKα RADIATION

FIG.22

Geology Department collection (no. 8243).

A number of serpentinised peridotites have been examined in the same way, lizardite was clearly identified in each case.

Many workers accept that antigorite is found where shearing has taken place, Hess et al. (1952), Francis (1956), Wilkinson (1953). Specimens F58 and Z32 are serpentines from a peridotite-basic dyke contact, with clear evidence of shearing effects. The serpentine is, however, identifiable as lizardite.

Deer, Howie and Zussman (1963) suggest however that antigorite may be found where there is no evidence of shearing. The chemical environment may have an important influence on the formation of chrysotile or antigorite. Hess et al. (1952) have suggested that in general olivine yields chrysotile, and enstatite, antigorite. However although the harzburgite contains enstatite there is no evidence for antigorite in the serpentinised varieties.

Six serpentinites (A2, F58, Z72A, F75, F101, F142) have been heated to 1200°C in the differential thermal analysis apparatus. The following reactions may be identified, fig.23. The serpentines lose H_2^-O at 104°C-113°C, iron is oxidised at 250°C-327°C and structural water lost from lizardite at 644°C-675°C. In some specimens a further endothermic reaction was observed at 687°C-720°C, this possibly relates to the loss of structural water from chrysotile. Further heating resulted in an

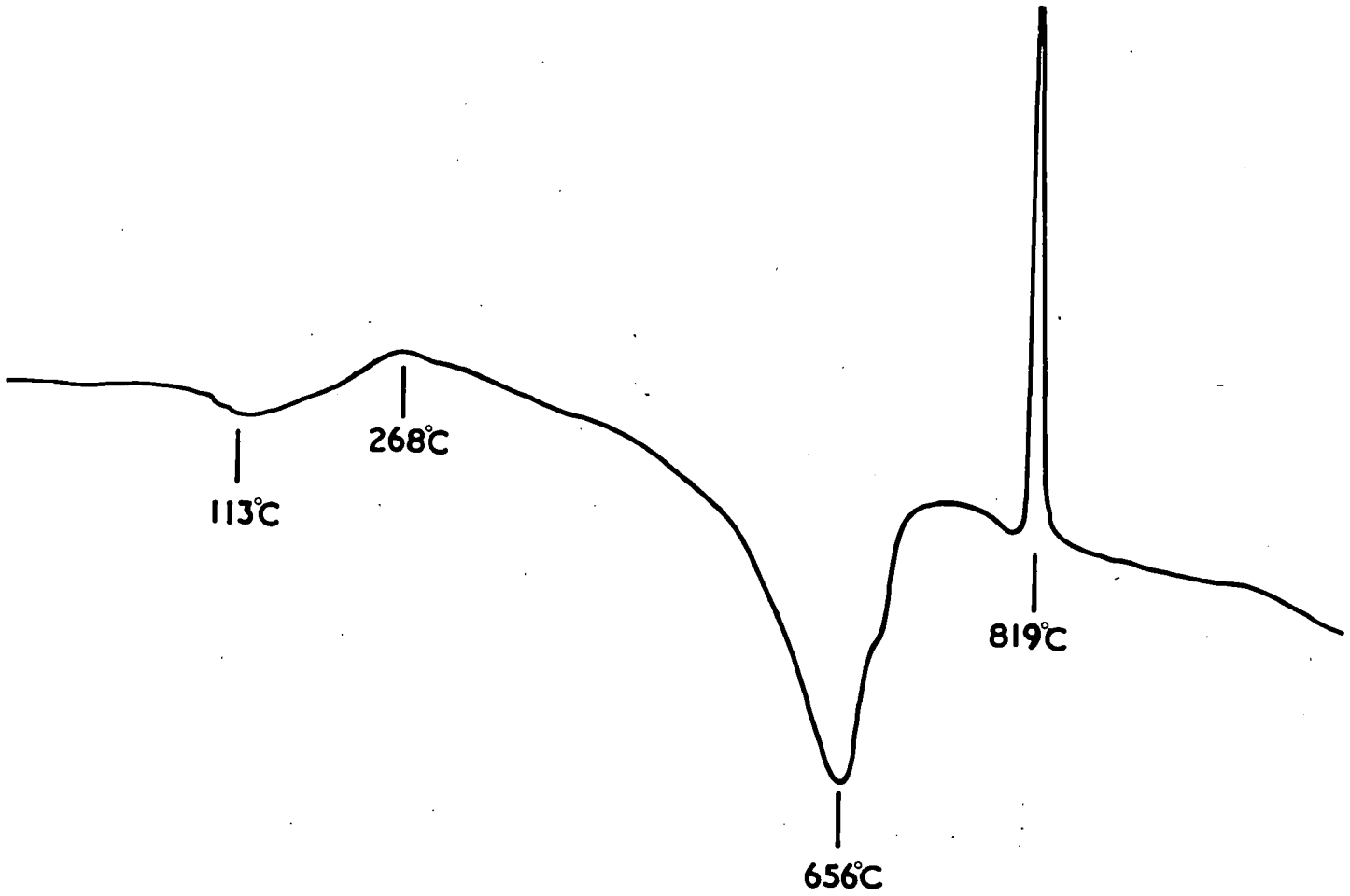

Differential thermal analysis record of serpentinite, F75

FIG. 23

exothermic reaction at 811°C-821°C which subsequent diffraction examination suggested was attributable to the formation of olivine and enstatite.

Pyroxenite

Pyroxenites occur as veins, ranging from a few cm up to 30-40 cm in thickness and cutting the peridotite with which they are in sharp contact. They constitute a very minor fraction of the entire peridotite mass but are known throughout the area and are particularly concentrated in the Andizlik and Zimparalik mine areas as previously described.

The pyroxenite veins are mainly composed of orthopyroxene although a single vein bearing considerable clinopyroxene is known.

Orthopyroxenite veins

In these veins orthopyroxenes constitute 60 to 85 percent of the rock with crystals up to 7 mm in length, mostly subhedral. Subsidiary clinopyroxene, olivine and very minor chromite comprise the remainder of the rock. Kink bands are strongly developed in the orthopyroxenes, and clinopyroxene exsolution lamellae are common, parallel to (100). The orthopyroxenes are of two kinds; biaxial positive enstatite and biaxial negative bronzite. The optic axial angle was measured at 77° in the specimen F51A. Many of the orthopyroxene crystals are crushed into smaller fragments along the crystal boundaries, where they are also partly altered to bastite.

The clinopyroxene occurs as lath like crystals, in parts altered to tremolitic amphibole and pale green chlorite, Plate 27. Olivine is rare, comprising no more than 1-2 percent of the vein, it is surrounded by a serpentine rim. Despite the fact that the pyroxenite veins are younger than the peridotite, some small anhedral to subhedral chromite crystals are seen enclosed in the orthopyroxenes. They constitute about 0.1 to 0.2 volume percent of the rock.

Orthopyroxenes from 11 pyroxenite veins have been examined by X-ray diffraction using the methods described previously, page 45. Table 2 indicates that the orthopyroxenes vary from En_{85} to En_{91}, in agreement with their optical identification as bronzite and enstatite. The orthopyroxenes of the harzburgites range from En_{89} to En_{99}, table 2, they are thus more Mg rich than those of the pyroxenites which is in agreement with the generation of the pyroxenite from peridotite at a late stage.

The clinopyroxenite vein

This type of vein was only found near Madenoyugu tepe in the north, specimen F135. The vein is 7 cm thick and can be followed for 2 to 3 m. It has a sharp contact with the host peridotite, though the boundary is marked by a thin serpentinised zone in the peridotite.

Clinopyroxene constitutes about 60 percent of the rock, the other minerals are orthopyroxene, olivine and altered varieties

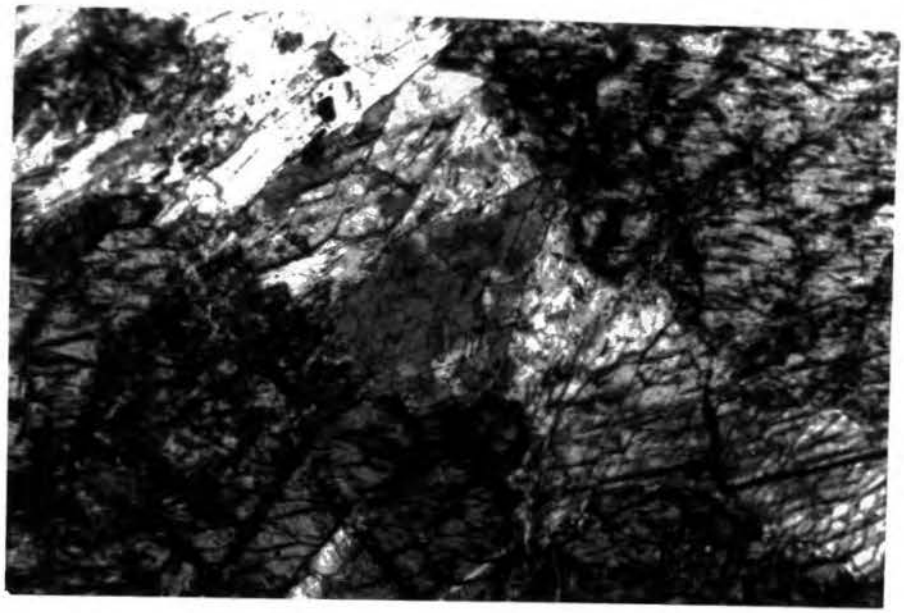

Plate 27 Tremolite developed in an orthopyroxenite vein (crossed polars, X32).

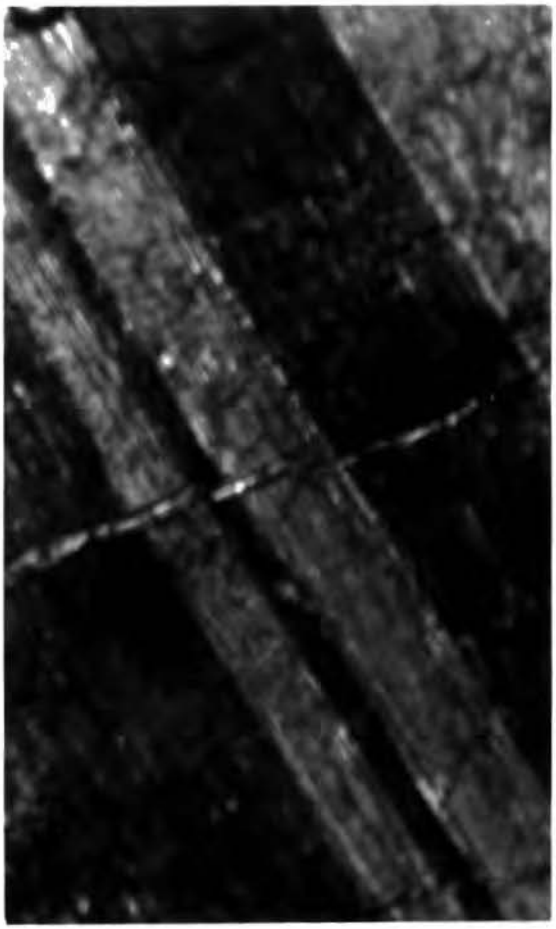

Plate 28 Polysynthetic twinning in clinopyroxene from the clinopyroxenite vein (crossed polars, X32).

of these minerals (bastite, tremolite, chlorite) together with very minor chromite.

The orthopyroxenes are subhedral and up to 5-6 mm in length, they include clinopyroxene exsolution lamellae parallel to (110) cleavage trace. The orthopyroxenes are bent or broken with no preferred orientation. They are identified optically as enstatite and bronzite and are partly altered to bastite.

The clinopyroxenes are subhedral ranging up to 1.5 cm in length, they show polysynthetic twinning, Plate 28, and an optic angle of 55°; in places they are partly altered to tremolite and chlorite.

Hand picked clinopyroxene crystals were examined by X-ray diffraction, using CuKα radiation, following the technique of Brown (1960). The Ca:Mg:Fe ratio of the clinopyroxene was estimated as $Ca_{43}:Mg_{43}:Fe_{14}$, from the position of the (060) and (600) reflections, fig.24. This composition was determined by plotting b ($=6.d_{060}=8.92686$) and a sin β ($=6.d_{600}=9.3723$) values on the pyroxene part of the $CaSiO_3$ - $MgSiO_3$ - $FeSiO_3$ triangular diagram, fig.25.

Basic dykes

The basic dykes are mainly composed of clinopyroxene, plagioclase feldspar, and ilmenite. The rock is dark greyish green in colour and individual minerals are difficult to distinguish in hand specimen. In places the dykes are heavily altered by

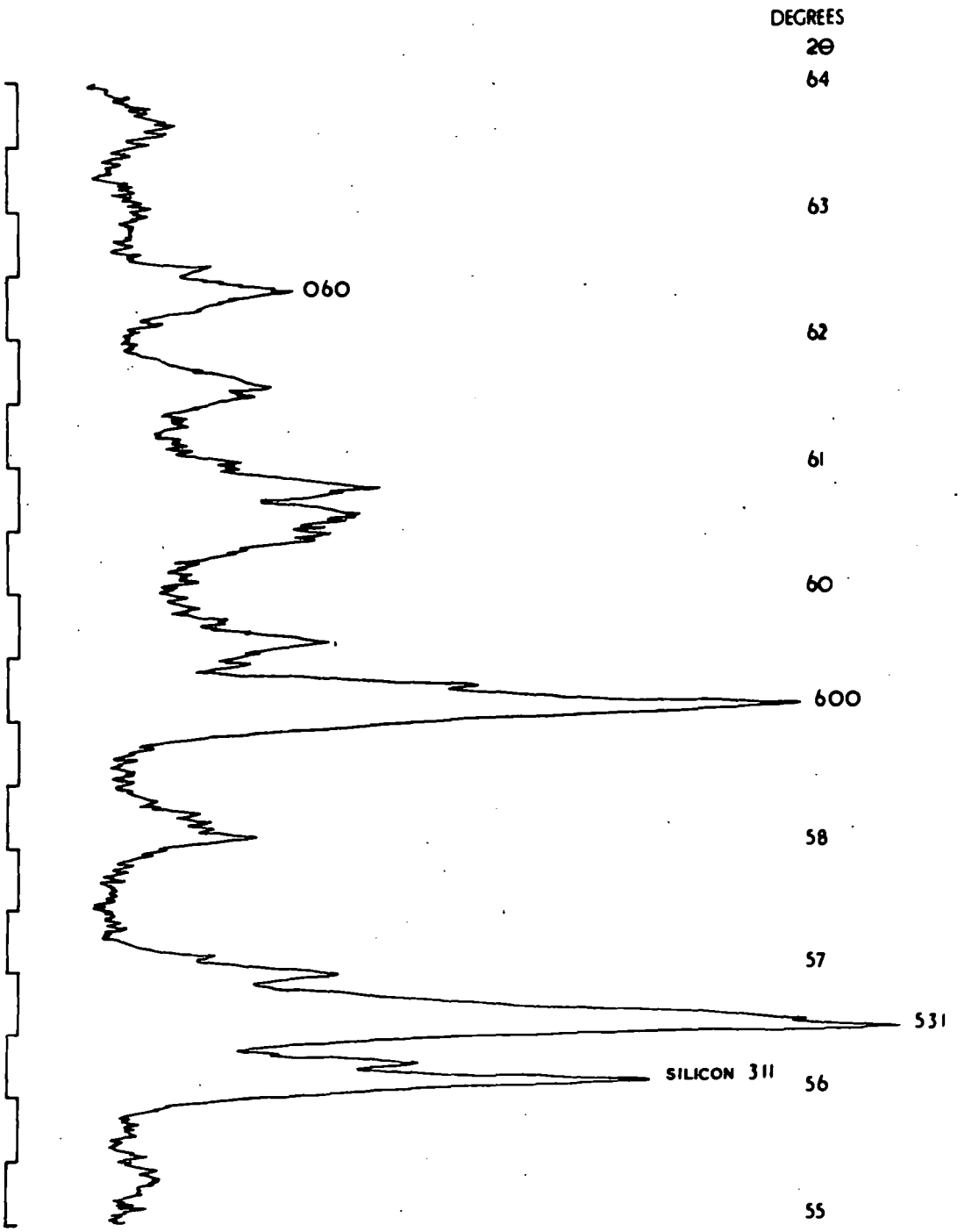

DIFFRACTOMETER RECORD OF CLINOPYROXENE NO F 135 CuKα RADIATION

FIG.24

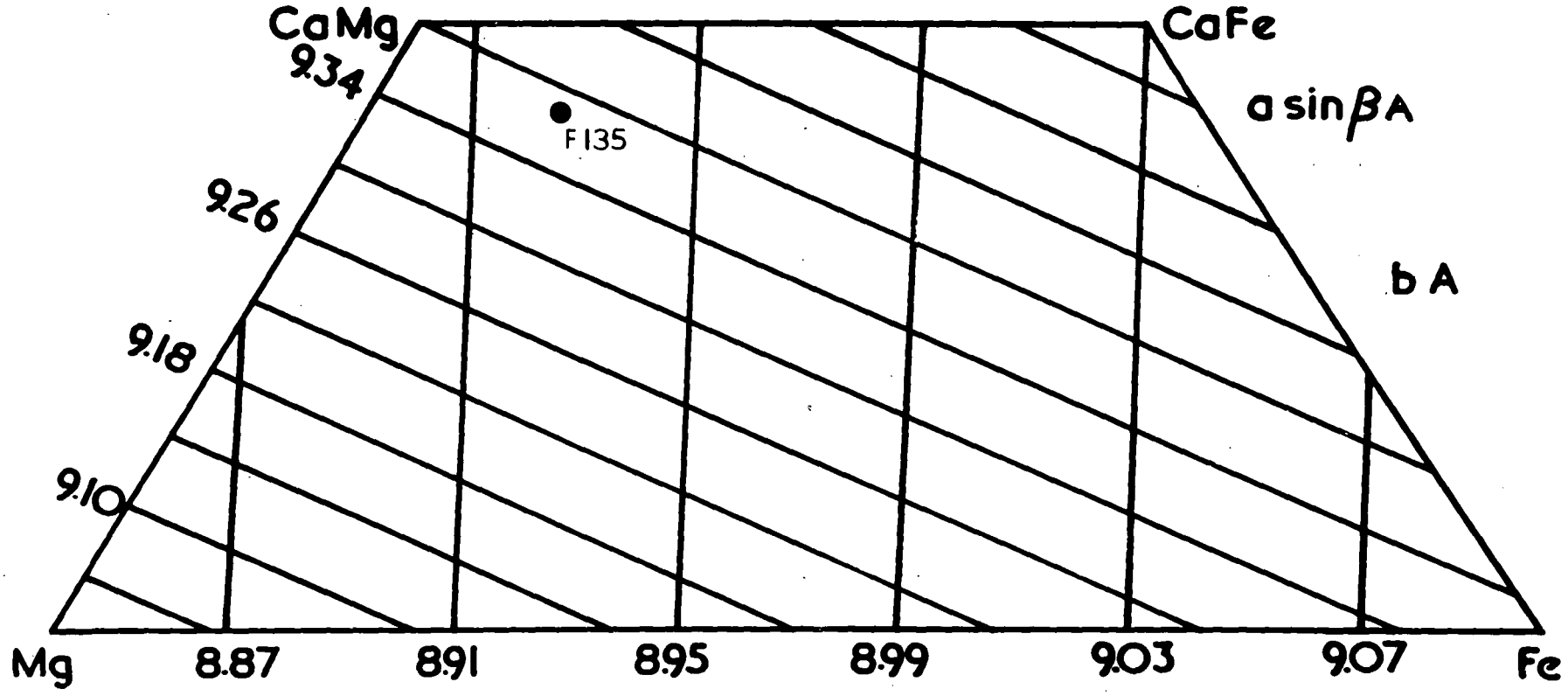

x-ray determinative chart for clinopyroxes (after Brown 1960)

FIG.25

weathering. Plagioclase constitutes about 50 percent of the rock and is heavily sausseritised. The grain size reaches 4 mm and shows moderate zoning. Albite, combined albite-carlsbad and pericline twinning are evident although albite twinning is most common.

The plagioclases range in composition from An_{33} Ab_{67} to An_{60} Ab_{40}; in the range andesine to labradorite.

Clinopyroxene comprises 30 to 40 percent of the rock, with anhedral to subhedral grains reaching 1 mm in length. Their optics identify them as augite, 2V measurements giving the optic axial angle as 48° (F7). Birefringence is strong, 2nd to 3rd order, and some of the pyroxenes show the 'hourglass' type of extinction. Most clinopyroxenes show some degree of alteration and have a light brown hornblende rim, Plate 29. In some grains the development of the hornblende is more extensive and augite is completely replaced by the former. The hornblende is pleochroic from Y, light brown to X, dark brown. Both augite and hornblende have been replaced by light green, faintly pleochroic; chlorite at a later stage.

Orthopyroxene is generally absent though some sections indicate a very small content.

Skeletal opaque minerals have been identified as ilmenite, Plate 30, grains range from 0.2 to 0.3 mm in diameter and comprise 2 to 3.5 percent of the rock. Reflectivity measurements taken

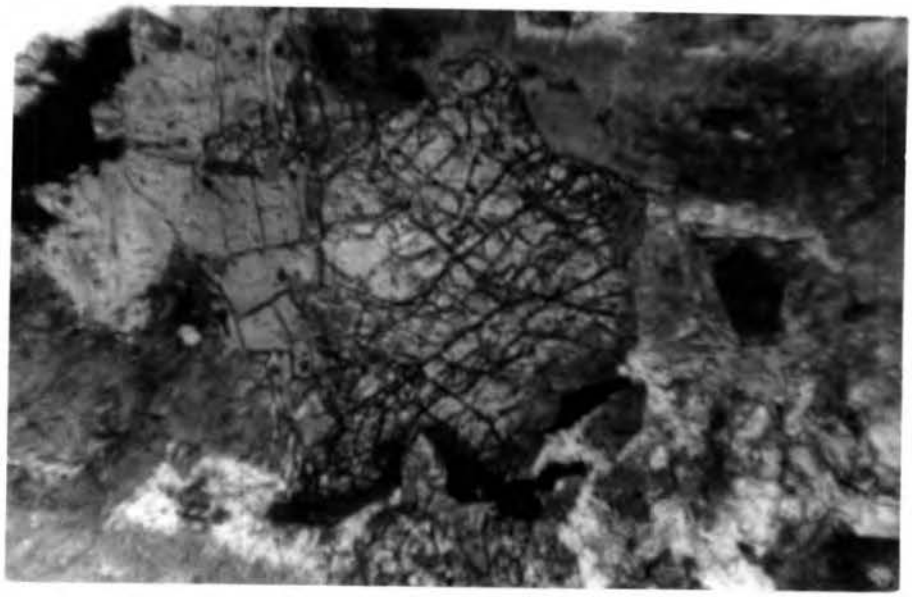

Plate 29 An amphibole rim to augite from a basic dyke (X32).

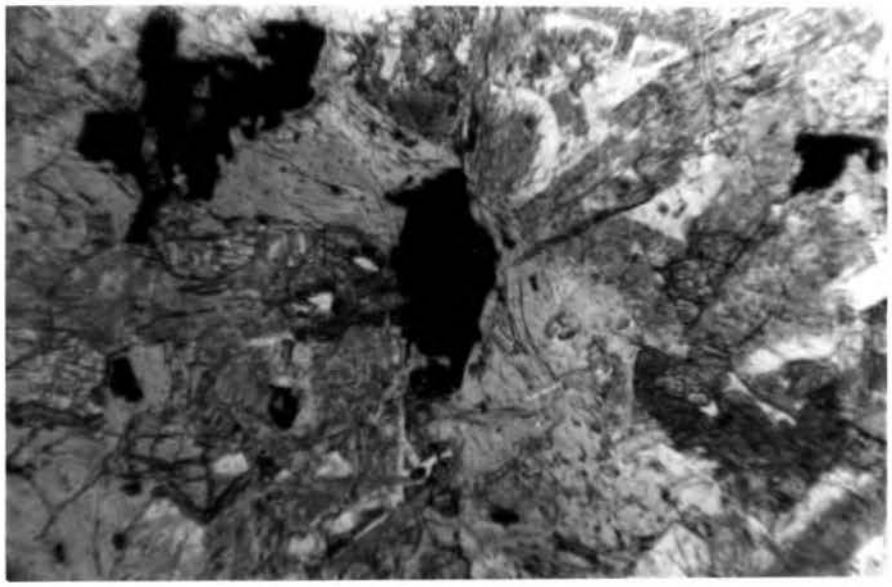

Plate 30 Skeletal ilmenite crystals from a basic dyke (X32).

at wavelengths of 480, 520, 580 and 640 mμare in the range of values reported for ilmenite by Uytenbogaardt (1951) and Schouten (1962). Apart from ilmenite, minor amounts of fine grained magnetite and pyrite are present. No native platinium was discovered in these dykes. The clinopyroxenes usually enclose the plagioclase laths and preserve an ophitic to subophitic texture, Plate 31. Near their contacts to the surrounding peridotite the dykes are sheared and the grain size diminishes, otherwise the rock is of fine to medium grain size and occasionally porphyritic, Plate 9.

The variability of plagioclase composition from andesine to labradorite, and the texture of the dykes suggest variation in composition from gabbro and dolerite to diorite. The distribution of these different rock types show no particular pattern.

Tremolite veins

Tremolite occurs as light to dark green, fibrous crystals in veins traversing the chromite ore bodies in an irregular manner. These fibres are 6-7 mm long forming subhedral crystals. They are colourless in thin section and show second order birefringence. The veins include minute chromite crystals. Some of the tremolite has been altered to talc.

It appears possible that primary magmatic water of the peridotite magma has been concentrated in the neighbourhood of the chromites, pneumatolitic and hydrothermal activity causing

Table 4 d spacings of tremolites

DPCJ*		F139B		ZU45		AU3		
dA°	Intensity	dA°	Intensity	dA°	Intensity	dA°	Intensity	hkl
-	-	9.025	19	8.99	22	9.035	11	020
8.43	s	8.432	83	8.425	92	8.457	65	110
5.10	w	5.094	18	5.088	7	5.101	9	130,001
4.89	m	4.855	22	4.879	8	4.778	10	$\bar{1}11$
4.52	m	4.502	27	4.524	18	4.517	16	040
4.22	w							
4.01	vw							
3.88	m	3.873	27	3.877	8	3.883	6	$\bar{1}31$
3.38	s	3.377	38			3.371	11	150,041
3.27	s	3.270	62	3.268	64	3.277	43	240
3.11	s	3.129	100	3.131	100	3.132	100	310
3.00	vvw							
2.94	s	2.935	60	2.934	33	2.938	42	$\bar{1}51$
2.80	w	2.809	24	2.809	28	2.810	17	330
2.74	vw	2.740	25	2.740	16	2.737	10	$\bar{4}21$
2.70	s	2.703	72	2.696	47	2.703	38	151
2.59	s	2.589	34	2.586	19	2.590	13	$\bar{1}12$,061
2.53	s	2.540	42	2.540	23	2.540	10	$\bar{2}02$,002
2.41	vvw	2.411	10	2.416	5			$\bar{1}32$
2.38	vw	2.386	16	2.384	11	2.387	7	350,400
2.33	w	2.337	36	2.336	22	2.338	22	$35\bar{1}$
2.298	vw	2.296	12	2.284	6			420,071
2.270	vw							
2.205	vvw					2.202	3	
2.182	vvw							
2.162	m	2.160	23	2.158	14	2.165	8	171,261
2.040	w	2.043	8			2.037	6	081,280
2.015	w	2.018	13					202
1.958	vw	1.963	7					$28\bar{1}$,190
1.934	vvw							
1.889	vw	1.897	4	1.898	5	1.899	9	
1.865	vw	1.865	11					460,$\bar{1}91$
1.837	vw							
1.808	vw							
1.746	vw			1.759	4			
1.686	w	1.686	7					003,$\bar{2}82$
1.648	w	1.651	7	1.649	7			$210\bar{1}$
1.635	vvw					1.640	4	
1.616	vw	1.616	7					
1.578	w							
1.555	vvw							
1.529	vw							
1.511	w	1.514	10					
1.501	vw	1.504	13	1.503	6	1.504	6	
1.468	vw							
1.455	vvw	1.457	10					
1.435	m	1.442	14			1.440	13	
1.362	vw							
1.340	vw							
1.333	vw							

DPCJ* Chrome tremolite from Hangha, Sierra Leone, Dunham, Phillips, Chalmers and Jones (1958) p.40.

the formation of tremolite veins along fractures. A possible reaction is:

$$3MgSiO_3+2CaMgSi_2O_6+SiO_2+H_2O \longrightarrow (OH)_2Ca_2Mg_5Si_8O_{22};$$

Three hand picked tremolite specimens (AU3, ZU45 and F139B) have been examined by X-ray diffraction and their d spacings compared with the values recorded by Dunham et al. (1958), table 4.

Amphibolites

The amphibolites, which occur locally as xenoliths within the ultramafics, have well developed schistocity and are shiny black in hand specimen; small white plagioclases can be identified with the naked eye. They are composed of amphibole, plagioclase, opaques and apatite. Amphiboles comprise 80 to 85 percent of the rock, they are greenish brown in colour with light brown to brown pleochroism, the grain size is around 1 mm. Identified as hornblende, they show strong orientation along the longer dimensions of the rhombohedral ~~faces~~ sections, Plate 32.

Plagioclase is interstitial to the amphibole and is heavily sausseritised. Normative plagioclase compositions have been calculated to $An_{54}Ab_{46}$ and $An_{63}Ab_{37}$, labradorites.

The opaque minerals comprise black anhedral crystals of ilmenite, oriented parallel to the schistosity direction. Six sided to round, fine grained apatite crystals occur as inclusions in the hornblende as well as interstitial to hornblende and ilmenite.

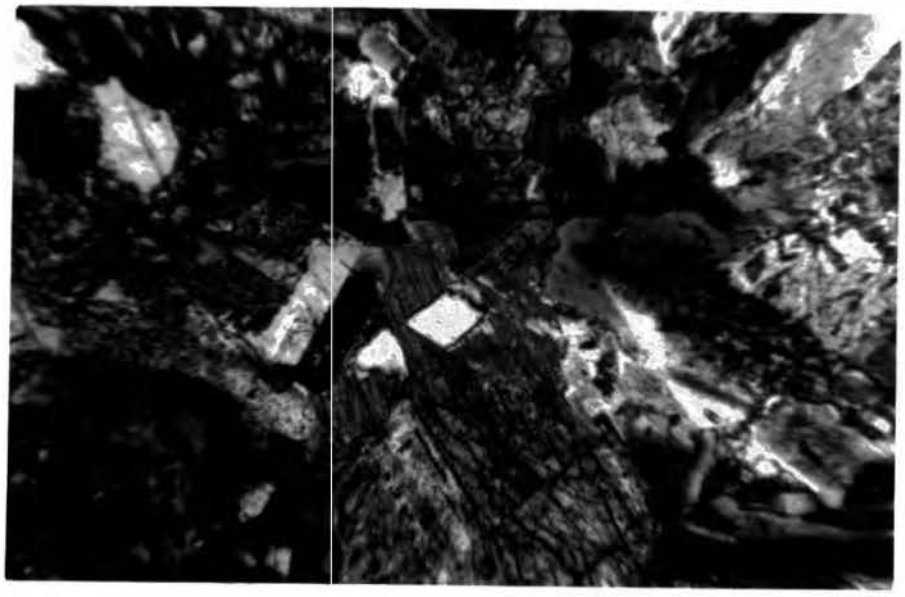

Plate 31 Ophitic and subophitic texture from a basic dyke (crossed polars, X20).

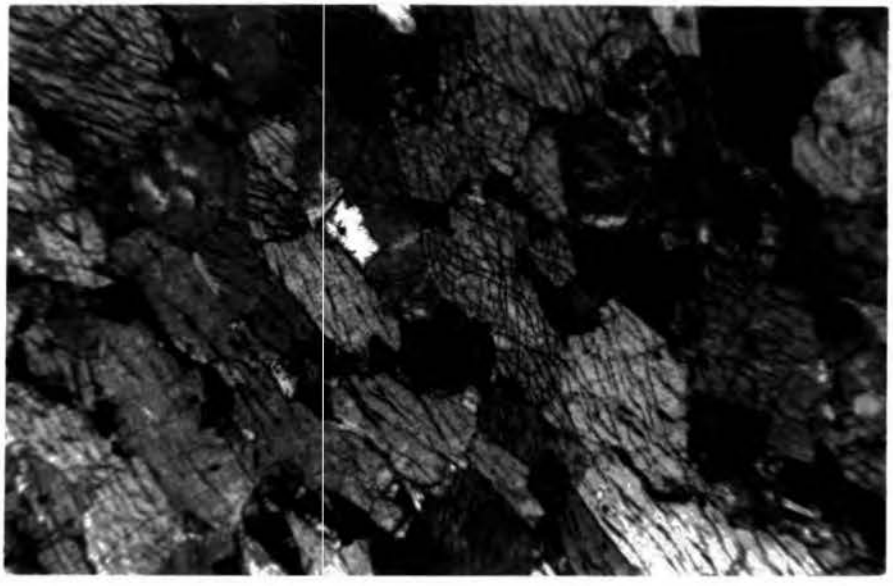

Plate 32 Amphibolite (crossed polars, X20).

CHAPTER 4

CHEMISTRY OF THE ULTRAMAFIC AND BASIC ROCKS

Analytical techniques

Silicate rocks from the Andizlik-Zimparalik area have been analysed by X-ray fluorescence spectrography and conventional wet-chemical techniques.

Sample preparation

The specimens were washed to remove dust, and the weathered parts were cut away and discarded. Preliminary crushing in the Sturtevant jaw crusher reduced the samples to chips of mm to cm size, this was followed by grinding in the tungsten carbide vials of the Tema disc mill which reduced the sample to a powder of around 300 mesh. The powders were pelletized under a pressure of 5 tons per square inch; 3 drops of "Mowiol" were added as a binder and the pellets backed with boric acid powder.

Analysis

11 elements have been determined by X-ray fluorescence spectrography and calculated as SiO_2, TiO_2, Al_2O_3, total Fe as Fe_2O_3, MgO, CaO, MnO, Na_2O, K_2O, P_2O_5 and S. (W-1) was used as master standard together with 25 secondary standards comprising chemically analysed rocks covering the whole compositional range. Mass absorbtion corrections were made by an iterative process using the computer technique described by Holland and Brindle (1966). Precision was high with coefficients of variation usually within $\pm$ 1 percent.

Line interference between MnKα and CrKβ was a problem in determination of Mn in peridotites containing chromite. The interference was substantially reduced by dropping the operative voltage of the X-ray tube below that required for optimum excitation of CrKβ.

Standards were prepared by an addition technique described by Hirst and Dunham (1963) for the determination of Cr and Ni by X-ray fluorescence. The X-ray method provides values for total Fe expressed as Fe_2O_3. Ferrous iron was determined by the conventional HF - H_2SO_4 dissolution followed by permanganate titration.

The Penfield tube was used for determination of total water and these values were subsequently adjusted for loss at 110°C to produce values for H_2O^+ and H_2O^-.

Chemistry of the peridotites

A total of 85 harzburgites and dunites showing all stages of serpentinisation have been analysed for the elements listed above, these analyses appear in tables 1 and 2 of the appendix except for those which appear in tables 5 and 6. The specimens were chosen to cover the representative rock types, and on an areal basis to give a measure of variation within the peridotite body as a whole. Some of the specimens are highly oxidized, the oxidation ratio $\left(\frac{\text{total iron (as } Fe_2O_3)}{Fe_2O_3}\right)$ changing from 9.96 (F251) to 1.05 (A90) in highly oxidized samples. Highly oxidized specimens

Table 5 Analyses (weight percent) and normative mineralogy of serpentinised ultramafics

	F251	F237	F233	F256	F225	F245	A13	F243	Z103	A21	Z101	F204	Z82	F239	F44	F6	F220	AU7	A91	ZU17	ZU37	$\bar{X}$
SiO_2	43.84	42.30	41.79	43.65	42.31	41.81	42.03	40.38	41.60	41.42	40.09	40.71	40.20	40.25	39.49	38.36	39.65	35.99	34.68	38.63	37.55	40.00
Cr_2O_3	0.34	0.31	0.33	0.37	0.33	0.32	0.36	0.28	0.29	0.30	0.27	0.33	0.28	0.27	0.26	0.27	0.26	0.22	0.28	0.23	0.23	0.28
Al_2O_3	0.29	0.14	0.33	1.72	0.56	0.43	0.24	0.26	0.26	0.30	0.16	0.38	0.19	0.05	0.22	0.30	0.25	-	-	0.17	-	0.21
Fe_2O_3	0.79	1.99	1.37	1.41	2.68	3.26	3.67	3.52	3.97	4.51	4.01	4.43	5.05	6.26	5.23	4.67	5.93	5.82	4.29	6.76	6.14	4.85
FeO	6.42	5.67	6.29	6.32	4.82	4.59	4.31	4.24	3.72	3.39	3.64	2.87	2.66	2.16	2.36	2.51	1.43	1.09	1.65	0.63	0.38	2.62
MgO	46.28	44.82	44.57	39.74	42.75	41.76	41.84	42.31	40.83	40.05	41.75	39.75	40.29	39,04	40.18	40.22	38.94	40.51	41.43	37.23	39.46	40.41
CaO	0.43	0.47	0.69	1.82	0.88	0.86	0.59	0.53	0.56	0.53	0.58	0.56	0.58	0.26	0.44	0.58	0.36	0.07	0.09	0.03	0.02	0.40
MnO	0.13	0.13	0.14	0.14	0.13	0.14	0.13	0.13	0.14	0.14	0.14	0.14	0.14	0.14	0.13	0.12	0.12	0.11	0.09	0.13	0.07	0.13
NiO	0.43	0.42	0.40	0.36	0.38	0.38	0.39	0.39	0.37	0.38	0.38	0.35	0.37	0.38	0.37	0.37	0.37	0.46	0.53	0.35	0.46	0.39
Na_2O	0.13	0.09	0.07	0.15	0.07	0.08	0.59	0.19	.0.13	0.11	0.05	0.12	0.12	0.11	0.13	0.06	0.10	0.13	0.11	0.05	0.12	0.11
K_2O	-	-	-	0.01	0.01	-	-	-	-	0.01	-	-	-	-	-	0.01	-	-	-	-	-	-
^+H_2O	0.22	2.42	2.73	2.98	3.84	4.02	5.16	6.18	6.60	7.12	7.59	8.52	9.00	9.39	9.74	10.97	11.25	13.47	13.88	13.96	14.53	8.93
^-H_2O	0.03	0.28	0.29	0.27	0.24	0.29	0.39	0.47	0.76	1.00	0.54	0.87	0.50	0.73	0.71	0.94	0.67*	1.51	1.77	1.46	0.91	0.84
S	0.03	0.37	0.38	0.42	0.40	0.67	0.34	0.67	0.37	0.35	0.40	0.67	0.33	0.71	0.49	0.34	0.50	0.47	0.51	0.30	0.09	0.41
								99.55														
Chromite	0.5	0.5	0.5	0.5	0.5	0.5	0.5	0.5	0.5	0.5	0.5	0.5	0.5	0.5	0.5	0.5	0.5	0.3	0.5	0.3	0.3	0.5
Pyrite	0.1	0.7	0.7	0.8	0.7	1.3	0.7	1.3	0.7	0.7	0.8	1.3	0.6	1.3	0.9	0.7	1.0	0.9	1.0	0.5	0.2	0.8
Magnetite	0.9	1.9	1.2	1.9	3.0	3.3	4.7	3.7	4.9	5.6	4.9	5.1	7.2	7.7	6.5	5.8	6.3	5.3	5.1	3.7	2.8	6.0
Hematite	-	-	-	-	-	-	-	-	-	-	-	-	-	-	-	-	0.9	2.1	-	3.8	4.2	-
Tremolite	-	-	-	-	-	-	-	-	-	-	-	-	-	-	3.2	4.1	2.4	0.4	0.4	0.4	-	-
Clinopyroxene	1.8	1.8	2.6	7.2	3.5	3.3	2.3	1.9	2.2	1.9	1.2	2.2	2.5	1.1	-	-	-	-	-	-	-	1.5
Chlorite	1.4	0.3	1.4	7.8	2.5	2.5	0.8	1.1	1.4	1.4	0.6	1.9	1.1	-	0.8	1.7	1.1	-	-	0.8	-	1.1
Olivine	73.3	63.1	65.1	44.3	45.7	38.1	37.7	39.4	26.2	21.7	30.0	16.9	15.3	7.3	13.8	12.4	-	-	8.1	-	-	17.1
Serpentine	0.3	18.2	19.6	15.2	29.4	37.7	38.8	46.4	49.3	53.3	57.7	63.3	67.9	72.0	73.3	69.7	87.1	82.0	71.4	84.7	86.4	67.5
Brucite	-	-	-	-	-	-	-	-	-	-	-	-	-	-	-	3.2	-	6.8	9.1	-	2.7	-
Orthopyroxene	22.1	12.3	7.6	21.5	13.5	13.2	13.6	4.3	14.1	13.2	2.6	7.4	4.6	8.9	-	-	-	-	-	-	-	4.0
^-H_2O	0.03	0.28	0.29	0.27	0.24	0.29	0.39	0.47	0.76	1.00	0.57	0.87	0.50	0.73	0.71	0.94	0.36*	1.51	1.77	1.46	0.91	0.84
Excess ^+H_2O																			1.78	2.77	2.41	
Excess MgO																						
Excess SiO_2																				1.44		
N	92	92	91	89	93	91	93	92	93	93	92	90	95	96	94	90			92		92	

N normative olivine and pyroxene compositions *Part of ^-H_2O used as ^+H_2O F251 through ZU37 - Harzburgites $\bar{X}$ Average Harzburgite

F68A	F208	94263 I	94263 IV	II	V
36.64	34.75	39.31	43.37	40.87	39.90
2.07	0.41	0.74	0.56	0.25	0.33
0.74	0.09	-	1.19	3.93	3.74
5.24	5.93	1.60	0.18	6.17	5.92
2.08	2.03	7.52	7.41	2.37	2.09
41.02	41.34	47.03	45.35	32.86	36.21
0.18	0.22	-	0.79	2.36	1.54
0.12	0.14	0.14	0.14	0.29	0.08
0.40	0.48	-	0.14	0.17	-
0.06	0.05	-	0.15	0.39	0.10
-	-	-	-	0.04	0.02
10.43	13.11	3.68	0.64	8.95	10.11
0.45	0.83	0.16	0.06	1.09	0.33
0.42	0.43	-	-	0.01	-
3.7	0.8	1.3	1.0	0.5	0.5
0.8	0.8	-	-	-	-
5.8	7.4	1.9	-	8.8	7.0
-	-	-	-	0.3	1.0
0.8	1.6	-	-	17.0	11.3
-	-	-	3.0	-	-
1.4	-	-	6.1	20.8	20.2
8.0	1.5	67.5	72.8	-	0.8
74.0	77.7	28.2	-	44.7	55.5
3.3	8.6	0.5	-	-	-
-	-	-	16.9	4.0	4.3
0.45	0.83	0.16	0.06	1.09	0.33
	0.27				
1.44		1.64			
				2.1	
90	90	89	90		

F68A and F208 - dunite

94263 I and IV from Challis (1965), II and IV from Green (1964)

Table 6 Analyses of harzburgites (weight percent) given in Table 5 calculated on a water free basis.

	F251	F237	F233	F256	F225	F245	A13	F243	Z103	A21	Z101	F204	Z82	F239	F44	F6	F220	AU7	A91	ZU17	ZU37	$\bar{X}$
SiO_2	43.45	43.47	43.09	45.12	44.21	44.11	44.50	43.26	44.91	45.08	43.64	44.93	44.42	44.78	44.10	43.55	45.02	42.33	41.11	54.67	44.41	44.40
Cr_2O_3	0.34	0.32	0.34	0.38	0.34	0.33	0.38	0.30	0.31	0.35	0.30	0.36	0.31	0.30	0.29	0.31	0.29	0.26	0.33	0.27	0.27	0.31
Al_2O_3	0.29	0.15	0.34	1.78	0.58	0.45	0.26	0.28	0.28	0.33	0.18	0.42	0.21	0.06	0.25	0.34	0.29	-	-	0.20	-	0.23
Fe_2O_3*	7.87	8.46	8.55	8.64	8.32	8.77	8.39	8.76	8.70	8.97	8.72	8.38	8.82	9.62	8.73	8.44	8.52	8.26	7.23	8.81	7.76	8.58
MgO	46.40	46.07	45.96	41.08	44.57	44.06	44.30	45.33	44.07	43.59	45.44	43.87	44.52	43.44	44.87	45.66	44.21	47.65	49.12	44.02	46.67	44.86
CaO	0.43	0.48	0.71	1.88	0.92	0.91	0.63	0.57	0.60	0.58	0.63	0.62	0.64	0.29	0.49	0.66	0.41	0.09	0.11	0.04	0.02	0.44
MnO	0.13	0.14	0.14	0.14	0.14	0.15	0.14	0.14	0.15	0.15	0.15	0.15	0.15	0.16	0.15	0.14	0.14	0.13	0.11	0.15	0.08	0.14
NiO	0.43	0.43	0.41	0.37	0.40	0.40	0.40	0.42	0.40	0.42	0.41	0.39	0.41	0.42	0.41	0.42	0.42	0.54	0.63	0.42	0.55	0.43
Na_2O	0.13	0.09	0.07	0.16	0.07	0.09	0.63	0.21	0.44	0.12	0.06	0.13	0.13	0.13	0.15	0.07	0.12	0.16	0.13	0.06	0.14	0.12
K_2O	-	-	-	0.01	0.01	-	-	-	-	0.01	-	-	-	-	-	0.01	-	-	-	-	-	-
S	0.03	0.38	0.39	0.43	0.42	0.71	0.36	0.72	0.40	0.38	0.44	0.74	0.37	0.79	0.55	0.39	0.57	0.56	0.61	0.36	0.11	0.45

*Total iron as Fe_2O_5

$\bar{X}$ average harzburgite

have been eliminated and play no part in conclusions regarding the chemistry of the silicate rocks.

The major difficulty in comparing ultramafic rocks from different parts of the intrusion lies in their variable serpentinisation. The degree of serpentinisation varies from zero to 100 percent, and thus the analyses of serpentinised peridotites should only be compared with those of unserpentinised or less serpentinised peridotites after allowance for the degree of serpentinisation. Comparisons of analyses are thus more likely to be relevant if made on a water free basis.

In the Andizlik-Zimparalik area the MgO content of the peridotite varies from 41.08 to 49.12 percent, characteristic of the alpine type of peridotite, while the SiO_2 content changes from 41.27 to 47.13 percent. Total iron, shown as Fe_2O_3 in table 6 and table 2 (in the appendix), varies from 7.23 to 9.61 percent. Other elements are generally in minor amounts in the peridotites.

Goles (1967) gives a list of minor elements present in peridotites, and his results, together with those of Turekian and Wedepohl (1961) and Vinogradov (1962) are shown in table 7. Minor element values for the Andizlik-Zimparalik area are also shown in this table they are in a good agreement with those from the literature except in the case of S, which is higher in the present samples. P, Ti and K are below the detection limit.

The source of Cr is mainly the chromite crystals present

Table 7 Minor elements range from the Andizlik-Zimparalik peridotite together with average values from the literature, in ppm.

Elements	A	B	C	D
Cr	1600	2000	2400	1650-3300
Mn	1620	1500	1040	620-1240
Ni	2000	2000	1500	3000-4950
Na	4200	5700	1040	0-3700
Al	20000	4500	10000	0-9420
P	220	170	-	-
S	300	100	-	300-10100
Ca	25000	7000	-	210-13400
Ti	300	300	-	-
K	40	300	200	-

A Turekian & Wedepohl (1961)
B Vinagradov (1962)
C Goles (1968)
D Andizlik-Zimparalik
- not detected

in the peridotite, S generally comes from pyrite and Ca is a reflection of the clinopyroxene or tremolite content of the specimen. Al will occur in the pyroxenes, or chlorite and chromite, while Na is probably present, in small amount, in the pyroxenes.

Only two of the analysed specimens, F68A and F208, table 5 and table 2 (in the appendix), have been identified as dunite by the thin section study. They show a lower SiO_2 but higher MgO content than the harzburgites. The dunites are also low in CaO reflecting the absence of clinopyroxene or tremolite. F208 is also low in Al_2O_3 but not F68A which contains 2.32 percent chromite. The average of 36 harzburgite analyses is given in tables 5 and 6.

The Si/Mg ratio of the peridotite changes from 0.839 to 1.098 and the Fe/Mg ratio from 0.16 to 0.22. No clear pattern emerges when these ratios are plotted on a map to study the compositional changes within the peridotite mass. There is a tendency for the Fe/Mg and Si/Mg ratios to be lower along the southern and northern contacts otherwise the distribution is haphazard, in accordance with the complicated tectonic history of the peridotite and its general uniformity of composition.

Representative harzburgite and dunite analyses have been recalculated on a water free basis and are plotted on an AFM triangular diagram with apices $Na_2O + K_2O$, MgO and FeO (total

iron), fig.26A, since the peridotites are true ultramafics the results are concentrated near the MgO corner of the diagram. This diagram confirms the uniformity of peridotite composition.

Because of the highly serpentinised nature of the peridotite the CIPW norm fails to give a realistic normative mineralogy, only in fresh peridotite does the CIPW norm approximate to the mode.

Hancock (1964) has presented a method for calculating the norms of serpentinised dunites. The method described here is a further development of Hancock's technique and is applicable not only to serpentinised dunites, but also to other types of serpentinised ultramafics.

Calculation of the normative mineralogy of serpentinised ultramafic rocks, after Engin and Hirst (1969), in press.

Since the olivine and pyroxene in peridotitic rocks are invariably deficient in iron, usually around Fo_{90}, it is very essential to have an accurate estimate of the amount of FeO available to form olivine in the norm. In this context it is incorrect to assign FeO to form either chromite or pyrite, these minerals are not soluble in the HF - H_2SO_4 used in determination of ferrous iron and their Fe contents therefore appear under Fe_2O_3 in the analyses. Allotment of iron for pyrite and chromite must therefore be made from Fe_2O_3 molecular proportions. Suppose (X) mol proportions of FeO are required for chromite

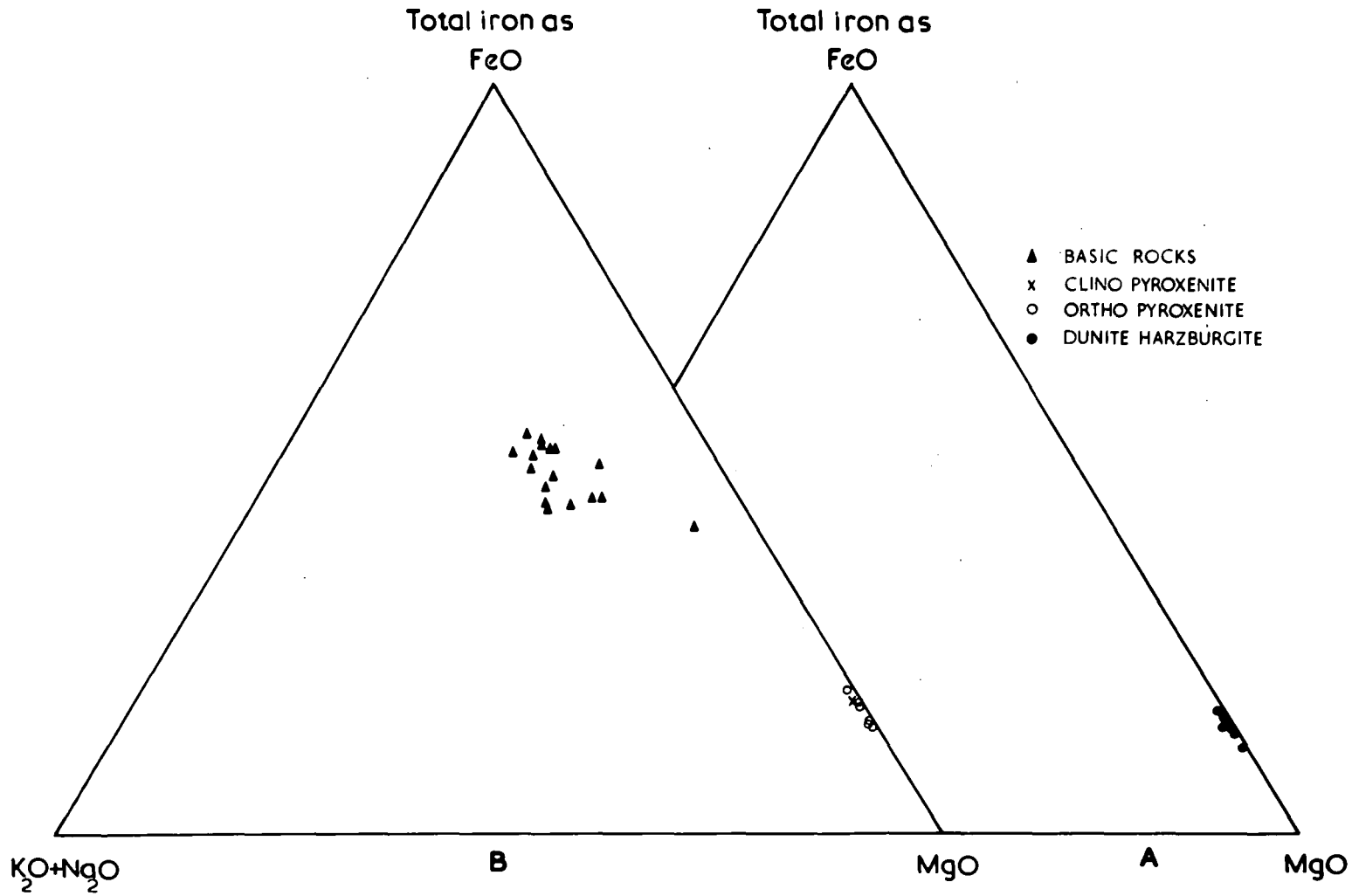

AFM DIAGRAMS OF BASIC AND ULTRAMAFIC ROCKS

FIG.26

(or pyrite) then the allotment of Fe_2O_3 would be $\frac{72}{160}$ 1.12X=0.5X. In the presence of considerable chromite the conventional CIPW allotment of $1Cr_2O_3:1FeO(\frac{1}{2}Fe_2O_3)$ would also result in errors in the FeO left for olivine. Chromite invariably contains Al_2O_3 and MgO and hence the suggested proportions are $3Cr_2O_3:1Al_2O_3:1Fe_2O_3:1MgO$.

Procedure

1. Determine molecular proportions and multiply by 1000.
2. Add MnO and NiO to FeO molecular proportion.
3. $3Cr_2O_3:1Al_2O_3:1Fe_2O_3:2MgO$ for chromite or $2Cr_2O_3:\frac{1}{2}Fe_2O_3:1$ MgO as explained above.
4. $1\ Fe_2O_3:4S$ for pyrite.
5. $1\ Fe_2O_3:1FeO$ for magnetite.

   residual Fe_2O_3 for hematite

   residual FeO to step 8 unless clinopyroxene is to appear.
6. $2\ CaO:5MgO:8SiO_2:1H_2O$ for tremolite

   or if clinopyroxene is known to occur from modal analyses then:

   $CaO:(MgO + FeO):2SiO_2$ for clinopyroxene.

   At this stage the ratio of available FeO + MgO is determined and preserved to the nearest significant figure in clinopyroxene.
7. $Al_2O_3:5MgO:3SiO_2:4H_2O$ for chlorite.
8. Using residual FeO from step 5 or 6, determine MgO for olivine from the known composition of olivine. (This must have been determined prior to this calculation by either X-ray

diffraction or electron probe analysis)

2 $FeO:SiO_2$

2 $MgO:SiO_2$ for <u>olivine</u>.

If no FeO were available at step 8, then forsterite will not appear in the norm.

9. 2 SiO_2:3MgO:2H_2O for <u>serpentine</u>.

The serpentine is determined by either remaining SiO_2, MgO or H_2O^+; four possibilities exist:

(1) If the serpentine content depends on available SiO_2, it is possible to have excess MgO and H_2O^+, these are reported as brucite, Step (10). If only MgO remains in excess it is reported as "<u>excess MgO</u>"; similarly in respect of H_2O^+.

(2) If the serpentine content depends on available MgO it is possible to have excess SiO_2 and H_2O^+. Excess SiO_2 is used to convert olivine to orthopyroxene, Step (11). The additional H_2O is reported as "<u>excess H_2O^+</u>".

(3) If the serpentine content depends on the available H_2O^+ it is possible to have excess MgO and SiO_2. The MgO is added to the available FeO+MgO for olivine (and/or orthopyroxene) thus modifying the original assumed Fo content. SiO_2 is added to the available SiO_2 for olivine and/or orthopyroxene. If the excess SiO_2 is more than one half the excess MgO, orthopyroxene will appear in the norm, Step (11). If the excess SiO_2 is less than one half the

excess MgO there will be more than sufficient MgO and FeO to satisfy olivine and a small excess of MgO would appear in the norm.

(4) If no H_2O is available at this stage to form serpentine, then Step 8 is re-determined. The olivine taking the Fo-Fa ratio corresponding to the available FeO+MgO. If excess SiO_2 remains after re-determining Step 8, then proceed to Step 11.

10. $MgO:H_2O$ for brucite.

Residual MgO as "excess MgO"

Residual H_2O as "excess H_2O"

11. Convert olivine into $(MgO+FeO):SiO_2$ for orthopyroxene. If available SiO_2 at this stage be insufficient to make over entirely to orthopyroxene distribute between x orthopyroxene and y olivine where

$$x + y = \text{total available MgO + FeO}$$

$$x + \frac{y}{2} = \text{total available } SiO_2$$

Weight percentages are obtained by multiplying the molecular proportions by the molecular weight of each mineral. The appearance of excess MgO, or excess H_2O, during Step 9 or 10 might reflect small errors in the analysis; particularly in H_2O at high contents. Alternatively the presence of excess MgO might imply that the assumed olivine composition of Step 8 was too rich in Fe. Other than assuming an arbitrary and more magnesian composition for the

olivine there is no alternative but to report as "excess MgO". Excess MgO can only be eliminated if the norm follows the course indicated in Steps 9(3) or 9(4). Step 9(3) raises the possibility of having additional oxidation (surface) effects manifest in the sample. In this case FeO values would be low, resulting in low normative olivine and creating excessive MgO and SiO_2 at this stage.

In the CIPW norm Na and K are calculated as feldspar. These constituents are in small amount and have been eliminated from the norm calculations. They are probably in pyroxene rather than feldspar.

Application

Norm calculations have been made on the peridotite analyses from the Andizlik-Zimparalik area, covering the whole range of serpentinisation, table 5. Two analyses from the New Zealand ultramafics, Challis (1965), and two analyses from the Lizard peridotite, Green (1964), have also been recalculated into their normative mineralogy, following the method outlined above.

The norm calculations show that the amount of normative serpentine changes from 0.27 to 86.39 percent. In some of the highly serpentinised specimens a small amount of brucite appears in the norm. Normative olivine varies from 73.3 to zero percent as the amount of normative serpentine increases.

Orthopyroxene likewise varies from 22.1 percent to zero. Clinopyroxene varies from 7.2 to zero percent, and chlorite from 7.8 percent to zero. CaO has been calculated as clinopyroxene while orthopyroxene appears in the norm, otherwise CaO is calculated as tremolite. The normative chromite content is constant and unaffected by serpentinisation. In the case of magnetite and pyrite there is a positive correlation between the degree of serpentinisation and the normative amount of these minerals, more noticeable for magnetite. In both cases there is a sudden fall in content coincident with the appearance of normative hematite, reflecting oxidation.

The serpentinisation process

The experimental work of Bowen and Tuttle (1949) has shown that when a mass of forsterite crystals in water cool from 1000°C, serpentine begins to form from the olivine at around 400°C. The presence of CO_2 in the hydrous phase allows removal of excess magnesia, as magnesite, and permits serpentine to form from olivine at 500°C. Conversely, increase in the Fe content of the olivine will lower the serpentinisation temperature. Serpentinisation of olivine, by addition of H_2O and SiO_2 or CO_2, without removal of MgO, would involve a large volume increase, these reactions may be summarised as:

(1) $3Mg_2SiO_4 + 4H_2O + SiO_2 \longrightarrow 2H_4Mg_3Si_2O_9$

olivine (420 gr: 131 cc) — introduced — serpentine (552 gr: 220 cc)

(2) $2Mg_2SiO_4 + 2H_2O + CO_2 \longrightarrow H_4Mg_3Si_2O_9 + MgCO_3$

olivine (280 gr: 88 cc) — introduced — serpentine (276 gr: 110 cc) — magnesite (84 gr: 28 cc)

Turner and Verhoogen (1960) suggest that a constant volume process of serpentinisation on the other hand would require the removal of about 30 percent by weight of the original bivalent oxides, the reaction may be summarised as:

$5Mg_2SiO_4 + 4H_2O \longrightarrow 2H_4Mg_3Si_2O_9 + 4MgO + SiO_2$

olivine (700 gr: 219 cc) — introduced (72 gr) — serpentine (552 gr: 220 cc) — 160 gr Removed in solution — 60 gr

This reaction would require the addition of a large volume of water, both for serpentinisation and removal of excess constituents from amongst the products. A conflict is thus developed posing the question: Is serpentinisation a constant volume process or is it a constant compositional process, except for hydration?

In the Andizlik-Zimparalik area chertification and Mg metasomatism are lacking ~~from~~ in the surrounding sedimentary rocks,

although magnesite occurrences are known in the eastern part of the area, particularly around the Upper Pliocene to Quaternary Conglomerates.

Magnesite is not the usual alteration product of the peridotite and results from the action of CO_2 rich waters. SiO_2 liberated by the reaction, crystallises as opal, near to the magnesite occurrences. The following equation may represent this localised alteration process:

$$3Mg_2SiO_4 + 2H_2O + 3CO_2 \longrightarrow 3MgCO_3 + H_4Mg_3Si_2O_9 + SiO_2$$

The formation of magnesite appears to be related to recent dislocations and eroded surfaces and occurs after consolidation of the peridotite and after serpentinisation. Magnesite deposition takes place around 250°C and seldom extends to depths greater than 150-200 m from the surface. Wijkerslooth (1945) considers that the CO_2 necessary for magnesite may be obtained in one of two ways:

(a) Rain and surface waters

(b) Juvenile waters associated with acidic magmatism; magnesite often occurs where aplitic and pegmatitic dykes cut peridotite. The absence of acidic rocks in the Andizlik-Zimparalik area suggests that CO_2 rich surface waters were probably responsible for the formation of magnesite. This is further supported by limited mining activity in the magnesite, which

have proved that they extend no more than 1-2 m below the surface.

Thayer (1966), (1967), by plotting bivalent oxides and SiO_2 against combined water for a large number of analyses of serpentinised ultramafic rocks, obtained a negative correlation between these oxides and their water contents. He concludes that serpentinisation mainly proceeded on a constant volume basis, because there was a loss of elements during the process. Page (1967) made a similar plot except that he plotted the bivalent oxides separately against water content. Page found that the loss of elements was not as significant as Thayer assumed, he did however, emphasise the loss of CaO with increase in water content.

In order to study the chemical changes during the serpentinisation process in the Andizlik-Zimparalik area, the constituents CaO, MgO, SiO_2, Al_2O_3 and total iron as Fe_2O_3, all on a water free basis, have been plotted against H_2O^+ for a selection of harzburgites. The results, shown in fig.27, indicate that these constituents are remarkably constant up to 10 percent H_2O^+; scattering is probably within the $\pm$ 1 percent attributable to experimental error. Above 10 percent H_2O^+ scattering is more noticeable for MgO and SiO_2. Total iron remains relatively constant while Al_2O_3 and CaO, constant up to 10 percent H_2O^+, decrease noticeably. Hess and Otalora

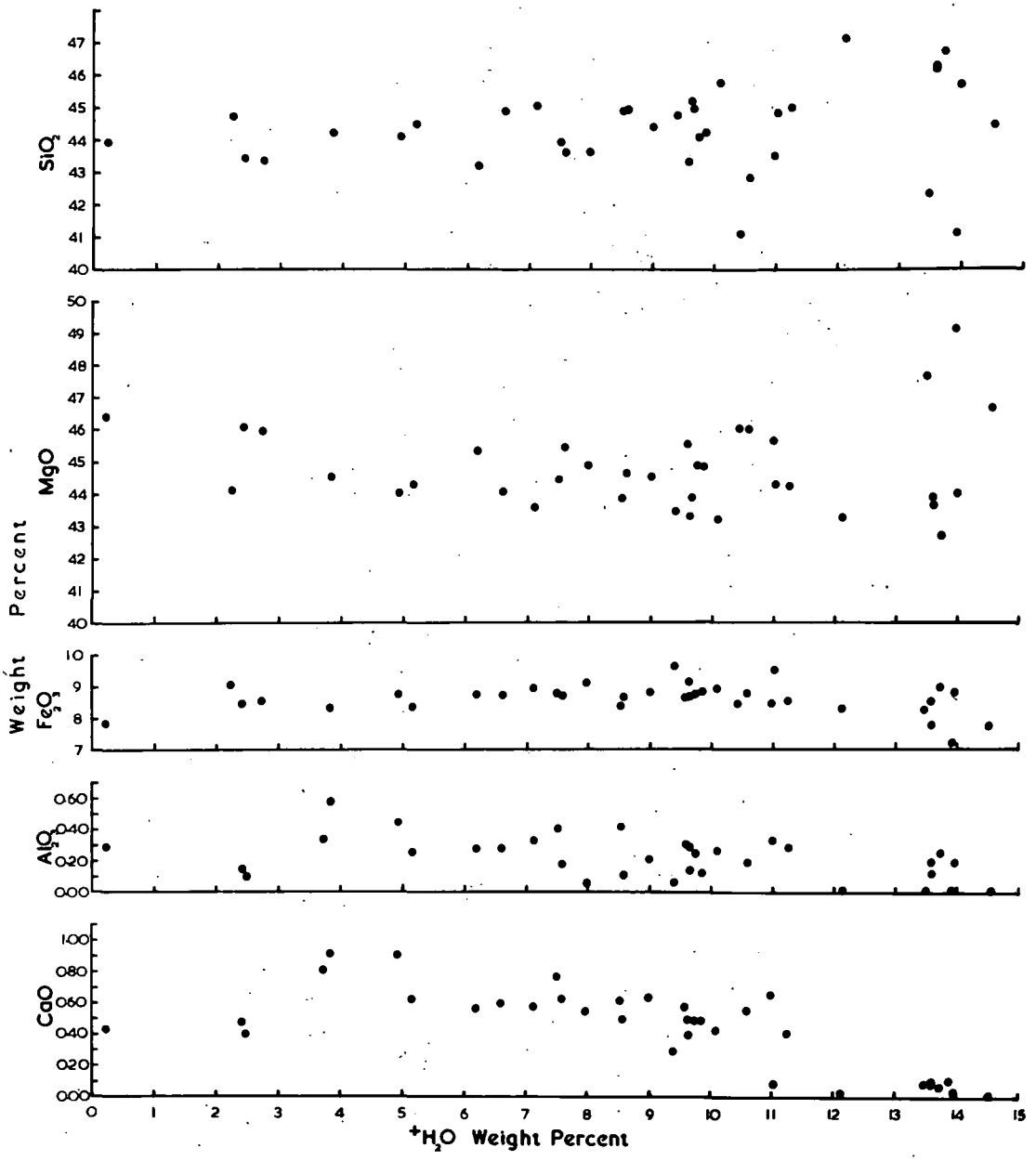

FIG.27

Correlation of CaO, Al_2O_3, Fe_2O_3, MgO and SiO_2 on a water free basis, against H_2O^+

(1964) have also shown that Al_2O_3 and CaO are lost in highly serpentinised rocks while Page (1967) has demonstrated loss in CaO with increase in water.

In fig.28 the H_2O^+ has been plotted against normative serpentine. Brucite appears in the norms of some serpentinites with more than 10 percent H_2O^+, when deviation from the straight line relationship is apparent. This is an obvious result, and depends on the presence of a water bearing mineral other than serpentine.

The norm calculations of two analyses from New Zealand, Challis (1965), and two from the Lizard, Cornwall, Green (1964), have also been recalculated into their normative mineralogy, New Zealand peridotites are similar in composition to the Andizlik-Zimparalik peridotites, but those peridotites from the Lizard, rich in Ca and Al have large amounts of normative chlorite and tremolite. The Lizard specimens consequently do not plot near the curve relating serpentine to H_2O^+. This curve thus enables an estimate of normative serpentine from the H_2O^+ content provided that water contents are below about 10 percent H_2O^+ and the CaO and Al_2O_3 are similar to the levels at Andizlik-Zimparalik.

Compositional changes in the peridotites as serpentinisation increases have been studied by means of the student's "t" test (Engin & Hirst, 1969). All comparisons have been made on

FIG.28

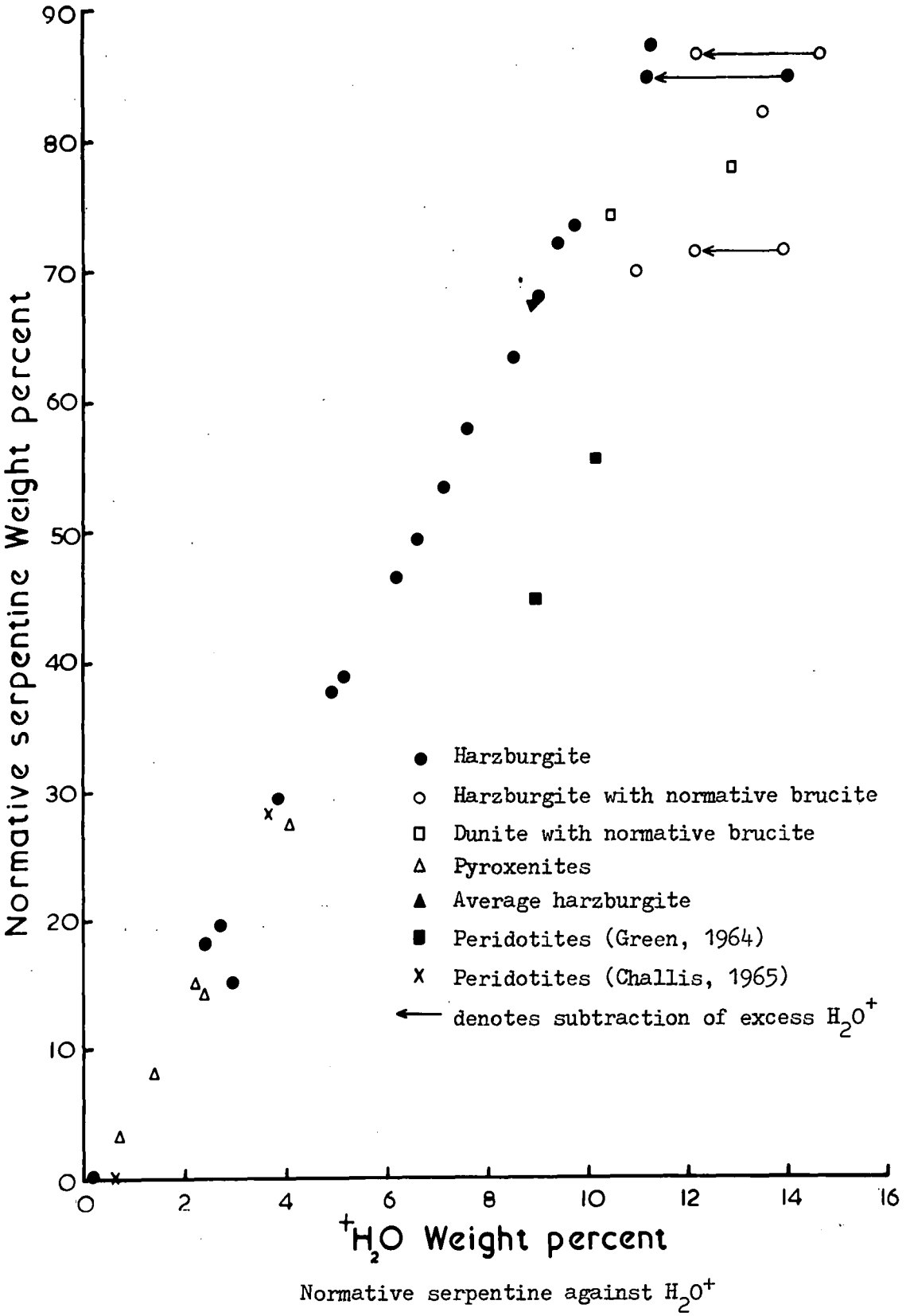

Normative serpentine against H_2O^+

the $t_{97.5}$ and $t_{99.5}$ significance levels and the results shown in table 8. Harzburgite specimens containing 0.2 to 5 percent H_2O^+ have been compared with specimens containing 5 to 10 percent H_2O^+. Except for MnO, all elements show no significant difference in their mean values. MnO which differs at the 99.0 percent confidence level, shows an increase in mean content in the group containing 5 to 10 percent H_2O^+. A further comparison has been made between the compound group containing 0.2 to 10 percent H_2O^+ and those peridotites with over 10 percent H_2O^+. This test clearly indicates that there is a loss of CaO, MnO, Al_2O_3 and a gain in NiO in the highly serpentinised rocks. The major components MgO, SiO_2 and total Fe as Fe_2O_3 show no significant changes in mean content between these two groups. In the case of MgO and SiO_2 however standard deviations are much higher in the highly serpentinised group, confirming the increased scatter, shown by fig.27.

Stueber and Goles (1967) studied the affects of serpentinisation on Na, Mn, Cr, Sc and Co and concluded that these elements were not affected by the process. No results are available for Sc or Co in the Andizlik-Zimparalik peridotites but the data on Na and Cr are in agreement with the conclusion of Stuber and Goles. The present data is at variance with Stuber and Goles in respect of Mn, although their histogram

Table 8 Statistical comparison of oxide contents on a water free basis for harzburgites with varying water contents

	A		B		C		D			
	$\bar{x}$	s	$\bar{x}$	s	$\bar{x}$	s	$\bar{x}$	s	tAB	tCD
SiO_2	43.930	0.532	44.371	0.626	44.251	0.633	44.754	1.752	1.460	1.183
Cr_2O_3	0.323	0.025	0.314	0.025	0.316	0.026	0.295	0.040	0.754	1.887
Al_2O_3	0.318	0.165	0.232	0.108	0.256	0.132	0.145	0.124	1.353	2.391
Fe_2O_3	8.507	0.372	8.813	0.289	8.730	0.342	8.533	0.554	1.944	1.258
MgO	45.197	0.969	44.432	0.678	44.641	0.840	44.951	1.856	1.981	0.655
CaO	0.642	0.217	0.555	0.103	0.579	0.149	0.207	0.214	1.203	5.864
MnO	0.142	0.007	0.149	0.006	0.147	0.007	0.135	0.021	2.583	2.374
NiO	0.417	0.014	0.411	0.012	0.413	0.012	0.482	0.076	0.880	4.053
Na_2O	0.098	0.027	0.147	0.135	0.134	0.118	0.101	0.038	0.835	0.949
S	0.417	0.209	0.558	0.174	0.519	0.195	0.344	0.202	1.523	2.463
t97.5									2.086	2.042
t99.0									2.528	2.457
t99.5									2.845	2.750

A - 0-5% H_2O^+ B - 5-10% H_2O^+ C - 0-10% H_2O^+ D - 10-15% H_2O^+

$\bar{x}$ = mean
s = standard deviation

(p.90 fig.8.) does suggest lower Mn in highly serpentinised rocks.

The data given above clearly favours the maintenance of a constant composition during serpentinisation, except for losses in respect of some minor components at high H_2O^+ contents, gain in NiO and fluctuation of MnO.

Most equations relating to serpentinisation which are reported in the literature (some are mentioned in connection with general aspects of serpentinisation at the beginning of this Chapter p. 68) refer to dunites, or more accurately to pure forsterite, and involve either addition of components such as SiO_2 during serpentinisation, or loss of components particularly SiO_2 and MgO. These equations have little relevance to the Andizlik-Zimparalik peridotites since they concern dunites and imply compositional changes. An alternative constant composition equation (to that involving magnesite see page 68), though again relating to dunite, is:

$$2Mg_2SiO_4 + 3H_2O \longrightarrow H_4Mg_3SiO_9 + Mg(OH)_2$$

introduced

(280 gr: 88 cc) (276 gr: 110 cc) (58 gr: 24 cc)

Brucite is produced by this reaction which involves an expansion of around 50 percent of the original volume. Brucite appears in the norms of some highly serpentinised harzburgites but the amounts are considerably less than those implied by this equation.

Thayer (1966, p.698) has evolved equations for the

serpentinisation of olivine and pyroxene, including appropriate amounts of Fe in their formula. Thayer's equations produce a considerable change in composition with serpentinisation, "the weight of material removed being about 30 percent in both natural olivine and enstatite.....although the presence of Fe reduces the amount of MgO to be removed in solution, it increases the SiO_2 reciprocally". Thayer does not attempt to combine olivine and pyroxene in the proportions normally encountered in harzburgites.

Following Engin and Hirst (1969) an equation may be produced in which olivine and pyroxene, amongst the reactants, approximate their weight percent proportions in harzburgite (75 olivine; 25 pyroxene). Apart from the addition of water the analytical data above demands that constant composition be maintained from reactants to products; minor constituents have been omitted.

The equation is:

$$7(Mg_{0.9}Fe_{0.1})_2SiO_4 + 3(Mg_{0.9}Fe_{0.1})SiO_3 + 10.57H_2O \longrightarrow$$

(1029 gr: 312 cc) (312 gr: 97 cc) introduced

$$0.3MgO + 0.57H_2 + 5H_4Mg_3Si_2O_9 + 0.57Fe_3O_4$$

(12 gr) (1385 gr: 543 cc) (132 gr: 24 cc)

Ferrous iron is represented by about 8.6 weight percent Fe_3O_4, magnetite, amongst the products; in reasonable agreement with

normative values in highly serpentinised rocks. This oxidation process implies generation of considerable gaseous hydrogen, as discussed by Thayer (1966, p.699,700). The excess MgO is very small, less than 1 percent by weight of the products, it might be located in minor constituents, such as chlorite, not included in the equation, or, if a little more water were made available, could form a small percentage of brucite. Given these small limitations the equation would appear to be a reasonably accurate representation of the serpentinisation process as applied to the harzburgites under consideration.

The conclusion to be drawn from this is that serpentinisation has been accompanied by an increase in volume of around 39 percent of the original volume. The chemistry of serpentinisation is thus basically related to a net addition of water. The scatter of SiO_2 and MgO in highly serpentinised rocks, together with the appearance of normative brucite, may reflect some chemical reorganisation within the peridotite. Since mean levels of both SiO_2 and MgO remain similar, in these rocks, to the values shown by the fresh rock, loss (or gain) to (or from) the surrounding sediments would seem improbable.

The main feature, in the field, which might support a volume increase is the extensive brecciation accompanying serpentinisation, particularly along the fault and fracture zones, and granulation

Plate 26. Kink bands in pyroxenes, lamellaer structure and undoluse extinction in the olivines may also result from strain due to internal pressures set up during expansion.

The normative mineralogy of the serpentinised ultrabasic rocks enables calculation of their average specific gravity using specific gravity data for individual minerals derived from the literature. By comparison with the specific gravity of the fresh harzburgite (F251), a measure of the volume increase may be calculated. Table 9 from Engin and Hirst (1969) gives relevant data for fresh harzburgite, three harzburgites with varying degrees of serpentinisation, and the average harzburgite of the Andizlik-Zimparalik area. The data suggests a volume increase of approximately 1 percent for each 4 percent of serpentine produced reaching a maximum of about 24.5 percent in fully serpentinised rocks. The average harzburgite of the area has 67.5 percent serpentine, representing an average volume increase of 17.8 percent relative to fresh harzburgite. Table 9 also gives measured specific gravities for the four harzburgites, these measurements were made by the rapid method, using Walker's steelyard. The measured specific gravities are in agreement with calculated values to within about 2 percent. Lower values might be expected for highly serpentinised rocks since pore space would lower the net value of the measured specific gravity; obviously no account of pore space can be taken

Table 9 Measured and calculated specific gravities for serpentinised harzburgites with relative volume increases

	F251	F245	F44	AU7	A*
Serpentine, percent	0.3	37.7	73.8	82.0	67.5
Brucite, percent	-	-	-	6.8	-
D_c	3.30	3.00	2.77	2.65	2.80
D_m	3.33	3.04	2.77	2.60	-
V_c	-	9.8	19.0	24.5	17.8
V_m	-	9.6	20.2	28.0	-

A* Average of 36 harzburgites from Andizlik-Zimparalik

D_c Calculated specific gravity

D_m Measured specific gravity

V_c Volume increase relative to F251 in percent, from calculated specific gravity

V_m Volume increase relative to F251 in percent, from measured specific gravity

in calculations based on normative mineralogy. The result of measured specific gravities would imply that the maximum volume increase is higher than 25 percent as calculated from norms, and probably in the region of 28 to 30 percent. These values are similar to those suggested by Hess (1955, p.403) of 25 percent for dunite, but less than the estimate of Hostetler et al. (1966) who suggest expensions of 35 to 40 percent.

The process of serpentinisation requires the addition of a large volume of water. Some large peridotite massifs are not serpentinised, a fact which has led to the suggestion that they include insufficient water to cause serpentinisation by autohydration on any extensive scale.

The source of water causing serpentinisation could lie outside the peridotite, and may come from the enclosing geosynclinal sediments, or from gases and solutions driven off and upward from similar rocks undergoing compaction, cementation and metamorphism at depths beneath the peridotite. Juvenile water is a further possibility.

In the Andizlik-Zimparalik area the serpentinisation appears to have been post magmatic and to be related to tectonic movements. The necessary water may have been supplied by the surrounding sediments, since serpentinisation is particularly intense in the marginal fault zones. Alternatively the process could be one of autohydration since association of serpentinisation with

fracture zones might imply that water had migrated to low pressure areas within the massif.

Pyroxenites

Orthopyroxenites

14 orthopyroxenite specimens have been analysed by the same method and for the same elements as the harzburgites and dunites. These analyses appear in table 3 of the appendix except for those which appear in table 10.

The SiO_2 content of the orthopyroxenites ranges from 53.73 to 56.03 percent, much higher than the level in the harzburgites and dunites. The MgO content varies from 32.40 to 36.56 percent and total iron as Fe_2O_3, from 6.61 to 8.73 percent. The pyroxenites are less oxidized than the other ultramafics, the FeO content varying from 3.89 to 6.68 percent.

The orthopyroxenites are slightly serpentinised with H_2O^+ contents ranging from 0.73 to 2.40 percent and representing minor normative serpentine, tremolite and chlorite.

The Al_2O_3 content varies from 0.51 to 0.95 percent, which is higher than the Al_2O_3 content of the harzburgites and dunites but is in general lower than the values given for orthopyroxene analyses in the literature (e.g. Deer, Howie and Zussman, 1963, Vol.2, pp. 16-22). It was shown by Zwaan (1954) and Hancock (1964) that the Al_2O_3 content of orthopyroxenes has a considerable effect on the diffraction results. The X-ray diffraction analyses of the

Table 10 Analyses (weight percent) and normative mineralogy of pyroxenites.

	A54	Z7	Z14	F36	F135
SiO_2	55.09	52.42	53.35	53.08	46.99
Cr_2O_3	0.31	0.45	0.33	0.50	0.26
Al_2O_3	0.49	0.60	0.50	0.57	0.67
Fe_2O_3	1.30	2.02	1.90	2.16	2.82
FeO	6.68	4.58	5.33	3.89	3.10
MgO	32.09	35.89	33.37	32.91	26.28
CaO	1.78	1.22	1.25	3.38	13.98
MnO	0.21	0.15	0.18	0.15	0.15
NiO	0.10	0.16	0.11	0.13	0.07
Na_2O	0.22	0.06	0.11	0.12	0.21
K_2O	0.01	-	-	0.02	0.01
^+H_2O	0.73	1.41	2.26	2.40	4.09
^-H_2O	0.21	0.42	0.53	0.11	0.57
S	0.10	0.15	0.20	0.08	0.44
Chromite	0.5	0.8	0.5	0.8	0.4
Pyrite	0.2	0.3	0.4	0.2	0.8
Magnetite	1.6	2.6	2.3	3.0	3.3
Hematite	-	-	-	-	-
Tremolite	-	-	-	-	-
Clinopyroxene	7.1	4.8	4.8	13.00	54.4
Chlorite	2.5	2.8	2.5	2.8	3.6
Olivine	-	8.7	-	-	6.3
Serpentine	3.2	8.0	14.9	14.2	27.4
Brucite	-	-	-	-	-
Orthopyroxene	83.6	71.2	71.5	64.1	2.2
^-H_2O	0.21	0.42	0.53	0.11	0.57
Excess ^+H_2O					
Excess MgO					
Excess SiO_2	0.66		3.78	1.20	
N	89	93	90	93	81

N normative olivine and pyroxene compositions

A54 through F36 orthopyroxenites

F135 clinopyroxenite

Andizlik-Zimparalik orthopyroxenes however fit on the orthopyroxene determinative curve, fig.20, within the limits of experimental error.

The CaO content is variable from 1.11 to 3.47 percent and is a reflection of the amount of clinopyroxene present in the rock.

Andizlik-Zimparalik pyroxenites are low in alkalis; K_2O is mostly below the detection limit of about 0.01 percent while Na_2O varies from 0.06 to only 0.22 percent. Upton (1967) describes pyroxenites associated with the alkaline volcanic fields of continental cratogenic areas. Here there is gradiation into peridotite and pyroxenite and Na_2O may reach 1.52 and K_2O 4.74 percent, MgO however varies from 7.78 to only 15.74 percent.

TiO_2 and P_2O_5 levels are very low, TiO_2 is below the detection limit but P_2O_5 may reach 0.03 percent. The S content is below that of the host peridotites, in the harzburgites and dunites the S may reach 1.05 percent but in the pyroxenites it varies from 0.01 to only 0.27 percent. NiO averages 0.12 percent and varies from 0.10 to 0.17 percent, considerably lower than the amount present in the harzburgites.

The amount Cr present in the orthopyroxenites is in general higher than in the harzburgitic host peridotite.

The pyroxenites are late stage features forming veins which cut the harzburgite and dunite; they may be derived from the peridotites with alterations by hydrothermal solutions circulating along

cracks (explained in p.18)

Thin section examination reveals fewer chromite crystals in the orthopyroxenites than in the host peridotite. These chromite crystals in specimen A55 were separated from the pyroxenite which was then analysed. Despite separation of chromite the analysis, shown in table 3(in appendix)still reveals a Cr_2O_3 content of 0.35 percent, still higher than the average value in peridotites in which chromite crystals are common. The S content of this separated pyroxenite is low suggesting that pyrite has also been removed during the separation.

The data leads to the conclusion that during the hydrothermal activity, responsible for the formation of pyroxenites small amounts of chromium were removed and transported from the chromite bodies by hydrothermal solutions. This chromium could enter into the pyroxenite structure, the chromite found in the pyroxenites may be residual chromite originally present in the peridotite (harzburgite) and unaffected by the hydrothermal process causing transformation of harzburgite to pyroxenite.

The pyroxenites are grouped as either northwest-southeast or northeast-southwest trending veins. The chemistry of the two groups is closely similar, only NiO shows a difference being higher in the northeast-southwest group.

Calculations of the normative mineralogy of four orthopyroxenites

are given in table 10, normative orthopyroxene ranges from 64.1 to 83.6 percent and clinopyroxene from 4.8 to 13.0 percent. H_2O^+ has been distributed between chlorite and serpentine which reaches 14.9 percent. Normative olivine is mainly absent from these pyroxenites, although it reaches 8.7 percent in Z7. On the AFM triangular diagram, fig. (26B), the orthopyroxenites plot close to, and overlapping, the harzburgites and dunites, with a tendency to be relatively enriched in Fe.

The clinopyroxenite vein

The chemical analysis of the clinopyroxenite vein (F135) is given in table 10. The chemistry of this specimen is obviously very different from that of the orthopyroxenites, being high in CaO (13.28 percent) and relatively low in SiO_2 and MgO. The normative mineralogy includes 54.4 percent clinopyroxene, 6.3 percent olivine and 2.2 percent orthopyroxene, table 10.

In the AFM triangular diagram fig. 26B, this analyses plots towards the iron rich end of the orthopyroxenite analyses.

Nomenclature

The peridotite norms have been plotted on an orthopyroxene-olivine-clinopyroxene triangular diagram, fig.29. For the most part they plot as harzburgites with 4 dunites, 1 lherzolite, 2 saxonites, 2 enstatites, 1 marchite, and 1 diopside peridotite.

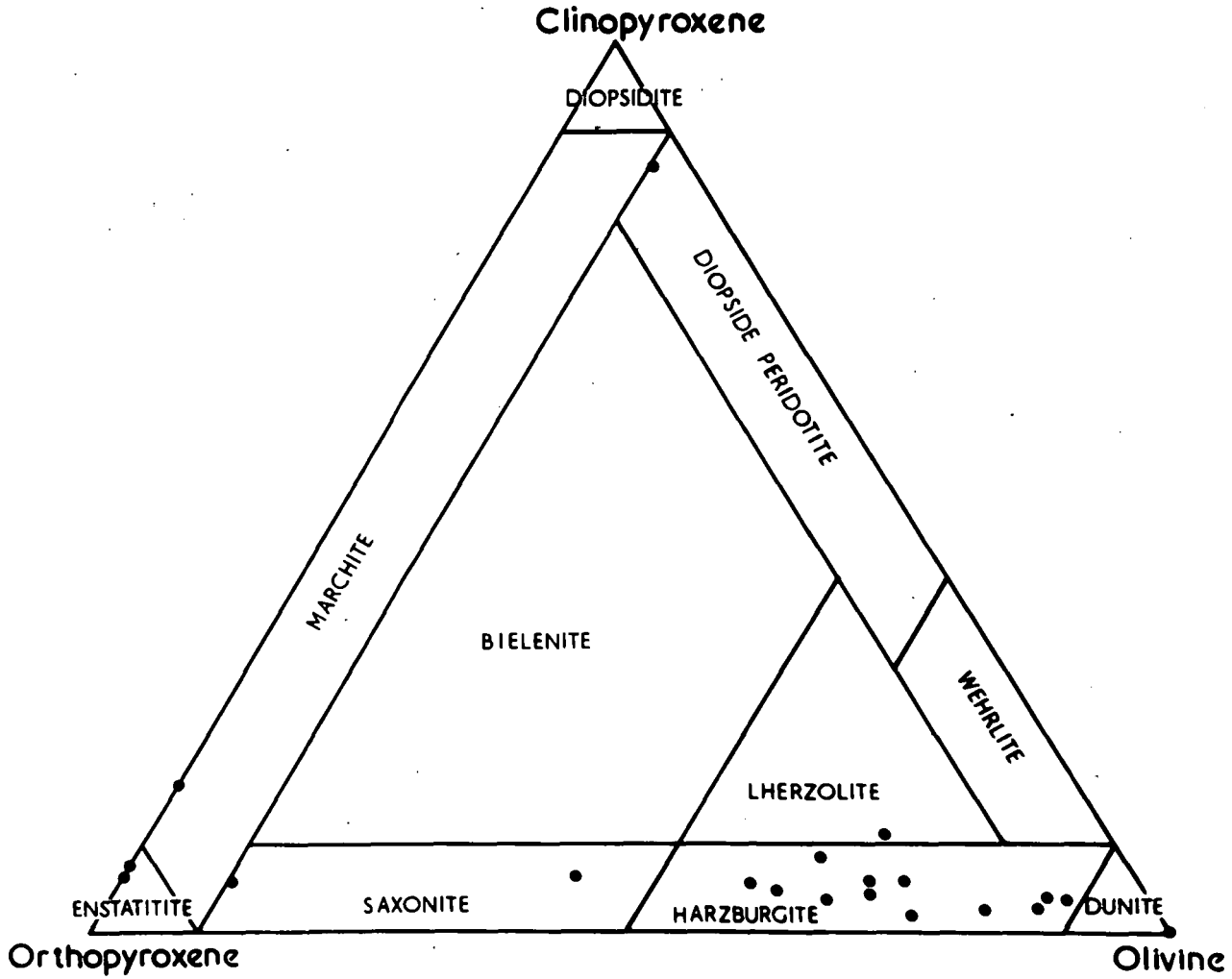

Normative mineral content of the Andızlık–Zımparalık peridotites

FIG.29

The chemistry of the basic dykes

18 basic dyke specimens have been analysed, these analyses appear in table 4 of the appendix except for those which are given in table 11. The SiO_2 content varies from 49.58 to 52.94 percent, with dykes from the central part of the field, around the Andizlik and Zimparalik mines, being slightly higher in SiO_2 than those of other areas. The Al_2O_3 content varies from 12.45 to 15.64 percent but has no regional pattern. MgO ranges from 5.28 to 8.18 percent with dykes from the central part of the field being slightly lower in MgO than elsewhere. The CaO content varies from 8.97 to 15.74 percent, Na_2O from 2.57 to 4.69 and K_2O from 0.06 to 0.56 percent. TiO_2 is generally over 1.20 percent but shows variation from 0.95 to 1.45 percent, reflecting the amount of ilmenite present. MnO is almost constant and lies within the range 0.18 to 0.23 percent, S varies from 0.14 to 0.56 percent and P_2O_5 from 0.13 to 0.21 percent. NiO is mostly below the detection limit but does reach 0.004 percent. The Cr_2O_3 content is low varying from 0.01 to 0.02 percent.

The dykes are chloritized with H_2O^+ ranging from 2.10 to 3.69 percent. The dykes have a similar chemistry and show no pronounced pattern of geographical distribution. Specimen A69, table 11, is chemically different to the other basic rock specimens being low in SiO_2 and high in MgO, this dyke is highly

Table 11 Analyses of basic rocks (weight percent) and their CIPW normative mineralogy

	A69	F241	F258	Z97B	Z34
SiO_2	40.85	49.43	49.53	50.58	50.93
TiO_2	0.37	1.37	1.02	1.26	1.22
Al_2O_3	16.08	14.50	14.71	13.77	14.96
Fe_2O_3	1.25	1.54	2.52	3.18	3.56
FeO	7.70	9.09	6.93	7.52	6.50
MgO	10.99	6.10	7.76	5.92	5.83
CaO	10.03	9.73	9.66	8.65	9.89
MnO	0.19	0.21	0.18	0.22	0.19
Na_2O	1.47	3.43	3.13	3.98	3.12
K_2O	0.05	0.23	0.30	0.26	0.22
^+H_2O	9.22	2.67	2.90	3.06	2.20
^-H_2O	0.52	0.20	0.27	0.48	0.35
P_2O_5	0.08	0.17	0.16	0.20	0.16
S	0.41	0.39	0.22	0.13	0.19
Quartz	-	-	-	0.3	4.1
Orthoclase	0.3	1.1	1.7	1.7	1.1
Albite	12.6	28.8	26.2	33.5	26.2
Anorthite	37.3	23.6	25.3	18.9	26.4
Diopside	10.1	20.3	17.7	18.7	17.8
Hypersthene	3.4	14.1	16.7	14.8	13.0
Olivine	22.6	2.8	2.2	-	-
Magnetite	1.9	2.3	3.7	4.6	5.1
Ilmenite	0.8	2.6	2.0	2.4	2.3
Pyrite	0.8	0.7	0.4	0.2	0.4
Apatite	0.2	0.3	0.3	0.3	0.3
H_2O^+	9.22	2.67	2.90	3.06	2.20
H_2O^-	0.52	0.20	0.27	0.48	0.35

chloritized with 9.22 percent H_2O^+

CIPW norms for 5 gabbroic rocks are given in table 11. Normative quartz and hypersthene or hypersthene and olivine appear, these have not been seen in thin section. Diopside reaches 20.3 percent and feldspar 54.1 percent. Plots of normative feldspar, in the triangular diagram of Hietanen (1963) fig.30, indicate that most of the dykes are quartz diorites, with one tonalite, two gabbros and one mafic gabbro (A69). On the AFM triangular diagram, the dykes plot in the iron and alkali rich part of the diagram, fig.26B.

Thayer (1967) mentions that the analyses of alpine type intrusives suggest a differention trend that crosses the AFM triangular diagram, fig.31, much closer to the typical calcalkaline plutonic trend than to the Skaergaard trend.

The Andizlik-Zimparalik harzburgites, dunites, ortho and clinopyroxenites, gabbros and diorites also show a compositional trend fig. 26A-B. This trend is not coincident with the calcalkaline plutonic trend of Hess (1960), as suggested by Thayer but agrees with Thayer's Syria-Turkey trend, fig.31.

Tremolites

Three tremolite specimens have been analysed after separation of contaminant chromite, they are of closely similar composition, table 12. The Cr_2O_3 content varies from 0.48 to 1.20 percent suggesting that they are chrome tremolites and

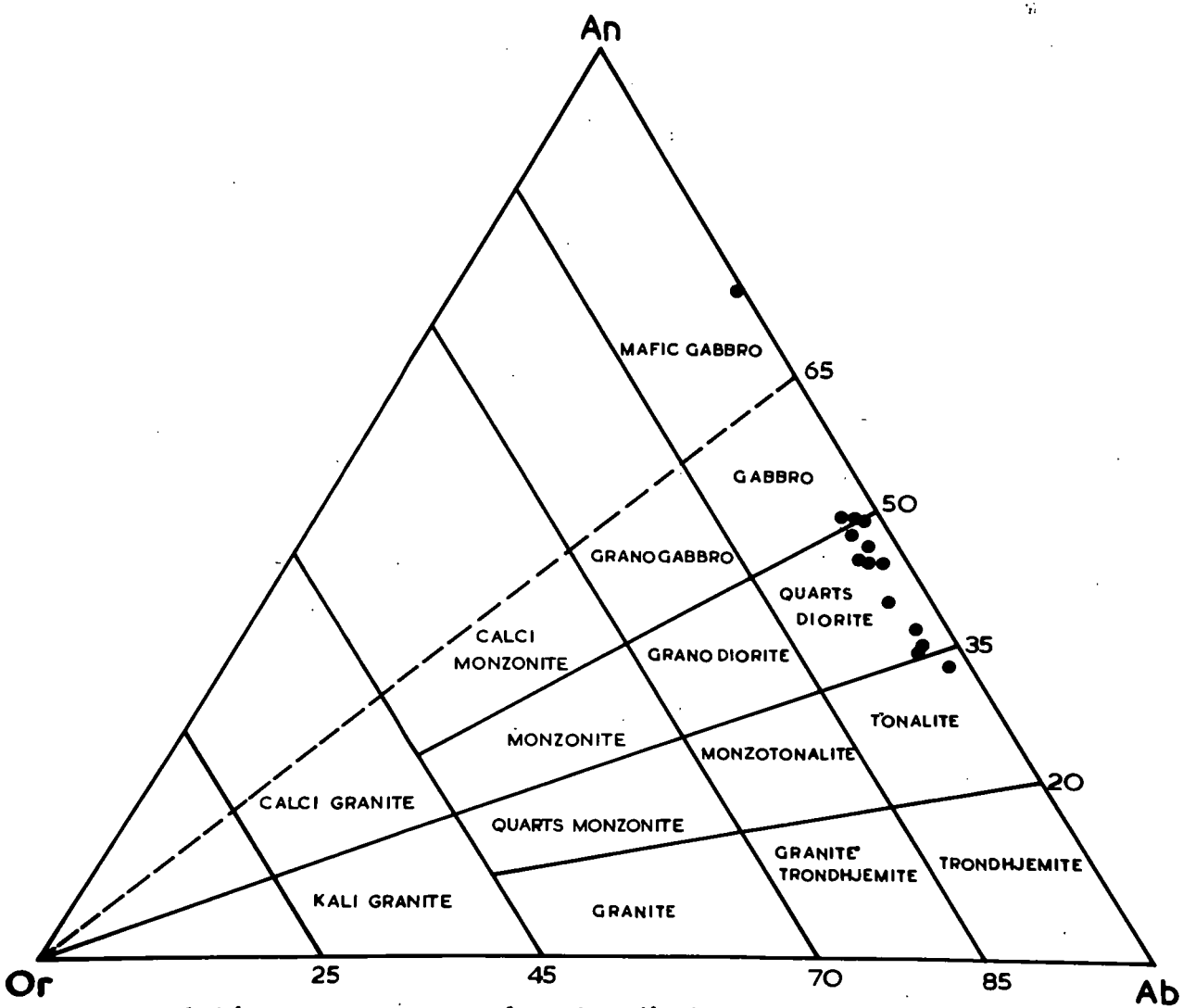

Normative feldspar content of calc-alkaline igneous rocks FIG.30

Table 12 Analyses of chrome tremolites (Weight percent)

	F139B	AU3	ZU45
SiO_2	51.58	52.68	48.33
TiO_2	0.11	0.08	0.36
Cr_2O_3	0.95	0.48	1.20
Al_2O_3	4.55	4.45	7.14
Fe_2O_3	-	1.92*	2.55*
FeO	1.65		
MgO	24.24	26.69	28.17
CaO	11.55	10.65	9.45
MnO	0.03	0.03	0.03
NiO	0.23	0.21	0.29
Na_2O	1.59	2.08	1.86
K_2O	0.11	0.12	0.12
H_2^+O	2.91		
H_2^-O	0.22		
S	0.07	0.55	0.43

*Total Fe as Fe_2O_3

AU3 and ZU45 analyses are on a water free basis

supporting the hypothesis that Cr is transported by hydrothermal solutions.

The formula of one of the chrome tremolites (F139B) ~~analysis~~ has been calculated from the analysis on the basis of 24 oxygens and on the basis of 23 oxygens, Phillips (1963), using a computer technique devised by R. Phillips (personal communication).

$$(K_{0.02}Na_{0.43}Ca_{0.02}H_{0.68})_{1.15}(Ca_{1.69}Mg_{0.31})_{2.00}(Mg_{4.67}Fe^{+2}_{0.22}Cr^{+3}_{0.10}Ti_{0.01})_{5.00}(Si_{7.11}Al_{0.74})_{7.85}O_{22}(OH)_{2.00}$$

and

$$(K_{0.02}Na_{0.43}Ca_{0.12}\square_{0.43})_{1.00}(Ca_{1.61}Mg_{0.39})_{2.00}$$

$$(Mg_{4.67}Fe^{+2}_{0.22}Cr^{+3}_{0.11}Ti_{0.01})_{5.01}(Si_{7.22}Al_{0.75})_{7.97}O_{22}(OH)_{2.72}$$

Amphibolites

The analyses of two amphibolites F185A and F202 are given in table 13; the amphibolites are found as xenoliths in the peridotite. Since amphiboles constitute 80-85 percent of the specimen, the two analyses have been calculated into amphibole formulae on the 24 and 23 oxygen basis, Phillips (1963), using a computer technique devised by R. Phillips (personal communication). F185A recalculated on the basis of 24 oxygen atoms:

$$(\square_{0.10}\ Na_{0.46}K_{0.04}Ca_{0.41})_{1.01}\ (Ca_{2.00})_{2.00}\ (Mg_{2.44}Fe^{++}_{0.66}Ti_{0.29}$$

$$\square_{0.29}\ Fe^{+++}_{0.16}\square_{0.08})_{3.92}\ (Al_{0.48}Fe_{0.44})_{0.92}\ (Si_{6.54}Al_{1.46})_{8.00}$$

$$O_{22}(OH)_{1.15}$$

F185A recalculated on the basis of 23 oxygen atoms:

$$(\square_{0.15}\ Na_{0.45}K_{0.03}Ca_{0.37})_{1.00}\ (Ca_{2.00})_{2.00}\ (Mg_{2.39}Fe^{++}_{0.65}$$

$$(Al_{0.33}Fe^{+++}_{0.59}Ti_{0.29})_{1.21}\ (Si_{6.43}Al_{1.58})_{8.01}\ O_{22}$$

F202 recalculated on the basis of 24 oxygen atoms:

$$(\square_{0.56}\ Na_{0.36}K_{0.07}H_{0.01})_{1.00}\ (Ca_{1.59}Na_{0.14}Fe_{0.27})_{2.00}$$

$$(Mg_{3.49}Fe^{++}_{0.88}Al_{0.23}Fe^{+++}_{0.18}Ti_{0.23})_{5.01}\ (Si_{6.58}Al_{1.42})_{8.00}\ O_{22}(OH)_{2.00}$$

F202 recalculated on the basis of 23 oxygen atoms:

$$(\square_{0.56}\ Na_{0.36}K_{0.07})_{0.99}\ (Ca_{1.59}Na_{0.14}Fe^{++}_{0.27})_{2.00}$$

$$(Mg_{3.49}Fe^{++}_{0.88}Al_{0.23}Fe^{+++}_{0.18}Ti_{0.23})_{5.01}\ (Si_{6.58}Al_{1.42})_{8.00}\ O_{22}$$

These analyses correspond with the general formula for pargasite although it must be remembered that they are whole rock and not mineral analyses.

Table 13 Analyses of amphibolites (Weight percent)

	F185A	F202
SiO_2	44.55	45.02
TiO_2	2.65	2.06
Cr_2O_3	0.03	0.07
Al_2O_3	11.19	9.59
Fe_2O_3	5.40	1.62
FeO	5.23	9.22
MgO	11.14	16.02
CaO	15.32	10.17
MnO	0.17	0.20
NiO	0.01	0.06
Na_2O	1.61	1.77
K_2O	0.19	0.39
H_2^+O	1.17	2.06
H_2^-O	0.10	0.32
P_2O_5	0.59	0.36
S	0.14	0.22

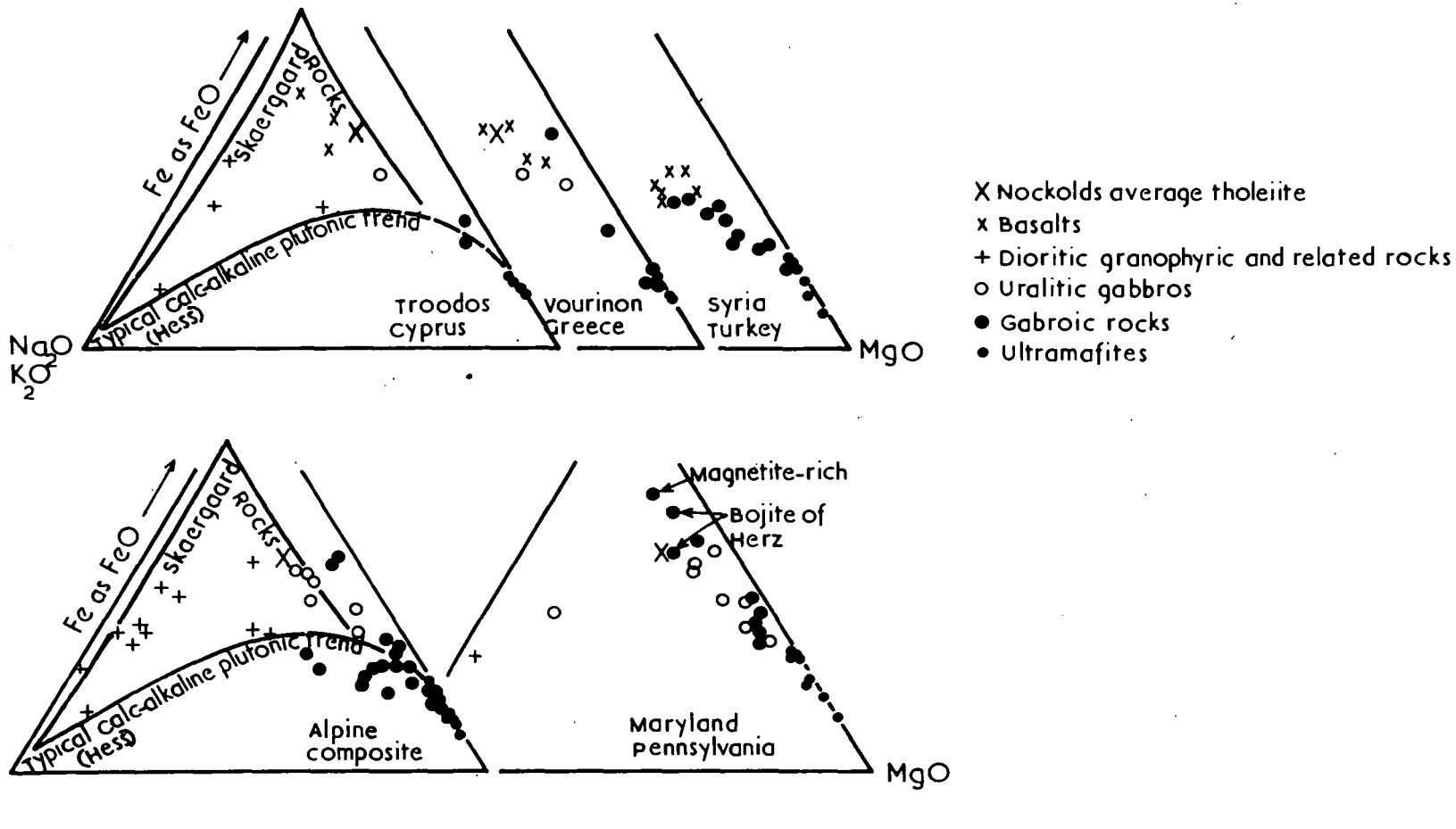

A F M diagrams of some alpine intrusive complexes and a compilation indicating the general alpine differentiation trend. (after T.P.Thayer 1967)

FIG.31

CHAPTER 5

CHROME ORE DEPOSITS, A SURVEY OF PREVIOUS WORK RELATED TO THEIR DISTRIBUTION AND GENESIS

Chromite deposits have been genetically grouped as either of stratiform or podiform (alpine) type. Apart from this generally accepted division there has been considerable discussion of the role of hydrothermal chromite deposition.

The possibilities of hydrothermal chromite formation

Sampson (1929) suggests that the segregation of chromite which takes place before intrusion, must have taken place in the magma chamber, the chromite and peridotite being injected contemporaneously. Chromite formed at an early stage seldom occurs in sufficient concentration to form an ore deposit. Where chromite does occur in workable concentration, it seems likely that some process, other than the unmodified accumulation of early formed crystals, has been effective. The complete absence of chromite as inclusions in basaltic lavas and basic dykes, in spite of frequent occurrence of olivine nodules, could be taken as evidence that chromite concentrations rarely form at an early magmatic stage. According to Singewald (1929) magmatic sulphide ores are not amongst the first minerals to separate and crystallize from a magma. These constituents are rendered more mobile by mineralizers and are kept in solution until after the rock forming minerals have solidified. Ore deposition takes

place through the introduction of these constituents into already solidified silicate rock. Thus when ore minerals are amongst the earliest constituents to crystalize, they are likely to be present only as accessory minerals, only those cases in which the ore constituents have been locally concentrated by some secondary process will form sulphidic and oxidic ores of economic value. Ore deposits may thus only result when mineralisers have retarded the early crystallization of the ore minerals facilitating their retention by the residual magmatic fluid, and their concentration within it.

According to Fisher (1929) the crystallization sequence in chromiferous rocks is as follows:

(1) Crystallization of early magmatic chromite which is well advanced before the initial crystallization of the groundmass minerals. Final freezing of early magmatic chromite overlaps the crystallization of the groundmass.

(2) Crystallization of late magmatic chromite which replaces, either partially or completely, the groundmass minerals and surrounds, embays, or cuts these minerals, or penetrates the cleavable minerals.

(3) Chromites of the hydrothermal period, which is distinctly later than the magmatic period, and is related to two distinct groups of minerals.

a. Early hydrothermal minerals, anthophyllite, actinolite

and tremolite.

b. Late hydrothermal minerals, chlorite, talc, penninite, serpentine and magnesite.

The chromite of this period was probably derived by hydrothermal solutions from the parent rock. Hydrothermal solutions causing serpentinisation may have played an important role in the formation of this type of chromite deposit, by dissolving magmatic chromite and re-depositing it with the hydrothermal silicates. Evidence presented in connection with serpentinisation suggests that this process is unlikely in the Andizlik-Zimparalik area. Despite this no fully supported hydrothermal chromite deposit has yet been recorded and recent workers have tended to rule out hydrothermal deposition at economic concentrations.

Sampson (1929) suggests that in the examination of chromite deposits the possibility of hydrothermal deposition should be kept in mind.

Small amounts of chromium can be transported by hydrothermal solutions and may be incorporated in the structure of other minerals such as tremolite and pyroxene, discussed in page 84.

Stratiform chromite deposits

The well known examples of stratifrom chromite deposits include those of the Bushveld Complex, South Africa, the Great Dyke - Rhodesia and the Stillwater Complex - Montana, U.S.A. All these deposits are characterized by a general sheet like form,

and exhibit many features in which they resemble sedimentary rocks. The most distinctive feature is that extremely thin layers can generally be traced over distances which are enormous relative to the thickness involved. The associated intrusions are also characterized by chilled margins of basaltic composition, high temperature metamorphic effects, and by a regular succession of comformable rocks changing upwards from ultramafic to gabbroic or noritic compositions. The chromite concentrations occur in tabular bodies, parallel to the layering of the enclosing rock. They have a sharp footwall and become disseminated upwards in the section. Most of the known stratiform chromite deposits are genetically related to pyroxenites.

Several hypotheses have been advanced to account for the origin of chromite deposition in the Bushveld Complex. The hypotheses are summarised by Cameron and Emerson (1959) as follows:

1. The chromite seams are due to selective replacement of certain layers in an original sedimentary sequence.
2. The chromite seams are magmatic in origin; but represent successive injections of chrome rich magma.
3. The chromite seams are magmatic in origin and are due to fractional crystallization and gravitative accumulation of successive crops of crystals.
4. The chromite seams represent chrome rich liquids derived:

a. as end stage liquids of magma crystallized in situ,

b. by separation and settling of an immiscible chrome rich liquid,

c. by resorption of settled chromite crystals.

Gravitative differentiation is still the preferred explanation although this process must have been complicated by other factors.

Despite differences of opinion on detail there is reasonable agreement concerning the genesis of stratiform chromites. They are generally believed to have formed in situ by crystal accumulation of cumulus chromite on the floor of a magma chamber. In this context the order of crystallization, and the specific gravity, of the specimen are important factors.

Wager and Brown (1968) suggest that layering is an igneous phenomen dependent largely on gravity and the chemical effects of magmatic fractionation. Repetition of layers may be attributed either to a rhythmic mechanical process or to rhythmic changes in the physico-chemical state of the magma. If mechanical sorting is responsible for the layers then convection currents must have been operative in the magma chamber, these may be either slow and continuous, or fast and sporadic, accounting for uniform and graded units in the sequence.

Recently Hawkes (1967) has postulated an attractive mechanism for rhythmic layering based upon the order of abundant crystal nucleation. Essentially related to undercooling, this mechanism

could account very simply for the type of layering seen in complexes such as Bushveld and Stillwater. Large scale cryptic layering is undoubtedly due to changes in the bulk chemistry of the magma.

Jackson (1964) suggests that primary disturbances of regular layering in stratiform chromites are for the most part of two types; slump structures and local unconformities. Slump structures are believed to have occurred by sliding of a partly consolidated crystal mush, on gentle slopes, penecontemporaneous with deposition.

As the result of a compositional study of chromites from the Stillwater complex, Jackson (1964) suggests that there is an upward increase in the amount of ferrous and ferric iron, in the chromite, relative to chromium and magnesium. Chromites from layers that contain olivine are richer in ferrous and ferric iron and poorer in chromium and magnesium than massive chromites from the same stratigraphic height. The most regular change of composition along the strike of the various chromitite zones is shown by the oxidation ratio of the chromites. The ratio of ferric iron to total iron decreases towards the centre of the complex.

Podiform chromite deposits.

Podiform deposits are lenticular concentrations of chromite ranging from massive to disseminated. They usually occur as tabular lenses, irregular pods, or a combination of these two

basic forms. The chromite in podiform deposits ranges from euhedral crystals, scattered as an accessory mineral through dunite, to massive aggregates of interlocking grains. They are genetically associated with olivine rich peridotites. The boundaries of podiform chromites may be well defined, many high grade deposits have sharp walls.

Magmatic movement of chromite crystal masses in a still liquid silicate matrix is probably of great importance in the development of podiform chromite deposits.

If ordinary basaltic magma is involved, it has to precipitate large amounts of olivine, with a slowly increasing Fe/Mg ratio, before the residual melt is sufficiently enriched in Cr for the precipitation of chrome spinel. Borchert (1964) assumes a primary concentration of 0.02 percent Cr_2O_3 in the parental magma, and 0.025 percent Cr_2O_3 as the lower limit of concentration to permit the separation of chrome spinel. Chromite will thus begin to crystallize after the separation of 20 weight percent of the solid phase. Borchert maintains that as chromite begins to crystallize from the residual melt, the necessary iron is subtracted from the immediate vicinity resulting in impoverishment in the surrounding silicates and an increase in the Mg/Fe ratio of the olivine associated with chromite in comparison to that in the surrounding harzburgite or dunite. Borchert suggests that reactions between crystallizing chromite and its silicate

environment are the key to the interpretation of the chemical composition of the chromite, its Cr/Fe, Cr/Al, Fe/Mg ratios on the one side and the Fe/Mg ratio of the paragenetic silicates on the other.

Many alpine peridotites, with associated chromite, occur in folded geosynclinal sediments of orogenic belts. Theories of origin include:

(1) Formation by crystal settling from basaltic magma, either at depth in stratifrom complexes, or in submarine lava flows.

(2) Crystallization from ultrabasic magmas.

(3) Intrusion of solid, primitive mantle material, or of residual mantle material after removal of a basaltic fraction.

(4) Incorporation of fragments of the oceanic crust into orogenic belts by mantle convection currents (Wyllie, 1967).

The structural features of alpine peridotites and their associated chromites are interpreted differently according to which theory of origin and emplacement is envisaged.

Borchert (1964), Petrascheck (1959), Helke (1962) and Dubertret (1955) interpret the structural features as primary, though modified by post magmatic tectonic movements. They consider that characteristic alpine peridotites result from differentiation of basaltic magma, with features governed by

magmatic layering.

Magmatic differentiation and segregation processes in basaltic magmas account for the development of chromite during the early stages of fractional crystallization. Borchert (1964) suggests that the differentiation process, accompanied by the crystallization and enrichment of chromite, has occurred in situ and at rather shallow depths. Large chromite accumulations are interpreted as developing by settling and downward rolling of the heavier chromite crystals on banks of silicates. During this stage much of the silicate may still be molten over distances of hundreds of miles or more. Nodular and lumpy ore masses may result especially in the deeper regions of the peridotite bodies.

In a crystallizing partial melt, zones exist which are enriched in volatiles. In these zones gliding and downward rolling of crystals and crystal aggregates proceeds with the greatest volocity leading to accumulation of massive chrome ore, neighbouring parts of the intrusion may be correspondingly impoverished in chromite. Thus the irregularity in form of the primary magmatic concentrations increase as the angle of inclination of the magmatic layers increase. Frequently the strike and the dip of magmatic layers will correspond to the foliation but local prototectonics and slump structures may produce many variations. Even irregular forms such as lenses,

podiform and bag like types of chromite will in most cases have some relation to the primary magmatic layering. The longest dimension of 'fusiform' ore bodies need not always lie in the dip direction but may often be oblique to the layering of the original residual melts. In most cases the regular orientation of the main faults and shear systems in relation to the magmatic layering can be regarded as evidence that primary differentiation processes have taken place in situ and prototectonic and post magmatic disturbances are in many cases strictly dependent on the original magmatic layering of the igneous intrusion. Thayer (1964), Hess (1955), Wijkerslooth (1954), Hiessleitner (1952) subscribe to an alternative hypothesis; they maintain that podiform and stratiform deposits are related in much the same way as metamorphic and sedimentary rocks. Structural relationships between podiform chromites and their host rocks are comparable to those in high grade metamorphic rocks, the layering being formed by flowage determined by upward movement of magma during emplacement.

In podiform deposits layered structures cross lithological contacts irrespective of their attitude, the latter have no recognizable control over the shape or location of the chromite. The chromite deposits are typically irregular in shape but the layered structure in the enclosing rocks is homoclinal and uniform.

Relict primary features in podiform chromites such as nodules, orbicules and settled textures can be compared to relict pebbles or cross bedding in metamorphosed conglomerates. Lineation is one of the most important structural features in podiform chromites. Distribution of chromite and dunite in torpedo or pencil shaped masses indicate the dominance of lineation which is best shown by the elongated nodules.

Chromite and olivine are both granular, foliation and schistocity are not well shown by the chromite but may be displayed in the associated peridotites. Flow layering, foliation and lineation may be simple and parallel to each other or angular and very complex. These features and relations are thought to point to the re-emplacement of podiform deposits as autoliths of solid chromite in a mobile crystal mush of peridotite. Relict textural features in chromite, and the wide range in proportion of associated peridotite can be explained by remobilization and re-emplacement of rocks partially differentiated by crystal settling in the lower part of the crust, or in the upper mantle. During the extensive travel from the site of primary differentiation most tabular or linear chromite deposits would be orientated in the direction of transport.

The crystal mush theory has also been supported by Bowen and Tuttle (1949) as the result of experimental work in the system

$MgO-SiO_2-H_2O$.

Ideas developed by Hutchinson (1963) for the re-emplacement of sulfide deposits during regional metamorphism seem to be applicable, in principle, to the movement of chromite bearing mafic rocks from their site of differentiation into eugeosynclines during major deep seated deformation. The sulfide ore minerals are rendered mobile, by plastic flow. In podiform chromites the evidence suggests that the oxide ore minerals were solid and immune to plastic deformation. The mobility of the alpine complexes may have resulted from crushing, local melting, and recrystallization of the silicates. The existence of thin dunite dykes in massive chromite suggests that the former have considerably higher relative mobility.

The lack of any significant contact metamorphism around most alpine peridotites is strongly in favour of the crystal mush theory. The contact relations between different components of alpine complexes are variable. The ultramafic parts of many complexes have serpentinised borders and are faulted against unaltered country rocks. This type of contact is now regarded as evidence for either cold diapiric emplacement or for serpentinisation. Serpentinisation could occur, during emplacement, by ground water moving towards the peridotite from the country rocks.

Moderate to high grade contact metamorphism, by peridotites

has been described by some workers; Green (1964), MacKenzie (1960) etc. Thermal metamorphism of country rocks to amphibole or pyroxene hornfels facies is accompanied by the development of strong foliation and lineation in both the peridotite and the country rock.

The chemical composition of high temperature peridotites (Green 1967) could be close to a possible mean composition for a peridotitic upper mantle. This type of peridotite has the potential for producing 10-20 percent of partial melt of basaltic composition. Alpine peridotites may thus represent complete mobilization, and intrusion to crustal levels, of portions of mantle peridotite. The primary origin of the high temperature peridotites is debatable, they provide evidence of:

(a) Mobility of high temperature, but entirely crystalline, peridotite within the crust.

(b) Movement of such high temperature peridotites through distances of 5-10 km, implying changes of load pressure of at least 2-3 Kb.

Van der Kaaden (1964) has summarised the main hypotheses for the genesis of alpine peridotites and podiform chromites as follows:

1. Emplacement of solid peridotitic material from the peridotitic substratum. The chromite is brought up in a

crystalline state. The observed layering, foliation and lineation are inherited from the substratum as a metamorphic texture. Chromite deposits were already deformed at depth by metamorphic processes and by flowage.

2. Emplacement of reactivated peridotitic material from the peridotitic substratum in the form of crystal mushes. The associated chromite deposits were brought up in a solid state and torn apart and stretched during their emplacement, by flowage of the crystal mush. Xenolitic blocks of gabbroic to pyroxenitic composition were also involved in these movements.

3. Emplacement of peridotitic magma. Large concentrations of chromite were formed at depth, after emplacement of the magma there was further crystallization but concentration of chromite from the magma was only possible on a very limited scale. Resorption of original chromite was also possible on a limited scale. Metamorphic textures were achieved by the disruption of early chromite by movement of the magma. Further disruption can be ascribed to post crystallisation tectonics.

4. Intrusion or even extrusion of basaltic material originating below the Mohorovic Discontinuity with differentiation in lacolithic bodies. The chromite deposits were formed in situ by gravitational-fractional crystallization. They have the same origin as the stratiform deposits.

5. Intrusion of basaltic magma forming stratiform complexes at depth, with later involvement in alpine tectonic movements.

6. The ultrabasic complexes were formed by local basification and rheomorphic mobilization of rocks in the basement complex.

Comparisons of podiform and stratiform chromite deposits.

T.P. Thayer (1960) has compared the two main types of chromite deposit and their related peridotite; the deposits are related in a similar manner to metamorphic and sedimentary rocks. Sedimentary principles should be applied to stratiform deposits and metamorphic rules for the podiform chromite deposits.

Stratiform chromites have been formed in situ by crystal accumulation of chromite on the floor of a magma chamber, they are characterised by a general sill like form. Layers can be followed for large distances with only small variations in thickness or other physical characters.

Two major hypotheses are advocated to explain the origin of podiform chromites and alpine peridotites.

1. They originate in a similar manner to stratiform deposits, but tectonic movements are responsible for their present positions and structural characters.

2. Peridotites of the orogenic belts have been emplaced as a crystal mush and originate from the lower part of the crust or

the upper mantle, they contain already differentiated chromites.

Podiform chromites are characteristically irregular. The size of each pod may vary from a few cm up to 150 m long. The contacts between chromite pods and the surrounding peridotites are sharp, and in most cases faulted. In stratiform deposits the bottom of the layers have sharp contacts but are disseminated upwards.

Examination of the peridotite enables a prediction of the type of associated chromite. Peridotites which include podiform chromites have been emplaced in major orogenic belts. The main associated rock types include dunite, harzburgite, troctolite and lherzolite. Poikilitic texture and plagioclase are rare. Contact relations with surrounding rocks are in most cases tectonic and thermal metamorphism is usually absent. The peridotites are commonly cut by numerous gabbroic dykes and pyroxenite veins, mainly parallel to the dominant joint directions.

The type of peridotite with which stratiform chromite is associated is pyroxenitic. Poikilitic texture and accessory plagioclase are common. Layering is continuous, with an upward progression from ultramafic to acidic rocks. Thermal metamorphism of surrounding rocks is common.

In stratiform complexes chromite layers are always parallel to the magmatic layering of the peridotite, whereas in podiform types, the position of the pods is not controlled by any magmatic layering.

The most common feature of podiform chromites is lineation, characterised by elongation of the pods. Lineation and foliation may be parallel to magmatic layering but may also be oblique.

Chromite crystals from stratiform deposits are more euhedral than those of podiform chromites. In stratiform chromites the amount of ferrous and ferric iron in the chromite increases at the expense of chromium and magnesium in the ascending sequence. Along the strike direction the ratio of ferric to total iron decreases towards the centre of the chromite layers. This is a generalized conception which may not apply for a particular example. Similar generalizations have been attempted for the podiform chromites, so far without success.

Podiform chromites are generally of metallurgical grade. The Cr_2O_3 content in the stratiform deposits varies in the range 35-50 percent while in podiform deposits the range is wide, from 15-65 percent. The average Cr:Fe ratio in stratiform deposits is 1.5:1 whereas in podiform deposits the values range from 2:1 to 4:1. The FeO:RO ratio is around unity in stratiform deposits and about 1:2 in the podiform type (Thayer, 1960).

A Regional survey of Podiform chromite deposits

Podiform chromite deposits are found in orogenic belts in association with highly disturbed peridotites. They occur in California, Cuba, Yugoslavia, Greece, Iran, Pakistan, India,

the Philippines, Russia and Turkey.

Californian chromite deposits

The peridotite zone of California, which contains numerous chromite concentrations, has a northwest-southeast trending, sill like form and occurs in Del Norte, Siskiyou, El Dorado, Amador Calaveros, Tuolumne and Mariposa counties. The deposits have been described by Wells et al. (1948, 1951). The peridotite is mainly saxonite with less common dunite and lherzolite. The chromite deposits are always related to the dunites and tend to occur near the margins of the mass. The chromites are mainly disseminated and podiform types. The term Californian type chromite has been used to describe other podiform deposits.

Chromite pods frequently occur in shear zones but there is no evidence that the chromite pods were formed after shearing took place. The pods possibly cause a weakness in the peridotite which make it liable to shearing at these points. There is no correlation between the size of the chromite deposits and that of the peridotite mass.

Chromite deposits of Cuba

The chromite deposits occur as irregular masses in belts of serpentinised peridotite along the north coast of Cuba, they have been described by Thayer (1943).

Gabbro, troctolite and anorthosite are associated with the

peridotite and form large masses. The chromite is associated with dunite and, to a lesser extent, with tractolite. It is commonly cut by dykes of banded troctolite and pegmatitic gabbro. The main chrome ore producing districts are Camaguey, Eastern Oriente and Matanzas province.

The primary structures in the chromite appear to bear little relation to the form of the ore bodies. The lateral contacts of massive ore bodies are usually sharp, whereas the ends may grade out through low-grade disseminated ore, to country rock. The chromite deposits of Cuba were formed early in the ultramafic sequence. The intergradation of gabbro, troctolite and anorthosite with peridotite is considered prima-facia evidence of essential contemporaneity of the feldspathic and non feldspathic rock types. The crosswise trend of planar structures in some disseminated ores, both with respect to the long axes of lenses and the trends of structures in the surrounding rock, suggest that, like the schistosity of metamorphic xenoliths, some of the structures in the ore may be inherited. The large number of sharp unfaulted contacts between massive ore and barren rock, and the lack of correlation between the size of the serpentine masses and the contained ore bodies, are taken as evidence against differentiation of the chromite in place, after intrusion of the peridotite. The very coarse grained chromite in some of the Cuban ore suggests, Thayer (1943)

that it was segregated at great depths, under conditions much more favourable to crystal growth than in any of the stratiform deposits where differentiation is presumed to have occurred after intrusion. The chromite is thus presumed to have segregated at great depth, before intrusion of the peridotite, and was carried up as solid (xenolithic) inclusions. Although the chromite itself was solid and subject to granulation under differential movements, the dunite matrix was sufficiently mobile to flow and penetrate minute fractures in the chromite. Analyses show a wide variation in Cr_2O_3 content, from 22.31 to 56.89 percent, and of Al_2O_3 from 13.77 to 44.73 percent.

Chromite deposits of Yugoslavia and Greece

Yugoslavian and Greek chrome ores have been described by Hiessleitner (1951, 1952). The tectonic movements along a northwest-southeast direction corresponding with the trend of the Dinaric mountains have influenced the shape of the serpentine masses, and the distribution of chromite ore, in Yugoslavia.

The chromite bearing peridotites of Greece extend along the Pindus mountains also on a northwest-southeast axis. Both podiform and stratiform deposits are found, they include:

a. Sinikl and Soufflion, Eastern Thrace.

Highly crystalline rocks border the serpentine mass. Magmatic banding is well exhibited, the chrome ore bodies are small in size.

b. Chalkidike peninsula.

The peridotites are distinctly layered, ranging in composition through dunite, pyroxenite, harzburgite, and gabbro to dolerite. Adjacent country rocks are crystalline schists. Chromite deposits are regularly developed ranging from 0.50 to 3 m thick bands of disseminated to solid chromite, conforming with the general layered structure.

c. The Mount Olympus area.

The chromite deposits are podiform with a low Cr_2O_3 content and are enclosed in northwest-southeast trending serpentine surrounded by crystalline limestone.

d. Domakos and Tsangli, Central Greece.

This area is the most productive in Greece. The main rock types are harzburgite and dunite. The chrome ore bodies are arranged along two to three axes parallel to the general northwest-southeast trend. The ore is of podiform type with a Cr_2O_3 content up to 40 percent and high Al_2O_3.

Chromite deposits of Iran

Haeri (1960) explains the chrome ore deposits of Iran, there are two main localities of chromite concentration, in the north in the Froumad district and the Ab-Dasht district in the south. The chromites are of podiform type with better grade ore in the south. The chromite occurs in serpentinised peridotite and in the

south is associated with magnesite veins.

Chromite deposits of Pakistan

Chromite bearing ultrabasic rocks are exposed along the western and northwestern border of West Pakistan, extending from the Malakard agency in the north to the Chagai district in the south, they have been described by Bilgrami (1964) and Asrarullah (1960). The ultrabasic rocks are mainly harzburgite, dunite and serpentinite. The ultrabasics follow the regional tectonic trends and appear to have been intruded, intermittently, along the central portions of large anticlines, or of an anticlinorium along the Zhob Valley. The Zhob Valley is the main chromite producing area. Metamorphosed sediments occur near the contacts. The ultrabasic rocks have been intruded by dolerite dykes which locally transgress into the surrounding sedimentary rocks.

Chromite occurs as disseminated crystals, veins, lenticular masses and tabular lenses. The contacts between the massive chromite and the enclosing rocks are well defined. There is no apparent directional relationship between the boundaries of the peridotites and the bands, layers and lenses of chromite which seem to be distributed at random in the host rock. In places there appears to be a definite relationship between the layering in the ultramafics and the chromite layers.

Many features in the Zhob Valley district point to its being

of the alpine type, except for the contact metamorphic effects on surrounding sediments. The Cr_2O_3 content of the chromites in the Zhob valley area decreases from west to east.

Chromite deposits of India

Chromite deposits occur quite extensively in the eastern part of the Indian peninsula, extending from Bihar in the north to Madras in the south. Chromite always occurs with serpentinised dunite, harzburgite and pyroxenites. The chromiferous ultrabasic rocks are of of Pre-Cambrian age being parallel or sub-parallel to the major tectonic zones of peninsular India.

In classifying the Indian chromites consideration must be given to the tectonic environment of the deposits. In many cases they show characters of both the podiform and stratiform types. The major chromite districts of India are:

(a) Singhbhum, Bihar; classified as stratiform.

(b) Keanjhar district, Orissa; the deposits are described as being of the fissure filling type (podiform type?).

(c) Kondapalle, Mdhra; small deposits of chromite occur, disseminated and in lenses.

(d) Sittampund, Madras; chromitite rocks occur in altered pyroxenites, interlayered with anorthosites.

(e) Byrapur and Sinduvalli, Mysore; chromites are of podiform type.

(f) Rotnagiri district, Maharashtra; altered peridotites are intruded into granite gneisses.

In general Indian chromites are ferromagnetic and have a high Al_2O_3 content. Accounts of Indian chromite deposits have been given by Prasada Rao and Malhotra (1964) and Chakraborty (1965).

Chromite deposits of the Philippines

Stoll (1958) has described these chromite deposits which form a belt 2500 m long and occur in a layered ultramafic complex. Norite and olivine gabbro form the upper zones of the layered complex. The dense chromite bodies are regarded as xenoliths that have been born upwards in intrusive saxonite. The main Masinloc deposit has the form of a thick irregularly curving plate and is classified as a sackform deposit (podiform). Contacts with the adjoining ore and rocks are generally sharp. The form, angularity and sharp definition of the bodies point to their xenolithic origin. Disseminated ore in bands 3-5 cm thick, 30-40 cm long, together with associated dunite, probably originated through corrosion and disruption of dense ore by peridotite accumulating next to the dense masses after movement had ceased. The platy banding, may be almost parallel to the long axis of the bodies and in places is set parallel to neighbouring contacts with massive chromite.

The chemistry of the massive ore and disseminated chromite is essentially the same. The Cr_2O_3 content ranges from 33.55 to 40.68 percent and Al_2O_3 from 23.04 to 33.44 percent, the ore being

mainly of refractory grade.

The ultramafic rocks may have originated by the partial refusion and intrusion of a concealed basal zone, possibly upper mantle material. The layers in the ultramafic mass are too uniform and continuous to have been produced by magmatic flowage, and too numerous and concordant to have arisen through multiple intrusion.

The petrographic relations between rock forming minerals and accessory chromite suggest that the latter crystallized after emplacement. Whatever may have been the exact physical-chemical state of the mass the evidence suggests that the peridotite possesed mobility.

Chromite deposits of Turkey

Chromite deposits are widespread in Turkey with more than 330 known groups of deposits. The chromites are related to ultrabasic rocks which are concordant with the trend of the orogenic belts, the age of emplacement is still controversial. The ultrabasic belts are associated with abyssal fractures which play an important role in the tectonic development of Turkey. Chains of ultrabasic rocks extend along these zones following the borders of geosynclinal foredeeps, they separate stable masses, such as Pre-Palaeozoic and Palaeozoic folded basement, from highly deformed units. A periodic rejuvenation of the abyssal fractures with

movement in the upper parts may explain the range of ages for emplacement of ultrabasic rocks in Turkey (Van der Kaaden, 1964).

Turkey is divided into three main peridotite and chromite zones which may be designated:

(a) The Northern zone

(b) The Southern zone

(c) The central Anatolian area

(a) In the Northern peridotite zone extending along the Pontic mountains, chromites are mainly of massive and podiform type, the latter having east northeast - west southwest and east-west trends. The Cr_2O_3 content of the ore is generally below 45 percent, with high values for FeO and Al_2O_3.

(b) The Southern peridotite zone extends east-west along the Tauros mountains. Chromite concentrations are extensive, but particularly significant near Fethiye in the west and the Elazig-Guleman district in the east. The chromites are of podiform type and have sharp contacts with the surrounding rocks. The pods are elongated in one of two general directions, north-northwest - south southeast or east northeast - west southwest. The grade of ore is metallurgical with up to 59 percent Cr_2O_3.

(c) In the central Anatolian area chromite concentrations are numerous, though generally of limited extent. The chromite occurs in podiform concentrations generally elongated north northwest - south southeast or northeast - southwest. Important mines include

Eskisehir-Dagardi, and of less significance the deposits at Bursa-Orhaneli, Kutahya-Domanic and Konya. In the Orhaneli area, however, the ore is classified as stratiform, with a Cr_2O_3 content of 48 percent. Thickness varies from 6 cm to 10 m and deposits are up to 70 m long. In the Dagardi mine the chromite ore body is 760 m long and has a sharp contact with the surrounding peridotite. The Cr_2O_3 content reaches 54 percent.

CHAPTER 6

THE PETROLOGY AND CHEMISTRY OF THE ANDIZLIK-ZIMPARALIK CHROME ORES

Introduction

Chromite is one of the few minerals which are useful as a source of metal, in the preparation of chemicals, and as a refractory material. The utility of a particular chrome ore depends both on its chemical composition and its physical properties.

Metallurgical[1] grade chrome ore is first converted to ferrochrome containing 60-75 percent chromium, it is mainly smelted in an electrical furnace. This grade of chromite should contain 45-50 percent Cr_2O_3 and have a Cr/Fe ratio of at least 2.8:1, silicate impurities should be low and combined Al_2O_3 and MgO should not exceed 25 percent.

Refractory grade chromite has a high resistance to corrosion and thermal change and is natural towards slags. For refractory purposes the combined Cr_2O_3 and Al_2O_3 should be over 57 percent, while SiO_2 is less than 5 percent and FeO less than 10 percent. Serpentine impurities should be as low as possible since they reduce the strength of the refractory at high temperatures.

Chemical grade chrome ore is first converted to alkali chromates or bichromates which may be used for tanning leather,

manufacture of pigments, dyeing and manufacture of dye stuffs, surface treatment of metals, wood preservation or as additives to drilling muds used for deep drilling. Specifications for chemical grade chromite include a Cr_2O_3 content above 44 percent while the Cr/Fe ratio should be about 1.6:1; Al_2O_3 should be less than 15 percent and SiO_2 less than 8 percent.

Chromite is a spinel with a general formula of $RO.R_2O_3$. In the chrome spinels the RO group is mainly MgO and FeO while the R_2O_3 group is mainly Cr_2O_3, Fe_2O_3 and Al_2O_3. Thayer (1956) suggests that the formula of chromite is best expressed by $(Mg.Fe^{++})(Cr\ Al\ Fe^{+++})_2O_4$.

Naturally occurring chromites are essentially solid solutions of the Mg and Fe members of the spinel and chromite series, magnesian chromite and ferro chromite, with minor amounts of the magnetite series. In nature pure end members are rarely found.

The high iron chromites resemble magnetite, they are hard with moderate to strong magnetic properties, opaque in thin section, and have a dark brown to black streak.

The high alumina chromites are black in hand specimen give a pale brown to brown streak and are coffee-brown in thin section; they are non-magnetic.

Chromite crystals have a wide variety of forms, the octahedron $\{111\}$ is predominant and combinations, even with $\{110\}$ and $\{100\}$ are

relatively rare.

The composition and chemical behaviour of chromite is complex. In theory the RO and R_2O_3 of chromite should balance in primary magmatic deposits since the host peridotite is a balanced system with no free MgO, periclase, Al_2O_3, corundum, or Fe_2O_3 hematite. In practise, however, many chromites are shown to have unbalanced formulae.

Ore types

In the Andizlik-Zimparalik area, apart from the chromite occurring as an accessory mineral in the peridotite, ore deposits are widespread and extensively mined.

Chrome ore concentrations of four types have been identified. They are massive chromite, nodular chromite, disseminated chromite, and a limited development of stratiform chromite.

The massive chromites comprise a closely packed mass of anhedral to subhedral chrome spinel crystals which reach 1-2 mm in size, Plate 12. Interstitial space has been filled by serpentine in most cases, and very rarely by tremolite and chlorite; the silicate matrix may reach 15 percent of the ore. Black to blackish brown in appearance, the ore deposits are generally brecciated and fragile.

Nodular chromites are common, with nodules ranging in size from a few mm to 2 to 3 cm in length and up to 1 cm in diameter, Plate 11.

They are embedded in a yellowish green serpentine matrix. The chromite nodules generally constitute some 50 to 60 percent of the ore. Nodules occasionally show lineation and pull-apart texture, as described by Thayer (1964).

Disseminated chromite (schliere) is transitional between massive and accessory chromite though generally closer to the former, Plate 13. The chromite content may reach 80 percent of the ore, although the matrix is easily seen in hand specimen.

Stratiform chromites are uncommon in the Andizlik-Zimparalik area; they occur in the east and southeast part of the field. The stratiform chromites do not reach economic grade but form 3-4 mm thick bands of euhedral to subhedral crystals with a grain size of about 1 mm, Plate 14.

Ore microscopy

Apart from the percentage of chromite crystals seen in the specimen there is no distinct criterion to facilitate the identification of a particular type of chromite by reflected light microscopy. The crystals are generally subhedral to euhedral in form though usually corroded. The interstitial spaces are filled by serpentine. Chromites often have numerous serpentine inclusions particularly in the nodular type, these inclusions occur mainly towards, and parallel with, the margins of the crystals, Plate 33. Fine-grained anhedral to subhedral pyrite, and some chalcopyrite

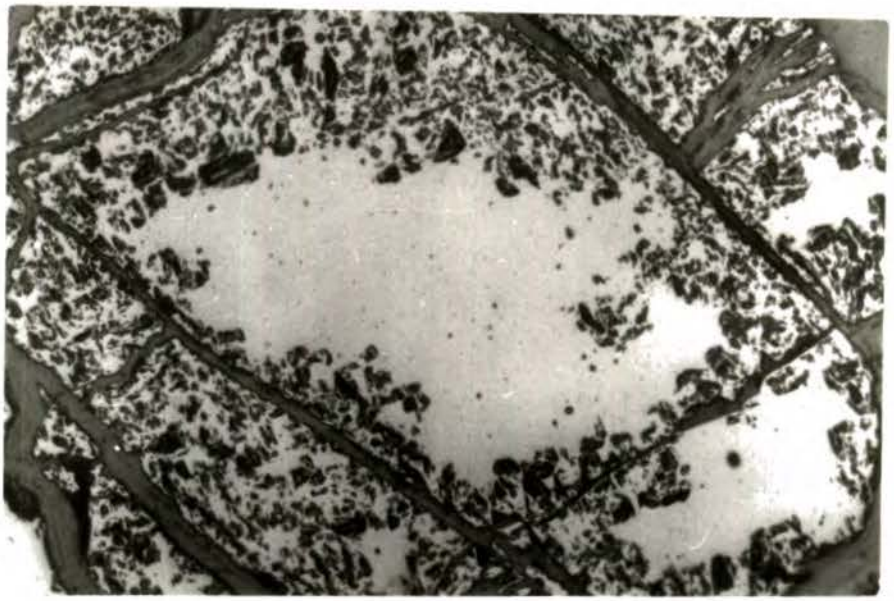

Plate 33 Silicate inclusions in chromite. These inclusions are parallel to the grain boundaries (Reflected light, X80).

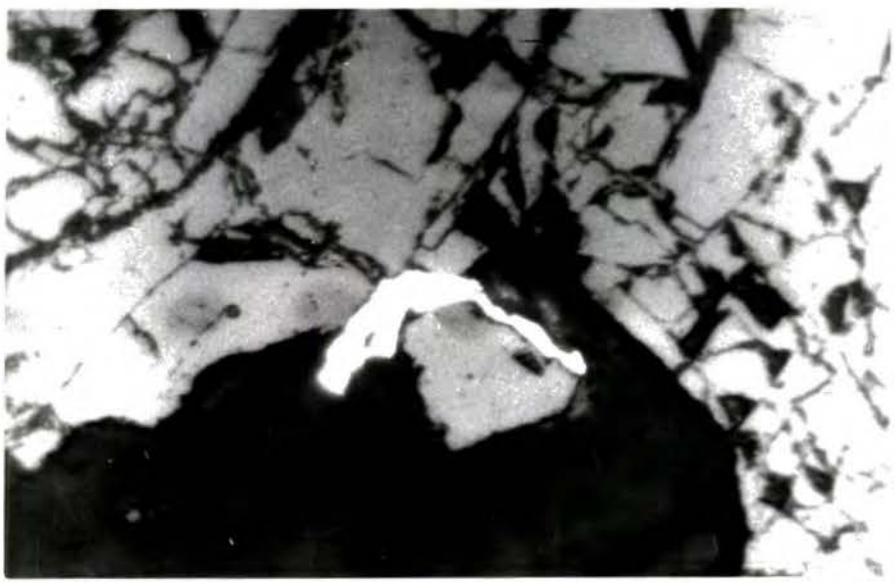

Plate 34 Intergranular anhedral pyrite associated with chromite (Reflected light, X200).

crystals, occur in the interstitial serpentine, Plate 34, but apart from this the mineralogy of the chromites is simple.

Wijkerslooth (1943) has described the occurrence of rutile and native platinium as inclusions in chromites from Turkey but neither of these two minerals, nor ilmenite, has been found in the microscopic study of the Andizlik-Zimparalik chromites.

Many corroded chromite crystals have a development of opaque material with relatively higher reflectivity along fine cracks within the crystals; rarely this material forms a narrow rim around the chromite, Plate 35. Attempts to measure the reflectivity of this phase have proved unsuccessful.

Wijkerslooth (1943) considers that resorption of chromite takes place in two stages.

1. Magmatic resorption, through early chromite sinking through and being affected by hot magma, preferably develops along fine cracks and crystal boundaries. This process can cause disruption of chromite grains.

2. Hydrothermal resorption, which also commences along fine cracks in the chromite and leads to the formation of an opaque mineral which has a higher reflectivity than the chromite. Horninger (1940) terms this mineral "ash coloured magnetite" while Spangenberg (1943) gives it the name "ferritchromit". Horninger (1940), Spangenberg (1943) and Wijkerslooth (1943) have attempted

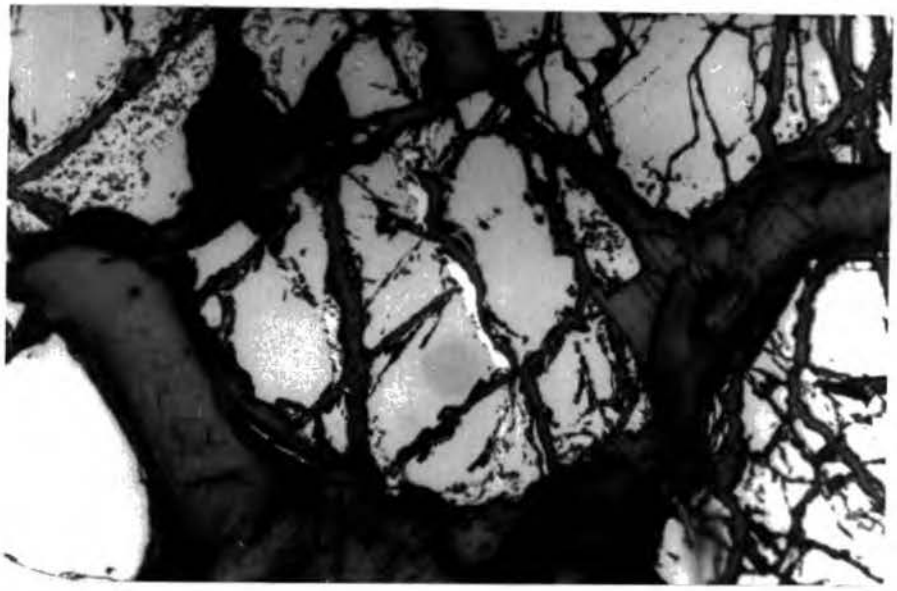

Plate 35 "Ferritchromit" zones developed along grain boundaries and cracks in chromite (Reflected light, X80).

to explain the development of this higher reflectivity material. They suggest that during hydrothermal activity Al_2O_3 and MgO from the chromite react with the serpentine to form tremolite and chlorite. Alternatively hydrothermal activity causes the removal of FeO and Fe_2O_3. The former process, removal of Al_2O_3 and MgO, seems more likely as the occurrence of "ferritchromit" is generally related to the formation of chlorite and tremolite.

Panagus and Ottemann (1966) describe "ferritchromit" occurring as rims around the chromite grains of the nodular chromites from Rodiani (Greece). They give the cell-edge of the host chromite as 8.24A° and 8.34A° for the "ferritchromit" rim.

Golding and Bayliss (1968) also mention similar occurrences in the chloritic chromites from Australia. They ~~both~~ show that in their "ferritchromit" Cr_2O_3 and Fe are higher but Al_2O_3 and MgO are lower than the associated primary chromite. These findings are in a close agreement with the explanation given above for the generation of "ferritchromit".

Reflectivity

Chromite reflectivities have been measured using the technique and apparatus described by Phillips and Bradshaw (1966); a digital voltmeter replaced the galvanometer in the original apparatus.

Reflectivity measurements were made at the wavelengths

440, 460, 480, 520, 540, 560, 580, 600, 620, 640 and 660 mμ. Black glass, carborundum, and silicon, calibrated by the "National Physical Laboratory" for the above wavelengths, were used as standards, appendix table 6.

Chromite specimens were repolished prior to reflectivity measurement. Background readings were taken for each specimen by covering the high power objective (40x) by a black box prepared for this purpose. For the measurements suitable areas on the specimen were selected by using the (10x) ocular and (10x) objective, but the actual readings were made with a (10x) ocular and (40x) objective. The field of view was reduced to 80μ diameter. Background and standard readings were recorded for every wavelength by sliding the wavelength filter from one wavelength to another for each specimen. Six measurements were made in different places on each sample, for each wavelength, after which standard and background readings were repeated, these measurements appear in table 5 of the appendix. The reflectivity of each specimen was calculated by reference to the relevant standard readings. The average of the two background readings was subtracted from the average of the Standard reading and from the average of six readings on the specimen. The reflectivity of each specimen was calculated separately for each of the three standards and the mean of these results accepted as the spectral reflectivity of

Table 14 Spectral reflectivities of chromites

Wave lengths mμ	F68	F65	F19	F62	ZU8	F128	ZU44	ZU9	A1	AU12	F70	A17	A78	F119	F31	AU32	ZU30E	ZU12	A10
440	11.12	11.28	12.19	12.25	12.65	12.87	12.74	12.94	13.06	12.73	12.81	13.17	13.15	13.33	13.18	13.25	13,20	13,21	13,28
460	10.93	11.06	12.09	12.04	12.63	12.80	12.69	12.94	12.79	12.72	12.77	13.12	12.92	13.04	13.01	12.88	13.04	13.00	13.14
480	10.88	11.05	12.04	11.92	12.51	12.70	12.42	12.82	12.73	12.60	12.69	12.88	12.80	12.91	12.86	12.91	12.86	12.91	13.06
520	10.74	11.00	11.81	11.73	12.31	12,49	12.23	12.58	12.55	12.35	12.47	12.66	12.60	12.74	12.62	12.68	12.68	12.69	12.85
540	10.64	10.88	11.75	11.61	12.15	12.36	12.10	12.49	12.43	12.21	12.33	12.55	12.50	12.62	12.50	12.54	12.53	12.61	12.73
560	10.58	10.73	11.62	11.51	12.08	12.29	12.03	12.42	12.30	12.10	12.24	12.45	12.37	12.53	12.40	12.47	12.43	12.53	12.66
580	10.49	10.69	11.49	11.42	11.99	12.15	11.90	12.28	12.21	12.12	12.15	12.36	12.29	12.44	12.29	12.35	12.32	12.40	12.53
600	10.43	10.63	11.41	11.32	11.93	12.12	11.81	12.16	12.17	11.91	12.08	12.22	12.12	12.32	12.20	12.25	12.21	12.37	12.45
620	10.34	10.70	11.33	11.34	11.81	11.90	11.78	12.15	12.15	11.94	11.84	12.29	12.16	12.35	12.06	12.00	12.20	12.24	12.29
640	10.42	10.37	11.30	11.21	11.85	11.87	11.70	11.72	11.94	11.57	11.92	12.29	12.08	12.04	12.05	11.99	12.32	12.13	12.15
660	10.23	10.13	11.33	10.74	11.65	11.71	11.79	11.47	11.58	11.33	11.64	12.21	12.08	11.98	11.67	11.78	11.82	11.97	11.66

that specimen for that particular wavelength.

Nineteen chromites have been examined in this way. As shown in table 14, the spectral reflectivities of the chromites vary by about 2 percent for a particular wavelength (for example at 480 μ, from 11.05 to 13.06).

Several traverses comprising a series of readings were made across grains, the readings were found to agree within the limits of experimental error and the specimens were presumed to be unzoned.

X-ray diffraction determinations of cell size

Ten chromite specimens have been studied by X-ray diffraction. X-ray powder photographs were taken with the Philips high angle diffractometer using a 114.6 mm Debye-Scherrer camera with fine collimators. Industrial G X-ray films were exposed to cobalt radiation for 24 hours. The d spacings have been compared in table 15, with the data given by A.S.T.M. and by Dunham et al. (1954).

Unit cell edges for the ten chromites have been calculated from back reflections and found to vary from 8.234A° (F68) to 8.305A° (Z68). The data is presented in table 16.

Chemistry

Chromites from the Andizlik-Zimparalik area have been analysed by X-ray fluorescence spectrography and optical spectrography.

Sample Preparation

Chrome ore specimens selected for chemical analysis included 6 to 90 percent silicate impurity. This impurity has been separated

Table 15 d spacings of Chromites

DPCJ*		F68		F76		ZU8		ZU9		F119		F242		
dA°	Intensity	dA°	Intensity	dA°	Intensity	dA°	Intensity	dA°	Intensity	dA°	Intensity	dA°	Intensity	hkl
		4.717	s	4.740	s	4.729	s	4.731	s	4.743	s	4.742	s	111
2.86	vw	2.896	s	2.905	s	2.906	s	2.902	s	2.921	s	2.916	m	220
2.45	s	2.467	vs	2.483	vs	2.481	vs	2.480	vs	2.488	vs	2.471	vs	311
				2.381	vvw	2.382	vvw	2.383	vvw	2.384	w	2.397	vvw	
2.04	m	2.051	m	2.057	s	2.060	s	2.058	s	2.064	s	2.060	s	400
1.67	vw	1.674	v	1.685	w	1.681	w	1.684	w	1.685	w	1.687	vvw	422
1.58	s	1.578	s	1.587	s	1.587	s	1.586	s	1.592	s	1.587	s	551,333
1.45	s	1.451	s	1.458	s	1.458	s	1.455	s	1.462	s	1.456	s	440
1.387	vvw	1.387	vw	1.394	vvw	1.393	vvw	1.395	vvw	1.400	w			531
1.300	vvw													620
1.254	vw													533
1.239	vvw													622
1.187	vw	1.189	vw	1.192	w	1.193	vvw	1.194	vvw	1.198	m	1.199	vvw	444
		1.152	vvw	1.157	vvw	1.159	vvw	1.156	vvw	1.162	w			117,155
1.101	vw	1.101	vvw	1.103	vvw	1.105	vvw	1.104	vvw	1.109	vvw	1.109	vvw	246
1.073	m	1.072	m	1.077	m	1.077	m	1.078	m	1.081	m	1.081	vvw	355,137
1.030	w	1.030	m	1.034	w	1.034	w	1.035	w	1.038	w	1.037	w	008
0.971	vvw	0.970	vvw											822,660
0.952	w	0.950	m	0.954	w	0.955	w	0.956	w	0.959	vvw	0.959	w	751,555
		0.944	vvw	0.948	vvw					0.953	w	0.952	w	662
0.922	w	0.921	m	0.924	w	0.925	w	0.926	w	0.928	w	0.928	w	840
		0.904	vvw											911,753
0.864	w													
0.843	m													
0.799														

DPCJ* Chromite from Hangha, Sierra Leone Dunham, Phillips, Challmers and Jones (1958) p.44

from the chromite.

Preliminary crushing in the Sturtevant jaw crusher reduced the sample to grains of mm to dust size. The samples were then passed through a 155 mesh sieve, and the fine fraction washed thoroughly to remove dust; a small proportion of the silicate impurity was removed by floatation at this stage. The dried specimens were then transferred to Clerici solution in a separation funnel, a process which was repeated several times. The separated chromite was recovered, washed, dried, and afterwards passed several times through a magnetic separator. The average purity achieved bytthis procedure was 99.50 percent, silicate inclusions present in the chromite crystals preventing a better degree of purification. After the separation, the chromite was reduced to around 300 mesh in a tungsten carbide ball mill. The powders were then pelletized at a pressure of 5 tons per sq inch, 3 drops of "Mowiol" were added as binder and boric acid powder added to form a backing to the specimen.

Analytical methods

Ten elements were determined by X-ray fluorescence spectrography and have been calculated as Cr_2O_3, Al_2O_3, total Fe as FeO, MgO, CaO, NiO, ZnO, CuO, SiO_2 and TiO_2. Nine chemically analysed chromites were used as standards, five secondary standards were produced by mixing known amounts of two of the primary standards.

Table 16 Unit cell edge lengths of chromites

No.	Unit cell edge length(A°)
F68	8.234
F65	8.245
F76	8.265
F62	8.268
ZU8	8.277
ZU9	8.291
F119	8.303
ZU12	8.296
Z68	8.305
F242	8.301

Mass absorbtion corrections were made by an iterative process using the computer technique described by Holland and Brindle (1966).

Interference from 4th order CrKβ is a problem in the determination of Al and required a correction to AlKα counts. Intensity readings from standards were plotted against Al_2O_3 content and a best-fit curve was drawn. The graphical deviation of each point was measured and divided by the corresponding CrKα count to produce values for X. The average modified deviation ($\bar{X}$) was then calculated and applied to unknowns:

$$AlK\alpha \text{ (corrected)} = AlK\alpha - (\bar{X}\ CrK\alpha)$$

Standards for the determination of Ca, Ni, Zn, Cu and Ti were prepared by an addition technique, as explained by Hirst and Dunham (1963). Standards for the determination of V and Mn were also compiled by an addition technique but the determinations were made by optical spectrography since X-ray fluorescence is subject to interferences; VKα by TiKβ and MnKα by CrKβ.

The Hilger and Watts automatic large spectrograph, E-742, with glass optical system E 744 was used for optical spectrography over the wavelength range 3800-5300μ. The wavelengths used were Mn 4034.49A° against Cr 4037.29A° and V 4400.58A° against Cr 4399.82A°, standard spectrographic techniques were employed; see for example Ahrens and Taylor (1961).

Results

Sixty-three chromite specimens have been analysed, including

one unseparated specimen, the results are shown in table 17. The samples include 15 from the Andizlik mine, 18 from the Zimparalik mine, 8 from Üçköprü and 8 from Damdir, the remainder are from the scattered occurrences shown on fig.10.

The Cr_2O_3 content varies from 37.09 to 58.43 percent, MgO from 10.58 to 14.47 percent, Al_2O_3 from 14.16 to 28.70 percent and total iron expressed as FeO from 12.16 to 18.64 percent. The remaining components are minor constituents, amongst which MnO shows variation from 0.21 to 0.59 percent and V_2O_3 from 0.15 to 0.33 percent. CuO is present in the range 50 to 250 ppm, probably representing minor chalcopyrite impurity. ZnO varies from 350 to 1312 ppm similar to the level in most other alpine chromites but considerably less than in the Zn bearing chromite from Norway described by Donath (1931) in which the content of ZnO reaches 2.62 percent.

The small silicate impurity remaining after separation is reflected in the SiO_2 content which varies from 0.11 to 1.54 percent. CaO varies from 46 to 1806 ppm, and this may also reflect the silicate impurity for-the content is particularly high in tremolite bearing chromites. (e.g. A17, 952 ppm). NiO varies from 880 to 2040 ppm and TiO_2 from 1340 to 4100 ppm. Thayer (1956), Malhotra and Rao (1964) and Ghisler and Windley (1967) etc. ascribe the TiO_2 content of chromite to impurities present in the analysed specimens. In the Andizlik-Zimparalik chromites neither ilmenite

Table 17 Chromite analyses (weight percent) and mineralogical formulae on the basis of 4 Oxygen atoms.

	A1	A88	AU12	AU4	A17	A78	AU29	AU17	AU13	AU32	AU18	AU10	AU6	AU28	A10
Cr_2O_3	53.44	53.98	54.09	54.29	55.30	55.39	56.27	56.38	56.86	56.96	56.99	57.19	57.83	57.87	58.31
Al_2O_3	18.72	17.47	19.11	18.70	17.04	16.58	16.27	17.57	14.68	16.06	15.75	15.37	14.70	14.75	15.25
V_2O_3	0.23	0.22	0.18	0.20	0.18	0.17	0.18	0.21	0.15	0.17	0.18	0.18	0.17	0.18	0.21
SiO_2	0.66	0.65	0.38	0.27	0.51	0.60	0.53	0.16	0.56	0.27	0.51	0.66	0.75	0.34	0.39
TiO_2	1619	1728	2972	1692	2271	4083	3390	1987	2914	3373	2037	2905	3794	2909	2859
MgO	12.73	10.58	12.88	12.28	11.05	13.16	12.99	12.20	12.54	12.65	12.46	13.21	12.92	12.39	12.25
FeO*	13.59	16.45	12.60	13.54	15.18	13.26	13.01	12.85	14.53	13.13	13.46	12.64	12.83	13.71	12.93
CaO	119	308	70	105	952	77	68	63	56	77	77	150	49	77	46
NiO	1835	1189	1790	1775	1030	1534	1368	1693	969	1349	1492	1816	1440	1279	1266
ZnO	378	525	385	410	487	385	385	373	375	373	385	348	339	385	388
CuO	128	88	63	81	98	122	87	62	75	88	112	95	76	78	81
MnO	0.24	0.27	0.26	0.33	0.27	0.23	0.24	0.23	0.24	0.25	0.25	0.23	0.25	0.30	0.21
Cr/Fe	3.46	2.89	3.78	3.53	3.21	3.68	3.81	3.86	3.45	3.82	3.73	3.98	3.97	3.72	3.97
Mg/Fe	0.73	0.50	0.79	0.70	0.56	0.77	0.77	0.74	0.67	0.75	0.72	0.81	0.78	0.70	0.73
Cr/Al	3.69	3.99	3.66	3.75	4.20	4.32	4.47	4.15	5.00	4.58	4.68	4.81	5.09	5.07	4.94
Cr	1.343	1.382	1.346	1.356	1.410	1.474	1.326	1.408	1.458	1.438	1.450	1.458	1.485	1.477	1.482
Al	0.701	0.666	0.709	0.695	0.644	0.658	0.613	0.655	0.561	0.604	0.594	0.582	0.561	0.559	0.576
Mg	0.576	0.483	0.592	0.570	0.423	0.635	0.600	0.571	0.584	0.594	0.577	0.608	0.593	0.584	0.572
Fe	0.356	0.442	0.325	0.353	0.402	0.363	0.340	0.333	0.387	0.342	0.356	0.332	0.337	0.361	0.339

*Total Fe as FeO

CaO, NiO, ZnO, CuO, TiO_2 are as p.p.m.

A1 through A10 from the Andizlik mine.

Table 17 continued

	ZU8	ZU19E	ZU44	Z58	Z59	ZU24E	ZU9	ZU36	ZU26E	ZU34A	ZU6	ZU5	Z57	ZU40E	ZU16	ZU30E	ZU12	Z68
Cr_2O_3	51.11	52.49	52.63	52.67	52.99	53.11	53.32	53.35	53.69	54.34	54.35	54.55	54.97	56.11	56.43	57.04	57.81	58.32
Al_2O_3	19.68	16.45	18.96	18.34	17.45	15.54	17.36	17.36	17.32	17.72	17.50	15.59	16.16	15.43	14.88	15.86	15.43	14.16
V_2O_3	0.29	0.23	0.23	0.27	0.20	0.29	0.23	0.19	0.23	0.21	0.20	0.28	0.23	0.17	0.19	0.20	0.19	0.18
SiO_2	0.62	1.16	0.48	0.62	1.27	1.30	0.93	0.81	0.88	0.33	0.44	0.39	0.62	0.67	0.71	0.35	0.39	0.57
TiO_2	1962	2079	2070	1770	3398	1444	2571	2722	2321	3340	2112	1636	1661	2730	2271	2421	2321	3147
MgO	12.93	14.33	13.22	11.90	13.87	14.47	13.24	13.33	12.76	12.74	13.24	12.33	11.85	12.76	13.20	12.38	11.86	12.65
FeO*	14.63	14.56	13.83	15.52	13.38	14.63	14.12	14.14	14.40	13.88	13.59	16.21	15.56	14.12	13.83	13.50	13.65	13.38
CaO	315	262	56	367	434	273	315	53	70	56	81	64	54	133	35	84	56	70
NiO	1539	1743	1463	1450	1678	1419	1667	2061	1539	1559	1673	1537	1520	1374	1179	1279	1352	1300
ZnO	622	522	491	547	472	541	485	522	475	385	491	465	476	373	408	404	404	361
CuO	125	106	53	122	115	112	158	75	101	99	78	88	115	88	88	115	100	43
MnO	0.29	0.31	0.25	0.25	0.24	0.28	0.30	0.28	0.27	0.25	0.25	0.29	0.23	0.29	0.28	0.25	0.27	0.24
Cr/Fe	3.08	3.17	3.35	2.99	3.49	3.20	3.32	3.32	3.28	3.45	3.52	2.96	3.11	3.50	3.60	3.72	3.73	3.84
Mg/Fe	0.69	0.76	0.74	0.59	0.80	0.77	0.73	0.73	0.69	0.71	0.75	0.59	0.59	0.70	0.74	0.71	0.67	0.73
Cr/Al	3.36	4.12	3.59	3.71	3.93	4.42	3.97	3.97	4.01	3.96	4.02	4.52	4.40	4.70	4.91	4.65	4.84	5.33
Cr	1.284	1.349	1.315	1.337	1.359	1.374	1.359	1.356	1.369	1.368	1.367	1.396	1.408	1.437	1.446	1.445	1.471	1.497
Al	0.737	0.629	0.708	0.693	0.666	0.598	0.661	0.658	0.658	0.663	0.655	0.595	0.616	0.588	0.569	0.588	0.585	0.541
Mg	0.586	0.642	0.605	0.544	0.608	0.645	0.597	0.605	0.576	0.592	0.610	0.580	0.546	0.588	0.607	0.579	0.555	0.588
Fe	0.383	0.390	0.359	0.410	0.354	0.396	0.373	0.374	0.382	0.360	0.356	0.433	0.417	0.375	0.368	0.356	0.361	0.354

*Total Fe as FeO

CaO, NiO, ZnO, CuO, TiO_2 are as p.p.m.

ZU8 through Z68 from the Zimparalik mine.

Table 17 continued

	F49	F31	F33	F242	F68	F65	F19	F218	F62	F115A	F70	F76	F244
Cr_2O_3	54.65	56.87	57.92	58.43	37.09	41.74	43.28	43.54	48.04	49.78	54.27	45.51	47.83
Al_2O_3	17.19	16.13	15.42	15.64	28.70	27.14	23.92	27.21	21.96	16.19	17.57	24.23	23.58
V_2O_3	0.19	0.21	0.17	0.17	0.29	0.30	0.28	0.31	0.33	0.22	0.26	0.24	0.29
SiO_2	0.70	0.45	0.43	0.14	0.65	0.51	0.72	0.20	0.47	0.66	0.26	0.37	0.48
TiO_2	2408	2012	2408	2371	2505	1828	2458	1639	1369	2922	2070	2872	1523
MgO	12.85	12.99	12.96	12.73	14.26	13.66	12.34	13.64	13.27	11.06	13.10	13.88	13.75
FeO*	13.73	12.74	12.46	12.16	17.92	15.89	18.64	14.38	15.21	21.20	13.86	14.98	13.35
CaO	56	38	56	868	154	266	434	87	630	56	399	126	227
NiO	1145	1421	1312	1378	1825	1701	878	2036	1593	1266	1357	1682	1908
ZnO	609	383	352	370	848	742	1312	634	734	1194	427	522	545
CuO	244	87	115	150	56	150	50	87	155	101	101	101	86
MnO	0.27	0.24	0.23	0.23	0.59	0.32	0.33	0.29	0.30	0.35	0.27	0.29	0.28
Cr/Fe	3.50	3.93	4.09	4.23	1.82	2.31	2.04	2.67	2.78	2.07	3.45	2.67	3.15
Mg/Fe	0.72	0.79	0.81	0.81	0.62	0.67	0.51	0.73	0.68	0.40	0.73	0.72	0.80
Cr/Al	4.11	4.56	4.86	4.83	1.67	1.99	2.34	2.07	2.83	3.97	3.99	2.43	2.62
Cr	1.386	1.436	1.465	1.470	0.902	1.013	1.083	1.045	1.191	1.303	1.361	1.114	1.169
Al	0.650	0.607	0.582	0.584	1.042	0.981	0.891	0.973	0.811	0.632	0.656	0.881	0.859
Mg	0.584	0.601	0.602	0.601	0.629	0.606	0.552	0.612	0.603	0.517	0.611	0.628	0.617
Fe	0.361	0.335	0.327	0.317	0.455	0.402	0.486	0.361	0.394	0.580	0.362	0.380	0.340

*Total Fe as FeO

CaO, NiO, ZnO, CuO, TiO_2 are as p.p.m.

F49 through F242 from the western part of the field

F68 through F70 from the eastern part of the field

F76 through F244 the Yassitepe mine

Table 17 continued

	F110	F248	F105	F112	F107A	F252B	F108	F104	F116	F128A	F136	F120A	F132	F207	F119	F126	F128Ao
Cr_2O_3	53.45	53.60	53.83	55.48	56.50	57.49	57.58	58.39	51.71	51.79	52.89	53.34	53.91	54.29	56.26	57.28	44.81
Al_2O_3	19.01	18.95	17.78	17.16	15.04	15.68	15.28	14.48	19.21	17.07	17.91	18.18	15.25	18.39	14.72	15.36	12.04
V_2O_3	0.19	0.19	0.21	0.19	0.23	0.17	0.17	0.19	0.21	0.25	0.23	0.19	0.22	0.18	0.17	0.15	0.25
SiO_2	0.35	0.21	0.44	0.36	0.72	0.38	0.51	0.38	0.54	0.97	0.39	0.78	1.54	0.11	1.00	0.39	6.85
TiO_2	2672	3548	2575	2805	1586	2613	3106	2613	2070	1636	2304	2964	1369	2672	1619	2805	1319
MgO	13.54	13.00	12.93	13.50	12.84	13.08	13.14	12.72	13.89	13.06	12.88	13.82	14.46	11.95	13.80	12.50	19.87
FeO*	12.71	13.22	14.10	12.58	14.11	12.49	12.60	13.17	13.76	16.04	14.96	12.92	13.95	14.30	13.44	13.62	14.50
CaO	63	63	59	77	57	84	54	66	63	1806	630	84	25	87	45	98	6650
NiO	1934	1578	1425	1677	1043	1629	1365	1243	1886	1450	1342	1879	1559	1762	1567	1190	2286
ZnO	398	413	399	367	424	360	350	384	381	460	429	385	454	472	354	385	441
CuO	102	104	100	102	106	102	87	77	78	75	100	87	165	88	63	88	87
MnO	0.24	0.27	0.27	0.23	0.25	0.24	0.24	0.23	0.26	0.29	0.28	0.24	0.31	0.29	0.24	0.25	0.58
Cr/Fe	3.70	3.57	3.36	3.88	3.53	4.05	4.02	3.90	3.31	2.84	3.11	3.64	3.40	3.34	3.69	3.70	
Mg/Fe	0.82	0.76	0.71	0.83	0.70	0.81	0.81	0.75	0.78	0.63	0.67	0.83	0.80	0.65	0.80	0.71	
Cr/Al	3.64	3.66	3.91	4.18	4.86	4.74	4.87	5.22	3.48	3.98	3.82	3.79	4.57	3.82	4.94	4.82	
Cr	1.328	1.334	1.354	1.392	1.448	1.451	1.462	1.486	1.292	1.328	1.334	1.344	1.400	1.357	1.445	1.457	
Al	0.705	0.702	0.668	0.640	0.574	0.592	0.578	0.551	0.713	0.652	0.673	0.681	0.590	0.686	0.565	0.581	
Mg	0.623	0.606	0.598	0.627	0.589	0.609	0.610	0.596	0.633	0.600	0.597	0.624	0.636	0.562	0.624	0.584	
Fe	0.326	0.338	0.369	0.326	0.378	0.326	0.330	0.348	0.358	0.430	0.393	0.337	0.378	0.371	0.360	0.359	

*Total Fe as FeO

CaO, NiO, ZnO, CuO, TiO_2 are as p.p.m.

F110 through F104 from the Uckopru mine area.

F116 through F126 from the Damdir mine area.

128Ao Analysis of chrome ore (unseparated analysis of F128A).

nor rutile have been identified during the episcopic study while, further, the TiO_2 content of the host peridotite is below the detection limit. The impurity which ranges up to 1.54 percent is thus unlikely to be the source of Ti, in fact the specimen with the highest impurity content does not carry high TiO_2. This evidence suggests that Ti must be present in the chromite lattice.

Comparative chemistry of chromite groups withinthe Andizlik-Zimparalik area.

The chromite occurrences have been divided into several groups, firstly according to their type or physical character; massive, nodular, disseminated or stratiform, and secondly according to structural disposition; east northeast - west southwest trending or northwest - southeast trending. It is also, of course, possible to have a geographical distribution depending on their position within the area, for example eastern chromites, western chromites, Üçköprü chromites etc.

Comparative chemistry of ore types

Most of the analysed specimens are massive chromites with Cr_2O_3 varying from 49.78 to 58.43 percent. Cr/Fe ratios range from 2.07 to 4.23, most are greater than 3 and the ore is thus of metallurgical grade.

Disseminated chromite is represented by 4 samples with Cr_2O_3 contents in the range 41.74 to 56.53, the Cr/Fe ratio varies from 2.31 to 3.60. The Al_2O_3 content of specimens F65 and F218 is

sufficient to classify them as refractory grade chromite.

Nodular chromites are also represented by 4 specimens with Cr_2O_3 contents of 56.87 to 58.39 percent and Cr/Fe ratios of 3.70 to 3.93.

Two chromites are of stratiform type (F19 and F68); they are low in Cr_2O_3, 37.09 and 43.28 percent, and high in Al_2O_3 and total Fe as FeO. Many minor constituents such as ZnO are at higher concentration than in other groups.

Student's "t" tests have been applied to these four types of chromites and the results are shown in table 18, together with values for the 97.5, 99.0 and 99.5 percent significance levels. To facilitate comparisons between the groups the significant differences at and above the 97.5 percent confidence level have been expressed in the form of a box diagram in fig.32. In this diagram, for example comparisons between massive and nodular chromite indicate that Al_2O_3 and CuO are relatively enriched in the massive type while Cr_2O_3 and Cr/Fe are higher in the nodular ore.

The data clearly suggest that nodular and massive chromites are significantly enriched in Cr_2O_3 relative to disseminated and particularly stratiform varieties. The latter, conversely, are enriched in Al_2O_3, FeO, ZnO, MnO and V_2O_3.

The comparisons are clearly demonstrated when average analyses

Table 18 Statistical comparisons between the compositions of the chrome ore types

	Disseminated (4)	St.Dev	Nodular (4)	St.Dev	Stratiform (2)	St.Dev	Massive (37)	St.Dev	Disseminated Nodular	Disseminated Stratiform	Disseminated Massive	Nodular Stratiform	Nodular Massive	Stratiform Massive
SiO_2	0.465	0.182	0.447	0.076	0.685	0.035	0.624	0.323	0.154	1.381	0.944	3.447	1.063	0.261
Cr_2O_3	48.910	6.374	57.715	0.657	40.185	3.095	54.201	2.465	2.380	1.495	3.189	8.859	2.770	7.517
Al_2O_3	21.753	5.519	15.032	0.771	26.310	2.390	17.031	1.842	2.089	0.912	3.562	7.010	2.096	6.643
MgO	13.358	0.308	12.715	0.178	13.300	0.960	12.925	0.862	3.132	0.089	0.971	0.963	0.475	0.579
FeO	14.550	0.798	13.228	0.323	18.280	0.360	14.286	1.503	2.661	5.144	0.337	14.176	1.371	3.655
CaO	111.750	90.938	68.000	21.260	294.000	140.000	191.757	302.376	0.811	1.566	0.514	2.577	0.798	0.463
TiO_2	2078.250	367.246	2644.250	412.103	2481.500	23.500	2345.486	581.969	1.776	1.267	0.877	0.456	0.975	0.322
NiO	1585.250	319.097	1288.500	85.821	1351.500	473.500	1526.784	239.354	1.555	0.584	0.436	0.210	1.929	0.916
ZnO	545.750	147.320	378.250	9.984	1080.000	232.000	461.973	138.497	1.965	2.798	1.114	4.930	1.179	5.728
CuO	106.250	25.772	73.750	18.267	53.000	3.000	97.919	22.016	1.782	2.378	0.689	1.303	2.066	2.809
MnO	0.290	0.019	0.240	0.007	0.460	0.130	0.269	0.029	4.330	2.093	1.386	2.755	1.938	6.282
V_2O_3	0.252	0.053	0.182	0.022	0.285	0.005	0.213	0.035	2.115	0.705	1.988	5.395	1.653	2.850
Cr/Fe	2.985	0.518	3.842	0.088	1.930	0.110	3.377	0.385	2.826	2.325	1.818	18.752	2.354	5.171
Mg/Fe	0.713	0.027	0.745	0.030	0.565	0.055	0.709	0.090	1.410	3.606	0.071	4.254	0.770	2.180
t97.5									2.447	2.776	2.021	2.776	2.021	2.021
t99.0									3.143	3.747	2.423	3.747	2.423	2.423
t99.5									3.707	4.604	2.704	4.604	2.704	2.704

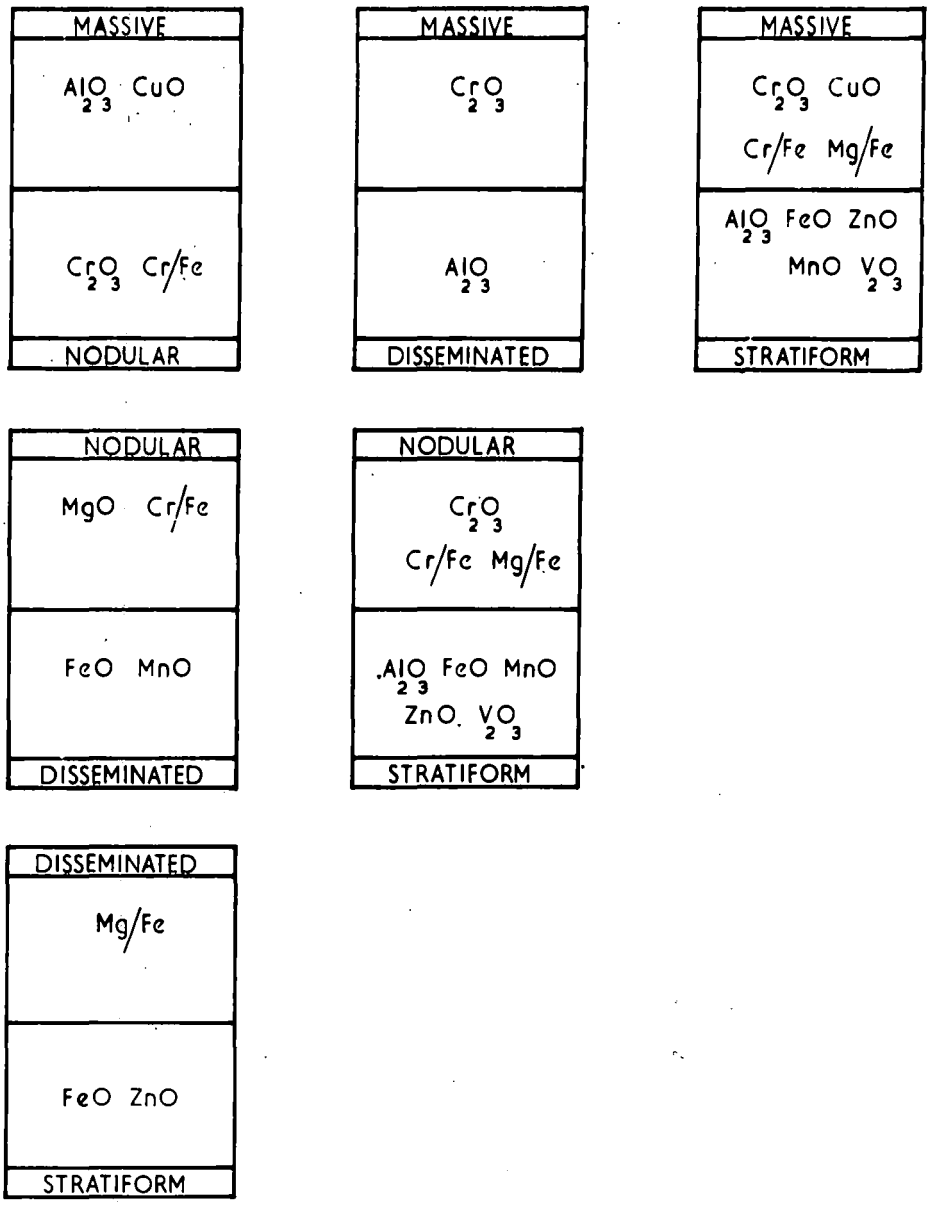

SIGNIFICANT DIFFERENCES IN THE CHEMISTRY OF CHROMITE TYPES AT THE 97.5 PERCENT CONFIDENCE LEVEL

FIG. 32

of the four types of chromite are plotted on a triangular diagram with apices Cr_2O_3 - Al_2O_3 - MgO + FeO, fig.33C. The diagram demonstrates a progressive trend from nodular chromite, plotting towards the Cr_2O_3 apex, through massive and disseminated varieties to stratiform chromite. This outcome may suggest a genetic connection between the four types, of nodular chromites being developed as early crystallized fractions of the magma, followed by massive and disseminated types, the stratiform type forming in the upper parts of the magma chamber.

Comparative chemistry in relation to structural disposition

East northeast - west southwest and northwest - southeast trending pods are clearly distinguishable in the Zimparalik mine. The Cr_2O_3 content of the former group varies from 51.11 to 57.81 percent and of the second group from 52.67 to 58.32 percent, levels of other elements are similar in both groups.

Student's "t" test, table 19, for these two groups show no significant difference in mean concentration for any element, consequently their average analyses plot very close to each other in the Cr_2O_3 - Al_2O_3 - FeO + MgO triangular diagram, fig.33B.

The two groups may have a common origin, compositions not having been modified during emplacement. Alternatively it is possible to envisage that originally different compositions have approached similarity in composition due to modifications during

Table 19 Statistical comparison between the compositions of chromites based on their structural disposition.

	NE-SW (12)	St.Dev	NW-SE (6)	St.Dev	NE-SW / NW-SE
SiO_2	0.742	0.280	0.607	0.311	0.874
Cr_2O_3	54.122	1.838	54.987	2.053	0.853
Al_2O_3	16.857	1.421	16.483	1.414	0.497
MgO	13.057	0.761	12.728	0.650	0.855
FeO	14.279	0.501	14.263	1.152	0.038
CaO	139.833	110.276	183.333	154.915	0.646
TiO_2	2291.000	489.542	2414.000	660.406	0.420
NiO	1534.583	212.717	1486.167	159.778	0.464
ZnO	475.333	69.984	456.667	59.957	0.527
CuO	101.667	24.974	93.500	27.561	0.595
MnO	0.275	0.022	0.253	0.017	2.010
V_2O_3	0.223	0.036	0.222	0.038	0.085
Cr/Fe	3.343	0.189	3.420	0.336	0.589
Mg/Fe	0.710	0.046	0.695	0.079	0.478
t97.5					2.120
t99.0					2.583
t99.5					2.921

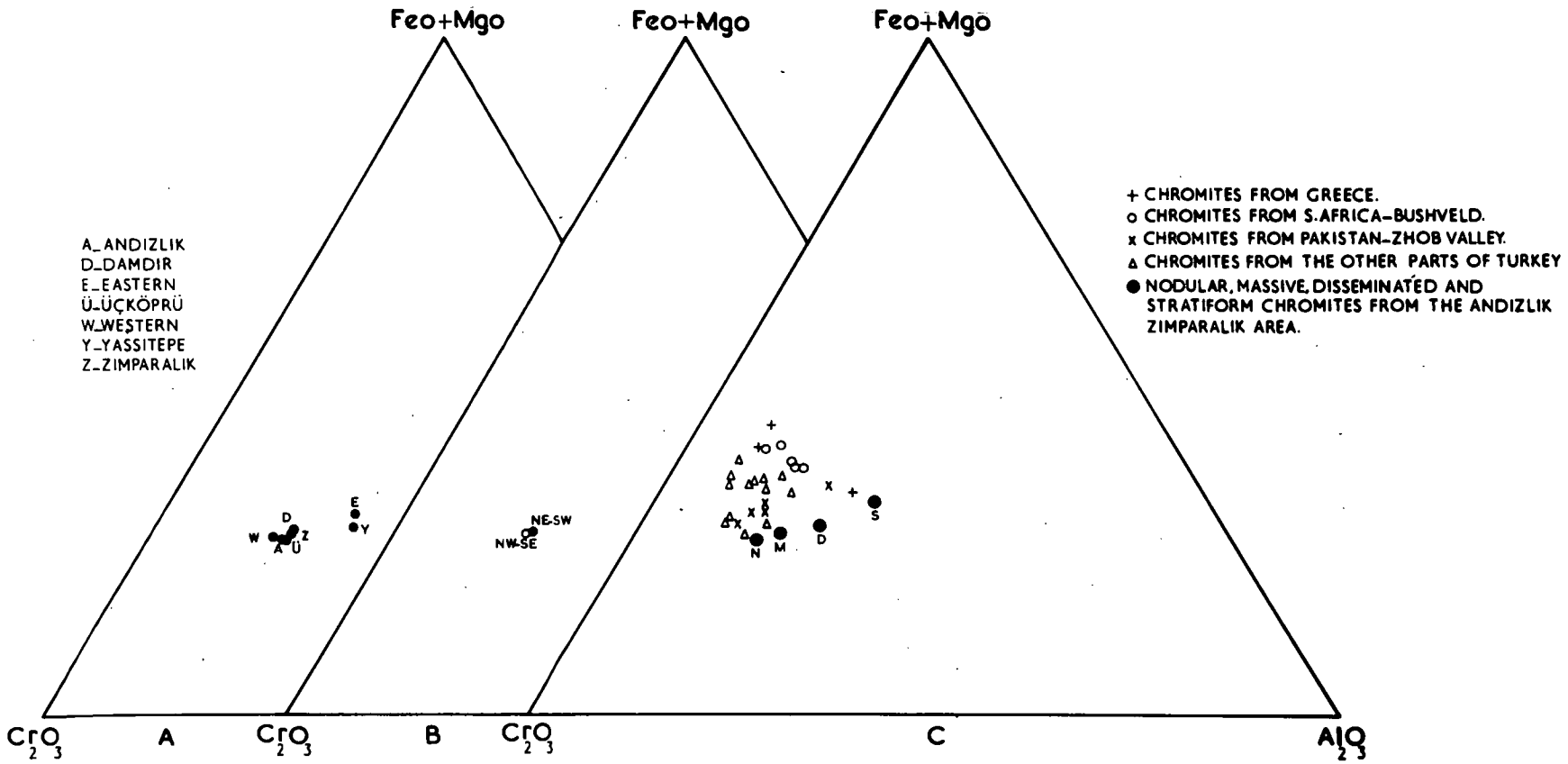

Cr_2O_3–Al_2O_3–FeO+Mgo DIAGRAMS OF CHROMITES

FIG.33

emplacement.

Comparative chemistry of ore groups from different parts of the intrusion

8 specimens from the Üçköprü mine area have Cr_2O_3 contents ranging from 53.45 to 58.39 percent and Cr/Fe ratios of 3.36 to 4.05. The ore is mainly massive.

15 chromites from the Andizlik mine have Cr_2O_3 contents varying from 53.44 to 58.31 percent and Cr/Fe ratio of 2.89 to 3.98.

The Zimparalik mine has contributed 18 chromite analyses with Cr_2O_3 contents of 51.11 to 58.32 percent, and Cr/Fe ratios of 2.96 to 3.84.

The Damdir mine area, fig 4 (see Volume 2), includes all specimens from Kilcan dere in the south to Madenoyugu tepe in the north. The Cr_2O_3 content varies from 51.71 to 57.28 percent, and Cr/Fe ratios from 2.84 to 3.70. The chromite in this sector is brecciated and frequently cut by basic dykes. The remaining analysed specimens have been grouped as either eastern or western occurrences.

The eastern group extends from east of the Damdir mine to the east of the Üçköprü mine, fig.4 (see Volume 2), and covers Kurudere, Karakaya, Tavuk tarlasi, Sarikaya, Kizlarmahallesi and the two stratiform occurrences. The area is represented by 7 chromite specimens. The grade of chromite in the eastern area is

comparatively low, with Cr_2O_3 ranging from 37.09 to 54.27 percent and Cr/Fe ratios from 1.82 to 3.45.

The western group occur around Incebel tepe and Dikmen tepe fig.4 (see Volume 2). 4 specimens from this group have been analysed. Cr_2O_3 contents range from 54.65 to 58.43 percent and Cr/Fe ratios from 3.50 to 4.23.

Student's "t" tests on these groups are shown in table 20. Significant differences in chemistry between these groups are summarised in box diagrams in fig.34.

The diagrams clearly indicate a progressive decrease in Cr_2O_3 and Cr/Fe and in increase in Al_2O_3, FeO, ZnO and V_2O_3 from western to eastern occurrences. Andizlik and Üçköprü chromites are closely similar to the western occurrences while Zimparalik and Damdir form an intermediate group.

The average analyses of each of these groups have been plotted on the Cr_2O_3 - Al_2O_3 - MgO + FeO triangular diagram, fig.33A. Andizlik, Zimparalik, Üçköprü, Damdir and the western occurrences congregate near the Cr_2O_3 corner of the diagram. The eastern chromites however, differ considerably and are displaced away from the Cr_2O_3 apex. This is undoubtedly due in part, at least, to the fact that the eastern occurrences include the two stratiform chromite samples.

Table 20 Statistical comparison between the compositions of chromites from different parts of the peridotite body

	Andizlik (15)	St.Dev	Zimparalik (18)	St.Dev	Uckopru (8)	St.Dev.	Damdir (8)	St.Dev.	Eastern outcrops (7)	St.Dev.	Western outcrops (4)	St.Dev
SiO_2	0.483	0.167	0.697	0.298	0.419	0.139	0.715	0.424	0.496	0.187	0.430	0.198
Cr_2O_3	56.077	1.515	54.410	1.955	55.790	1.856	53.934	1.861	45.391	5.281	56.967	1.451
Al_2O_3	16.535	1.465	16.733	1.430	16.672	1.677	17.011	1.581	23.241	4.547	16.095	0.682
MgO	12.419	0.706	12.948	0.743	13.094	0.275	13.295	0.783	13.047	0.978	12.882	0.102
FeO	13.581	1.024	14.274	0.781	13.122	0.620	14.124	0.918	16.729	2.444	12.773	0.590
CaO	152.933	222.544	154.333	128.558	65.375	9.578	354.750	579.073	289.429	193.926	254.500	354.281
TiO_2	2702.200	754.128	2332.000	555.435	2689.750	520.417	2179.875	563.826	2113.000	505.464	2299.750	166.818
NiO	1455.000	274.093	1518.444	197.980	1486.750	259.748	1579.375	235.163	1522.286	358.685	1314.000	105.012
ZnO	394.733	47.003	469.111	67.386	386.875	24.538	415.000	41.334	841.571	288.343	428.500	104.791
CuO	88.933	18.763	98.944	26.150	98.750	10.779	93.000	29.086	100.000	38.045	149.000	59.216
MnO	0.253	0.029	0.268	0.023	0.246	0.015	0.270	0.024	0.350	0.101	0.242	0.016
V_2O_3	0.187	0.021	0.223	0.037	0.193	0.019	0.200	0.031	0.284	0.033	0.185	0.017
Cr/Fe	3.657	0.295	3.368	0.251	3.751	0.234	3.377	0.281	2.449	0.519	3.938	0.274
Mg/Fe	0.715	0.082	0.705	0.060	0.774	0.048	0.734	0.073	0.620	0.114	0.782	0.037

Table 20 continued

	Andizlik Zimparalik	Andizlik Uckopru	Andizlik Damdir	Andizlik Eastern	Andizlik Western	Zimparalik Uckopru	Zimparalik Damdir	Zimparalik Eastern	Zimparalik Western	Uckopru Damdir	Uckopru Eastern	Uckopru Western	Damdir Eastern	Damdir Western	Eastern Western
SiO_2	2.399	0.883	1.784	0.156	0.508	2.420	0.121	1.594	1.628	1.756	0.849	0.104	1.777	1.165	0.496
Cr_2O_3	2.612	0.381	2.845	6.889	0.997	1.621	0.559	5.976	2.355	1.868	4.853	1.014	3.986	2.606	3.882
Al_2O_3	0.380	0.195	0.690	4.926	0.552	0.090	0.426	5.201	0.830	0.389	3.539	0.604	3.382	1.012	2.825
MgO	2.017	2.482	2.604	1.629	1.237	0.519	1.039	0.262	0.167	0.641	0.120	1.355	0.507	0.957	0.304
FeO	2.137	1.106	1.200	4.054	1.431	3.541	0.411	3.637	3.454	2.392	3.749	0.855	2.604	2.448	2.881
CaO	0.022	1.063	1.141	1.329	0.667	1.878	1.339	1.942	0.906	1.322	3.038	1.377	0.265	0.290	0.191
TiO_2	1.571	0.040	1.643	1.792	1.003	1.484	0.616	0.870	0.110	1.758	2.020	1.334	0.224	0.380	0.649
NiO	0.746	0.257	1.039	0.462	0.955	0.327	0.656	0.033	1.910	0.699	0.206	1.167	0.343	1.965	1.026
ZnO	3.495	0.422	0.981	5.566	0.891	3.223	2.020	4.922	0.927	1.548	4.135	0.974	3.850	0.290	2.499
CuO	1.202	1.304	0.388	0.871	3.167	0.019	0.496	0.076	2.495	0.490	0.083	2.122	0.375	2.005	1.509
MnO	1.549	0.615	1.318	3.256	0.675	2.356	0.216	3.116	2.007	2.190	2.672	0.362	2.019	1.853	1.911
V_2O_3	3.203	0.557	1.101	7.876	0.194	2.120	1.464	3.694	1.915	0.546	6.234	0.624	4.706	0.821	5.045
Cr/Fe	2.950	0.745	2.106	6.614	1.622	3.523	0.080	5.699	3.847	2.704	5.953	1.120	4.078	2.994	4.819
Mg/Fe	0.380	1.799	0.529	2.118	1.531	2.764	1.015	2.326	2.378	1.214	3.244	0.294	2.170	1.148	2.507
t97.5	2.042	2.080	2.080	2.086	2.110	2.064	2.064	2.069	2.086	2.145	2.160	2.228	2.160	2.228	2.262
t99.0	2.457	2.518	2.518	2.528	2.567	2.492	2.492	2.500	2.528	2.624	2.650	2.764	2.650	2.764	2.821
t99.5	2.750	2.831	2.831	2.845	2.898	2.797	2.797	2.807	2.845	2.977	3.012	3.169	3.012	3.169	3.250

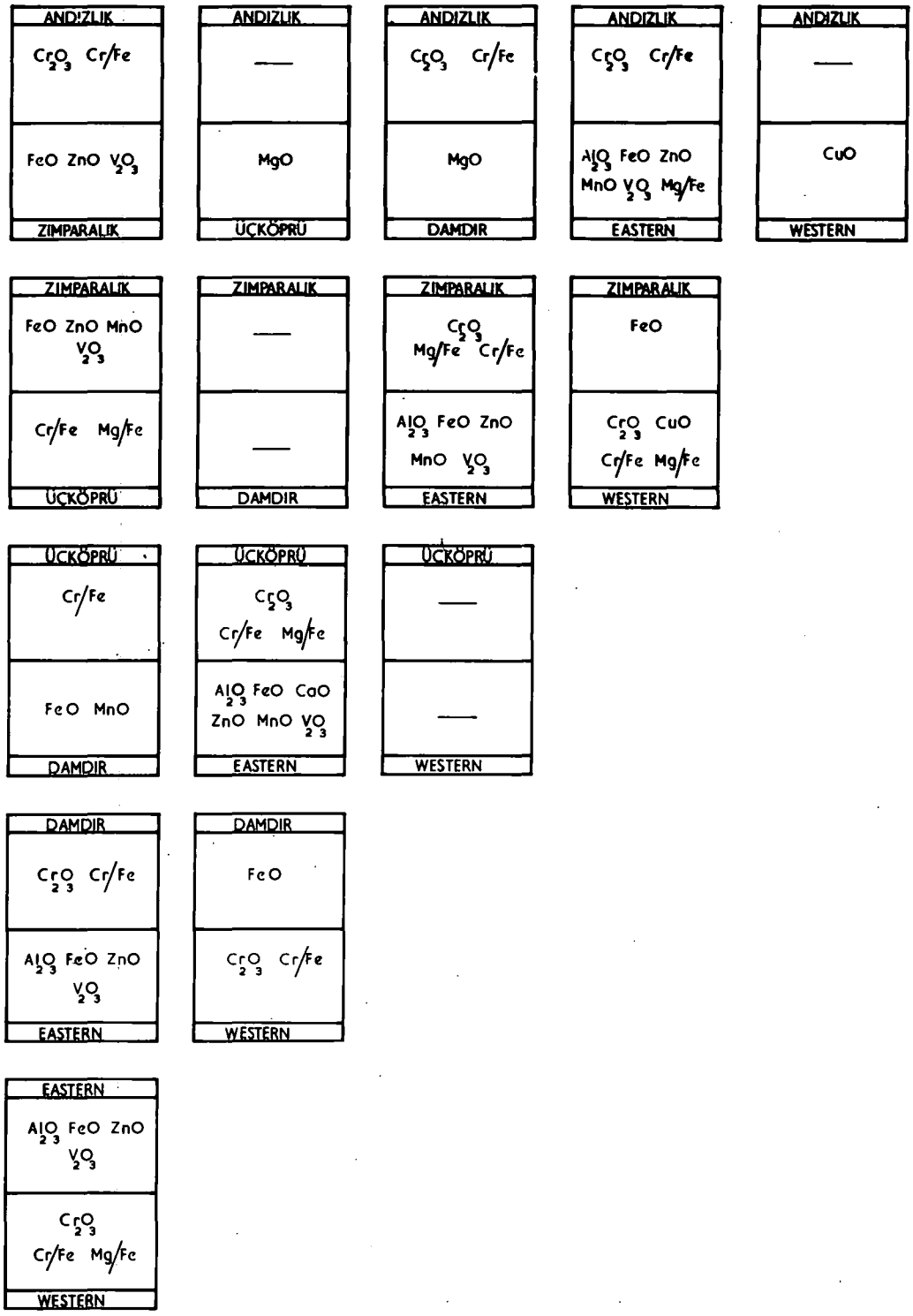

SIGNIFICANT DIFFERENCES IN THE CHEMISTRY OF CHROMITES FROM DIFFERENT PARTS OF THE PERIDOTITE AT THE 97.5 PERCENT CONFIDENCE LEVEL.

FIG.34

Chemical variation within a chromite pod

Variations in chromite chemistry have been studied within pods both along their strike and in the dip direction. This investigation was readily achieved by establishing a sample pattern based on the surface and subsurface maps of the Andizlik and Zimparalik mines, fig. 5A, 5B, 5C and 6A, 6B, 6C, 6D, (see Volume 2) compositional variation is apparent but does not conform to any recognizable pattern.

Chemical variations within chromite grains based on electron microprobe analyses

Electron microprobe scans have been made on "ferritchromit" associated with the normal chromite grains. Fig.35 reveals that the Mg and Al contents of the "ferritchromit" are lower than in the host chromite while conversely Fe and Cr are higher. These findings are in agreement with those of Panagus and Ottemann (1966) and Golding and Bayliss (1968), discussed previously.

In order to study quantitatively the compositional changes in chromite grains 43 spots in three chromite specimens have been analysed for Cr, Al, Mg and Fe. The results are given in table 21, and the disposition of the analysed spots in specimens F47 and F115 is shown in fig.36.

The standards used for the analyses were Cr metal for Cr, synthetic Fe_2O_3 for Fe, and synthetic enstatite, containing 10 percent

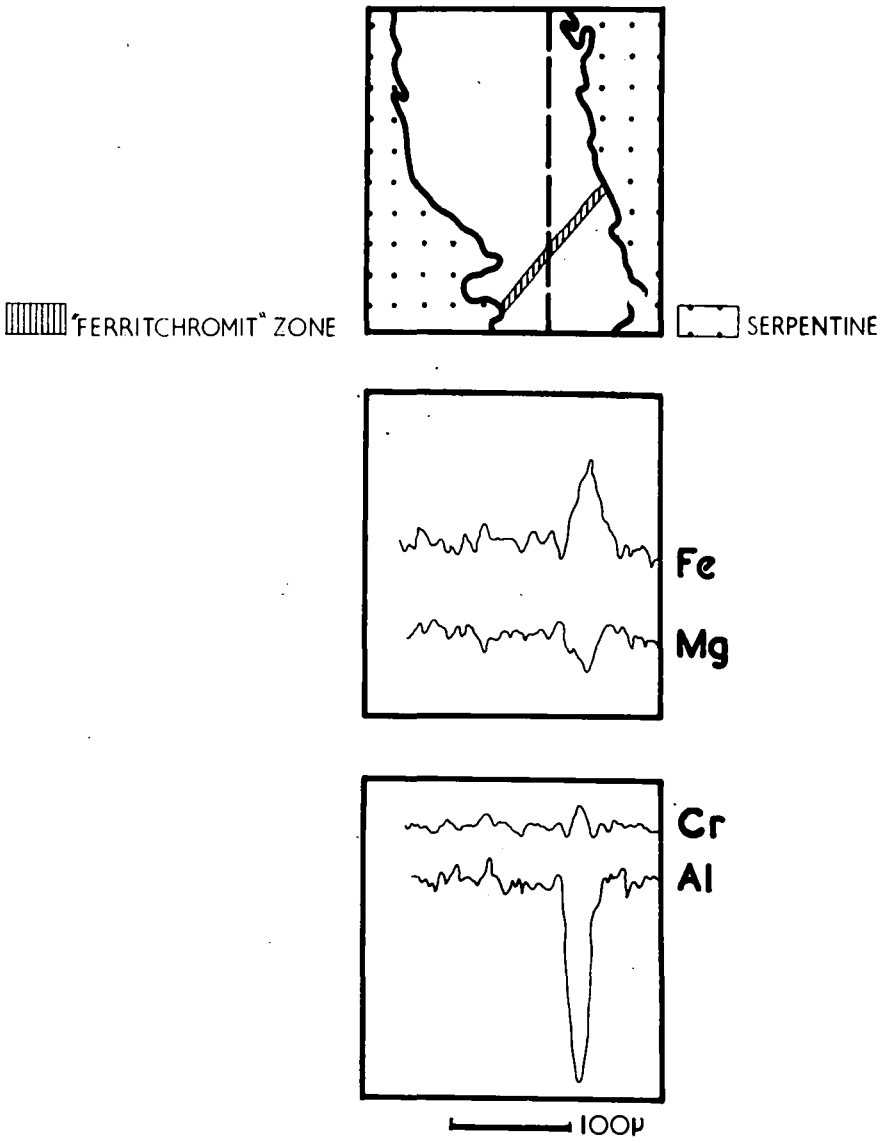

Electron probe scan along the broken line in a chromite grain

FIG.35

Al_2O_3, for Mg and Al. Dead time, drift, mass absorbtion, atomic number and fluorescence corrections were made by means of a computer program based on J.V.P. Long, University of Cambridge (Private publication), T. Padfield, University of Leeds and J.W. Aucott, University of Durham (Personal communication).

Analysed spots 3,4,5 and 6 in grain F47.1, fig 36, are from the "ferritchromit" zone. Their analyses confirm previous statements that this material is lower in Al_2O_3 and MgO but higher in FeO and Cr_2O_3 than associated host chromite, see table 21.

The analysed spots from specimen F115 can be placed in two groups, F115.1 spot 4; F115.1 spot 6; F115.1 spot 7; F115.2 spot 5; F115.2 spot 6; constitute one group which distinct from the remainder. The first group are generally lower in MgO and Al_2O_3 and higher in total Fe; the differences in Cr_2O_3 are insignificant. Normal episcopic examination fails to reveal these differences but they can be resolved by measurements of the reflectivity, in this particular example.

No significant change in composition was detected from the analyses of 11 spots in sample F31, table 21.

The electron probe chemical results indicate that the changes in composition within grains from F115 are similar to the changes leading to the formation of the "ferritchromit" of F47. This suggests that the compositional variation may be a result of

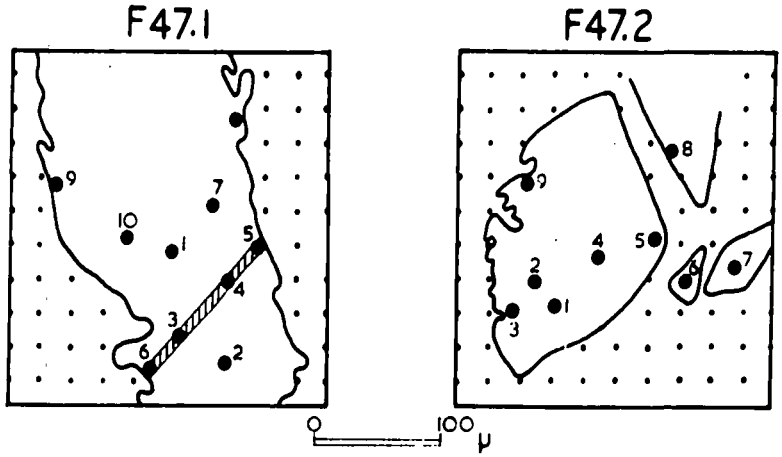

"FERRITCHROMIT" ZONE SERPENTINE IN F47 AND CHLORITE IN F115

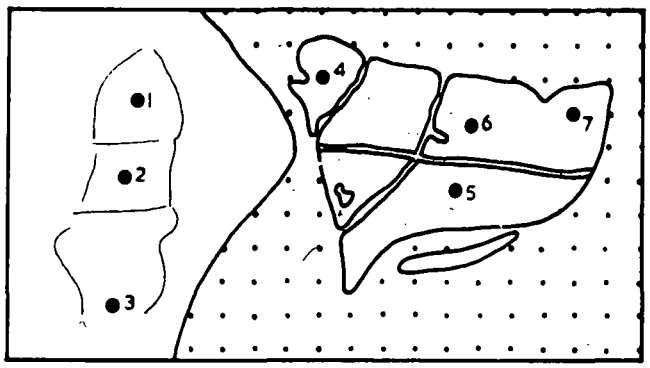

F115.1

CHROMITE

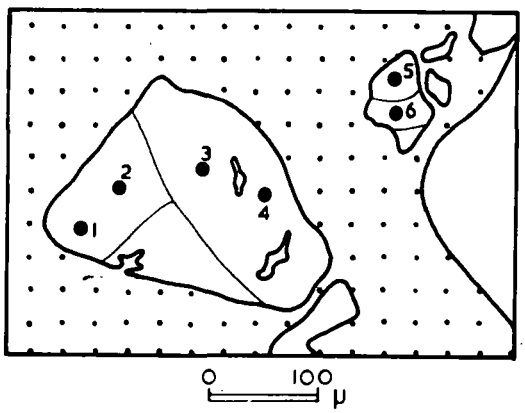

F115.2

Disposition of analysed spots in chromite grains

FIG.36

Table 21 Electron microprobe spot analyses of chromites (weight percent)

	F47.11	F47.12	F47.13	F47.14	F47.15	F47.16	F47.17	F47.18	F47.19	F47.110	F47.21	F47.22	F47.23	F47.24	F47.25	F47.26	F47.27	F47.28	F47.29
Cr_2O_3	56.48	57.02	62.59	63.56	62.04	61.92	56.33	57.88	55.84	56.21	56.75	57.51	53.82	56.80	57.23	57.36	57.57	57.13	56.29
Al_2O_3	12.78	12.87	3.24	1.27	2.81	2.66	12.68	13.17	13.92	12.60	12.76	13.25	12.39	12.88	12.78	12.65	12.85	12.95	14.34
FeO*	17.93	17.78	23.92	26.04	28.13	28.14	18.34	18.57	18.11	18.56	17.48	16.88	21.26	17.46	17.09	16.98	16.84	17.10	21.80
MgO	12.81	12.33	10.25	9.13	7.02	7.29	12.65	10.38	12.13	12.63	13.00	12.36	12.52	12.86	12.90	13.01	12.73	12.82	7.56

	F115.11	F115.12	F115.3	F115.14	F115.15	F115.16	F115.17	F115.21	F115.22	F115.23	F115.24	F115.25	F115.26
Cr_2O_3	54.59	54.53	54.31	48.34	54.14	54.17	53.97	54.63	53.71	54.28	54.79	51.74	54.40
Al_2O_3	14.65	14.55	14.55	15.02	14.60	9.22	8.12	13.97	14.73	14.02	13.15	9.73	9.27
FeO*	16.99	17.00	17.13	28.31	18.12	28.43	28.93	21.40	19.04	20.03	21.51	29.04	27.62
MgO	13.78	13.92	14.00	8.33	13.13	8.18	8.98	10.00	12.52	11.67	10.55	9.48	8.72

	F31.11	F31.12	F31.13	F31.14	F31.15	F31.16	F31.17	F31.18	F31.19	F31.110	F31.111
Cr_2O_3	60.37	59.28	59.48	58.77	58.25	58.28	60.65	58.59	58.27	58.31	58.54
Al_2O_3	11.39	11.59	12.24	11.28	11.82	11.90	10.03	11.36	11.48	11.66	11.66
FeO*	14.50	15.30	14.72	15.72	15.27	15.10	15.80	15.68	15.66	15.13	15.09
MgO	13.74	13.82	13.56	14.23	14.66	14.72	13.52	14.36	14.60	14.91	14.71

*Total iron as FeO

hydrothermal activity as discussed by Wijkerslooth (1943), Golding and Bayliss (1968) etc. The compositional changes are not however as extreme as in the formation of "ferritchromit".

If the pyroxenite veins and Cr bearing tremolites are formed by the same hydrothermal solutions involved in the above alterations, it is difficult to envisage their Cr being supplied from chromite since there is in fact relative enrichment of Cr in the alteration products.

Comparison of electron microprobe and X-ray fluorescence analyses

Direct comparison of X-ray fluorescence and electron probe analyses is difficult, due to fundamental differences in excitation, in correction procedures used, and in standardisation. Compositional changes within grains, which are detectable by electron microprobe but not by X-ray fluorescence analyses raise further difficulties.

Analyses have been obtained on samples F31 and F115 by both methods, table 22. Electron probe and X-ray analyses of F115 are similar if the small amount of hydrothermally altered material impoverished in Al_2O_3 and MgO is eliminated from the probe results. F31 however is noticeably deficient in Al_2O_3 by electron probe analyses.

Electron probe analyses tend to be low in Al when compared with those obtained by more conventional methods. It is difficult to recognise bad analyses by either X-ray fluorescence or electron

Table 22 Comparison of electron probe and X-ray fluorescence analyses of chromites.

	Analyses by electron probe		Analyses by X-ray fluorescence	
	F115*	F31*	F115	F31
Cr_2O_3	53.66	58.98	50.68	57.60
Al_2O_3	12.74	11.49	16.48	16.35
FeO**	22.58	15.27	21.58	12.90
MgO	11.02	14.25	11.26	13.15

	Uncorrected electron probe analysis example for the low total group	After correction of the low total group
	F115.11	F115.11
Cr_2O_3	52.33	54.59
Al_2O_3	14.96	14.65
FeO **	16.59	16.99
MgO	11.44	13.78

	Uncorrected electron probe analysis example for the high total group	After correction of the high total group
	F115.14	F115.14
Cr_2O_3	48.66	48.34
Al_2O_3	15.75	15.02
FeO **	28.62	28.31
MgO	6.87	8.33

*Electron probe analyses of F115 and F31 are the average of 13 and 11 spots given in Table 21.

** Total iron as FeO

probe since the necessary corrections to the raw data are made by iterative procedures and hence a normalisation factor is involved.

Probe analyses may be assessed in terms of their uncorrected totals before normalisation. In the present study the chromites fall into two groups; iron poor giving low totals of about 95 percent, and iron rich producing totals of 99 percent. A comparison of the two types in terms of the uncorrected analyses shows that the correction procedures are similar, except for Cr_2O_3. After correction MgO increases by 2 to 3 percent, Al_2O_3 and iron are slightly decreased. In the low iron group Cr_2O_3 increase by up to 3 percent, whilst in the other group, Cr_2O_3 totals are unchanged after correction. The 3 percent increase is due to the atomic number correction but the increase is lost due to normalisation in the high iron group, table 22.

The comparatively low Al_2O_3 figures are not due to correction procedures. The chromite analyses were checked against other synthetic standards such as Al_2O_3 and $MgAl_2O_4$, and gave good agreement. Results determined by using Al_2O_3 were low, this was due to a peak shift in the 2Θ angular setting of the $AlK\alpha_1$ line. There was no detectable peak shift in relation to the other standards.

Despite these uncertainties the agreement between X-ray and electron probe analyses are good. Electron probe results should be

consistent within themselves and differences shown in sample F115 and F47 are real.

General Considerations

Van der Kaaden and Müller (1953), Van der Kaaden (1959), Borchert (1964) have suggested that there are regular variations in chemistry within ultrabasic massifs, chromites being relatively rich in Cr and poor in Al, with metallurgical Cr/Fe ratios, in the deeper parts of the intrusion. Borchert (loc.cit) suggests that Al increases in rocks which formed at later stages of the magmatic differentiation process, reaching the highest values in noritic rocks towards the top of a complex. Borchert infers that the Al content of chromites from the upper part of a massif will also increase, forming refractory grade chromites rich in Al and having a low Cr/Fe ratio.

Van der Walt (1941) showed that in Bushveld chromites there was an increase in the Al_2O_3 and decrease in Cr_2O_3 content from stratigraphically lower to upper levels.

Jackson (1964) also showed in the Stillwater complex, chromites near the base of the intrusion are rich in MgO and increase in iron upward in the section.

Chromites from different parts of the Andizlik-Zimparalik peridotite show some significant differences which despite the complex tectonic history of the area, present a recognizable pattern,

Cr_2O_3, Cr/Fe, Mg/Fe and Cr/Al increasing from east to west. The Cr/Fe ratios of the analysed chromites have been plotted on fig. 37; average values have been used where more than one analysis was available from a small area. Accepting Borchert's suggestion these results could be taken as an indication that the western deposits represent chromites from the deeper parts of the magma chamber, eastern deposits conversely having come from a higher stratigraphic level. However during the emplacement of the peridotite pressure acting from the west in an east-west direction must have contributed to the above pattern. Further there is no obvious conformable pattern in the related ultramafics, particularly if analyses on a water free basis are used.

Similar compositional trends are reported by Asrarullah (1960) for the Hindubagh area of West Pakistan, where the ore grade decreases from west to east, and by Hancock (1964) for the Mount Tawai area, North Borneo, where the Cr_2O_3 content of the chromite increases from northwest to southeast.

Green (1963) explains the formation of aluminous spinel by recrystallization of aluminous pyroxene with deformation and a large decrease in load pressure, thus:

$$n\ MgSiO_3.Al_2O_3 + Mg_2SiO_4 \longrightarrow MgAl_2O_4 + (m+1)MgSiO_3$$

Irvine (1967) suggests that this reaction may be applicable to aluminium rich chromium spinels. He further suggests however that

DISTRIBUTION OF Cr/Fe RATIOS IN CHROMITES FROM THE ANDIZLIK–ZIMPARALIK AREA

FIG.37

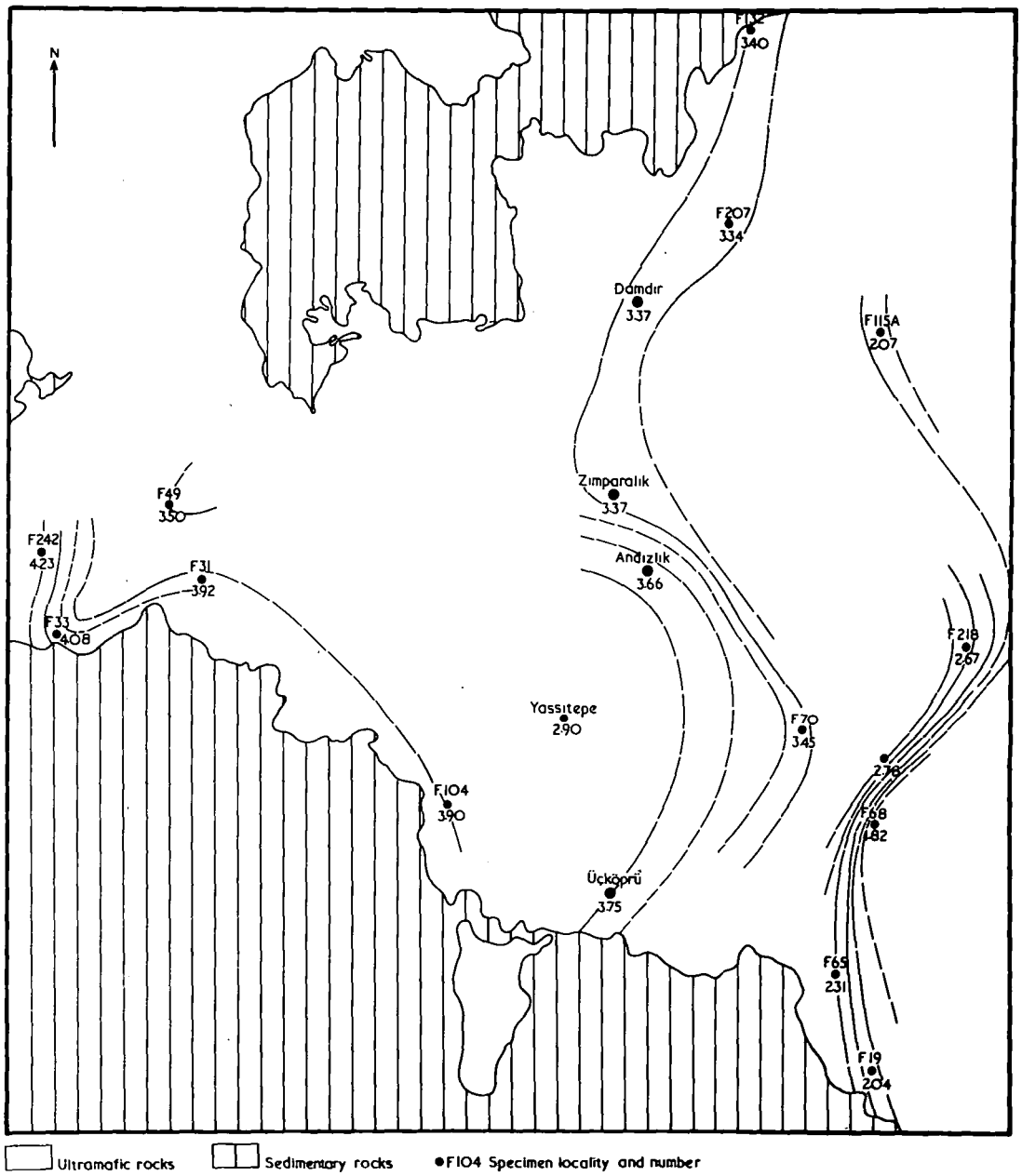

some alumina rich chromites in alpine peridotites may be the product of primary magmatic crystallization and reaction.

Cr and Al rich spinels form continuous solid solution series. If the aluminous spinel is supposed to be a product of crystal fractionation then they may, in some cases, reflect continued growth of fractionated grains of moderately aluminous spinel from interstitial basaltic magma. The most important factor in the formation of aluminous spinel in alpine type peridotite is moderately high pressure.

In the Andizlik-Zimparalik area two Cr_2O_3 poor, and relatively Al_2O_3 rich, chromite specimens (F19, F68) are derived from two, very thin, stratifrom chromite bands which occur in association with serpentinised dunite. Their chemistry suggests that they may be from the upper part of the magma chamber, although the dunitic nature of their host rocks ~~might~~ conflicts with this hypothesis.

Comparisons with other chromites

The Andizlik-Zimparalik chromites have been compared with chromites from Greece, Hiessleitner (1951), Pakistan, Bilgrami (1963), and South Africa, Cameron and Emerson (1959); the analyses given by these authors are listed in table 23. These data together with analyses of some Turkish chromites taken from Van der Kaaden (1959), Hiessleitner (1951) and M.T.A. Report 132 (1966), have been plotted on the Cr_2O_3 - Al_2O_3 - FeO+MgO triangular diagram, fig.33C.

Table 23 Composition of Chromites, from Pakistan, Greece and South Africa

	Zhob Valley (Pakistan)				Greece			Bushveld (South Africa)				
	1	2	3	7	Domokos	Soufflion	Fteri	1	2	3	4	5
Cr_2O_3	58.72	54.41	53.91	45.21	40.03	40.64	47.65	47.12	47.31	47.31	46.93	49.31
Al_2O_3	11.64	13.86	13.35	20.24	21.94	7.38	8.1	15.74	13.88	14.49	11.04	9.49
Fe_2O_3	5.36	3.98	3.46	4.41	0.6	0.19	0.74	-	7.84	7.44	-	8.87
SiO_2	0.21	0.24	0.29	0.31	5.3	11.52	6.64	0.12	0.07	0.13	0.22	0.13
TiO_2	0.16	0.45	0.26	0.21	n.d.	n.d.	n.d.	0.44	0.58	0.58	0.55	0.66
V_2O_5	0.06	0.07	0.08	0.12	n.d.	n.d.	n.d.	0.62	0.28	0.28	0.62	0.33
FeO	8.47	12.26	13.89	14.26	12.0	16.30	19.43	25.15*	20.22	19.03	29.46*	24.35
MgO	14.52	14.24	13.86	15.12	18.18	19.62	16.65	11.13	9.21	10.07	9.10	5.90
CaO	-	0.08	0.07	0.01	0.10	0.2	n.d.	0.53	-	-	0.48	-
NiO	0.23	0.16	0.09	0.21	n.d.	n.d.	n.d.	n.d.	-	-	n.d.	n.d.
MnO	0.17	0.20	0.18	0.25	0.28	0.36	n.d.	n.d.	-	0.44	n.d.	0.16

*Total iron expressed as FeO

Zhob Valley, Bilgrami, S.E. (1963) p.581

Greece, Hiessleitner, G. (1951) p.228

Bushveld, Cameron, E.N., M.E. Emerson (1959 p.1195.

Despite the fact that these Pakistani and Greek chromites are genetically similar to the Andizlik-Zimparalik chromites they have a different chemistry. The Pakistani chromites have comparable Cr_2O_3 and Al_2O_3 contents to the nodular and massive chromites of Andizlik-Zimparalik but have a higher FeO+MgO content. Chromites from Greece are also relatively enriched in FeO+MgO. The chromites of the South African Bushveld complex are similar to the stratiform chromites of the Andizlik-Zimparalik area though they are somewhat higher in Cr_2O_3 and FeO+MgO.

Recalculation of chromite analyses into mineralogical formulae

The iron determinations made by X-ray fluorescence spectrography, were total iron expressed as FeO. Ferrous iron determinations are particularly difficult because of the resistance to acids shown by chromite. If RO^{2+} is assumed to be equal to $R_2O_3^{3+}$ in the spinel formula then FeO and Fe_2O_3 values may be calculated. Most of the chromites show $RO \leq R_2O_3$, these chromites are, in effect, unbalanced. Only 5 specimens (F68, F65, F19, F115A, F128A) are balanced.

The chromite analyses were first corrected in respect of MgO, sufficient MgO being subtracted to satisfy the SiO_2 in forming serpentine. Minor constituents were also eliminated and the 4 major oxides Cr_2O_3, MgO, Al_2O_3, FeO recalculated to 100 percent total.

Now given that RO equals R_2O_3 then

$$\frac{A}{40.32} + \frac{B-0.909y}{71.85} = \frac{y}{459.70} + \frac{C}{101.96} + \frac{D}{152.01}$$

where A, MgO; B, total Fe as FeO; C, Al_2O_3; D, Cr_2O_3 and y, Fe_2O_3; and X+0.909y=B where X=FeO.

Distribution of total Fe between FeO and Fe_2O_3 may thus be evaluated from this formula, this gives the following results for the 5 balanced chromites:

F68A	FeO = 15.06	Fe_2O_3 = 3.48
F128A	FeO = 15.81	Fe_2O_3 = 0.66
F65	FeO = 15.87	Fe_2O_3 = 0.24
F19	FeO = 17.59	Fe_2O_3 = 1.48
F115A	FeO = 18.09	Fe_2O_3 = 3.77

The general formula of chromite, $RO^{2+}\ R_2O_3^{3+}$, may be written as $(Mg,Fe)O(Cr.Al.Fe)_2O_3$, and therefore as a result of the substitution of Fe^{2+} for Mg^{2+}, and of Al^{3+} and Fe^{3+} for Cr^{3+}, chromites may vary widely in composition.

Thayer (1956) has suggested that chromite compositions may be expressed in terms of the molecular ratio of the RO and R_2O_3 constituents. After making corrections for impurities, omitting oxygen, subscripts, and iron, which can be calculated by difference, the shortened formula may be expressed as $(Mg_a)\ Cr_x\ Al_y$.

The formulae of the chromites have been calculated on the basis of 4 oxygens for example specimen A1 becomes:

$$(Mg_{0.576}\ Fe_{0.356})_{0.932}\ (Cr_{1.343}\ Al_{0.701})_{2.044}\ O_4$$

Or in the shortened form:

$$(Mg_{0.576})\ Cr_{1.343}\ Al_{0.701}$$

the chromite formulae are listed in table 17, together with the analyses.

Elimination of impurity effects by recalculating the analyses may result in considerable errors if the impurity is more than 2-3 percent. To demonstrate this, one specimen (F128A) has been analysed twice. The separated ore, containing 0.97 percent SiO_2, gave the following results after allowance for silicate impurity; Cr_2O_3, 53.48; Al_2O_3, 17.63; MgO, 12.47; FeO, 16.41. The ore has 6.85 percent SiO_2 which, after recalculation for silicate impurity gives; Cr_2O_3, 53.22; Al_2O_3, 14.30; MgO, 15.40; FeO, 17.07. If the assumed composition of the impurity had been correct these recalculations should have produced closely similar results.

Inter-element correlation data

Inter-element correlation coefficients are given in table 24; correlations significant at the 99.9 percent confidence level have been underlined. Al_2O_3, V_2O_3, MnO, FeO and ZnO have negative correlation with Cr_2O_3, Al_2O_3 has positive correlations with V_2O_3, MnO, ZnO and NiO, the first three being dependent on the correlation with Cr_2O_3 given above: MgO has positive correlation with NiO and

Table 24 Inter-element correlation data for chromites

	V_2O_3	MnO	CuO	ZnO	NiO	TiO_2	CaO	FeO	MgO	Al_2O_3	Cr_2O_3
V_2O_3											
MnO	0.468										
CuO	0.136	-0.063									
ZnO	0.580	0.594	0.050								
NiO	0.220	0.145	-0.030	-0.116							
TiO_2	-0.601	-0.162	-0.167	-0.177	-0.094						
CaO	0.273	0.104	0.092	0.157	-0.143	-0.250					
FeO	0.526	0.633	-0.049	0.848	-0.208	-0.241	0.251				
MgO	0.225	0.177	0.095	-0.096	0.510	-0.050	-0.074	-0.282			
Al_2O_3	0.679	0.589	-0.001	0.556	0.439	-0.213	0.111	0.379	0.292		
Cr_2O_3	-0.756	-0.725	0.011	-0.728	0.348	0.263	0.177	-0.620	0.326	-0.935	
SiO_2	0.140	0.152	0.195	0.160	-0.001	-0.186	0.142	0.208	0.406	-0.158	-0.102

Significance levels

%99	0.408
%90	0.325
%80	0.295

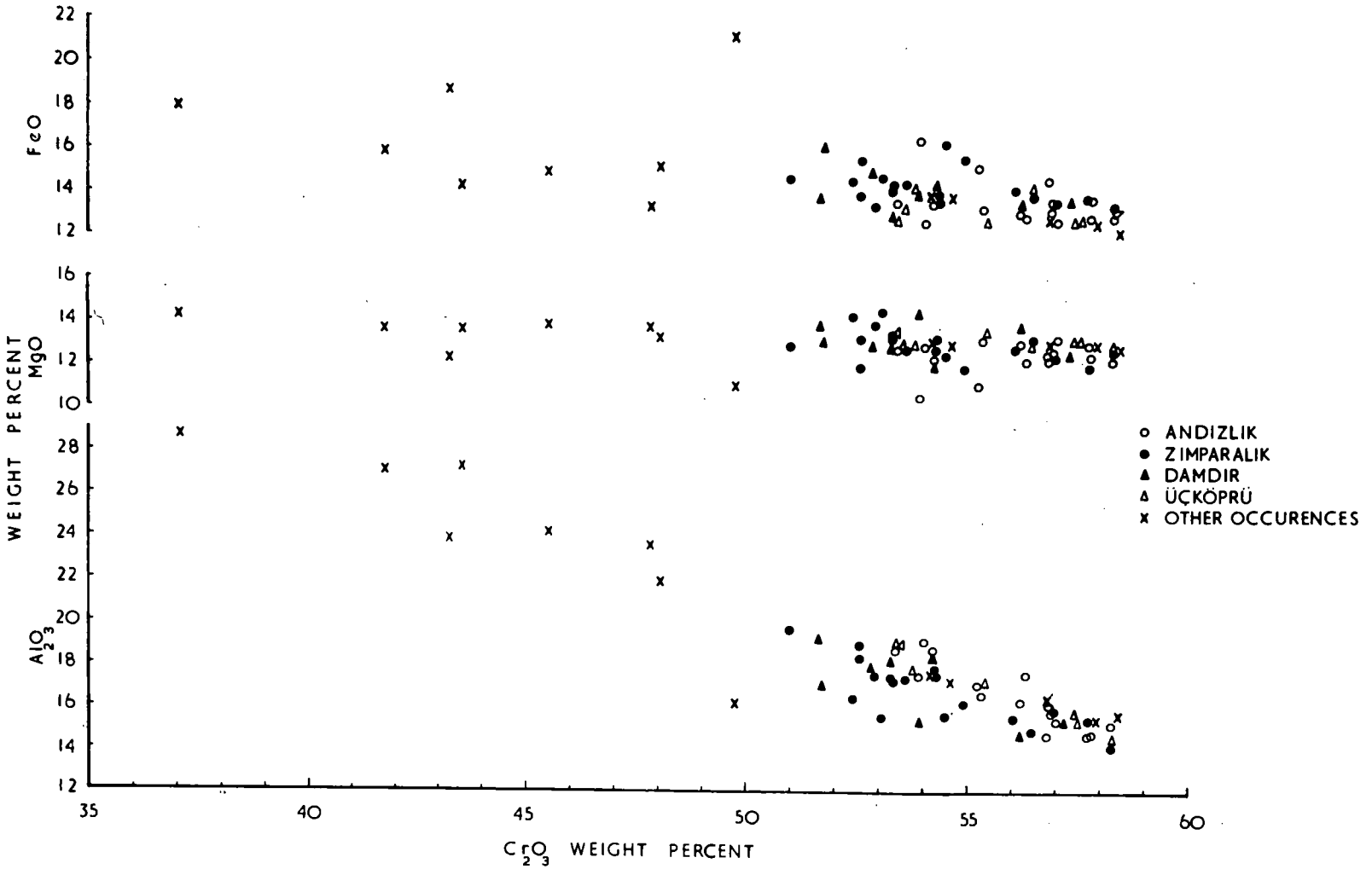

Correlation between Al_2O_3 MgO and Fe as FeO with Cr_2O_3 in chromite

FIG.38

FeO positive correlation with V_2O_3, MnO and ZnO. TiO_2 against V_2O_3 shows negative correlation, ZnO has positive correlation with V_2O_3 and MnO and MnO positive correlation with V_2O_3. All other correlations are below the 99.9 percent confidence level.

Correlations between FeO, MgO and Al_2O_3 with Cr_2O_3 are shown in fig.38.

The data presented above connected with intercorrelations of the elements agrees with the main features of differentiation process as Al shows negative correlation with Cr and Fe with Mg.

Relations between the chemistry and physical properties of the chromites

Cell size

Cell edge lengths of 10 analysed chromites are listed in table 16. The cell edge lengths have been correlated with the chemical components and correlation coefficients are given in table 25.

Cr_2O_3, Al_2O_3, FeO and ZnO show correlation with cell size at the 99.9 percent confidence level, Cr_2O_3 has a positive correlation while ZnO, FeO and Al_2O_3 have negative correlations. Similar relationships between cell size Al_2O_3 and Cr_2O_3 have been demonstrated by Stevens (1944) and Hancock (1964), etc.

Statistical details connected with correlations between the unit cell edge, Cr_2O_3 and Al_2O_3 of the chromites are given in table 26.

Table 25 Correlation of the composition of the chromites with their unit cell edge lengths.

	Correlation Coefficients
SiO_2	0.075
Cr_2O_3	0.988
Al_2O_3	-0.993
MgO	-0.657
FeO	-0.942
CaO	0.047
TiO_2	0.161
NiO	-0.820
ZnO	-0.940
CuO	0.091
MnO	-0.792
V_2O_3	-0.818
Significance levels	
%99	0.872
%90	0.765
%80	0.715

Table 26 Statistical data for the correlation of unit cell edge lengths with Cr_2O_3 and Al_2O_3 content of chromite.

$\underline{Cr_2O_3}$

Regression equation	Cell edge=295.0401Cr_2O_3-2391.7267
Correlation coefficient	0.9877
Number of data points	10
Student "t"	17.8669
Standard deviation of cell edge	0.0250
Standard deviation of Cr_2O_3	7.4966
Standard error of estimate on cell edge	0.0039
Standard error of estimate on Cr_2O_3	1.1721

$\underline{Al_2O_3}$

Regression equation	Cell edge=211.4739Al_2O_3+1770.5889
Correlation coefficient	-0.9926
Number of data points	10
Student "t"	-23.2357
Standard deviation of cell edge	0.0250
Standard deviation of Al_2O_3	5.3464
Standard error of estimate on cell edge	0.0030
Standard error of estimate on Al_2O_3	0.6460

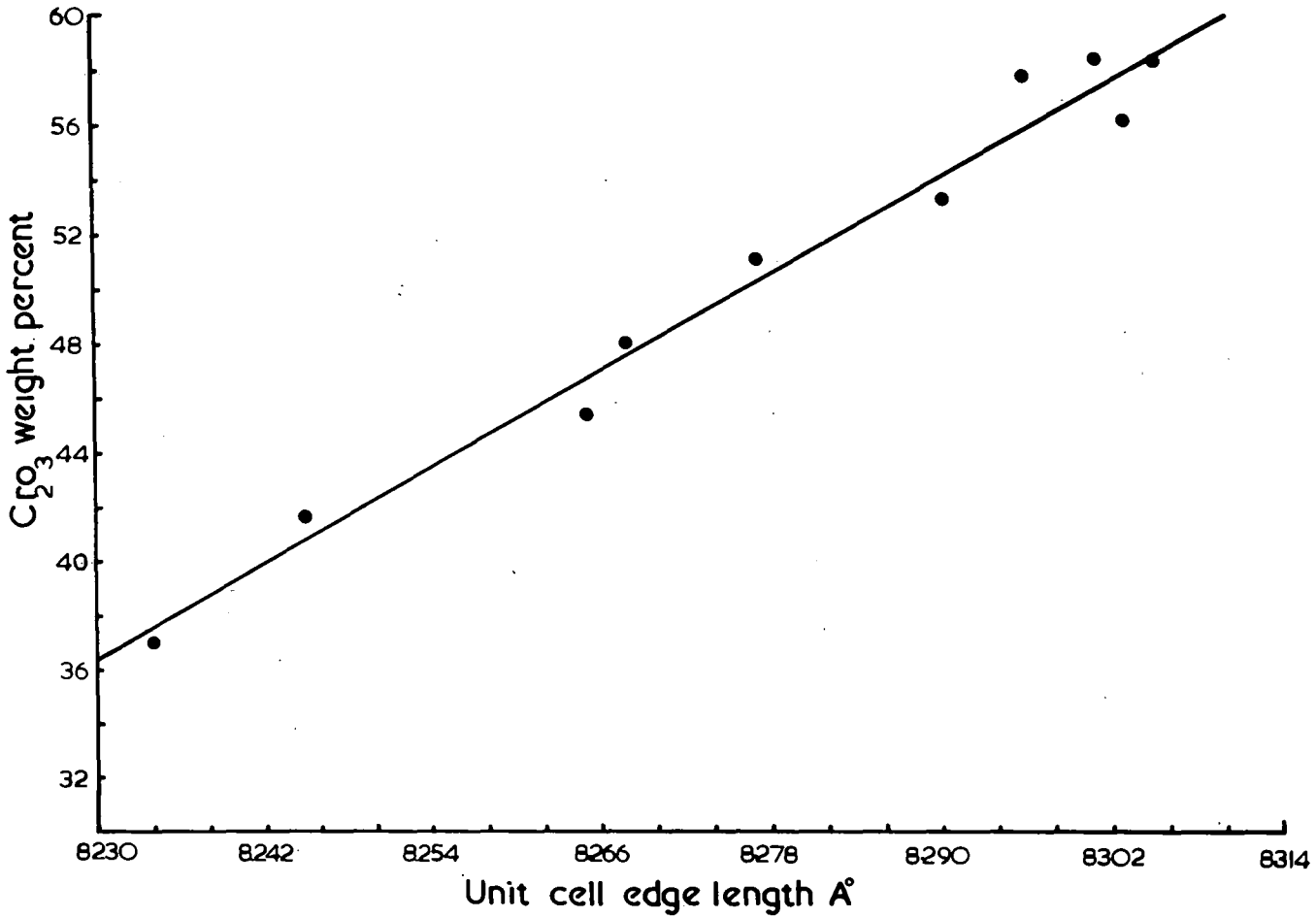

Correlation between unit cell edge and Cr_2O_3 in chromite

FIG. 39

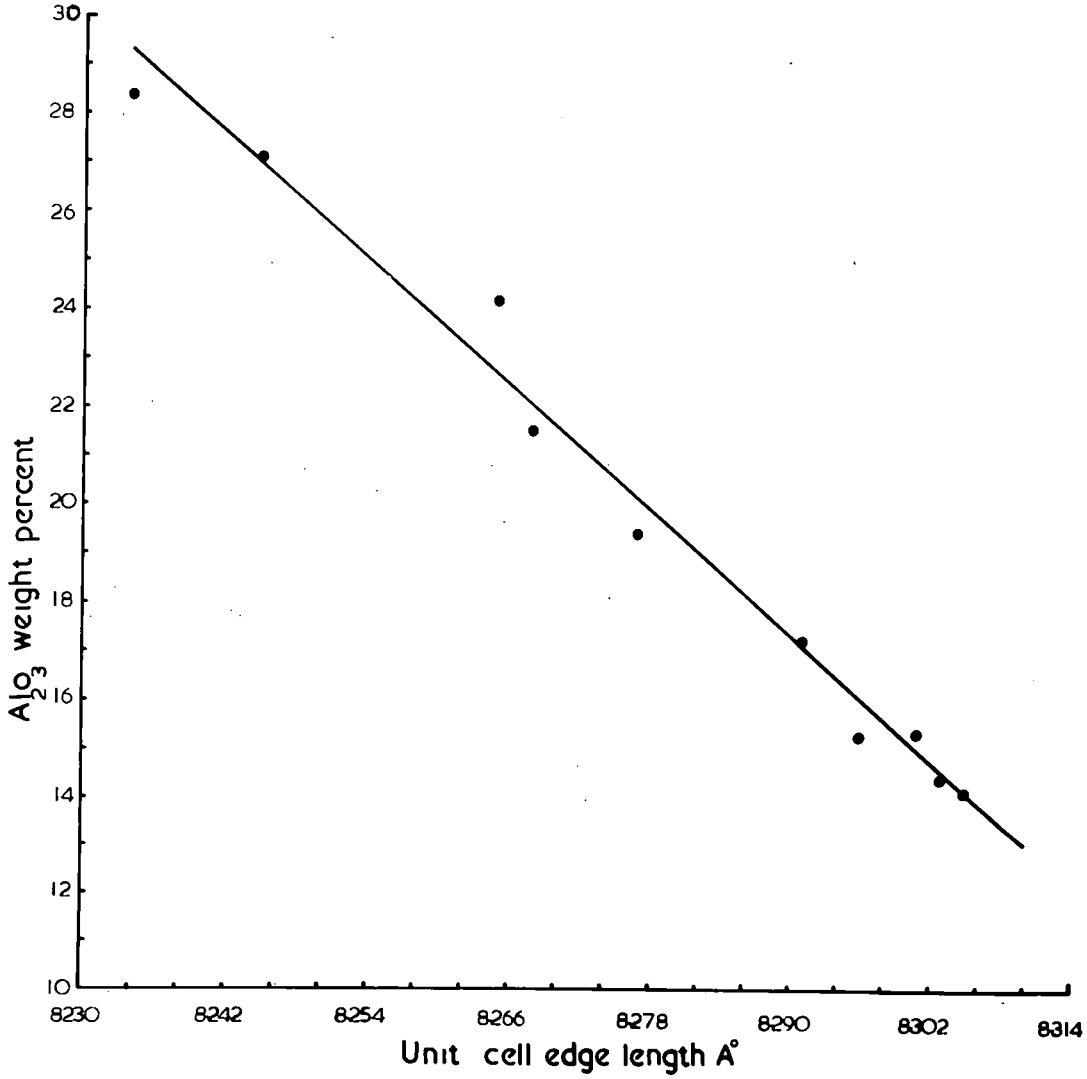

Correlation between unit cell edge and Al_2O_3 in chromite

FIG.40

Fig.39 and 40 show these correlations. The correlations can be used to estimate the Cr_2O_3, Al_2O_3, FeO and ZnO percentage of the chromites providing that the length of cell edge has been determined from X-ray diffraction studies.

Reflectivity

The spectral reflectivity values, given in table 14, have been correlated with the chemistry of the chromites, correlation coefficients are given in table 27.

Cr_2O_3 has positive correlation at the 99.9 percent confidence level with the measured reflectivity values, V_2O_3, MnO, Al_2O_3 have negative correlation while FeO has negative correlation at the 99.9 percent confidence level except for the wavelengths 640 and 660 mμ. ZnO has negative correlation with the reflectivity values at the 440, 520, 560, 580, 600 and 620 mμ wavelengths. Correlations between MgO and reflectivity are weaker with negative correlation only at the 85 percent confidence level.

Correlations between reflectivity values at 480, 540, 580 and 640 mμ wavelengths and 4 major components of the chromites (Cr_2O_3, Al_2O_3, FeO and MgO) have been further studied, regression equations and other statistical details are given in table 28. In figs 41 and 42, the relationship between Cr_2O_3 and Al_2O_3 and reflectivity are shown, together with 95 percent confidence limits.

The data indicate that the Cr_2O_3, Al_2O_3, MnO, V_2O_3, FeO and ZnO

Table 27 Correlation coefficients between reflectivity and composition of chromites, for various wavelengths

	440mμ	460mμ	480mμ	520mμ	540mμ	560mμ	580mμ	600mμ	620mμ	640mμ	660mμ
SiO_2	-0.075	-0.060	-0.067	-0.063	-0.050	-0.047	-0.063	-0.055	-0.016	-0.120	-0.010
Cr_2O_3	0.966	0.953	0.955	0.962	0.957	0.956	0.963	0.958	0.954	0.932	0.855
Al_2O_3	-0.982	-0.972	-0.975	-0.980	-0.977	-0.980	-0.979	-0.978	-0.965	-0.952	-0.898
MgO	-0.539	-0.564	-0.558	-0.550	-0.559	-0.551	-0.548	-0.552	-0.560	-0.618	-0.591
FeO	-0.742	-0.716	-0.720	-0.732	-0.718	-0.715	-0.739	-0.722	-0.739	-0.662	-0.552
CaO	-0.069	-0.013	-0.024	-0.032	-0.032	-0.027	-0.042	-0.023	-0.055	-0.005	-0.027
TiO_2	0.206	0.190	0.216	0.204	0.212	0.210	0.220	0.180	0.177	0.190	0.245
NiO	-0.327	-0.349	-0.342	-0.331	-0.344	-0.341	-0.316	-0.325	-0.288	-0.422	-0.472
ZnO	-0.714	-0.688	-0.688	-0.707	-0.691	-0.695	-0.713	-0.708	-0.712	-0.661	-0.567
CuO	-0.035	-0.047	-0.036	-0.018	-0.022	-0.035	-0.031	-0.027	-0.028	-0.047	-0.180
MnO	-0.807	-0.796	-0.799	-0.813	-0.808	-0.791	-0.803	-0.796	-0.823	-0.751	-0.700
V_2O_3	-0.766	-0.728	-0.732	-0.738	-0.742	-0.738	-0.754	-0.726	-0.757	-0.711	-0.745

Significance levels	
%99.9	0.693
%90	0.575
%80	0.528

Table 28 continued

FeO	480mμ	540mμ	580mμ	640mμ
Regression equation	R=-0.2627FeO+16.2945	R=-02470FeO+15.7498	R=-0.2516FeO+15.6236	R=-0.2175FeO+14.8723
Correlation coefficient	-0.7199	-0.7181	-0.7392	-0.6615
Number of data points	19	19	19	19
Student "t"	-4.2770	-4.2553	-4.5266	-3.6375
Standard deviation of FeO	1.6880	1.6880	1.6880	1.6880
Standard deviation of R	0.6161	0.5805	0.5745	0.5551
Standard error of estimate on FeO	1.1715	1.1746	1.1367	1.2658
Standard error of estimate on R	0.4276	0.4040	0.3868	0.4163

MgO				
Regression equation	R=-0.4771MgO+18.6505	R=-0.4510MgO+17.9978	R=-0.4376MgO+17.6420	R=-0.4763MgO+17.8706
Correlation coefficient	-0.5575	-0.5591	-0.5484	-0.6177
Number of data points	19	19	19	19
Student "t"	-2.7691	-2.7826	-2.7045	-3.2392
Standard deviation of MgO	0.7200	0.7200	0.7200	0.7200
Standard deviation of R	0.6161	0.5805	0.5745	0.5551
Standard error of estimate on FeO	0.5977	0.5968	0.6020	0.5662
Standard error of estimate on R	0.5115	0.4812	0.4803	0.4365

R = Reflectivity

Table 28 Statistical data for the correlation of reflectivity at wavelengths 480, 540, 580 and 640 mμ with the Cr_2O_3, Al_2O_3, FeO and MgO contents of chromite.

$\underline{Cr_2O_3}$

	480mμ	540mμ	580mμ	640mμ
Regression equation	$R=0.1003Cr_2O_3+7.2486$	$R=0.0946Cr_2O_3+7.2288$	$R=0.0942Cr_2O_3+7.0562$	$R=0.0882Cr_2O_3+7.1118$
Correlation coefficient	0.9552	0.9565	0.9627	0.9324
Number of Data points	19	19	19	19
Student "t"	13.3227	13.5281	14.6807	10.6412
Standard deviation of Cr_2O_3	5.8656	5.8656	5.8656	5.8656
Standard deviation of R	0.6161	0.5805	0.5745	0.5551
Standard error of estimate on Cr_2O_3	1.7341	1.7100	1.5859	2.1191
Standard error of estimate on R	0.1821	0.1692	0.1553	0.2005

$\underline{Al_2O_3}$

Regression equation	$R=-0.1514Al_2O_3+15.3494$	$R=-0.1430Al_2O_3+14.8759$	$R=-01417Al_2O_3+14.6590$	$R=-0.1333Al_2O_3+14.2394$
Correlation coefficient	-0.9745	-0.9773	-0.9788	-0.9524
Number of data points	19	19	19	19
Student "t"	-17.9286	-19.0580	-19.7043	-12.8856
Standard deviation of Al_2O_3	3.9662	3.9662	3.9662	3.9662
Standard deviation of R	0.6161	0.5805	0.5745	0.5551
Standard error of estimate on Al_2O_3	0.8889	0.8386	0.8123	1.2087
Standard error of estimate on R	0.1380	0.1227	0.1176	0.1691

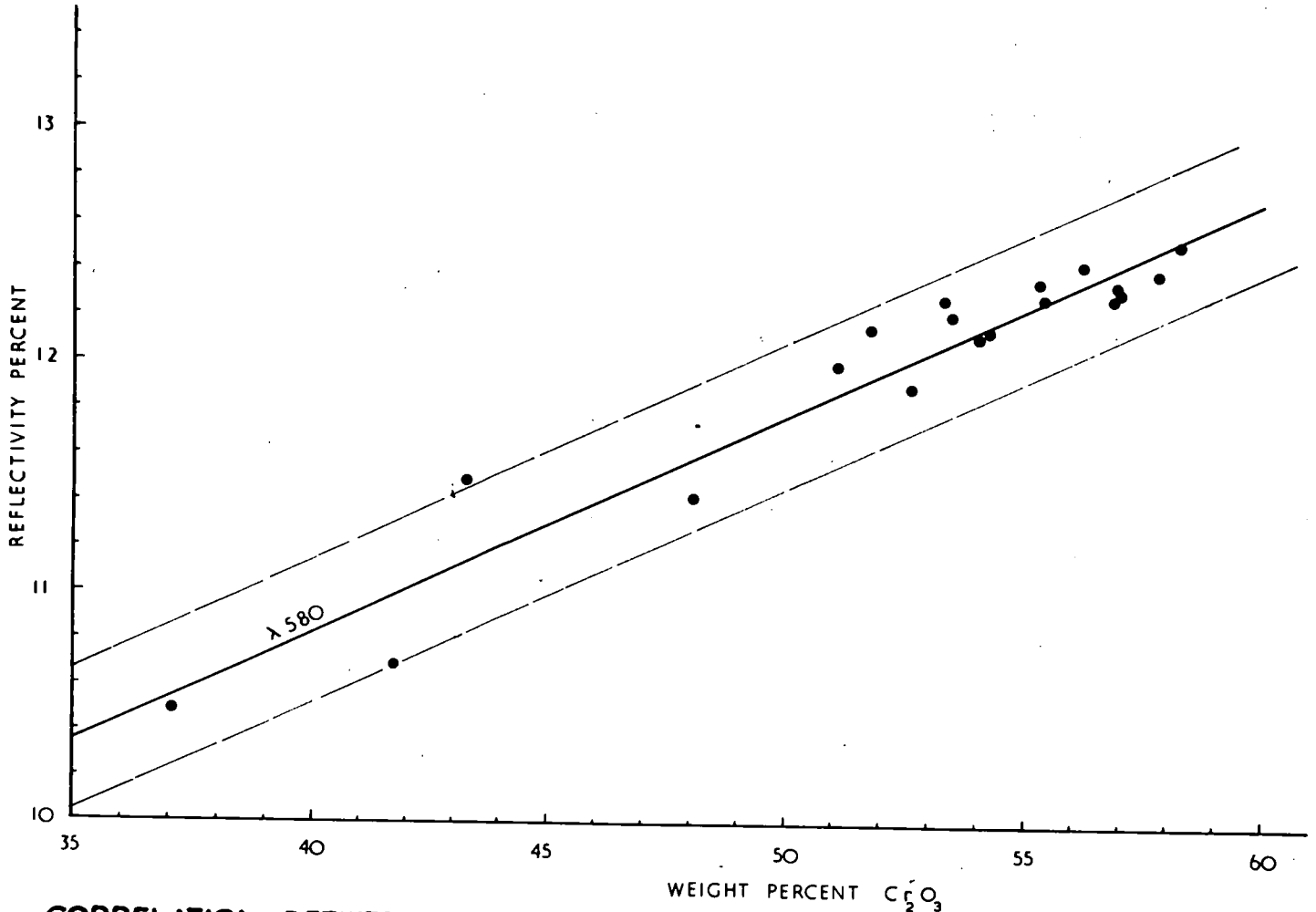

CORRELATION BETWEEN SPECTRAL REFLECTIVITY AND Cr_2O_3 IN THE CHROMITES

FIG. 41

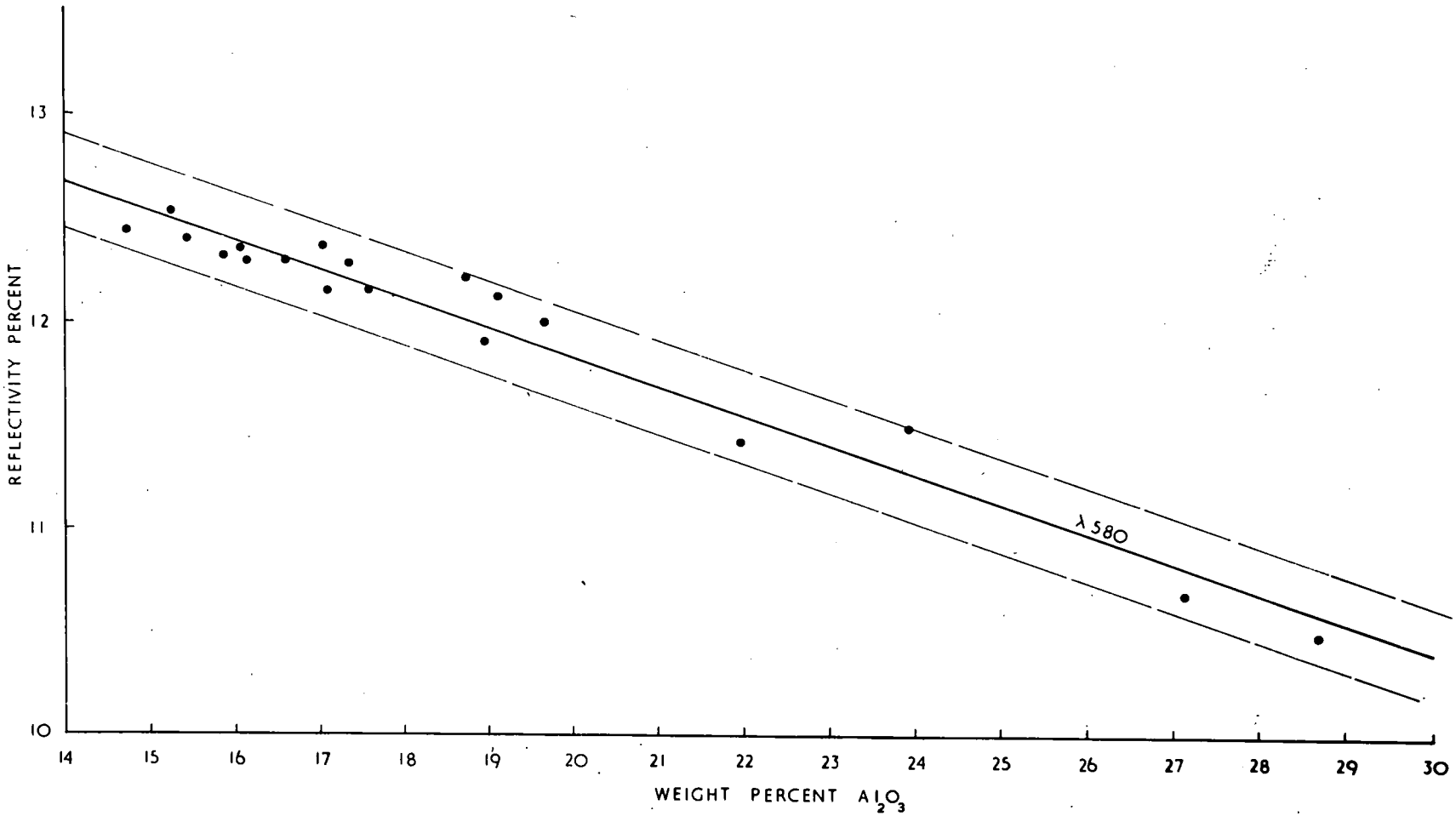

CORRELATION BETWEEN SPECTRAL REFLECTIVITY AND Al_{23} IN THE CHROMITES

FIG.42

contents of the chromites may be estimated from reflectivity measurements within the 95 percent confidence limits, but MgO may only be estimated within the 85 percent confidence limits. For all these elements there may be higher accuracy at relatively high concentration.

The relationships between spectral reflectivity and chemical composition prove of use in studying the chemistry of accessory chromite which can only be recovered from the host peridotite with considerable difficulty. The reflectivity of the specimen should be measured at the 4 wavelengths 480, 540, 580 and 640 mμ providing four values for each oxide content Cr_2O_3 etc; these values should then be averaged to produce the analysis.

The chemical composition of 5 chromites which occur in an accessory amount in the peridotite have been estimated from reflectivity measurements at wavelengths of 480, 540, 580 and 640 mμ, table 29. These reflectivity values have been used in the equations given in table 28 to produce values for Cr_2O_3, Al_2O_3, FeO and MgO. The number of determinations made are insufficient for any conclusions to be made, although the accessory chromite from the eastern sector F208, F204 and F67A is relatively impoverished in Cr_2O_3 and enriched in Al_2O_3, in agreement with conclusions based on chemical analyses of chrome ores from this part of the body.

Table 29 Reflectivity measurements of accessory chromites from the peridotite with chemical compositions derived (weight percent) from the equations relating reflectivity and chemistry.

λmμ	A13	F67A	F204	F208	F251
480	13.31	12.68	11.61	10.84	12.35
540	13.03	12.53	11.38	10.62	11.94
580	12.70	11.97	10.99	10.48	11.70
640	12.29	11.42	-	10.19	11.36
Cr_2O_3	60.1	52.8	43.0	35.7	49.5
Al_2O_3	13.7	18.5	25.0	29.8	20.7
FeO	11.5	14.3	14.3	20.9	15.5
MgO	11.3	12.8	14.9	16.3	13.5

CHAPTER 7

PETROGENESIS

Theories relating to the genesis of large peridotite bodies

There are two main hypotheses concerning the nature of the parent magma from which alpine peridotites are derived, that of Hess (1938) who advocated a primary peridotite magma and that of Bowen and Tuttle (1949).

The main objections to the hypothesis advocated by Hess are that effusive equivalents of ultramafic magmas are never found at the surface, and that ultramafic magmas can only exist at very high temperatures. Bailey and McCallien (1953), however, have described serpentine lavas from Turkey and Gass (1958) has described ultrabasic pillow lavas from Cyprus. Gass suggested that these pillow lavas were formed either by complete fusion of part of the peridotite substratum or from a peridotite body nearer to the surface.

Vogt (1923) suggested that peridotites were emplaced as liquids with temperatures of 1500°C to 1600°C. Although high temperature metamorphism related to alpine peridotites has been described, e.g. Green (1964), Bilgrami (1964), MacKenzie (1960), the metamorphism is not consistent with the high temperatures suggested by Vogt. Bowen and Tuttle (1949) investigated the system $MgO - SiO_2 - H_2O$ at temperatures ranging up to 900°C and pressures

up to 15.000 lb per sq. inch, they concluded that there is no possibility of the existence of a serpentine magma below 1000°C.

Peridotites consist largely of olivine crystals, gravitational differentiation of olivine, separating from basaltic magma, is an established mechanism capable of producing crystal accumulations of this type.

Bowen and Tuttle (1949) suggest that mobility of peridotitic accumulates can be achieved by the lubricating effect of small quantities of intergranular magmatic liquid, or water vapour. If the alpine peridotites are the early cumulus fraction of differentiated basaltic magma, they should be accompanied by considerable quantities of basaltic rocks and later differentiates such as rhyolite or trachyte.

Turner and Verhoogen (1960) suggest that some alpine peridotites may represent mobile masses that have been separated from a peridotite substratum of the upper mantle.

Gass and Masson-Smith (1963) suggest that the mineralogical and geophysical evidence relating to the Troodos complex of Cyprus are consistent with the derivation of ultrabasic material from the mantle. The composition and nature of the Troodos peridotites are comparable to those of alpine type complexes suggesting a comparable parent magma although not necessarily a comparable tectonic setting.

Rocks that have seismic velocities equal to the observed values for the upper mantle are limited to ultramafic and eclogitic compositions. On the assumption that chondritic meteorites are representative of the average cosmic material Urey (1952), Macdonald (1959) and Ringwood (1959) have suggested a carbonaceous chondrite composition as a reasonable model for the composition of the earth. Macdonald (1959b) has indicated that the rate of heat loss at the earth's surface is in agreement with the rate of heat production of a chondritic earth. Kovach and Anderson (1965) suggested that the astronomical data on the terrestrial planets may be satisfied on the assumption that they have a chemical similarity, but Gast (1960) has shown that the minor element distribution in the crust of the earth is not entirely consistent with a chondritic model. The crust and upper mantle do not contain K, Rb, Cs, U, Ba and Sr in the proportions found in the chondrites, the alkali metals being depleted with respect to U, Sr and Ba. MacGregor (1967) concludes that either the earth is not chondritic or differentiation of a chondritic parent into the crust, mantle and core has resulted in concentration of U, Sr and Ba in the crust, with K, Rb and Cs being concentrated in the lower mantle or lost from the system through a primitive atmosphere (Ringwood, 1966). MacGregor (1967) reviews the chondritic hypothesis and concludes that the mantle is ultramafic and probably corresponds closely in composition to a four

phase spinel or garnet peridotite.

The system CaO - MgO - Al_2O_3 - SiO_2 is the model system for the peridotite phase assemblage and phase changes in an ultramafic upper mantle will be governed by a limited number of reactions. The relationship of these reaction boundaries to the earth's thermal gradient indicates that for the two pyroxene peridotites the geothermal gradient for a Precambrian shield or an oceanic region does not intersect the spinel peridotite field. Spinel peridotites may thus only be formed as precipitates from basaltic or picritic magmas or exist in regions with an exceptionally high geothermal gradient.

In a consideration of garnet peridotites O'Hara (1967) suggests that layered, spinel bearing ultrabasic masses containing high Al_2O_3 pyroxenes have formed by accumulation from basic magmas which were crystallizing near the base of the crust prior to orogenesis. During rapid downbuckling these dry, relatively cold rocks were subjected to high pressures and recrystallised to eclogite facies assemblages with reaction between the layers produced by original igneous processes before the temperature could rise to the normal values appropriate to the depth of burial, or water gain access from the country rocks. Survival of the eclogite facies assemblage requires the coincidence of a second event, the rapid and extensive isostatic or tectonic uplift of the garnet peridotites before

recrystallization in response to rising temperature or access of water.

Simulikowski (1968) suggests that the most convincing evidence for the occurrence of eclogite in the upper mantle is the presence of eclogite nodules in the diamond bearing kimberlite pipes of South Africa. Experimental work suggests that diamond can not form in the earth's crust but must originate from deeper zones which have been submitted to considerable pressures. Simulikowski however has examined the pressure-temperature conditions of eclogite and concludes that true eclogites could be formed in a very wide range of pressure and temperature, frequently relatively low. Eclogites are metamorphic products of the earth's crust, particularly in such zones where the increase of pressure with depth was accompanied by a very small increase of temperature. Eclogites of this type cannot be expected below the Mohorovic discontinuity. Garnet pyroxenites (griquaites) may occur in the upper mantle as subordinate differentiation products of garnet pyrolite. The concensus of opinion would be that large volumes of ultramafic rock originate from the upper mantle.

Wyllie (1967) suggests that when ultramafic materials are first derived from the upper mantle, they could be in one of several states. Complete or nearly complete fusion of upper mantle material would yield an ultrabasic liquid magma. Partial fusion

of the upper mantle material would yield basaltic magma from which mafic minerals such as olivine and pyroxene may later be concentrated to form ultramafic rocks. Partial fusion of the upper mantle could also yield a crystal mush composed of basaltic or picritic liquid and refractory olivine crystals. Transportation of the mush and subsequent crystallization of the liquid would yield an ultramafic rock. Finally an ultramafic rock could be derived directly from the upper mantle in the solid state either by plastic flow or by tectonic transport.

Yoder and Tilley (1962) have suggested that the peridotite masses may be cold intrusions derived as crystalline rocks from the upper mantle.

O'Hara (1967) has examined the equilibration conditions of the ultramafic rocks in the system CaO - MgO - Al_2O_3 - SiO_2 and concludes that the alpine type peridotites appear to have equilibrated under varying conditions in the range 0 to 20 kb, 400 to 1200°C, thus reinforcing the conclusion that special tectonic conditions are necessary for their transport and emplacement.

A summary of the data relating to the genesis of the Andizlik-Zimparalik peridotite and associated chrome ore.

(a) Structural evidence

In the Andizlik-Zimparalik area the peridotite body trends, in general, in a northwest-southeast direction and is bounded by thrust

zones, to the north and south, which dip towards the peridotite. The peridotite is serpentinised, on average to over 50 percent, although the range is from fresh to fully serpentinised.

The main structural features, faults, pyroxenite veins, and internal contacts are aligned in two dominant directions, northwest-southeast and northeast-southwest; the chromite bodies and basic dykes are also aligned in this direction. These features make acute angles in the east-west direction suggesting that the maximum pressure direction was east-west. The sedimentary rocks are free from any sign of contact metamorphism but the peridotite at the contacts is characterised by heavy brecciation and serpentinisation. Slickensides, measured along these thrust zones, indicate movement in the northwest-southeast direction.

Lack of contact metamorphism, intense brecciation and serpentinisation indicate that the peridotite was cool and in a solid state when it was emplaced in its present position. Basic rocks, mainly dioritic in composition and intrusive to the peridotite, comprise some 9 percent of the area. Unless considerable quantities of basaltic material has been removed by erosion the derivation of the peridotite as a cumulus fraction of a differentiating basaltic magma seems unlikely. Magmatic layering is obscure, it is known in one locality, plate 15, where pyroxene rich bands are

seen in the harzburgite. Very thin, localized chromite bands occur in several localities and suggest that the peridotite has been differentiated at some period in its history.

The observed features in the area, suggest that the peridotite body was probably derived from the upper mantle or lower crust. At this level the bulk of the chromite had already crystallized and segregated into separate, and possibly stratiform bodies. Textural relations between olivine and chromite suggest that probably the bulk of the silicate fraction was also crystallized at this stage. Under the influence of the regional stress field, probably set up at the onset of the alpine orogeny, this particular solidified mush rose through the crust, chromite concentrations moving differentially and becoming aligned in response to the stress field, pods resembling the boudinage structure. Fracturing along directions determined by the stress field commenced and was particularly strong marginally where the peridotite cooled more quickly and became solid. Fig.4 and 4A (see Volume 2) illustrates the much higher density of faulting and fracturing of the marginal zones in comparison to the central part of the area, this high density of fracturing is responsible for the comparative difficulty of working chrome ore at Damdir and Uckopru in contrast to either Andizlik or Zimparalik. During this stage of emplacement country rocks including Carboniferous, Permian, Jurassic, and Cretaceous

limestones, Radiolarian cherts and amphibolites were caught up in the peridotite as xenoliths, thus dating the movement as post Cretaceous. These xenoliths are highly sheared but are not metamorphosed.

(b) Chemical evidence

Except for the degree of serpentinisation the peridotites lie within a narrow compositional range. The olivine composition changes from Fo_{88} to Fo_{91} (based on electron probe analyses) while the orthopyroxene composition of the harzburgites changes from En_{89} to En_{99} (based on X-ray diffraction results); no pattern is evident.

The chromite chemistry indicates a general increase in Mg/Fe, Cr/Fe, and Cr/Al ratios from east to west. Chemical trends resulting from fractional crystallization may be related systematically to stratigraphic elevation, provided the chromite grains have not been modified greatly by reaction with interstitial magma and associated silicates. In this context the chromites from the eastern part of the field must have been generated at stratigraphically higher levels than the remaining chromites.

Except for F19 and F68 all analysed chromites have no genetic connection with their present host rock with which they are in tectonic contact. They have been brought to their present position during emplacement of the peridotite from the deeper levels. Bearing

in mind the extent of tectonic transport, regularity in compositional trend would not be expected. Yassitepe chromites illustrate this point for their analyses are more in keeping with those occurring much further east, fig.37. Analysed eastern chromites contain those examples where primary magmatic segregation may still be identified, plate 14. To maintain these primary magmatic relations the chromite and the associated silicate must have been entirely crystallised prior to tectonic movement or differential movement should have occurred as postulated for development of podiform ore. This conclusion leads to the suggestion that the eastern stratiform chromites, which also have considerably different chemistry from the bulk of the chromite, crystallised at a relatively high level in the crust after the initial tectonic uplift responsible for the inception of the podiform structures and strong marginal faulting. Thus the final consolidation of the ultramafic "magma" may have taken place at a relatively high level, it probably preceded the crystallisation of the residual dioritic dregs which form the dykes.

Basic dykes must have resulted from the residual magma. They are late stage intrusive features and where the primary relations are preserved the peridotite is sheared as well as cooked, Plate 7, and the basic dykes have chilled margins. The basic dykes are clearly later than the chromite bodies which they cut and brecciate, they

often have a narrow chilled margin against the chromite, Plate 9. The intrusion of the basic dykes probably occurred before the peridotite was emplaced in its present position. The residual magma moved to the low pressure areas particularly abundant in the highly fractured southern and northern thrust zones and consequently the dykes follow the zones of weakness and conform with the northwest-southeast directions. Boundary planes of the basic dykes dipping northeast in the north and southwest in the south of Kilcan dere and also opposite dip directions of these planes observed along the southern thrust zone, fig.7, could result from continued tectonic uplift after consolidation of the dykes or may simply reflect the dominant directions of the fracture pattern.

Plagioclase is not present in the peridotite although examination of the system CaO - MgO - Al_2O_3 - SiO_2 shows that it is not possible to arrive at an enstatite, diopside, forsterite spinel assemblage without involving anorthite. Yoder and Tilley (1962), however, showed that the anorthite - forsterite assemblage is not stable at very high load pressures while Rothstein (1961) has also suggested that high pressure causes depression of liquidus temperatures to the point where the spinel and diopside fields converge.

Irvine (1966) has compared spinels from alpine and stratiform complexes, he states that the ratio $Fe^{+++}/Cr+Al+Fe^{++}$ in the spinels of the alpine type is relatively constant and is low compared with

the stratiform chromites. Irvine concludes that most spinels of alpine type peridotite bodies must have crystallized at relatively low oxygen fugacity. The contrast in Fe_2O_3 content between the spinels of alpine type peridotites and chromites of stratiform intrusions may represent a contrast between a low, relatively uniform state of oxidation in the deep crust or upper mantle and more variable, and generally higher, oxygen fugacities in the rocks and fluids of the near surface environments where the stratiform intrusions are crystallized.

Most of the Andizlik-Zimparalik chromites are unbalanced, only five requiring Fe_2O_3 values in the range 0.24 to 3.72 percent. This, also, might suggest that these balanced chromites were formed in the upper part of a magma chamber, or at a higher position in the crust, relative to the other unbalanced chromites; the stratiform chromites occur in this group.

Hydrothermal solutions saturated with SiO_2, probably at temperatures above 650°C have formed localised pyroxenite veins along the two dominant structural directions, northwest-southeast and northeast-southwest in the peridotite. Tremolite veins associated with the chrome ore bodies may also have formed at this stage. During this hydrothermal activity a limited amount of Cr has been removed, presumably from the ore bodies, and taken into the tremolite and orthopyroxene structures.

The development of "ferritchromit" zones in the chromite grains is believed to be the result of hydrothermal activity; Al_2O_3 and MgO have been removed preferentially from the chromites, leaving behind zones enriched in Cr_2O_3 and FeO. This suggests that Cr is not easily removed from chromite by hydrothermal solutions, and this may have some bearing on the source of Cr in the tremolite and pyroxenites. If no Cr is leached from chromite during the formation of the "ferritchromit" zones, then it is probable that the chrome tremolite, and pyroxenites were formed during a separate hydrothermal phase. If on the other hand some Cr is leached during the formation of "ferritchromit", although little relative to the amounts of Al_2O_3 and MgO leached with resultant enrichment in Cr, then the formation of chrome tremolite, pyroxenites, and the ferritchromit zones could be contemporaneous.

Low temperature hydrothermal solutions possibly moving from the surrounding sediments into the peridotite, caused serpentinisation. Analyses of serpentinised rocks has shown that the serpentinisation is a constant compositional process and, in the area generally, has been accompanied by a volume increase of around 20 percent. This volume increase, and resultant drop in density, must have provided some of the impetus for the further uplift of the peridotite and emplacement in its present position.

Pliocene to Quaternary conglomerates and marls rest unconformably on the peridotite while Van der Kaaden (1959 p.2) has described Eocene flysch formations which include peridotite fragments. This information suggests that the final emplacement of the peridotite was or shortly after, the Eocene. During this period the Laramian phase of the alpine orogeny was effective all along the Tauros mountains and in southern Turkey,(Ketin, 1966, p.30).

Finally, exposure of the peridotite to atmospheric weathering and surface oxidation has resulted in the formation of limited magnesite deposits.

A Relative time sequence for the emplacement of the peridotite and chrome ore deposits in the Andizlik-Zimparalik area.

The events can be grouped in 6 stages:

1. Chromite segregation into initially stratiform bodies and crystallisation of the bulk of the "ultrabasic magma".

Position:

Upper Mantle to lower crust.

Time:

Unknown, probably starts crystallising in response to changes induced by the onset of the alpine orogeny.

2. Intrusion, possibly initially magmatic, but mainly tectonic. Solid chromite moves differentially in relation to the crystal

mush, podiform and lenticular disposition develops in response to stress.

Margins become entirely solidified but not the central parts, brecciation and fracturing of marginal areas, attitudes of joints, faults and contacts determined by the stress field.

Position:

Achieves a position in the lower to middle crust.

Time:

Post Cretaceous to Early Tertiary.

3. The bulk of the residual silicates crystallise, local but insignificant development of stratiform chromite towards the top of the igneous body.

Position:

~~Achieves a position in the~~ Lower to middle crust.

4. Residual magma (gabbroic to dioritic) occupies low pressure areas and is particularly abundant in the brecciated and faulted margins of the intrusion. The dykes are aligned mainly in the northwest-southeast direction.

Position:

~~Achieves a position in the~~ Lower to middle crust.

5. "High" temperature, SiO_2 bearing, hydrothermal activity, localised along joints forms pyroxenite veins, tremolite forms

in association with chromite. Possibly some localised serpentinisation, and some modification of chromite composition due to hydrothermal activity - "ferritchromit" development.

Position:

~~Achieves a position in the~~ Lower to middle crust.

6. Low temperature hydrothermal activity causes serpentinisation, particularly in fault zones and marginal areas where further intense brecciation results from expansion. Continued expansion, leading to a volume increase of about 20 percent, provides the impetus for further tectonic uplift to the present position and present level. The direction of movement is governed by the stress field operating, and previously imposed. Chromite bodies found in the eastern part of the field have chemical compositions which indicate an origin in the upper part of the magma chamber. Their present position suggests some degree of easterly movement in the later stages of emplacement. Lineation of podiform chromites however, suggest that easterly movement was an early developed feature. The basic dykes pre-date the last uplift, since some of them are substantially faulted and none have been recorded transgressing the marginal faults into the country rocks.

Position:

Movement to present level.

Time:

Late Eocene or post Eocene and pre Pliocene.

REFERENCES

Ahrens, L.H., and S.R. Taylor (1961) Spectrochemical analysis. Addison-Wesley, Massachusetts, U.S.A., 454p.

Altinli, I.E., (1955) The geology of Southern Denizli. Istanbul Universitesi fen fakultesi mecmuasi Cilt 20, sayi 1-2.

Asrarullah., (1960) Geology of chromite in West Pakistan. Symposium on chrome ore Cento, Ankara-Turkey pp 38-53.

Bailey, Sir E.B., and W.J. McCallien, (1953) Serpentine lavas, the Ankara Melange and the Anatolian thrust. Tran. Roy. Soc. Edin., 1 x ii, pt.ii.

Badgley, P.C., (1959) Structural Methods for the exploration geologist. Harper and Brothers, New York.

Bilgrami, S.A., (1963) Further data on the chemical composition of Zhob Valley chromites. Am. Mineral. 48, pp 573-587.

(1964) Mineralogy and petrology of the central part of the Hindubagh igneous complex, Hindubagh mining district, Zhob Valley, West Pakistan. Rec.Geol.Survey. Pakistan vol 10, part 2-C.

Borchert, H., (1958) Turkiye de inisiyal ofiolitik magmatizmaya ait Krom ve Bakir cevheri yataklari. M.T.A. enstitisu yayinlarindan ANKARA No.102. 162 p. (in Turkish and German).

(1961) Gurleyik koy kuzeyindeki peridotit masifinin tektonik ve ic yapisi. M.T.A. unpublished report No.2816. (in Turkish and German).

(1964) Principles of the genesis and enrichment of chromite ore deposits. In Methods of prospection for chromite. Edited by R. Woodtli. Proc. of an OECD seminar Paris pp 175-202.

Bowen, N.L., (1928) The evolution of the igneous rocks. Dover Publications, Inc. New York.

and O.F. Tuttle., (1949) The system $MgO-SiO_2-H_2O$. Bull. Geol. Soc. Am. Vol.60, pp 439-460.

Brothers, R.N., (1960) Olivine nodules from New Zealand. Int. Geol. Cong. Reports, 21st sess. pt.13, pp 68-81.

Brown, G.M., (1960) The effect of ion substituation on the unit cell dimensions of the common clinopyroxenes. Am. Mineral. Vol 45, pp 15-38.

Cameron, E.N., and M.E. Emerson., (1959) The origin of certain chromite deposits of the eastern part of the Bushveld complex. Econ. Geol. V.54, pp.1151-1213.

Chacrobarty, K.L., (1965) Geology and Mineralogical characters of the Indian chromites. Econ. Geol, V.60 pp 1660-1668.

Challis, G.A., (1965) The origin of New Zealand ultramafic intrusions. Jour. Pet. Vol.6, No.2 pp 322-364.

Colin, H.J., (1962) Fethiye-Antalya-Kas-Finike (Guneybati Anadolu) bolgesinde yapilan jeolojik etudler. M.T.A. dergisi sayi 59 pp 19-59. (in Turkish and French).

Davies, L.O., (1954) Statistical methods in research and production. Oliver and Boyd, 292p.

Deer, W.A., Howie, R.A., and Zussman, J., (1963) Rock-forming minerals. Five Volumes. Longmans Press.

Donath, M., (1931) Zinc-bearing chromite. Am.min. Vol. 16 p.484-487.

Dubertret, L., (1955) Geologie des roches vertes du Nord-Ouest de la syrie et du Hatay, (Turquie). Notes et Mem. sur le Moyen-Orient. Mus. Nat. d'Hist. Naturelle, Paris Bd.6. p.5/224.

Dunham, K.C., Phillips, R., Chalmers, R.A., and Jones, D.A., (1958) The chromiferous ultrabasic rocks of eastern Sierra Leone. Col. Geol. Min. Resources. Bull. Supply No.3.

Engin, T., and Hirst, D.M., (1969) The Serpentinisation of harzburgites from the alpine peridotite belt of S.W. Turkey (in preparation).

Erentoz, C., (1966) Contribution to the stratigraphy of Turkey. M.T.A. Bull. 66 pp.1-41.

Fisher, L.W., (1929) Origin of chromite deposits. Econ. Geol. Vol.24 pp 691-721.

Francis, G.H., (1956) The serpentine mass in Glen Urquhart, Inverness-shire, Scotland. Am. Jour. Scie. Vol 251 pp 201-226.

Gass, I.G., (1958) Ultrabasic pillow lavas from Cyprus. Geol. Mag. 95 pp 241-251.

and D, Masson-Smith., (1963) The geology and gravity anomalies of the Troodos massif, Cyprus. Phil. Trans. Roy. Soc. A255 pp 417-467.

Gast, P.W., (1960) Limitations on the composition of the upper mantle. J. Geophys. Res. 65. pp 1287-1297.

Ghisler, M., and B.F. Windley., (1967) The chromite deposits of the Fiskenaesset region, West Greenland. The Geol. Surv. of Greenland Report No. 12 39 p.

Golding, H.G., and P. Bayliss., (1968) Altered chrome ores from the Coolac serpentine belt, New South Wales, Australia. Am. Mineral. Vol. 53 pp 162-183.

Gales, G.G., (1967) Trace elements in ultramafic rocks. In ultramafic and related rocks. Edited by P.J. Wyllie. Wiley, New York. 1967 pp 352-362.

Graciansky, P. de., (1967) Existance d'une Nappe ophiolitique a l'extremite occidentale de la chaine sud-anatolienne relations avec les autres unites charriees et avec les terrains autochtones (Province de Mugla, Turquie). C.R. Acad. Sc. Paris, t.264, pp 2876-2879.

Green, D.H., (1964) The petrogenesis of the High-temperature peridotite intrusion in the Lizard area, Cornwall. Jour. Pet. Vol. 5 pp 134-188.

(1967) High temperature peridotite intrusions. In ultramafic and related rock edited by P.J. Wyllie. Wiley, New York. 1967 pp 212-222.

Haeri, Y., (1960) Geology of Iran's chromite deposits. Symposium on chrome ore, cento Ankara - Turkey. pp 21-26.

Hancock, W.G., (1964) The mount Tawai peridotite, North Borneo. Ph.D. thesis unpublished. Durham University.

Hawkes, D.D., (1967) Order of abundant crystal nucleation in a natural magma. Geol. Mag. Vol.104, No.5, pp 473-486.

Helke, A., (1962) The metalogeny of the chromite deposits of the Guleman district, Turkey. Econ. Geol., Vol.57 pp 954-962.

Hess, H.H., (1938) A primary peridotite magma. Am. Jour. Sci. 5th ser. Vol.35, pp 321-344.

(1952) Orthopyroxenes of the Bushveld type, ion substitution and changes in unit cell dimensions. Am. Jour. Sci. Bowen Vol. pp 173-187.

G. Dengo., and R.J. Smith., (1952) Antigorite from the vicinity of Caracas, Venezuela. Am. Mineral., Vol.37, pp 68-75.

(1955) Serpentines, orogeny and epirogeny. Geol. Soc. Amer. Special paper 62, pp 391-408.

(1960) Stillwater igneous complex. Geol. Soc. Am. Memoir 80, 230 p.

and G. Otalora., (1964) Mineralogical and chemical composition of the Mayaguez serpentine cores. U.S. Nat. Acad. Sci-Nat. Res. Council, Publ. 1188, pp 152-168.

Hiessleitner, G., (1951-1952) Serpentine und chromerz-Geologie der Balkanhalbinsel und eines Teiles Von Kleinasian. Bed.1, II.

(1954) Guney Anadolu torosu kromitli peridotit serpantinlerinin jeolojisine yeni ilaveler. M.T.A. dergisi sayi 46/47 (in Turkish and German).

Hietanen, A., (1963) Idaho batholith near pierce and Bungalow. U.S. Geol. Surv., prof. paper. 344.D.

Hirst, D.M., and K.C. Dunham., (1963) Chemistry and petrography of the marl slate of S.E. Durham, England. Econ. Geol, Vol. 58, pp 912-940.

Holland, J.G., and D.W. Brindle., (1966) A self-consistent mass absorption correction for silicate analysis by X-ray fluorescence. Spectrochimica Acta. Vol.22. pp 2083-2093.

Horninger, G., (1940) Beobachtungen am Erzinhalt von Gesteinen und am chromerz aus tampadel in schlesien, min. Petr. Mitt., Bd.52.

Hostetler, P.B., R.G. Coleman., F.A. Mumpton., and B. Evans, (1966). Brucite in alpine serpentinites. Am. Mineral. Vol.51. pp 75-98.

Hutchinson, R.W., (1963) Discussion of the ore Knob massive sulfide copper deposit, North Carolina: an example of recrystallised ore: Econ. Geol. v.58. pp 997-998.

Irvine, T.N., (1965) Chromian spinel as a petrogenetic indicator Part 1. Theory. Canadian Journal of Earth Sciences Vol.2 pp 647-672.

(1966) Chromian spinel as a petrogenetic indicator. Part 2 Petrologic applications. Canadian Journal of Earth Sciences Vol.4. pp 71-103.

Jackson, E.D., (1963) Stratigraphic and lateral variation of chromite composition in the Stillwater complex (Montana). Min. Soc. America, Spec. paper 1, pp 46-54.

(1964) ~~Principles of the genesis and enrichment of chromite ore deposits.~~ Primary features of stratiform chromite deposits. In methods of prospection for chromite. Edited by R. Woodtli. proc. of an OECD seminar. Paris pp 111-134.

Kaaden, G. Van der., (1953) Gurleyik koyu (Mugla) kuzeyindeki bloke bolge icinde Kalan krom yataklarinin jeolojisi hakkinda rapor. M.T.A. unpublished report No.2039. (in Turkish and German).

and G. Muller., (1953) Chemische Zusammensetzung von chromiterzen aus der gegend von Gurleyik koy (S.V. Turkei) und vergleiche mit chromiten der Balkanhalbinsel. Turkiye jeoloji Kurumu bulteni cilt.4. sayi 2 pp 61-78 (in German with a Turkish summary).

and K. Metz., (1954) Datca-Mugla-Dalaman cay (Guneybati anadolu) arasindaki bolgenin jeolojisi. Turkiye jeoloji kurumu bulteni cilt 5. sayi 1-2 pp 71-170. (in German with a Turkish summary).

(1959) On relationship between composition of chromites and their tectonic-magmatic position in peridotite bodies in the S.W. of Turkey. M.T.A. Bull. Turkey No.52 pp 1-15.

(1960) On the geological-tectonic setting of the chromite province of Mugla (Turkey). Symposium on chrome ore, Cento Ankara-Turkey pp 109-121.

(1964) The different concepts of the genesis of alpine-type emplaced ultrabasic rocks and their implications on chromite prospection. Methods of prospection for chromite. Edited by R. Woodtli. proc. of an OECD seminar Paris, pp 175-202.

Ketin, I., (1966) Tectonic units of Anatolia (Asia Minor). M.T.A.Bull. Turkey No.66 pp 23-34.

Kovach, R.L., and D.L. Anderson., (1965) The interiors of the terrestrial planets. J. Geophysics. Res.70, 2873-2882.

Kuno, H., (1954) Study of orthopyroxenes from volcanic rocks. Am. Mineral. Vol.39, pp.30-46.

Macdonald, G.J.F., (1959) Chondrites and the chemical composition of the earth, in P.H. Abelson, ed. Researches in geochemistry. John Wiley and Sons, New York pp 476-494.

(1959b) Calculations on the thermal history of the earth. J. Geophys. Res. 64 pp 1967-2000.

Malhotra, P.D. and Prasado Rao, G.H.S.V., (1964) Investigations on the chemical composition of Indian chromites. Records of the Geol. Survey of India Vol.93 part 2, pp 215-248.

M.T.A. yayini (1966) Turkiye Krom yataklari. No. 132, 102 p.(in Turkish)

Nebert, K, (1959) Ultrabazic ve bazik sahre masiflerinin serpantinlesmesi ile ilgili musahedeler. M.T.A. mecmuasi. No.52 pp 46-48. (in Turkish and German).

O'Hara, M.J., (1967) Garnetiferous ultrabasic rocks of orogenic regions. In ultramafics and related rocks, edited by P.J. Wyllie, Wiley, New York 1967, pp 167-172.

(1967) Mineral paragenesis in ultramafic rocks. In ultramafics and related rocks, edited by P.J. Wyllie, Wiley, New York 1967, pp 393-403.

Page, N.J., (1967) Serpentinisation considered as a constant volume metasomatic process. A discussion. Am. Mineral. Vol.52, pp 545-549.

(1968) Chemical differences among the serpentine polymorphs. Am. Mineral. Vol.53, pp 201-215.

Pamir, H.N., (1964) Turkiye jeoloji haritasi, Denizli, olcek 1:500,000 M.T.A. Yayini.

Panagus, A., and Ottemann, J., (1966) Chemical differentiation of chromite grains in the nodular chromite from Rodiani (Greece). Mineralium Deposita 1 pp 72-75.

Petrascheck, W.E., (1958) Dogu Turkiye krom ihtiva eden ofiolitlerinin jeolojisi hakkinda. M.T.A. dergisi sayi 50 pp 1-15. (in Turkish and German).

(1959) Intrusiver und extrusiver peridotitmagmatismus in alpinotypen Bereich. Geol. Rundschau, Vol.48, pp 205-217.

Philippson, A., (1910-1915) Reisen U. Forschungen in Westl. Kleinoien, Pet. Mit. Erg. H., Gotha.

Phillips, F.C., (1963) The use of stereographic projection in Structural Geology. Edward Arnold (Publishers) Ltd.

Phillips, R.,(1963) The recalculation of amphibole analyses. Min. Mag. Vol.33, pp 701-711.

and P.M.D. Bradshaw., (1966) A test of the linearity of a photomultiplier used for reflectivity measurement. Min. Mag. Vol.35, pp 756-758.

and N.G. Ware., (1967) The spectral reflectivity of synthetic calcium monoferrite. Min. Mag. Vol.36 pp 422-424.

Poldervaart, A., and H.H. Hess., (1951) Pyroxenes in the crystallisation of basaltic magma. The Jour. of Geology Vol.59, pp 472-489.

Ringwood, A.E., (1959) On the chemical evolution and densities of the planets. Geochim. Cosmochim. Acta, Vol.15, pp 257-283.

I.D. MacGregor, and F.R. Boyd., (1964) Petrological composition of the upper mantle. Carnegie Inst. Wash. Yearbook, 63 pp 147-152.

(1966) Chemical evolution of the terrestrial planets. Geochim. Cosmochim. Acta, Vol.30 pp 41-104.

Rothstein, A.V.T., (1957) The Dawros peridotites, Connemara, Eire. Quart. Jour. Geol. Soc., Vol.113, pp 1-25.

(1961) A synorogenic peridotite at Dawros, Connemara. Acta Geologica (Budapest). Tomus 6, pp 221-232.

Sampson, E., (1929) May chromite crystallize late. Econ. Geol. Vol. 24 pp 632-641.

Schouten, C., (1962) Determination tables for ore microscopy. Elsevier publishing company. Amsterdam - New York.

Singewald, J.T. (1929) Discussion on chromite. Econ. Geol, Vol.24, pp 645-649.

Simulikowski, K., (1968) Theoretical and geological arguments for eclogite occurrences. 23rd Inter. Gong. Vol 1, pp 165-174.

Snetsinger, K.G., K.Keil, and T.E. Bunch., (1967) Chromites from equilibrated chondrites. Am. Mineral. Vol.52 pp 1322-1331.

Spangenberg, K., (1943) Die chromerzlagerstaette von Tampadel am Zobten, Ztschr. F. Pr. Geol. 1931.

Stoll, W.C., (1958) Geology and petrology of the Masinloc chromite deposit, Zambales, Luzon, Phillipine Islands. Bull. Geol. Soc. Am. Vol.69 pp 419-448.

Streckeisen, L.A., (1967) Classification and nomenclature of igneous rocks. N.Jb.Miner. Abh. 107, 2 und 3, S.144-240, Stuttgart.

Stueber, A.M., and G.G. Gales, (1967) Abundances of Na, Mn, Cr, Sc, and Co in ultramafic rocks. Geochim. Cosmochim. Acta. Vol.31, pp 75-93.

Tchihatcheff, P. de (1886-1889) Asie Mineure (Geologie et Paleontologie), Paris.

Tertsch, H., (1922) Studien am Westrande des Dunkelsteiner Granulitmassives. Min. Pet. Mitt, Band 35, pp 177-214.

Thayer, T.P., (1943) Chrome resources of Cuba. Geol. Surv. Bull. U.S.A. 935-A.

(1946) Preliminary chemical correlation of chromite with containing rocks. Econ. Geol. Vol.41 pp 202-217.

(1956) Mineralogy and Geology of chromium. Am. Chem. Soc. Monograph series. Edited by Marvin, J.Udy. Reinhold publ. Corp. pp 14-52.

(1960) Application of geology in chromite exploration and mining. Symposium on chrome ore, Cento Ankara-Turkey. pp 197-223.

(1960) Some critical differences between alpine type and stratiform peridotite-gabbro complex. Norden. Intern. Geol. Cong. Part 13 pp 247-259.

and C.E. Brown (1961) Is the Tinaquille, Venezuela, "Pseudogabbro" metamorphic or magmatic? Geol. Soc. Amer. Bull. Vol.72 pp 1565-1570.

(1963) Flow-layering in alpine peridotite-gabbro complexes. Min. Soc. Amer. special paper 1 pp 55-61.

(1963) The Canyon Mountain complex, Oregon and the alpine mafic magma stem. U.S. Geol. Survey spec. paper 475-C pp c82-c85.

(1964) Principal features and origin of podiform chromite deposits and some observations on the Guleman-Soridag, Turkey. Econ. Geol. Vol.59 pp 1497-1524.

(1966) Serpentinisation considered as a constant volume metasomatic process. Amer. Mineral. Vol.51 pp 685-710.

(1967) Serpentinisation considered as a constant volume metasomatic process. A reply. Amer. Mineral. Vol.52 pp 549-553.

(1967) Chemical and structural relations of ultramafic and feldspathic rocks in alpine intrusive complexes. In ultramific and related rocks. Edited by P.J. Wyllie. Wiley, New York, 1967, pp 222-239.

and G.R. Himmelberg., (1968) Rock succession in the alpine-type mafic complexes at Canyon Mountain, Oregon. 23rd Inter. Cong. Vol.1 pp 175-186.

Tokay, M., (1960) Investigations on chrome ore deposits made by the mineral research and exploration institute of Turkey. Symposium on chrome ore, Cento Ankara-Turkey pp 82-91.

Turekian, K.K. and K.H. Wedephhl., (1961) Distribution of the elements in some major units of the earth's crust. Bull. Geol. Soc. Am. Vol.72. pp 175-192.

Turner, F.J., (1942) Preferred orientation of olivine crystals in peridotites with special reference to New Zealand examples. Trans. Roy. Soc. N.Z. Vol.72, pp 280-300.

H.Heard., and D.T.Griggs (1960) Experimental determination of enstatite and accompanying inversion to clino enstatite. 21st Inter. Geol. Cong. Report, Copenhagen section 15, pp 339-408.

J. Verhoogen., (1960) Igneous and Metamorphic petrology. McGraw-Hill. Book Company, Inc.

Upton, B.G.J., (1967) Alkaline pyroxenites. In ultramafic and related rocks. Edited by P.J. Wyllie, Willey, New York, 1967, pp 281-288.

Urey, H.C., (1952) The planets, their origin and development. Yale University press.

Uytenbogaardt, W., (1951) Tables for microscopic identification of ore minerals. Princeton University press, New Jersey.

*

Vinagradov, A.P., (1962) Average contents of chemical elements in the principal types of igneous rocks of the earth's crust. Geochemistry, pp 641-664.

Vogt, J.H.L., (1923) The physical chemistry of the crystallization and magmatic differentiation of igneous rocks. Pt.8. J. Geol. 31 pp 407-419.

Wager, L.R. and G.M. Brown (1968) Layered Igneous rocks, Publishers Oliver and Boyd.

Wells, F.G. and F.W. Cater Jr. (1950) Geological investigations of chromite in California, Part 1 Klamath Mountains, chromite deposits of Siskiyou County, California. California Div. Mines Bull. 134.

*Van der Walt, C.J., (1942) Chrome ores of the western Bushveld Complex. Geol. Soc. South Africa Trans., Vol. 44, pp. 79-112.

Whittaker, E.J.W., (1953) The structure of chrysotile. Acta crystallogr. 6, pp 747-748.

and J. Zussman., (1956) The characterization of serpentine minerals by X-ray diffraction. Min. Mag. Vol.31 pp 108-126.

Wijkerslooth, P. de., (1942) Turk Krom cevherindeki istihaleler. M.T.A. dergisi sayi 2-27 pp 267-277 (in Turkish and German).

(1942) Turkiye ve Balkanlardaki Krom cevheri zuhurati ile bunlarin bu ulkelerin buyuk tektonigine olan munasebatleri. M.T.A. dergisi, sayi 1-26 pp 35-53 (in Turkish and German).

(1943) Anadolu Krom cevherleri uzerine mikroskopik tetkikler. M.T.A. dergisi sayi 2-30 pp 254-259 (in Turkish and German).

(1945) Bati Anadoludaki kromitlerin magnezik tesekkullerine esit hidrotermal degisiklikleri. M.T.A. dergisi, sayi 2-34 pp 354-358 (in Turkish and German).

(1946) Anadolu Krom cevherlerinin istihalesi ve bunlarin magmatik oluslorla ilgisi. M.T.A. yayini seri B, No. 10 (in Turkish and German).

(1954) Einiges uber die Entstehung von chromitkonzentration enu chromerzlagerst atten an hand von neuen beobachtungen in Anatolien. Neues Jb. Mineral. Abh. 9 pp 190-200.

Wilkinson, J.F.G., (1953) Some aspects of alpine type serpentinites of Queensland. Geol. Mag. Vol.90 pp 305-321.

Wyllie, P.J., (1967) Review. In ultramafics and related rocks. Willey, New York 1967, pp 403-416.

Yoder, H.S., and G.Th. Sahama., (1957) Olivine X-ray determinative curve. Amer. Min. Vol.42, pp 475-491.

and C.E. Tilley., (1962) Origin of basalt magmas: an experimental study of natural and synthetic rock systems. Jour. Pet. 3, pp 342-532.

Zwan, P.C., (1954) On the determination of pyroxenes by X-ray powder diagrams. Leidse Geol. Medelelingen, Vol.19 p 167.

APPENDIX

Appendix Table 1 Analyses of harzburgites (weight percent)

	F39	F200	F216	F217	F223	F226	F240	A24	A74	A90	Z1	Z12	Z22	Z89	Z93
SiO_2	40.62	37.86	39.99	38.96	40.42	39.67	43.40	40.82	40.07	39.22	40.52	39.23	39.17	40.88	39.28
Cr_2O_3	0.25	0.25	0.28	0.27	0.29	0.27	0.26	0.27	0.30	0.32	0.19	0.27	0.29	0.28	0.21
Al_2O_3	0.13	0.17	0.05	0.28	0.38	0.12	0.10	0.10	0.26	-	-	0.17	0.22	0.24	0.11
Fe_2O_3	6.13	2.21	4.58	4.15	4.82	5.69	6.52	4.52	5.56	7.90	6.65	6.63	7.00	5.79	6.99
FeO	1.91	2.32	3.42	3.31	2.97	2.02	2.07	3.05	1.98	0.37	0.45	0.59	0.50	2.01	0.44
MgO	38.91	40.65	41.10	40.92	40.88	40.22	42.79	40.51	39.09	38.73	37.21	37.29	35.82	38.58	37.10
CaO	0.44	0.49	0.50	0.52	0.71	0.44	0.39	0.45	0.40	0.08	0.03	0.07	0.06	0.38	0.07
MnO	0.13	0.13	0.15	0.12	0.14	0.13	0.15	0.14	0.13	0.14	0.10	0.11	0.13	0.13	0.13
NiO	0.38	0.37	0.36	0.37	0.36	0.39	0.42	0.38	0.36	0.42	0.54	0.36	0.38	0.37	0.40
Na_2O	0.05	0.05	0.05	0.09	0.07	0.05	0.14	0.05	0.20	0.12	0.10	0.05	0.11	0.05	0.05
K_2O	-	-	-	-	-	-	-	-	-	-	-	-	-	-	-
H_2O^+	9.63	10.57	7.98	9.57	7.51	9.85	2.24	8.58	9.65	11.03	12.12	13.59	13.72	10.08	13.59
H_2O^-	0.50	1.06	0.45	0.53	0.53	0.44	0.78	0.60	1.26	1.53	1.90	1.45	2.38	0.63	1.44
S	0.70	0.62	0.71	0.56	0.61	0.50	0.55	0.20	0.49	0.10	0.15	0.10	0.16	0.34	0.15

Appendix Table 2 Analyses of harzburgites and dunites (weight percent) on water free basis

No.	F11	F53	F56	F67	F113	F168	F172	F173	F178	F206	F213	F214	F215	F219
SiO_2	44.52	45.07	43.68	42.70	44.98	45.32	46.33	44.67	44.48	44.76	43.22	43.00	43.50	45.37
Cr_2O_3	0.28	0.29	0.37	0.32	0.32	0.37	0.28	0.46	0.31	0.29	0.30	0.33	0.30	0.28
Al_2O_3	0.51	0.21	0.24	0.44	0.27	0.51	0.02	0.07	0.18	0.15	0.05	0.11	0.17	0.33
Fe_2O_3*	8.60	9.08	8.80	8.15	8.76	8.32	8.93	8.93	8.45	8.71	8.79	8.84	8.74	8.55
MgO	44.36	43.77	45.29	46.88	44.05	43.51	42.73	44.48	44.90	44.51	45.54	45.57	45.32	44.15
CaO	0.81	0.37	0.38	0.65	0.65	0.88	0.33	0.41	0.45	0.36	0.40	0.46	0.62	0.36
MnO	0.14	0.15	0.15	0.13	0.14	0.15	0.15	0.15	0.14	0.15	0.13	0.13	0.15	0.13
NiO	0.42	0.44	0.42	0.43	0.41	0.38	0.45	0.43	0.44	0.43	0.50	0.42	0.41	0.42
Na_2O	0.10	0.07	0.20	0.18	0.08	0.11	0.08	0.06	0.10	0.06	0.11	0.06	0.06	0.14
K_2O	0.01	-	-	-	-	-	0.01	-	-	-	-	-	-	-
P_2O_5	-	-	-	-	-	-	-	-	-	-	-	-	-	-
S	0.24	0.56	0.47	0.11	0.33	0.43	0.69	0.34	0.54	0.57	0.95	1.08	0.72	0.27

No.	F231	F232	F234	F235	F249	A4	A24	A28	A39	A51	A68	A74	A84	A86
SiO_2	44.09	43.32	43.62	44.11	44.86	46.68	44.95	45.41	43.86	44.85	45.05	44.98	43.85	44.01
Cr_2O_3	0.30	0.27	0.26	0.31	0.30	0.29	0.30	0.34	0.26	0.30	0.34	0.34	0.31	0.28
Al_2O_3	0.57	-	0.28	0.24	0.33	0.18	0.11	0.21	0.16	0.21	0.62	0.29	0.30	0.12
Fe_2O_3*	8.48	9.19	8.87	8.97	8.43	8.91	8.67	8.70	8.86	9.02	8.44	8.69	8.74	8.87
MgO	44.53	45.58	45.11	44.51	43.86	42.71	44.61	43.86	44.54	43.86	44.13	43.88	44.96	44.91
CaO	0.78	0.27	0.70	0.68	0.72	0.24	0.50	0.60	0.53	0.52	0.48	0.45	0.54	0.58
MnO	0.14	0.15	0.15	0.15	0.15	0.15	0.15	0.15	0.15	0.15	0.14	0.15	0.15	0.15
NiO	0.41	0.43	0.40	0.41	0.35	0.43	0.42	0.40	0.41	0.42	0.41	0.41	0.41	0.42
Na_2O	0.10	0.12	0.06	0.06	0.13	0.06	0.06	0.11	0.14	0.10	0.06	0.23	0.21	0.06
K_2O	-	-	-	-	0.01	-	-	-	-	-	-	-	-	-
P_2O_5	-	-	-	-	-	0.17	-	-	0.04	0.03	0.03	0.03	0.01	0.02
S	0.58	0.67	0.54	0.55	0.85	0.18	0.22	0.22	1.05	0.53	0.29	0.55	0.51	0.56

*Total iron as Fe_2O_3

F11 through A86 harzburgites

F68 and F208 dunites

Appendix Table 2 continued

No.	A90	AU11	AU19	AU27	AU34	Z1	Z12	Z13	Z15	Z22	Z43	Z46	Z48	Z49
SiO_2	44.85	45.06	42.41	41.21	44.46	47.13	46.17	46.84	45.39	46.69	46.75	46.76	46.26	45.23
Cr_2O_3	0.37	0.29	0.26	0.32	0.32	0.22	0.32	0.28	0.31	0.35	0.32	0.32	0.33	0.27
Al_2O_3	-	0.17	0.02	-	0.25	-	0.20	0.32	0.15	0.26	0.15	0.15	0.16	0.41
Fe_2O_3*	9.51	8.70	8.91	7.83	8.65	8.30	8.57	8.42	8.85	9.00	9.02	9.16	9.16	8.80
MgO	44.29	44.20	46.31	49.37	45.03	43.28	43.89	43.19	43.97	42.70	42.13	42.56	42.52	43.57
CaO	0.09	0.45	0.33	0.11	0.57	0.03	0.09	0.10	0.36	0.07	0.60	0.17	0.45	0.72
MnO	0.16	0.15	0.14	0.12	0.15	0.12	0.13	0.13	0.15	0.15	0.15	0.15	0.16	0.15
NiO	0.48	0.42	0.46	0.50	0.41	0.63	0.42	0.44	0.42	0.45	0.42	0.47	0.42	0.41
Na_2O	0.14	0.07	0.68	0.22	0.06	0.12	0.06	0.06	0.11	0.13	0.06	0.06	0.15	0.08
K_2O	-	-	-	-	-	-	-	-	-	-	-	-	-	-
P_2O_5	-	0.03	-	-	-	-	0.03	0.02	0.04	0.02	0.03	0.03	0.04	0.03
S	0.12	0.45	0.47	0.33	0.10	0.18	0.12	0.20	0.26	0.19	0.37	0.17	0.35	0.34

No.	Z55	Z60	Z61	Z63	Z67	Z70A	Z89	Z93	Z104	ZU13	ZU34	ZU35	ZU46	F68	F208
SiO_2	47.86	46.59	45.42	46.35	44.85	41.70	45.79	46.23	46.17	43.11	44.01	45.35	46.05	41.11	40.35
Cr_2O_3	0.30	0.29	0.29	0.36	0.28	0.29	0.31	0.25	0.30	0.33	0.28	0.24	0.28	2.32	0.48
Al_2O_3	-	0.23	0.16	0.22	0.17	-	0.27	0.13	0.30	-	-	0.12	0.10	0.83	0.11
Fe_2O_3*	7.87	9.01	8.80	8.44	8.90	7.86	8.96	8.79	9.24	8.54	8.83	8.85	8.45	8.45	9.48
MgO	42.84	42.67	44.16	43.20	44.07	49.02	43.21	43.66	42.05	45.79	45.61	44.41	43.73	46.03	48.04
CaO	0.03	0.22	0.37	0.32	0.37	0.06	0.43	0.09	0.46	0.09	0.03	0.08	0.05	0.20	0.26
MnO	0.12	0.15	0.15	0.15	0.15	0.12	0.15	0.15	0.15	0.14	0.12	0.15	0.09	0.14	0.16
NiO	0.61	0.43	0.41	0.40	0.42	0.57	0.42	0.47	0.43	0.53	0.58	0.42	0.45	0.45	0.56
Na_2O	0.12	0.06	0.06	0.19	0.27	0.11	0.06	0.06	0.13	0.12	0.06	0.15	0.50	0.07	0.06
K_2O	-	-	-	-	-	-	-	-	-	-	-	-	-	-	-
P_2O_5	0.02	0.03	0.03	0.03	0.03	0.04	0.02	-	0.03	-	0.02	0.03	0.02	-	-
S	0.24	0.33	0.16	0.34	0.50	0.24	0.38	0.18	0.73	1.35	0.46	0.21	0.28	0.47	0.50

*Total iron as Fe_2O_3

A90 through ZU46 harzburgites

F68 and F208 dunites

Appendix Table 3 analyses of Orthopyroxenites (weight percent) on water free basis

	F20	A18	A55	A76	Z25	Z62	Z94
SiO_2	53.73	56.03	56.00	54.89	55.65	55.04	54.39
Cr_2O_3	0.39	0.55	0.35	0.48	0.46	0.59	0.51
Al_2O_3	0.95	0.61	0.63	0.88	0.78	0.87	0.47
Fe_2O_3*	8.07	6.69	6.88	7.27	6.54	7.04	7.78
MgO	34.32	34.36	34.63	33.98	34.71	34.00	35.04
CaO	1.73	1.26	1.11	1.79	1.40	1.75	1.17
MnO	0.19	0.16	0.16	0.18	0.15	0.16	0.18
NiO	0.15	0.13	0.13	0.13	0.12	0.12	0.12
Na_2O	0.14	0.07	0.08	0.11	0.06	0.22	0.12
K_2O	0.01	0.01	-	0.01	-	0.01	-
P_2O_5	-	-	-	0.01	-	0.02	0.02
S	0.32	0.12	0.01	0.27	0.13	0.18	0.19

*Total Fe as Fe_2O_3

A55 analysis after chromite has been separated from the sample

Appendix Table 4 Analyses of basic rocks (weight percent) on water free basis

No	F7	F23	F34A	F35	F205	F209	F221	F238	F247	F253	Z19	Z99
SiO_2	49.58	52.17	50.79	49.71	51.12	51.78	51.05	51.81	50.35	49.56	51.97	52.94
TiO_2	1.29	1.37	1.17	1.23	1.12	0.95	1.45	1.50	1.26	1.24	1.29	1.00
Al_2O_3	16.50	15.58	15.29	15.64	15.46	14.88	14.89	15.52	14.84	12.45	15.23	15.18
Fe_2O_3*	11.39	11.55	10.68	10.79	10.52	10.25	11.31	11.42	11.50	10.58	10.96	10.45
Cr_2O_3	0.01	-	0.02	-	0.02	0.02	0.01	0.01	0.01	0.01	-	-
MgO	7.04	5.28	7.65	7.33	6.55	8.18	5.70	5.28	6.29	7.17	6.53	6.42
CaO	9.16	9.39	10.04	9.78	10.24	10.10	11.24	9.31	10.51	15.74	9.29	10.65
MnO	0.20	0.21	0.20	0.20	0.19	0.18	0.21	0.21	0.21	0.22	0.20	0.19
NiO	-	-	-	-	-	-	-	-	-	-	-	-
Na_2O	3.84	3.34	3.41	4.58	3.92	3.00	3.34	4.30	4.29	2.62	3.56	2.57
K_2O	0.38	0.56	0.26	0.29	0.39	0.29	0.37	0.28	0.33	0.06	0.52	0.17
P_2O_5	0.18	0.18	0.17	0.15	0.14	0.16	0.21	0.17	0.21	0.19	0.14	0.13
S	0.43	0.35	0.33	0.28	0.34	0.21	0.21	0.18	0.19	0.14	0.30	0.26

*Total iron as Fe_2O_3

Appendix Table 5 Reflectivity readings (mV) of six chromite grains and standards at various wave-lengths as recorded on the digital voltmeter

	BACKGROUND											BLACK GLASS										
No.	440mμ	460mμ	480mμ	520mμ	540mμ	560mμ	580mμ	600mμ	620mμ	640mμ	660mμ	440mμ	460mμ	480mμ	520mμ	540mμ	560mμ	580mμ	600mμ	620mμ	640mμ	660mμ
F68	0.013	0.028	0.048	0.067	0.060	0.045	0.029	0.015	0.005	0.000	-0.003	0.062	0.126	0.213	0.318	0.293	0.239	0.168	0.100	0.051	0.022	0.008
F62	0.009	0.023	0.039	0.055	0.049	0.036	0.023	0.011	0.003	-0.001	-0.004	0.053	0.111	0.189	0.286	0.263	0.215	0.151	0.090	0.044	0.019	0.006
F119	0.008	0.021	0.036	0.050	0.044	0.033	0.021	0.010	0.003	-0.001	-0.003	0.051	0.106	0.180	0.273	0.251	0.204	0.144	0.084	0.042	0.018	0.006
A1	0.008	0.021	0.036	0.052	0.045	0.034	0.021	0.011	0.003	-0.001	-0.004	0.050	0.105	0.179	0.270	0.249	0.203	0.143	0.084	0.042	0.018	0.006
ZU8	0.008	0.021	0.037	0.052	0.045	0.034	0.021	0.010	0.003	-0.002	-0.004	0.050	0.103	0.176	0.268	0.246	0.201	0.141	0.083	0.041	0.018	0.005
F65A	0.008	0.019	0.034	0.048	0.042	0.032	0.021	0.011	0.003	-0.001	-0.003	0.041	0.086	0.148	0.228	0.212	0.173	0.123	0.072	0.036	0.016	0.005
F31A	0.035	0.068	0.110	0.146	0.128	0.101	0.068	0.037	0.017	0.006	0.000	0.113	0.217	0.362	0.522	0.473	0.386	0.272	0.159	0.082	0.037	0.015
A17	0.001	0.007	0.016	0.025	0.022	0.016	0.009	0.003	-0.001	-0.004	-0.006	0.029	0.064	0.112	0.175	0.162	0.133	0.093	0.055	0.026	0.010	0.001
AU12	0.002	0.008	0.017	0.026	0.023	0.017	0.010	0.004	-0.001	-0.003	-0.004	0.029	0.063	0.111	0.172	0.160	0.131	0.092	0.054	0.026	0.010	0.003
ZU9	0.001	0.008	0.016	0.023	0.017	0.017	0.009	0.003	-0.001	-0.004	-0.006	0.028	0.061	0.108	0.168	0.156	0.128	0.090	0.052	0.024	0.009	0.002
F19	0.002	0.008	0.017	0.026	0.023	0.017	0.010	0.004	-0.001	-0.004	-0.005	0.028	0.062	0.109	0.170	0.158	0.130	0.091	0.053	0.026	0.010	0.001
A10	0.001	0.007	0.014	0.023	0.020	0.015	0.008	0.004	-0.001	-0.003	-0.005	0.028	0.061	0.107	0.165	0.154	0.126	0.088	0.052	0.025	0.010	0.002
F70A	0.000	0.006	0.013	0.021	0.019	00.14	0.008	0.003	-0.001	-0.003	-0.004	0.027	0.060	0.104	0.162	0.151	0.124	0.087	0.051	0.025	0.010	0.002
AU32	0.000	0.005	0.011	0.018	0.016	0.012	0.007	0.002	-0.002	-0.004	-0.005	0.026	0.058	0.101	0.157	0.147	0.120	0.084	0.049	0.024	0.009	0.002
ZU30E	0.035	0.067	0.109	0.145	0.127	0.100	0.067	0.037	0.016	0.005	-0.001	0.113	0.220	0.366	0.528	0.478	0.389	0.274	0.161	0.083	0.037	0.015
A78	0.036	0.068	0.111	0.149	0.129	0.102	0.069	0.037	0.017	0.006	-0.001	0.113	0.219	0.363	0.526	0.476	0.388	0.272	0.160	0.082	0.037	0.014
ZU44	0.036	0.068	0.111	0.149	0.129	0.102	0.069	0.037	0.017	0.006	-0.001	0.112	0.218	0.362	0.524	0.474	0.386	0.273	0.159	0.082	0.037	0.014
ZU12	0.036	0.069	0.111	0.148	0.129	0.102	0.068	0.038	0.017	0.006	0.000	0.114	0.220	0.365	0.527	0.476	0.388	0.273	0.160	0.082	0.037	0.015
F128	0.033	0.063	0.102	0.136	0.118	0.094	0.063	0.035	0.016	0.005	-0.001	0.109	0.210	0.349	0.505	0.458	0.374	0.263	0.154	0.080	0.036	0.014

Appendix Table 5 continued

	CARBORANDUM											SILICON										
No.	440mμ	460mμ	480mμ	520mμ	540mμ	560mμ	580mμ	600mμ	620mμ	640mμ	660mμ	440mμ	460mμ	480mμ	520mμ	540mμ	560mμ	580mμ	600mμ	620mμ	640mμ	660mμ
F68	0.246	0.487	0.825	1.252	1.156	0.953	0.680	0.406	0.215	0.103	0.045	0.484	0.935	1.544	2.253	2.058	1.678	1.190	0.708	0.373	0.179	0.080
F62	0.216	0.433	0.735	1.124	1.039	0.858	0.613	0.368	0.193	0.092	0.040	0.437	0.840	1.394	2.051	1.870	1.526	1.080	0.646	0.339	0.162	0.072
F119	0.204	0.409	0.695	1.065	0.986	0.813	0.583	0.349	0.184	0.087	0.038	0.416	0.805	1.333	1.968	1.796	1.463	1.040	0.619	0.325	0.156	0.070
A1	0.202	0.407	0.691	1.057	0.979	0.810	0.578	0.346	0.182	0.086	0.038	0.401	0.777	1.289	1.904	1.740	1.421	1.008	0.601	0.316	0.151	0.067
ZU8	0.200	0.401	0.683	1.044	0.967	0.799	0.571	0.342	0.178	0.084	0.036	0.395	0.763	1.266	1.882	1.724	1.409	1.003	0.596	0.313	0.149	0.067
F65A	0.165	0.331	0.567	0.884	0.822	0.682	0.491	0.294	0.155	0.074	0.033	0.327	0.635	1.063	1.603	1.472	1.209	0.864	0.514	0.272	0.130	0.058
F31A	0.400	0.775	1.300	1.913	1.746	1.433	1.016	0.602	0.318	0.153	0.068	0.776	1.461	2.385	3.403	3.053	2.480	1.745	1.027	0.544	0.260	0.117
A17	0.131	0.268	0.463	0.715	0.669	0.554	0.396	0.237	0.124	0.059	0.025	0.271	0.533	0.893	1.326	1.223	1.001	0.710	0.423	0.222	0.106	0.046
AU12	0.128	0.262	0.449	0.693	0.648	0.537	0.384	0.231	0.121	0.058	0.025	0.262	0.516	0.865	1.277	1.180	0.967	0.685	0.410	0.216	0.103	0.046
ZU9	0.126	0.258	0.441	0.683	0.639	0.531	0.379	0.227	0.119	0.056	0.023	0.255	0.506	0.847	1.251	1.160	0.950	0.673	0.402	0.210	0.101	0.044
F19	0.126	0.257	0.442	0.681	0.637	0.527	0.378	0.227	0.120	0.056	0.023	0.260	0.511	0.857	1.269	1.170	0.960	0.681	0.406	0.214	0.102	0.045
A10	0.126	0.259	0.442	0.680	0.635	0.526	0.376	0.225	0.118	0.056	0.024	0.260	0.511	0.853	1.259	1.160	0.948	0.672	0.402	0.211	0.101	0.045
F70A	0.124	0.256	0.438	0.671	0.628	0.518	0.371	0.222	0.117	0.056	0.024	0.258	0.505	0 846	1.246	1.146	0.938	0.663	0.396	0.208	0.100	0.044
AU32	0.122	0.250	0.430	0.657	0.615	0.509	0.363	0.218	0.113	0.053	0.022	0.252	0.500	0.830	1.222	1.125	0.920	0.651	0.388	0.203	0.098	0.043
ZU30E	0.406	0.784	1.314	1.938	1.767	1.452	1.030	0.610	0.323	0.154	0.069	0.779	1.464	2.396	3.414	3.077	2.500	1.760	1.039	0.549	0.262	0.119
A78	0.403	0.781	1.308	1.930	1.761	1.445	1.025	0.609	0.323	0.154	0.069	0.786	1.479	2.420	3.445	3.098	2.516	1.772	1.042	0.550	0.263	0.120
ZU44	0.404	0.780	1.307	1.925	1.756	1.443	1.024	0.606	0.321	0.154	0.069	0.788	1.477	2.416	3.438	3.095	2.509	1.767	1.040	0.551	0.263	0.120
ZU12	0.404	0.783	1.308	1.926	1.756	1.441	1.023	0.605	0.321	0.153	0.069	0.787	1.480	2.419	3.441	3.092	2.509	1.766	1.039	0.548	0.263	0.119
F128	0.388	0.750	1.257	1.860	1.696	1.394	0.991	0.587	0.313	0.149	0.067	0.765	1.437	2.335	3.350	2.998	2.434	1.712	1.008	0.535	0.255	0.116

Appendix Table 5 continued

	CHROMITE GRAIN 1											CHROMITE GRAIN 2										
No.	440mμ	460mμ	480mμ	520mμ	540mμ	560mμ	580mμ	600mμ	620mμ	640mμ	660mμ	440mμ	460mμ	480mμ	520mμ	540mμ	560mμ	580mμ	600mμ	620mμ	640mμ	660mμ
F68	0.134	0.269	0.455	0.684	0.629	0.516	0.366	0.217	0.113	0.053	0.022	0.134	0.267	0.451	0.681	0.626	0.513	0.365	0.217	0.113	0.053	0.022
F62	0.130	0.262	0.443	0.670	0.617	0.505	0.359	0.213	0.111	0.052	0.021	0.130	0.260	0.440	0.670	0.616	0.505	0.358	0.214	0.111	0.051	0.021
F119	0.134	0.270	0.457	0.696	0.641	0.524	0.373	0.222	0.116	0.053	0.022	0.133	0.267	0.454	0.687	0.634	0.520	0.369	0.220	0.115	0.053	0.022
A1	0.128	0.257	0.438	0.665	0.612	0.502	0.357	0.213	0.110	0.051	0.021	0.128	0.257	0.438	0.665	0.613	0.502	0.357	0.213	0.110	0.051	0.021
ZU8	0.124	0.250	0.424	0.649	0.598	0.493	0.350	0.208	0.108	0.050	0.020	0.123	0.248	0.422	0.643	0.593	0.487	0.347	0.207	0.107	0.050	0.020
F65A	0.092	0.186	0.320	0.493	0.456	0.377	0.270	0.162	0.083	0.039	0.016	0.090	0.183	0.315	0.487	0.451	0.373	0.267	0.159	0.082	0.038	0.016
F31A	0.261	0.504	0.837	1.218	1.106	0.902	0.638	0.376	0.197	0.093	0.040	0.262	0.503	0.837	1.221	1.108	0.904	0.639	0.376	0.198	0.093	0.040
A17	0.083	0.171	0.295	0.453	0.422	0.348	0.247	0.147	0.076	0.035	0.013	0.083	0.171	0.295	0.454	0.422	0.349	0.248	0.147	0.076	0.035	0.013
AU12	0.078	0.161	0.277	0.424	0.396	0.326	0.232	0.158	0.072	0.033	0.013	0.078	0.162	0.279	0.429	0.400	0.330	0.235	0.140	0.072	0.034	0.013
ZU9	0.079	0.166	0.286	0.439	0.413	0.340	0.242	0.144	0.074	0.033	0.012	0.079	0.165	0.285	0.437	0.408	0.337	0.239	0.143	0.073	0.033	0.012
F19	0.075	0.154	0.266	0.408	0.380	0.313	0.222	0.132	0.068	0.031	0.012	0.076	0.157	0.270	0.415	0.386	0.318	0.227	0.135	0.070	0.031	0.012
A10	0.080	0.166	0.286	0.437	0.406	0.334	0.237	0.141	0.073	0.034	0.013	0.080	0.165	0.284	0.436	0.405	0.333	0.236	0.141	0.073	0.033	0.013
F70A	0.076	0.158	0.272	0.416	0.387	0.318	0.225	0.134	0.069	0.032	0.012	0.076	0.158	0.271	0.416	0.385	0.317	0.226	0.134	0.069	0.032	0.012
AU32	0.076	0.158	0.271	0.415	0.386	0.318	0.225	0.134	0.068	0.031	0.012	0.077	0.159	0.275	0.419	0.390	0.320	0.226	0.134	0.069	0.031	0.012
ZU30E	0.265	0.510	0.847	1.238	1.124	0.918	0.648	0.383	0.201	0.095	0.041	0.263	0.509	0.847	1.235	1.121	0.915	0.647	0.381	0.201	0.095	0.041
A78	0.261	0.503	0.839	1.224	1.110	0.907	0.641	0.378	0.199	0.094	0.040	0.264	0.509	0.848	1.239	1.125	0.919	0.649	0.382	0.201	0.095	0.041
ZU44	0.257	0.495	0.825	1.204	1.093	0.892	0.631	0.372	0.196	0.092	0.040	0.256	0.494	0.819	1.198	1.086	0.887	0.627	0.371	0.194	0.091	0.040
ZU12	0.264	0.508	0.844	1.234	1.116	0.913	0.646	0.381	0.201	0.094	0.041	0.263	0.506	0.844	1.233	1.118	0.914	0.646	0.381	0.201	0.094	0.041
F128	0.250	0.484	0.807	1.181	1.073	0.876	0.619	0.364	0.193	0.091	0.040	0.254	0.489	0.817	1.198	1.085	0.887	0.623	0.369	0.194	0.091	0.040

Appendix Table 5 continued

	CHROMITE GRAIN 3											CHROMITE GRAIN 4										
No.	440mμ	460mμ	480mμ	520mμ	540mμ	560mμ	580mμ	600mμ	620mμ	640mμ	660mμ	440mμ	460mμ	480mμ	520mμ	540mμ	560mμ	580mμ	600mμ	620mμ	640mμ	660mμ
F68	0.133	0.264	0.450	0.679	0.625	0.512	0.364	0.217	0.112	0.053	0.022	0.134	0.267	0.454	0.684	0.629	0.515	0.366	0.218	0.114	0.053	0.022
F62	0.128	0.259	0.439	0.666	0.613	0.502	0.357	0.213	0.110	0.051	0.021	0.128	0.257	0.436	0.659	0.607	0.498	0.353	0.210	0.109	0.051	0.020
F119	0.131	0.263	0.445	0.677	0.625	0.512	0.365	0.217	0.113	0.052	0.022	0.131	0.263	0.448	0.677	0.624	0.511	0.364	0.217	0.113	0.053	0.022
A1	0.128	0.258	0.436	0.663	0.610	0.501	0.357	0.212	0.110	0.051	0.021	0.127	0.256	0.433	0.660	0.608	0.499	0.355	0.211	0.110	0.051	0.021
ZU8	0.123	0.248	0.421	0.643	0.591	0.486	0.347	0.206	0.107	0.050	0.020	0.123	0.247	0.420	0.641	0.591	0.485	0.346	0.206	0.106	0.049	0.020
F65A	0.090	0.183	0.315	0.487	0.451	0.372	0.267	0.159	0.083	0.038	0.016	0.088	0.178	0.306	0.483	0.437	0.360	0.257	0.153	0.079	0.036	0.014
F31A	0.261	0.503	0.836	1.219	1.104	0.901	0.637	0.375	0.197	0.093	0.040	0.261	0.501	0.836	1.218	1.105	0.903	0.637	0.376	0.198	0.093	0.040
A17	0.083	0.172	0.296	0.453	0.423	0.348	0.247	0.147	0.076	0.035	0.013	0.083	0.172	0.295	0.453	0.422	0.348	0.247	0.147	0.076	0.035	0.013
AU12	0.079	0.163	0.280	0.430	0.401	0.330	0.234	0.139	0.072	0.033	0.013	0.078	0.161	0.278	0.426	0.397	0.327	0.233	0.139	0.072	0.032	0.012
ZU9	0.078	0.162	0.279	0.428	0.398	0.328	0.233	0.138	0.071	0.032	0.012	0.078	0.161	0.279	0.427	0.399	0.329	0.234	0.139	0.072	0.032	0.012
F19	0.074	0.154	0.266	0.407	0.379	0.312	0.222	0.132	0.069	0.031	0.012	0.076	0.158	0.271	0.416	0.387	0.318	0.227	0.135	0.070	0.031	0.012
A10	0.080	0.166	0.285	0.437	0.407	0.335	0.238	0.142	0.073	0.034	0.013	0.079	0.163	0.282	0.433	0.401	0.330	0.234	0.139	0.071	0.033	0.013
F70A	0.076	0.157	0.271	0.414	0.384	0.316	0.224	0.134	0.069	0.032	0.012	0.076	0.157	0.270	0.414	0.384	0.316	0.224	0.134	0.069	0.032	0.012
AU32	0.076	0.158	0.272	0.416	0.386	0.317	0.224	0.134	0.068	0.031	0.011	0.077	0.159	0.274	0.417	0.388	0.318	0.226	0.135	0.069	0.032	0.012
ZU30E	0.264	0.511	0.848	1.237	1.121	0.915	0.646	0.381	0.201	0.095	0.041	0.264	0.507	0.845	1.237	1.117	0.911	0.644	0.380	0.200	0.094	0.041
A78	0.262	0.508	0.848	1.237	1.123	0.917	0.649	0.382	0.200	0.095	0.041	0.260	0.502	0.838	1.224	1.113	0.910	0.644	0.380	0.200	0.094	0.041
ZU44	0.254	0.490	0.814	1.192	1.078	0.880	0.623	0.367	0.193	0.091	0.040	0.255	0.491	0.819	1.193	1.082	0.885	0.624	0.368	0.193	0.091	0.040
ZU12	0.263	0.506	0.843	1.230	1.116	0.912	0.644	0.380	0.200	0.094	0.041	0.263	0.507	0.844	1.233	1.119	0.914	0.645	0.381	0.201	0.094	0.041
F128	0.249	0.482	0.804	1.175	1.066	0.871	0.615	0.363	0.191	0.090	0.039	0.250	0.481	0.805	1.176	1.067	0.872	0.616	0.363	0.192	0.090	0.039

Appendix Table 5 continued

	CHROMITE GRAIN 5											CHROMITE GRAIN 6										
No.	440mμ	460mμ	480mμ	520mμ	540mμ	560mμ	580mμ	600mμ	620mμ	640mμ	660mμ	440mμ	460mμ	480mμ	520mμ	540mμ	560mμ	580mμ	600mμ	620mμ	640mμ	660mμ
F68	0.133	0.265	0.446	0.676	0.621	0.510	0.362	0.216	0.113	0.052	0.021	0.134	0.266	0.448	0.678	0.624	0.511	0.364	0.217	0.112	0.053	0.022
F62	0.127	0.256	0.433	0.657	0.605	0.496	0.352	0.210	0.109	0.050	0.020	0.128	0.257	0.436	0.661	0.608	0.499	0.355	0.211	0.109	0.050	0.020
F119	0.131	0.264	0.446	0.677	0.624	0.512	0.364	0.217	0.113	0.052	0.021	0.130	0.261	0.443	0.673	0.620	0.508	0.362	0.215	0.112	0.052	0.021
A1	0.127	0.256	0.439	0.660	0.613	0.504	0.358	0.214	0.111	0.051	0.021	0.130	0.260	0.443	0.671	0.618	0.507	0.360	0.215	0.112	0.052	0.021
ZU8	0.123	0.248	0.423	0.643	0.594	0.488	0.348	0.207	0.107	0.050	0.020	0.122	0.246	0.419	0.637	0.589	0.484	0.345	0.206	0.106	0.050	0.020
F65A	0.087	0.177	0.304	0.469	0.435	0.358	0.256	0.153	0.080	0.037	0.015	0.087	0.176	0.302	0.467	0.433	0.356	0.256	0.152	0.079	0.036	0.014
F31A	0.260	0.502	0.837	1.219	1.105	0.903	0.638	0.375	0.198	0.093	0.040	0.261	0.502	0.838	1.221	1.108	0.905	0.639	0.378	0.198	0.093	0.041
A17	0.082	0.171	0.295	0.452	0.422	0.348	0.247	0.147	0.076	0.035	0.013	0.082	0.172	0.295	0.452	0.422	0.348	0.247	0.147	0.076	0.034	0.013
AU12	0.078	0.161	0.277	0.424	0.396	0.326	0.232	0.137	0.071	0.032	0.012	0.078	0.161	0.278	0.425	0.396	0.326	0.232	0.138	0.071	0.032	0.013
ZU9	0.077	0.162	0.279	0.429	0.400	0.330	0.235	0.140	0.072	0.032	0.012	0.078	0.164	0.283	0.432	0.402	0.331	0.236	0.140	0.072	0.032	0.012
F19	0.075	0.154	0.266	0.407	0.378	0.311	0.221	0.132	0.068	0.031	0.012	0.075	0.156	0.268	0.411	0.382	0.314	0.223	0.133	0.068	0.032	0.012
A10	0.079	0.163	0.281	0.429	0.399	0.328	0.233	0.138	0.071	0.032	0.012	0.078	0.162	0.280	0.428	0.398	0.330	0.233	0.139	0.071	0.032	0.012
F70A	0.077	0.159	0.273	0.417	0.388	0.319	0.227	0.135	0.070	0.032	0.012	0.077	0.159	0.272	0.416	0.387	0.317	0.225	0.135	0.070	0.032	0.012
AU32	0.076	0.158	0.271	0.413	0.383	0.314	0.223	0.133	0.068	0.031	0.012	0.076	0.158	0.272	0.414	0.385	0.316	0.224	0.134	0.068	0.031	0.011
ZU30E	0.262	0.504	0.841	1.230	1.115	0.912	0.645	0.380	0.200	0.094	0.041	0.262	0.507	0.841	1.229	1.116	0.914	0.645	0.380	0.200	0.094	0.041
A78	0.260	0.504	0.839	1.225	1.112	0.909	0.643	0.379	0.199	0.093	0.041	0.262	0.506	0.843	1.233	1.118	0.914	0.645	0.380	0.201	0.094	0.041
ZU44	0.254	0.487	0.811	1.184	1.075	0.878	0.622	0.365	0.193	0.091	0.039	0.254	0.490	0.817	1.193	1.082	0.884	0.625	0.369	0.195	0.092	0.040
ZU12	0.261	0.506	0.844	1.230	1.115	0.912	0.644	0.381	0.200	0.094	0.041	0.262	0.504	0.841	1.229	1.116	0.912	0.646	0.381	0.200	0.095	0.041
F128	0.248	0.478	0.800	1.164	1.058	0.866	0.613	0.360	0.189	0.089	0.039	0.247	0.479	0.801	1.168	1.060	0.866	0.612	0.361	0.189	0.089	0.039

Appendix Table 5 continued

	BACKGROUND											BLACK GLASS									
No.	440mμ	460mμ	480mμ	520mμ	540mμ	560mμ	580mμ	600mμ	620mμ	640mμ	660mμ	440mμ	460mμ	480mμ	520mμ	540mμ	560mμ	580mμ	600mμ	620mμ	640mμ	660mμ
F68	0.013	0.029	0.049	0.068	0.060	0.046	0.029	0.016	0.006	0.000	-0.004	0.061	0.125	0.212	0.319	0.294	0.239	0.169	0.100	0.051	0.022	0.007
F62	0.008	0.022	0.038	0.054	0.047	0.036	0.022	0.011	0.003	-0.001	-0.004	0.052	0.108	0.186	0.282	0.260	0.212	0.149	0.088	0.044	0.019	0.006
F119	0.008	0.021	0.035	0.050	0.044	0.033	0.020	0.010	0.003	-0.002	-0.004	0.049	0.103	0.176	0.267	0.246	0.201	0.141	0.083	0.042	0.018	0.006
A1	0.008	0.021	0.037	0.052	0.046	0.034	0.021	0.011	0.003	-0.001	-0.004	0.050	0.104	0.178	0.268	0.247	0.202	0.142	0.084	0.042	0.018	0.006
ZU8	0.008	0.020	0.036	0.051	0.045	0.034	0.021	0.010	0.002	-0.001	-0.004	0.049	0.101	0.173	0.263	0.243	0.198	0.140	0.082	0.042	0.018	0.005
F65A	0.007	0.018	0.031	0.045	0.039	0.030	0.019	0.010	0.003	-0.002	-0.003	0.039	0.081	0.140	0.215	0.200	0.163	0.115	0.068	0.034	0.014	0.004
F31A	0.034	0.066	0.106	0.143	0.125	0.098	0.066	0.036	0.016	0.005	-0.001	0.110	0.214	0.356	0.515	0.466	0.380	0.267	0.156	0.081	0.036	0.014
A17	0.001	0.007	0.015	0.023	0.020	0.015	0.008	0.003	-0.002	-0.004	-0.006	0.029	0.062	0.111	0.172	0.161	0.132	0.093	0.054	0.026	0.010	0.001
AU12	0.001	0.007	0.015	0.024	0.021	0.016	0.009	0.004	-0.001	-0.003	-0.005	0.028	0.061	0.107	0.167	0.156	0.128	0.090	0.052	0.026	0.010	0.002
ZU9	0.001	0.008	0.017	0.026	0.023	0.017	0.010	0.004	-0.001	-0.004	-0.005	0.028	0.061	0.109	0.170	0.158	0.129	0.091	0.053	0.025	0.010	0.001
F19	0.001	0.008	0.017	0.026	0.023	0.018	0.011	0.004	0.000	-0.003	-0.005	0.029	0.063	0.111	0.171	0.159	0.130	0.092	0.054	0.027	0.010	0.002
A10	0.000	0.006	0.012	0.020	0.018	0.013	0.007	0.003	-0.002	-0.004	-0.005	0.026	0.059	0.103	0.160	0.150	0.122	0.086	0.050	0.025	0.009	0.001
F70A	0.000	0.005	0.012	0.019	0.018	0.012	0.007	0.002	-0.002	-0.003	-0.005	0.026	0.058	0.102	0.159	0.148	0.120	0.085	0.049	0.024	0.010	0.001
AU32	-0.001	0.004	0.011	0.017	0.016	0.012	0.006	0.001	-0.002	-0.004	-0.005	0.025	0.057	0.101	0.156	0.145	0.118	0.083	0.048	0.023	0.009	0.001
ZU30E	0.035	0.067	0.108	0.145	0.126	0.100	0.067	0.037	0.016	0.005	-0.001	0.111	0.215	0.359	0.519	0.469	0.383	0.269	0.158	0.081	0.037	0.014
A78	0.035	0.067	0.108	0.145	0.126	0.100	0.067	0.037	0.016	0.005	-0.001	0.111	0.216	0.360	0.521	0.472	0.385	0.271	0.158	0.081	0.036	0.013
ZU44	0.035	0.067	0.109	0.146	0.127	0.101	0.067	0.037	0.016	0.005	-0.001	0.111	0.215	0.358	0.518	0.468	0.382	0.269	0.157	0.081	0.037	0.014
ZU12	0.033	0.065	0.106	0.141	0.123	0.097	0.065	0.036	0.016	0.005	-0.001	0.110	0.214	0.356	0.514	0.466	0.381	0.268	0.156	0.081	0.037	0.014
F128	0.031	0.060	0.098	0.132	0.115	0.091	0.061	0.032	0.014	0.004	-0.001	0.106	0.205	0.343	0.497	0.451	0.367	0.259	0.151	0.079	0.036	0.013

Appendix Table 5 continued

	CARBORANDUM											SILICON									
No.	440mμ	460mμ	480mμ	520mμ	540mμ	560mμ	580mμ	600mμ	620mμ	640mμ	660mμ	440mμ	460mμ	480mμ	520mμ	540mμ	560mμ	580mμ	600mμ	620mμ	640mμ	660mμ
F68	0.240	0.476	0.807	1.231	1.138	0.939	0.670	0.402	0.212	0.101	0.044	0.477	0.918	1.513	2.223	2.028	1.657	1.171	0.698	0.369	0.176	0.079
F62	0.213	0.425	0.722	1.108	1.026	0.847	0.606	0.363	0.191	0.091	0.040	0.429	0.833	1.379	2.033	1.857	1.515	1.077	0.640	0.336	0.161	0.071
F119	0.201	0.403	0.687	1.052	0.974	0.803	0.577	0.346	0.182	0.087	0.037	0.404	0.783	1.299	1.920	1.754	1.434	1.019	0.606	0.318	0.152	0.068
A1	0.199	0.398	0.680	1.041	0.963	0.795	0.569	0.341	0.180	0.085	0.038	0.400	0.776	1.286	1.904	1.739	1.419	1.009	0.600	0.314	0.151	0.068
ZU8	0.195	0.391	0.666	1.028	0.951	0.787	0.566	0.338	0.177	0.084	0.037	0.391	0.756	1.256	1.869	1.709	1.398	0.995	0.593	0.310	0.148	0.066
F65A	0.155	0.313	0.538	0.836	0.778	0.645	0.463	0.278	0.147	0.070	0.030	0.311	0.607	1.016	1.523	1.398	1.146	0.817	0.488	0.257	0.123	0.055
F31A	0.395	0.768	1.280	1.888	1.723	1.416	1.005	0.595	0.318	0.151	0.068	0.770	1.443	2.363	3.370	3.038	2.466	1.736	1.020	0.540	0.258	0.117
A17	0.132	0.269	0.464	0.715	0.671	0.557	0.399	0.239	0.125	0.059	0.024	0.268	0.529	0.884	1.313	1.212	0.994	0.706	0.421	0.221	0.106	0.046
AU12	0.125	0.257	0.441	0.681	0.637	0.529	0.378	0.227	0.119	0.057	0.024	0.258	0.508	0.850	1.261	1.166	0.955	0.677	0.405	0.213	0.102	0.046
ZU9	0.126	0.260	0.446	0.688	0.643	0.533	0.381	0.229	0.120	0.056	0.023	0.257	0.507	0.847	1.258	1.160	0.951	0.676	0.404	0.214	0.102	0.045
F19	0.127	0.258	0.445	0.686	0.642	0.533	0.382	0.229	0.120	0.057	0.024	0.260	0.514	0.860	1.273	1.176	0.964	0.684	0.409	0.215	1.104	0.045
A10	0.124	0.252	0.434	0.668	0.625	0.519	0.370	0.222	0.116	0.055	0.023	0.255	0.503	0.840	1.242	1.143	0.936	0.663	0.395	0.208	0.100	0.044
F70A	0.123	0.251	0.431	0.660	0.617	0.511	0.364	0.219	0.114	0.054	0.022	0.252	0.498	0.830	1.223	1.124	0.920	0.651	0.390	0.205	0.098	0.043
AU32	0.122	0.250	0.428	0.656	0.612	0.505	0.361	0.217	0.113	0.053	0.022	0.254	0.499	0.830	1.220	1.123	0.918	0.649	0.387	0.203	0.097	0.043
ZU30E	0.399	0.770	1.293	1.909	1.744	1.432	1.018	0.602	0.320	0.153	0.069	0.776	1.459	2.380	3.405	3.068	2.491	1.754	1.034	0.548	0.262	0.119
A78	0.400	0.772	1.296	1.914	1.746	1.436	1.019	0.605	0.319	0.153	0.069	0.780	1.470	2.398	3.415	3.082	2.500	1.763	1.037	0.548	0.261	0.118
ZU44	0.400	0.774	1.293	1.908	1.741	1.429	1.017	0.603	0.319	0.152	0.068	0.779	1.467	2.397	3.415	3.072	2.493	1.760	1.037	0.546	0.261	0.118
ZU12	0.394	0.765	1.275	1.881	1.720	1.413	1.004	0.595	0.316	0.152	0.067	0.763	1.432	2.343	3.340	3.014	2.445	1.723	1.013	0.538	0.258	0.116
F128	0.383	0.742	1.244	1.836	1.678	1.380	0.979	0.583	0.309	0.149	0.066	0.754	1.420	2.324	3.318	2.990	2.427	1.711	1.006	0.533	0.254	0.116

Appendix Table 6 Spectral reflectivity values of Glass, Carborundum and Silicon standards calibrated by the National Physical Laboratory at various wavelengths.

Wavelength mμ	Black Glass	Carborundum	Silicon
440	4.52	21.0	43.1
460	4.50	20.8	41.3
480	4.49	20.6	39.9
500	4.47	20.5	38.9
520	4.46	20.4	38.0
540	4.44	20.3	37.2
560	4.43	20.2	36.6
580	4.42	20.1	36.0
600	4.41	20.0	35.5
620	4.40	20.0	35.1
640	4.39	19.9	34.8
660	4.38	19.9	34.4